eman ta zabal zazu

Universidad del País Vasco   **Euskal Herriko Unibertsitatea**

Universidad del País Vasco / Euskal Herriko Unibertsitatea

Facultad de Medicina y Enfermería

Departamento de Neurociencias

Microglial phagocytosis

from development to neurodegenerative diseases

Tesis doctoral para optar al grado de Doctor, presentada por:

Marlene Soledad Beccari Galeano

2021

Directora de Tesis:

Dra. Amanda Sierra

TABLE OF CONTENTS

1. ABBREVIATIONS

1. ABBREVIATIONS

act-casp3	Activated-caspase 3
AD	Alzheimer´s disease
ALS	Amyotrophic lateral sclerosis
ANPs	Amplifying neuroprogenitors
AP	Antero-posterior
APP	Amyloid precursor protein
ATP	Adenosine triphosphate
Aβ	Amyloid βeta
BAMs	Border-associated macrophages
BBB	Blood brain barrier
BM	Bone marrow
BrdU	5-Bromo-2´-deoxyuridine
CA	Cornus Ammonis
Ca^{2+}	Calcium ion
CBF	Cerebral blood flow
CCA	Common carotid artery
CCR2	Chemokine receptor 2
CD68	Macrosialin or ED1
CL	Contralateral side
CNS	Central nervous system
CR3	Complement receptor 3
CRT	Calreticulin
CSFR1	Colony stimulating factor 1 receptor
CX3CL1	Chemokine fractalkine
d	Days
DAM	Disease-associated microglia
E	Embryonic day
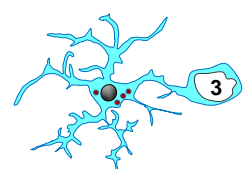
EAE	Experimental autoimmune encephalomyelitis
ECA	External carotid artery
EEG	Electroencephalography
EMP1	Progressive myoclonus epilepsy 1
EMPs	Erythromyeloid precursors
ER/SR	Endoplasmic/sarcoplasmic reticulum membranes
EtOH	Ethanol
F1	Filament 1
F2	Filament 2
Gal-3	Galectin-3
GAS6	Arrest-specific protein 6
GCL	Granule cell layer
GDNF	Glial cell-derived neurotrophic factor
GFP	Green fluorescent protein
GPR34	G protein-coupled receptor 34
h	Hours
HD	Huntington´s disease
HIE	Hypoxia-ischemia encephalopathies
HSc	Hematopoietic stem cells
HT	Hypothermia
i.p	Intraperitoneal
ICA	Internal carotid artery
IFN- γ	Interferon gamma
IFN-β	Interferon beta
IL	Ipsilateral side
IL-10	Interleukin 10
IL-1β	Interleukin 1 beta
IL-4	Interleukin 4
IL-6	Interleukin 6
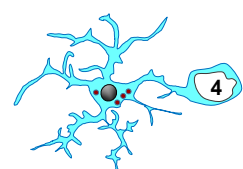
KA	Kainic acid
KO	Knock-out
LAMP1	Lysosome-associated membrane protein 1
LDF	Laser-Doppler flowmetry
LL	Latero-lateral
LPC	Lysophosphatidylcholine
LPS	Lipopolysaccharides
LTs	Leukotrienes
m	Month
M_1	Muscarinic acetylcholine receptor 1
MCA	Middle cerebral artery
MerTK	Mer tyrosine kinase
MFG-E8	Milk fat globule EGF factor 8
MIC-1	Macrophage-inflammatory protein 1
MS	Multiple sclerosis
MTLE	Mesial temporal lobe epilepsy
N_2	Nitrogen
NGF	Nerve growth factor
NMDA	N-methyl-D-aspartic acid
NSCs	neural stem cells
OGD	Oxygen and glucose deprivation
OND	Oxygen and nutrient deprivation
P	Postnatal days
PBR	Peripheral benzodiazepine receptor
PD	Parkinson´s disease
PET	Positron emission tomography
PGE_2	Prostaglandin E2
PGs	Prostanglandins
Ph capacity	Phagocytic capacity
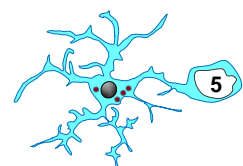
Ph index	Phagocytic index
Ph/A coupling	Phagocytosis/Apoptosis coupling
PH3	Phospho-histone 3
PM	Postmortem
ProS	Protein S
PS	Phosphatidylserine
RANTES	Chemokine ligand 5
RFP	Red fluorescent protein
RNS	Reactive nitrogen species
ROS	Reactive oxygen species
rt-PA	Recombinant tissue plasminogen activator
S1P	Sphingosine-1-phosphate
SE	Status epilepticus
SGZ	Subgranular zone
Siglec-H	Sialic acid-binding immunoglobulin-like lectin H
Stab-1	Stabilin-1
SVZ	Subventricular zone
TAM	Tyro2, AXl, and MerTK family
TBI	Traumatic brain injury
TC	Time to contact
TR	Time to remove
TD	Time to descend
TGF-β	Transforming growth factor beta
TLE	Temporal lobe epilepsy
TLR2	Toll-like receptor 2
TLR4	Toll-like receptor 4
TMEM119	Transmembrane protein 119
TNF-α	Tumor necrosis factor alpha
TREM2	Myeloid cells 2

6
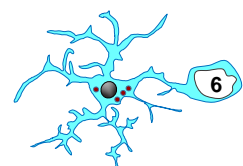
TSPO	Translocator protein
TT	Time to turn
UDP	Uridine 5´-triphosphate
VNR or αvβ3	Vitronectin receptor
γ-H2AX	γ-histone 2A, member X
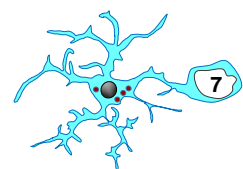
2. SUMMARY/RESUMEN

2. SUMMARY

2.1 RESUMEN

La microglía es el macrófago residente del sistema nervioso central (SNC). Estos centinelas cerebrales "escanean" continuamente el parénquima cerebral con sus procesos delgados, largos y ramificados que ayudan a mantener la homeostasis tisular y desempeñar una de sus funciones principales: fagocitosis o "comer células".

La microglía es el fagocito profesional en el cerebro y pueden fagocitar diferentes tipos de material durante condiciones fisiológicas y patológicas. No obstante, en esta tesis doctoral nos centramos en la fagocitosis de células en proceso de apoptosis o muerte celular programada. La apoptosis es un fenómeno generalizado que ocurre durante el desarrollo del cerebro pero también en patología. La eliminación eficaz de las células muertas es crucial para evitar que las células apoptóticas pierdan la integridad de la membrana y filtren contenidos intracelulares potencialmente tóxicos en el tejido circundante. Para garantizar un aclaramiento eficaz del parénquima, la microglía está dotada de una variedad de receptores de membrana para detectar y reconocer diferentes moléculas liberadas por dianas apoptóticas, como las señales "búscame" y "cómeme". Una vez que estas señales son reconocidas por la microglía, las células muertas son envueltas en un fagosoma, que posteriormente se fusionará con los lisosomas para su completa degradación. Por lo tanto, la fagocitosis microglial es un proceso crucial para mantener la homeostasis tisular.

En los últimos años, nuestro grupo estableció por primera vez la fagocitosis microglial basal en condiciones fisiológicas en el cerebro adulto, utilizando como modelo la cascada neurogénica del hipocampo, donde las células recién nacidas sufren apoptosis de forma natural y son fagocitadas rápidamente por la microglía. Además, también descubrimos que, bajo el desafío apoptótico inducido por excitotoxicidad o inflamación, la microglía mostraba diferentes estrategias para hacer frente al mayor número de células muertas, como aumentar la capacidad fagocítica por célula o reclutar más microglía. Sin embargo, en ciertas condiciones patológicas, como la epilepsia del lóbulo temporal mesial (mesial temporal lobe epilepsy, MTLE), un trastorno neurológico caracterizado por convulsiones, excitotoxicidad e inflamación, la fagocitosis microglial se altera rápidamente en las primeras etapas de la enfermedad, correlacionando con el desarrollo de una respuesta inflamatoria. Estos hallazgos nos llevaron a plantear la hipótesis que **la fagocitosis microglial también se ve afectada en otras condiciones**
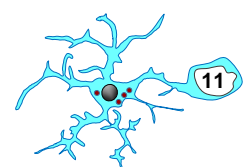
neuropatológicas que comparten características principales, como la muerte neuronal, la excitotoxicidad y/o la inflamación.

En esta tesis doctoral, exploramos la respuesta fagocítica de la microglía hipocampal postnatal y adulta en diferentes modelos in vivo: inflamación inducida por lipopolisacáridos bacterianos (LPS), administración de etanol (EtOH), encefalopatía hipóxica-isquémica (HIE), irradiación craneal (CIR), oclusión transitoria de la arteria cerebral media (tMCAo) como modelo de accidente cerebrovascular, e inyección de ácido kaínico intrahipocampal (KA) como modelo de MTLE. Además, analizamos otro tema relacionado con la fagocitosis del hipocampo hasta la edad adulta: la supervivencia de las células recién nacidas en la cascada neurogénica del hipocampo adulto.

Nuestro **objetivo 1** fue analizar la eficacia de la fagocitosis microglial en el hipocampo posnatal temprano a día 9 y 14 (P9-P14) bajo diferentes desafíos apoptóticos inducidos por lipopolisacárido bacteriano (LPS), EtOH y HIE. El tratamiento con LPS no provocó un aumento de la apoptosis en ninguna edad posnatal y, por lo tanto, no fue un modelo útil para estudiar la fagocitosis microglial. Por el contrario, EtOH aumentó el número de células muertas, pero la respuesta fagocítica al desafío fue diferente a P9 y P14. En P14, la fagocitosis permaneció estrechamente acoplada a la apoptosis, es decir, el aumento en el número de células apoptóticas se corresponde con un aumento en la fagocitosis microglial. Por lo tanto, en este escenario hubo acoplamiento entre fagocitosis/apoptosis (Ph/A). En P9, sin embargo, el incremento en la capacidad fagocítica no fue suficiente para compensar la cantidad de células muertas, lo que condujo al desacoplamiento de la relación fagocitosis/apoptosis. Se encontró una respuesta fagocítica similar en ratones P9 sometidos a HIE, donde la microglía también aumentó su capacidad fagocítica y el número de células microgliales, pero ambas estrategias no pudieron igualar el incremento de la apoptosis y, como resultado, se perdió el acoplamiento fagocitosis/apoptosis. Estos hallazgos sugirieron una maduración del potencial fagocítico microglial entre P9 y P14.

Nuestro **objetivo 2** fue analizar la eficacia de la fagocitosis microglial en el hipocampo adulto a los 2-3 meses (2-3 m) bajo desafíos apoptótico inducido por CIR, HIE, tMCAo e inyección intrahipocampal de KA. Nuestro estudio mostró que la cantidad de apoptosis inducida por CIR se eliminó del parénquima a las 24h, lo que indica la capacidad de la microglía para volverse "superfagocítica". Sin embargo, la fagocitosis microglial se vio gravemente afectada después del tratamiento con HIE, tMCAo y KA. Es importante destacar que esta disfunción microglial no se compensó con la invasión de células periféricas (monocitos) y/o células residentes (astrocitos y células madre
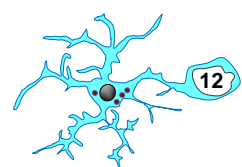
neurales) con potencial fagocítico, lo que convierte a la microglía deteriorada en el fagocito más determinante del hipocampo. Además, el deterioro de la fagocitosis microglial se acompañó de fagoptosis, es decir, el engullimiento de células no apoptóticas, aunque este fenómeno se produjo con menor frecuencia que la fagocitosis de células apoptóticas. Por lo tanto, la microglía no usó su reservorio fagocítico para enfrentar el desafío apoptótico inducido por el tratamiento con HIE, tMCAo y KA y, como consecuencia, la eficiencia fagocítica microglial se redujo notablemente.

Nuestro **objetivo 3** fue analizar otro tema relacionado con la fagocitosis en el nicho neurogénico del hipocampo hasta la edad adulta: la supervivencia de las células del recién nacido, que utilizamos para establecer la línea de base de la fagocitosis microglial. Hace unos años, nuestro grupo descubrió que las células recién nacidas del hipocampo mueren en dos períodos: 1, un período crítico temprano principal, en el que el 56% de las células se pierden en los primeros 1-4 días después del nacimiento celular, y 2, un período secundario tardío, en el que otro 25% de las células recién nacidas perecen a los 4-8 días de vida celular. Ahora exploramos si estos períodos de supervivencia se mantuvieron durante la edad adulta y, por lo tanto, si la cascada neurogénica adulta podría usarse como modelo para analizar la fagocitosis en ratones en etapas más maduras. Nuestro estudio mostró que la dinámica de la producción y supervivencia de las células del recién nacido fue en gran medida idéntica durante la edad adulta (de 1m a 12m). Además, descubrimos que el número de células recién nacidas que se diferencian en nuevas neuronas era proporcional al número de neuroprogenitores en proliferación de 1m a 12m. Sin embargo, el número de células recién nacidas se diferencia en nuevos astrocitos aumentó en ratones maduros (6-12 m) y se relacionó con una mayor supervivencia neta a los 30 días, y como resultado, el nicho cambia de neurogénico a neuro/astrogénico en ratones maduros. Finalmente, nuestros datos demostraron que la cascada neurogénica del hipocampo es un modelo útil para estudiar la fagocitosis microglial en ratones envejecidos.
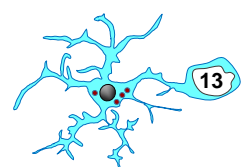
2.2 SUMMARY

Microglia are the resident macrophages of the central nervous system (CNS). These brain sentinels continuously survey the brain parenchyma with their thin, long, and branched processes and help to maintain the tissue homeostasis by exerting one of their main functions: phagocytosis or "cell eating".

Microglia are the professional phagocytes in the brain and can phagocytose different types of cargo during physiological and pathological conditions. In this PhD thesis we focused on phagocytosis of cells undergoing apoptosis, or programmed cell death. Apoptosis is a widespread phenomenon that occurs during brain development but also in several pathologies. The efficient clearance of dead cells is crucial to prevent apoptotic cells from losing membrane integrity and leak potentially toxic intracellular contents into the surrounding tissue. To guarantee an efficient clearance of the parenchyma, microglia are endowed a variety of receptors attached to their membrane to detect and recognize different molecules released by apoptotic targets, such as "find-me" and "eat-me" signals. Once these signals are recognized by microglia, dead cells are engulfed in a phagosome, which subsequently will fuse with lysosomes for its complete degradation. Therefore, microglial phagocytosis is a crucial process to maintain tissue homeostasis.

In the last few years, our group established for the first time the basal microglial phagocytosis in physiological conditions in the adult brain, using as a model the hippocampal neurogenic cascade, where newborn cells naturally undergo apoptosis and are rapidly phagocytosed by microglia. Moreover, we also discovered that under apoptotic challenge induced by excitotoxicity or inflammation, microglia displayed different strategies to cope with the increased number of dead cells such as increasing the phagocytic capacity per cell or recruiting more microglia. Nevertheless, in certain pathological conditions, such as mesial temporal lobe epilepsy (MTLE), a neurological disorder characterized by seizures, excitotoxicity, and inflammation, microglial phagocytosis was rapidly impaired at early stages of the disease, correlating with the development of an inflammatory response. These findings prompted us to hypothesize that **microglial phagocytosis is also impaired in other neuropathological conditions with share main hallmarks, such as neuronal death, excitotoxicity and/or inflammation**.

In this PhD Thesis, we explored the phagocytic response of postnatal and adult hippocampal microglia in different in vivo models: inflammation induced by bacterial lipopolysaccharides (LPS), ethanol (EtOH) administration, Hypoxia-Ischemia
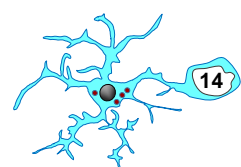
encephalopathies (HIE), cranial irradiation (CIR), transient Middle Cerebral Artery occlusion (tMCAo) as a model of stroke, and intrahippocampal kainic acid (KA) injection as a model MTLE. In addition, we analyzed another issue related to hippocampal phagocytosis through adulthood: newborn cell survival in the adult hippocampal neurogenic cascade.

Our **Aim 1** was to analyze microglial phagocytosis efficiency in early postnatal hippocampus at day 9 and 14 (P9-P14) under different apoptotic challenge induced by bacterial *Lipopolysaccharide* (LPS), EtOH, and HIE. LPS treatment did not evoke an increased apoptosis at any postnatal ages, and therefore, was not a useful model to study microglial phagocytosis. In contrast, EtOH increased the number of dead cells, but the phagocytic response to challenge was different between P9 and P14. At P14, phagocytosis remained tightly coupled to apoptosis, i.e., the rise in apoptotic cell numbers is matched with an increase in microglial phagocytosis. Therefore, in this scenario there was phagocytosis/apoptosis (Ph/A) coupling. At P9, however, the increment in the phagocytic capacity was not enough to compensate the amount of dead cells, leading to phagocytosis/apoptosis ratio uncoupling. Similar phagocytic response was found in P9 mice subjected to HIE, where microglia also increased their phagocytic capacity and microglial cell numbers but both strategies could not match the increment of apoptosis, and as a result, the phagocytosis/apoptosis coupling was lost. These findings suggested a maturation of the microglial phagocytic potential between P9 and P14.

Our **Aim 2** was to analyze microglial phagocytosis efficiency in adult hippocampus at 2-3 month (2-3m) under apoptotic challenge induced by CIR, HIE, tMCAo, and intrahippocampal KA injection. Our study showed that the amount of apoptosis induced by CIR was surprisingly cleaned from the parenchyma 24h later, indicating the capacity of microglia to become "superphagocytic". However, microglial phagocytosis was severely impaired after HIE, tMCAo, and KA treatment. Importantly, this microglial dysfunction was not compensated by invading peripheral cells (monocytes) and/or resident cells (astrocytes and neural stem cells) with phagocytic potential, which renders the impaired microglia the most determinant phagocyte in the hippocampus. Moreover, microglial phagocytosis impairment was accompanied by phagoptosis, i.e, engulfment of non-apoptotic cells, although this phenomenon occurred at lower frequency than the phagocytosis of apoptotic cells. Therefore, microglia did not use their phagocytic reservoir to confront apoptotic challenge induced by HIE, tMCAo, and KA treatment, and as a consequence, microglial phagocytosis efficiency was remarkably reduced.
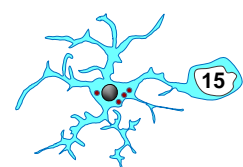
Our **Aim 3** was to analyze another issue related to phagocytosis in the hippocampal neurogenic niche through adulthood: the survival of newborn cells, which we used to establish the baseline of microglial phagocytosis. a few years ago, our group discovered that hippocampal newborn cells decline in two periods: 1, a main early critical period, in which 56% of cells are lost in the first 1-4 days after cell birth, and 2, a secondary late critical period, in which other 25% of newborn cells die from 4-8 days of cell life. We now explored whether these periods of survival were maintained throughout adulthood, and therefore whether the adult neurogenic cascade could be used as a model to analyze phagocytosis in older mice. Our study showed that the dynamics of newborn cells production and survival was largely identical through adulthood (from 1m to 12m). In addition, we discovered that the number of newborn cells differentiates into new neurons was proportional to the number of proliferating neuroprogenitors from 1m-12m. However, the number of newborn cells differentiates into new astrocytes increased in mature mice (6-12m) and was related to an increased net survival at 30d, and as a result, the niche switches from neurogenic to neuro/astrogenic in mature mice. Finally, our data showed that the hippocampal neurogenic cascade is a useful model to study microglial phagocytosis in older mice.
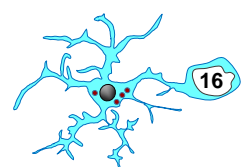
3. INTRODUCTION

3. INTRODUCTION

3.1 INTRODUCTION TO MICROGLIA

"A raíz de nuestras primeras observaciones no vacilamos en inclinarnos a admitir la naturaleza neuróglica de la nueva especie celular y la denominamos microglía, en atención a su tamaño diminuto, considerablemente menor que el de los gliocitos fibrosos y protoplásmicos; pero la suposición ulterior de que la microglía posee un origen mesodérmico nos va inclinando a designarla con el nombre, más significativo, de mesoglía" [del Rio-Hortega, 1919].

"As a result of our first observation, we are convinced that this new cell type is a glial cell and we call it microglia due to the tiny size of their soma, which is considerably smaller than that of fibrous and protoplasmic astrocytes. Nonetheless, the subsequent assumption that microglia have a mesodermal origin inspired us also to name them mesoglia" [Sierra et al., 2016]. These words were written a century ago by the Spanish neurohistologist Pío del Río Hortega to describe one of the most fascinating cells in the brain: microglia.

Microglia are the resident immune cells and expert phagocytes of the central nervous system (CNS), responsible for orchestrating the innate immune response [Sierra et al., 2013]. They are part of the glial population, alongside astrocytes, oligodendrocytes, and ependymal cells, which supports and maintains the hundred billion neurons that compose the mammalian CNS. Microglia are ubiquitously distributed throughout the brain, including the spinal cord, although their density and morphology are region-dependent [Abbott et al., 2010; Lawson et al., 1990; Stowell et al., 2018; Takagi et al., 2019; Verdonk et al., 2016]. They continuously patrol the brain parenchyma by extending and retracting their processes, without overlapping each other [Davalos et al., 2005; Nimmerjahn et al., 2005a]. This extraordinary vigilance capacity coupled with its immune nature enable microglia to perform critical functions within the brain parenchyma in physiological and pathological conditions, as we will discuss in a later section (**"3.2 Microglial functions"**).

Microglia are myeloid cells that arise from the yolk sac during early embryogenesis [Ginhoux and Prinz, 2015; Ginhoux et al., 2013; Hoeffel and Ginhoux, 2018; Kierdorf and Prinz, 2013; Schulz et al., 2012; Wieghofer and Prinz, 2016]. These tiny cells are the only true CNS parenchyma macrophages [Aguzzi et al., 2013] due to a unique combination of origin and environmental exposures, although other macrophages reside in the meninges, choroid plexus and perivascular space (BAM, border associated
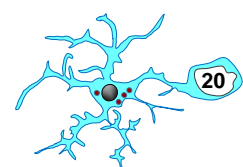
macrophages). In the next section, we will address the relevance about the origin of microglia compared to peripheral macrophages/monocytes.

3.1.1 Ontogeny of microglia and peripheral macrophages/monocytes

The origin of microglia was a long-lasting controversial debate for many generations of neuroscientists. Río-Hortega phenotypically characterized microglia and proposed that they originated from the mesodermal tissue [del Rio-Hortega, 1919, 1932]. Several investigators followed del Río-Hortega´s hypothesis and presented evidence supporting a mesodermal origin of microglia based on their morphological and phenotypic similarities with macrophages [Hume et al., 1983; Murabe and Sano, 1982, 1983; Perry et al., 1985]. In the last decade a series of lineage-tracing experiments [Ginhoux et al., 2010; Gomez Perdiguero et al., 2015; Hoeffel et al., 2012; Schulz et al., 2012] in parallel with parabiosis experiments [Ajami et al., 2007; Hashimoto et al., 2013], and neonatal bone marrow (BM) transplantations [Ginhoux et al., 2010; Hashimoto et al., 2013] definitively demonstrated that microglia are generated from yolk sac erythromyeloid precursors (EMPs) around embryonic day 7.5 (E7.5) to E8 in mice [Ginhoux and Guilliams, 2016]. These primitive cells migrate into the cephalic mesenchyme at E10.5 and expand perinatally within the neuroepithelium with little or no inputs by peripheral monocytes, which derive from fetal hematopoietic stem cells (HSCs) [Ginhoux and Guilliams, 2016; Ginhoux et al., 2010; Goldmann et al., 2016; Hoeffel and Ginhoux, 2015; Prinz et al., 2019]. Similarly, BAMs residing in the meninges, choroid plexus, and perivascular spaces of the brain also derive from yolk sac EMPs instead of fetal monocytes [Goldmann et al., 2016]. In the adult brain, microglia maintain their population by self-renewal, with no significant contribution from liver or BM-derived macrophages [Ginhoux et al., 2010; Hashimoto et al., 2013; Hoeffel et al., 2012; Schulz et al., 2012; Yona et al., 2013]. Therefore, microglia share a myeloid origin with other macrophages.
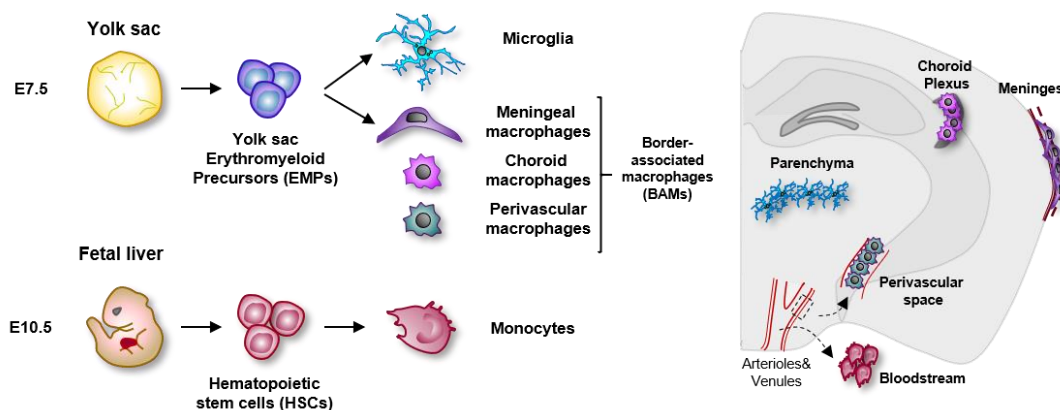
Figure 1. Origin of microglia and peripheral macrophages/monocytes. Microglia are generated from yolk sac erythromyeloid precursors (EMPs) around embryonic day 7.5 (E7.5). Other brain-border associated-

macrophages (BAMs) residing in the meninges, choroid plexus, and perivascular spaces also derive from yolk sac EMPs. In contrast, blood monocytes are generated from hematopoietic stem cells (HSCs) located in fetal liver around E10.5 and maintain their capacity to self-renew throughout adulthood.
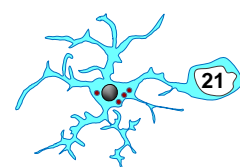
After it was demonstrated that microglia originate from the yolk sac, investigators turned their attention to develop the precise tools to discriminate these cells from other myeloid populations. This point is particularly critical during certain diseases or injuries that involve breach of the blood brain barrier (BBB), leading to the infiltration of peripheral monocytes into the CNS. In the recent years, significant effort has been made to develop tools to distinguish microglia from other BAMS and circulating blood monocytes. In the next section, we will explain the current antibodies and transgenic mice used to study microglial cells **(Fig. 2)**.

3.1.2 Tools to discriminate microglia from peripheral macrophages/monocytes

Antibodies. The most widely immunohistochemical markers used to identify microglia are ionized calcium-binding adapter molecule 1 (Iba1; [Ito et al., 1998]), cluster of differentiation receptors CD11b, CD45, and CD68 [Chakrabarty et al., 2010; Holness and Simmons, 1993; Rice et al., 2017], fractalkine receptor (CX3CR1; [Jones et al., 2010]), F4/80 ([Lawson et al., 1990]), and colony stimulating factor 1 receptor (CSF1R) [Jenkins et al., 2013]**(Fig. 2)**. However, these proteins are also expressed by BAMs and peripheral macrophages/monocytes and, therefore, the precise distinction between these populations in the CNS is a challenge. In some cases, it is possible discriminate both macrophages populations based on the amount of protein levels (marked as "high" or "low") using flow cytometry. For instance, a common strategy used in several laboratories is the combination of CD11b and CD45, in which microglia are $CD11b^+/CD45^{low}$, whereas peripheral macrophages are $CD11b^+/CD45^{high}$ [Ford et al., 1995; Grabert et al., 2016; Zhang et al., 2002]. Nonetheless, caution should be taken because CD45 expression increases in microglia under inflammation conditions and with aging [Abiega et al., 2016; Benmamar-Badel et al., 2020; Haage et al., 2019; Roesch et al., 2018].

Recent transcriptomic analysis have identified several microglial-specific genes [Butovsky et al., 2014; Gautiar et al., 2012; Hickman et al., 2013] such as *Tmem119*, *P2yr12*, *Hexb*, *Siglech*, *Fcrls*, *Gpr34*, and *Sall1*, among others, which have been the starting point for the development of new tools, including specific microglial antibodies and transgenic mice **(Fig. 2)**. For example, the transmembrane protein 119 (TMEM119) [Bennett et al., 2016] and the purinergic receptor P2Y12R [Butovsky et al., 2014] are
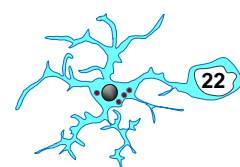
only expressed by mouse and human microglia. In addition, the Fc receptor-like molecules (FCRLs) were reported in mouse microglia but not in peripheral macrophages/monocytes [Butovsky et al., 2014]. Finally, the sialic acid-binding immunoglobulin-like lectin H (Siglec-H) was identified as an exclusive microglial-marker in mouse [Konishi et al., 2017]. The development of these new antibodies is a useful tool to identify microglia during physiological conditions. Nonetheless, their efficiency is compromised during development and disease. For instance, TMEM119 expression does not occur until postnatal day 14 (P14) in mice [Bennett et al., 2016], which limits its use at early postnatal stages. In addition, microglial homeostatic genes such as *Tmem119*, *P2yr12*, and *Siglech* are downregulated in CNS diseases [Butovsky et al., 2014; Holtman et al., 2015; Keren-Shaul et al., 2017; van der Poel et al., 2019], which could limit their use. In contrast, [van der Poel et al., 2019] reported a stable expression of these genes in multiple sclerosis (MS), suggesting a disease-dependent expression. Thus, further studies are required to validate these antibodies during neuropathological conditions.

Transgenic mice. The first and most commonly used mice line for in vivo imaging of microglia is based on the fractalkine receptor gene *Cx3cr1*. In CX3CR1-GFP, microglia express the green fluorescent reporter GFP under the control of the *Cx3cr1* promoter [Jung et al., 2000]. These transgenic mice have two crucial limitations: 1, they are either heterozygous (Cx3cr1$^{GFP/+}$) or deficient (Cx3cr1$^{GFP/GFP}$) for Cx3cr1, and therefore neuron-microglia communication (mediated by CX3CL1-CX3CR1 signaling) is impaired compared to WT mice, which can alter the synaptic transmission, learning, and memory [Maggi et al., 2011; Rogers et al., 2011]; and 2, Cx3cr1 is also expressed by other cell populations including BAMs, peripheral monocytes, dendritic cells, and natural killer cells [Jung et al., 2000] **(Fig. 2)**. Therefore, GFP labeling is not restricted to microglia in these animals. Another transgenic mouse available is Iba1-EGFP, in which microglia and peripheral macrophages/monocytes express GFP under the control of the *Iba1* promoter [Hirasawa et al., 2005] **(Fig. 2)**. More recently, several knock-in mouse lines have been developed based on microglia-specific genes such as Tmem119^{EGFP}/+ [Kaiser and Feng, 2019], Tmem119$^{tdTomato/+}$ [Ruan et al., 2020], Sall1$^{GFP/+}$ [Buttgereit et al., 2016; Takasato et al., 2004], and Hexb$^{tdTomato/+}$ [Masuda et al., 2020], in which the expression of fluorescent reporter is largely limited to microglia **(Fig. 2)**. There are also available several tamoxifen inducible Cre lines including Cx3cr1^{CreER} [Parkhurst et al., 2013; Yona et al., 2013], Tmem119$^{cre/ERT2}$/+ [Kaiser and Feng, 2019], Sall1^{CreER} [Buttgereit et al., 2016], Hexb^{CreERT2} [Masuda et al., 2020], and P2ry12 ^{CreERT2}/+ [McKinsey et al., 2020], although they have some limitations **(Fig. 2)**. For instance, Tmem119^{CreERT2}/+, and
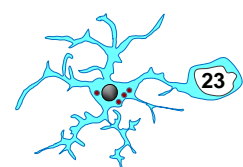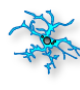
P2ry12[CreERT2]/+ mice are not completely specific to microglia since recombination also occurs in some BAM subsets after tamoxifen administration [Kaiser and Feng, 2019; McKinsey et al., 2020]. Moreover, recombination is also detected in astrocytes and oligodendrocytes in Sall1[CreER] mice [Chappell-Maor et al., 2020; Masuda et al., 2020]. Finally, it is reported that Hexb[CreERT2] mice have the highest microglia specificity, although not all microglia are targeted (brain region dependent) and recombination also happens in a very small proportion of perivascular macrophages [Masuda et al., 2020]. Despite these limitations, these transgenic mice are powerful tools to study and comprehend the behavior of microglia.

In addition to the previous mouse lines, researchers also made an effort to generate other transgenic mice to discriminate microglia from peripheral monocytes. For instance, the Cx3cr1[GFP/+] Ccr2[RFP/+] strain **(Fig. 2)**, in which resident microglia express the green fluorescent protein GFP and peripheral monocytes express the red fluorescent protein RFP under the control of the C-C motif chemokine receptor 2 (CCR2) promoter [Saederup et al., 2010].

In this PhD Thesis, we use the following transgenic mouse lines to identify microglia and/or peripheral monocytes in the CNS **(Fig. 2)**: 1, fms-EGFP (MacGreen), in which the green reporter is expressed under the promoter of *c-fms*, which encodes for CSF1R, leading to GFP expression in microglia and peripheral macrophages/monocytes [Geissmann et al., 2010; Sasmono et al., 2003]; 2, fms-EGFP Ccr2[RFP/+], in which microglia and peripheral monocytes express the GFP and RFP, respectively; and 3, Ccr2^{-/-}, with deficits in the recruitment of monocytes to sites of inflammation or injury [Serbina and Pamer, 2006].

The rise of innovative genetic, immunological, as well as imaging tools brought to light the remarkable high dynamism and plasticity of microglial cells under physiological conditions unmasking their crucial role in maintaining brain homeostasis. In the next section we will cover the microglial functions in the CNS.
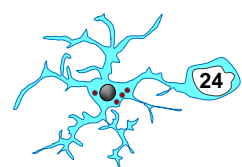
	Microglia	BAMs	Monocytes	Oligodendrocyte	Astrocyte
Iba-1	✓	✓	✓	X	X
CD11b	✓	✓	✓	X	X
CD45	✓	✓	✓	X	X
CD68	✓	✓	✓	X	X
CX3CR1	✓	✓	✓	X	X
F4/80	✓	✓	✓	X	X
CS1FR	✓	✓	✓	X	X
TMEM119	✓ (*)	X	X	X	X
P2Y12R	✓ (*)	X	X	X	X
Siglec-H	✓ (*)	X	X	X	X
Cx3cr1$^{(GFP/+)}$	✓	✓	✓	X	X
Cx3cr1$^{(GFP/GFP)}$	✓	✓	✓	X	X
Cx3cr1^{CreER}	✓	✓	✓	X	X
Iba1-EGFP	✓	✓	✓	X	X
Tmem119^{EGFP}/+	✓	X	X	X	X
Tmem119$^{tdTomato/+}$	✓	X	X	X	X
Tmem119^{CreERT2}/+	✓	✓ (*)	X	X	X
Sall1$^{GFP/+}$	✓	X	X	X	X
Sall1^{CreER}	✓	X	X	✓	✓
Hexb$^{CreERT2/+}$	✓	✓ (*)	X	X	X
P2yr12^{CreERT2}/+	✓	✓ (*)	X	X	X
Cx3cr1$^{(GFP/GFP)}$ CCR2$^{(RFP/+)}$	GFP+	GFP+	RFP+	X	X
fms-EGFP	✓	X	✓	X	X
fms-EGFP CCR2$^{(RFP/+)}$	GFP+	X	RFP+	X	X
CCR2$^{(-/-)}$	X	X	/	X	X

Figure 2. Tools to discriminate microglia from peripheral macrophages/monocytes. Antibodies and transgenic mice used to study microglia and peripheral macrophages/monocytes. (✓ and X) positive and negative expression, respectively; (*) crucial considerations: <u>Antibodies</u> (TMEM119 expression does not occur until postnatal day 14. Tmem119, P2yr12, and Siglech genes are downregulated in CNS diseases, which could limit their efficiency as antibodies. However, it was reported a stable expression of these genes in MS, suggesting a possible disease-dependent expression. <u>Transgenic mice</u> (some BAM subsets are detected in Tmem119^{CreERT2}/+ and P2ry12^{CreERT2}/+ mice; astrocytes and oligodendrocytes are identified in Sall1^{CreER} mice, and small proportion of perivascular macrophages are detected in Hexb^{CreERT2} mice. The nomenclature used for each transgenic model corresponds to that of the paper where each was originally published.

3.2 MICROGLIAL FUNCTIONS

Microglia are the most susceptible sensors of changes in the brain [Hickman et al., 2013], which allows them to perform a wide range of functions [Ginhoux et al., 2013; Nayak et al., 2014]. Some of these functions include synapse monitoring/pruning,
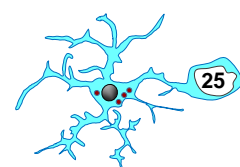
myelinization, vasculogenesis, and neurogenesis during development and adulthood in physiological and pathological conditions **(Fig. 3)**.

3.2.1 Neurogenesis

During development, microglia modulate neuron production in the subventricular zone (SVZ) of prenatal brain directly by phagocytosing neuroprogenitors cells in rats and macaque monkeys [Cunningham et al., 2013a]. Moreover, during adulthood, microglia also remove apoptotic newborn cells both in the subrgranular zone (SGZ) of the hippocampus [Sierra et al., 2010] and in the SVZ [Fourgeaud et al., 2016]. In addition, microglia can be a detrimental factor in neurogenesis. In pathological conditions such as aging and/or neurodegenerative diseases, microglia release pro-inflammatory cytokines during the inflammatory response, which trigger negative consequences for neurogenesis [Sierra et al., 2014].

3.2.2 Vasculogenesis

Several studies suggested the role of microglia in the formation of new blood vessels or angiogenesis, since microglia are temporally and spatially associated with the developing vasculature [Imamoto and Leblond, 1978; Rezaie et al., 1997, 2005]. In addition, microglia could induce vasculature alterations in pathologies such as Alzheimer´s disease (AD) or Parkinson´s Disease (PD) [Zhao et al., 2018a]. Nonetheless, the functional implications between microglia and vasculogenesis is not well defined.

3.2.3 Astrogliogenesis

Microglia also could be implicated in the production of astrocytes or astrogliogenesis by activating specific signaling pathways [Zhu et al., 2008]. Moreover, the production of pro-inflammatory mediators by microglia induce the appearance of reactive astrocytes, which lose the ability to promote neuronal survival, outgrowth, and synaptogenesis, and evoke the death of neurons and oligodendrocytes [Liddelow et al., 2017].

3.2.4 Synapse monitoring/pruning

Some evidences support the fact that microglia contribute to synapse formation [Coull et al., 2005; Parkhurst et al., 2013], maturation [Hoshiko et al., 2012; Paolicelli et al., 2011; Schafer et al., 2012; Zhan et al., 2014], function, and plasticity [Paloneva et al., 2002; Roumier et al., 2004, 2008; Walker and Lue, 2013]. In the adult CNS, synapse elimination was suggested to occur via microglia trogocytosis (defined as a partial
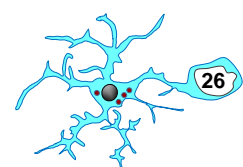
elimination or nibbling) rather than via phagocytosis [Weinhard et al., 2018]. Nonetheless, an excessive removal of synapses could negatively impact on several pathological diseases such as schizophrenia, AD, among others [Vilalta and Brown, 2018].

3.2.5 Myelination

Microglia are also related to myelination through the production of grown factors that was proposed to regulate the proliferation and survival of oligodendrocytes and their fate [Pang et al., 2013]. Moreover, phagocytosis executed by microglial is a crucial process for remyelination, since the engulfment of myelin debris facilitates the recruitment and differentiation of oligodendrocytes precursors [Domingues et al., 2016; Kotter et al., 2006]. On the contrary, microglia could be a negative role in remyelination by the release of pro-inflammatory cytokines during neuropathological conditions [Bennett and Barres, 2017; Pang et al., 2000].
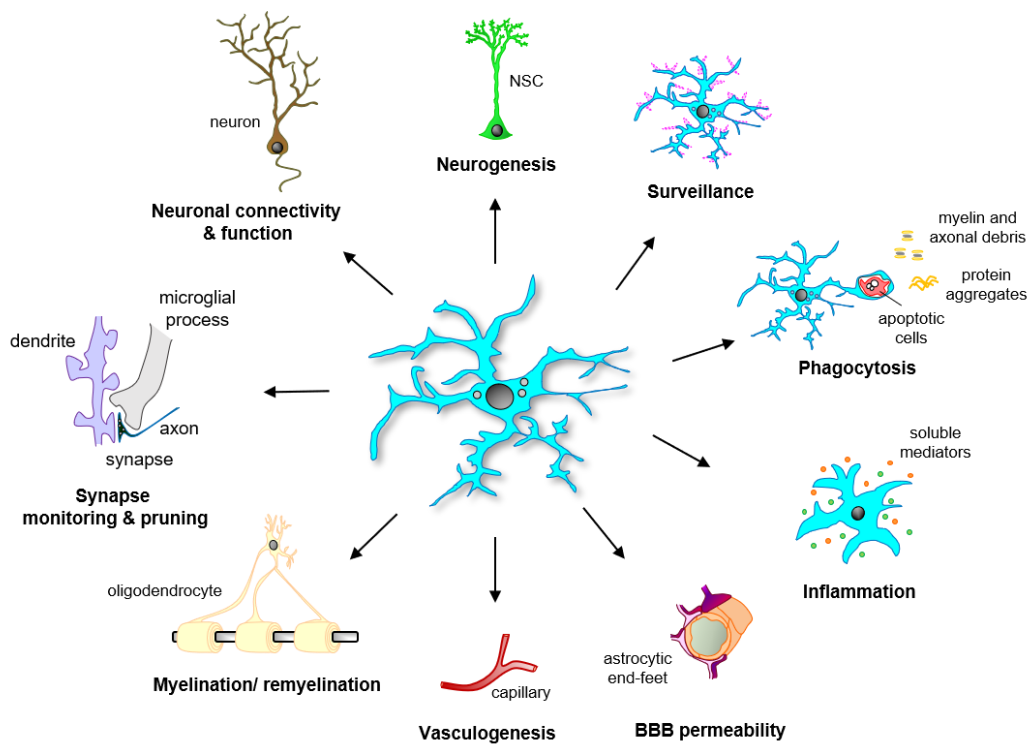
Figure 3. Microglia: key functions. Microglia continuously patrol the brain parenchyma with their processes, which allows them to perform a wide range of functions in physiological and pathological conditions. For instance, microglia perform classical immune functions, such as release of inflammatory mediators and phagocytosis of cellular debris (apoptotic cells, axonal, and myelin waste). In addition, these brain sentinels also interact with other brain cells, affecting on their function: neurons and their connectivity; neural stem cells (NSCs) and neurogenesis; oligodendrocytes and myelination/remyelination; endothelial cells and vasculogenesis; and astrocytes and blood-brain barrier (BBB) permeability. Adapted from [Sierra et al., 2019].
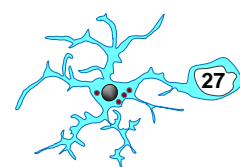
This variety of microglial functions are closely related to the two main abilities of microglia: control of inflammatory response and phagocytosis, which we will cover in the next section.

3.3 INFLAMMATORY RESPONSE

Microglia are the innate immune cells in the CNS parenchyma and, therefore, one of their main roles is to orchestrate the brain inflammatory response. The innate immune system represents the first line of defense to an intruding pathogen by triggering an inflammatory response.

Inflammation is a complex biological response of the body to harmful stimuli including pathogens or damaged cells [Isailovic et al., 2015]. The four cardinals of inflammation to counteract noxious stimuli include heat, pain, fever, redness, swelling, and loss of function [Lucas et al., 2006]. The main function of inflammation is to remove the injurious stimuli, initiate the healing process, and to restore both structure and function [Chen et al., 2018].

In the brain, several resident cells types such as astrocytes, oligodendrocytes, endothelial cells, perivascular and meningeal macrophages, and even neurons can release inflammatory mediators, although not to the same extent as microglia [Cámara-Lemarroy et al., 2010; Jeong et al., 2013; Lucas et al., 2006]. During an inflammatory insult, microglia respond by releasing different inflammatory mediators such cytokines, chemokines, proteins of the complement system, prostaglandins, leukotrienes, trophic factors, and ROS, [Nayak et al., 2014], which will be cover below.

3.3.1 Cytokines

Cytokines are small proteins produced by nearly every cell to regulate and influence immune response [Takeuchi and Akira, 2010]. These proteins bind to their receptors on target cells (neurons and glia) and activate a cascade of intercellular signals, regulating several cellular functions such as cell adhesion, cell survival, cytokine secretion, angiogenesis, proliferation, and/or cell dead [Devi, 2000; Foster, 2001; Zhang et al., 2009]. Cytokines are classically divided in two groups: pro- and anti-inflammatory factors.

Pro-inflammatory cytokines. These proteins facilitate the inflammatory response [Dinarello, 2000]. The most widely investigated pro-inflammatory cytokines are interlukin-1β (IL-1β), interlukin-6 (IL-6), and tumor necrosis factor-α (TNF-α) [Vezzani et al., 2011].
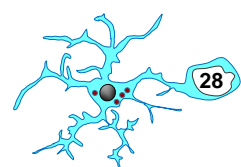
While pro-inflammatory cytokines play an essential role in the maintenance of normal brain function as well as in repair after damage, their massive and uncontrolled release can also induce an additional detrimental injury in the surrounding brain tissue. In line with this assumption, different studies demonstrated that the levels of these pro-inflammatory cytokines are increased in many neurodegenerative diseases including epilepsy, stroke, AD, MS, and/or PD, significantly aggravating the progression of the disease [Rocha et al., 2012; Zheng et al., 2016].

Anti-inflammatory cytokines. These proteins control both the extent and the duration of inflammatory response [Opal and DePalo, 2000]. Major anti-inflammatory cytokines include interleukin 4 (IL-4), interleukin 10 (IL-10), and transforming growth factor β (TGF-β) [Su et al., 2016]. In addition, there are described specific cytokines inhibitors and soluble cytokines receptors that play as anti-inflammatory [Opal and DePalo, 2000]. The main function of these cytokines is to resolve the pro-inflammatory response and promote tissue repair [Loftis et al., 2010], preventing the negative effects associated with chronic inflammation [Vezzani et al., 2013]. Nonetheless, anti-inflammatory cytokines also have a negative role in the inflammatory response. For instance, TGF-β is related to epileptogenesis [Vezzani et al., 2013] and the macrophage inhibitory cytokine 1 (MIC-1), is associated with microglial phagocytosis impairment in brain tumors [Wu et al., 2010].

3.3.2 Chemokines

Chemokines are a large family of small cytokines secreted during the inflammatory response [Griffith et al., 2014]. Their main function is to regulate the motility of immune cells, in particular leukocytes, towards the infection site through a process called chemotaxis [Hughes and Nibbs, 2018]. Chemokines CCL2 and CX3CL1 and their receptors CCR2 and CX3CR1, are one of the factors that control monocytes and macrophages infiltration into the inflamed CNS [Hughes and Nibbs, 2018]. In addition, CX3CL1/CX3CR1 are an important neuron/microglia communication axis [Wolf et al., 2013]. Many reports showed that chemokines and their receptors are especially involved in the pathogenesis of neurodegenerative diseases such as stroke, brain trauma, MS, and/or AD [Mennicken et al., 1999; Savarin-Vuaillat and Ransohoff, 2007; Ubogu et al., 2006].

3.3.3 The complement system

Complement is a central part of the innate immunity that serves as a first line of defense against foreign and altered host cells [Ricklin et al., 2010]. The complement
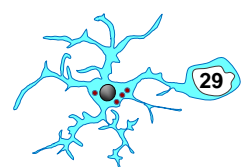
system refers to small soluble proteins produced mainly by the liver, circulating in the blood initially as inactive pro-enzymes that become functionally active on cleavage by proteases [Ling and Murali, 2019]. Its main function is to opsonize pathogens and induce a series of inflammatory responses that help immune cells to fight infection and maintain homeostasis. It can be activated through three pathways: classical, alternative, and lectin pathways. All three share the common step of activating the central component C3, but they differ according to the nature of the target recognition [Bonifati and Kishore, 2007]. However, an exaggerated or insufficient activation of the complement system can have deleterious effect, allowing the secretion of many proinflammatory cytokines, and generation of oxidative products [Bonifati and Kishore, 2007]. Several studies support both a protective and a deleterious effect of the complement in neurodegenerative diseases including stroke, epilepsy, traumatic brain injury (TBI), MS, AD, and/or ALS [Schartz and Tenner, 2020].

3.3.4 Prostaglandins (PGs)

PGs are small lipid molecules derived from arachidonic acid [Kuehl and Egan, 1980] and produced by almost all nucleated cells. Prostaglandin E2 (PGE_2) is one of the most abundant PGs produced in the body and is implicated in numerous physiological and pathological process [Park et al., 2006]. Under physiological conditions, PGE_2 is an important mediator of many biological functions, such as regulation of immune responses, blood pressure, gastrointestinal integrity, and fertility. However, dysregulated PGE_2 synthesis or degradation is associated with a wide range of pathological conditions including MS, AD, PS, Huntington's disease (HD), and/or Amyotrophic Lateral Sclerosis (ALS) [Famitafreshi and Karimian, 2020; Legler et al., 2010].

3.3.5 Leukotrienes (LTs)

Together with PGs, LTs are a group of inflammatory lipid mediators derived from arachidonic acid [Funk, 2001]. They play a pivotal role in acute and chronic inflammation [Ricciotti and Fitzgerald, 2011]. In the periphery, LTs are generated by leukocytes [Funk, 2001; Peters-Golden and Henderson, 2007], however, in the CNS the cellular source of these mediators is poorly explored [Michael et al., 2020]. Several reports proposed that LTs contribute to the neuropathology of many neurodegenerative diseases such as stroke [Fang et al., 2006, 2007; Hijioka et al., 2020; Ji et al., 2013; Zhao et al., 2011], brain trauma [Hu et al., 2005; Zhang et al., 2004], epilepsy [Takahashi et al., 2013], MS [Mirshafiey and Jadidi-Niaragh, 2010], AD [Chu and Praticò, 2011; Michael et al., 2020], and/or brain tumors [Nozaki et al., 2010].
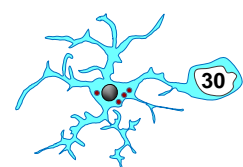
3.3.6 Trophic factors

Trophic factors are small proteins with a crucial role in both developing and mature brain, where they support the growth, survival, and differentiation of neurons and glial cells [Allen et al., 2013; Chao, 2003; Linker et al., 2009]. The glial cell-derived neurotrophic factor (GDNF), the nerve growth factor (NGF) and brain-derived neurotrophic factor (BDNF) are the main factors studied as a promising therapeutic method for neurodegenerative diseases such as stroke, MS, PD, and/or ALS [Gutiérrez-Fernández et al., 2012; Paul and Sullivan, 2019; Razavi et al., 2015; Tovar-y-Romo et al., 2014].

3.3.7 Reactive oxygen species (ROS)

ROS refers to a series of reactive molecules and free radicals derived from molecular oxygen. These molecules serve as cell signaling molecules for normal biologic processes such as cell survival, cell death, cell signaling, differentiation, gene expression, and/or immune response [Milkovic et al., 2019; Sies and Jones, 2020]. However, they can also provoke damage to multiple cellular organelles and processes, which ultimately disrupt normal physiology. Many evidences support the significant connection between ROS and neurodegenerative diseases such as epilepsy, stroke, AD, PD, HD as well as aging [Kumar and Ratan, 2016; Manoharan et al., 2016; Martinc et al., 2012; Rodrigo et al., 2013].

3.4 A CONSIDERATION ON MICROGLIAL ACTIVATION NOMENCLATURE

Traditionally, neuroscientist have classified microglia in two different and opposite categories: "resting" and "activated" **(Fig. 4)**. Microglia in the healthy brain are in a "resting" state, characterized by a highly ramified morphology as well as being immunologically quiescent. When subjected to different types of stimuli microglia rapidly shift to an "activated" state, marked by a morphological transformation from ramified to ameboid, and becoming cytotoxic cells [Banati et al., 1993]. In addition, the "activated" state was assumed to play a critical role in neurodegenerative diseases [Streit et al., 2004]. However, two pioneer studies using 2-photon microscopy demonstrated that microglia constantly monitor their domains [Davalos et al., 2005; Nimmerjahn et al., 2005b]. In fact, this microglial motility invited researchers to enquire and identify new roles of microglia in the non-pathological brain. Nowadays, we know that microglia
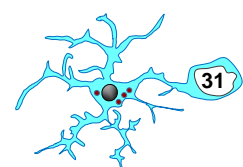
modulate neurogenesis, regulate synapse plasticity and myelin formation, phagocytose synaptic elements and apoptotic cells throughout the entire lifespan, and new physiological roles will emerge in the future [Miyamoto et al., 2016; Salter and Stevens, 2017; Schafer and Stevens, 2015; Weinhard et al., 2018; Wolf et al., 2017]; therefore, microglia are never "resting". In addition, the "activated" nomenclature is based on morphological changes, and is, thus, ambiguous. There is not a unique "activation" response but, rather, it depends on the stimulus, for instance, danger signals from damaged cells, altered neurotransmitter levels, loss of neuronal input, serum proteins, among others [Ransohoff and Perry, 2009]. Under pathological conditions, the morphological changes undergone by "activated" microglia are assumed to be detrimental however, these changes cannot be directly translated into function. Therefore, we need to change our conception of these cells and understand that microglial functions cannot be solely explained by morphological variations.

Another controversial classification used is "M1/M2" **(Fig. 4)**. This dichotomy was adopted from inflammatory response of macrophages, initiated by interferon-γ (IFN-γ) or IL-4 [Stein et al., 1992]. These categories were designated as M1 or "classical" (driven by IFN-γ) and M2 or "alternative" (driven by IL-4) activation [Stein et al., 1992]. M1 is considered a pro-inflammatory and neurotoxic phenotype, in which microglia release ROS and pro-inflammatory cytokines such as TNF-α, IL-1β, and/or IL-12. In contrast, M2 is considered an anti-inflammatory and neuroprotective phenotype, in which microglia release trophic factors, such as TGF-β, BDNF, and higher expression of scavenger receptors [Tang and Le, 2016]. Nonetheless, this assumption derived from in vitro studies, in which cultured macrophages were stimulated with a defined set of factors and does not represent the same pattern of response in vivo. In fact, single-cell RNA sequencing of infiltrating macrophages after TBI showed the absence of M1 and M2 profile [Kim et al., 2016]. Moreover, transcriptional profile analysis of human macrophages also failed to correlate with the M1/M2 polarization [Xue et al., 2014a], indicating that macrophages have a much broader repertoire of response depending on the different environmental signal received.

As brain macrophages, microglia inherited the "bad" (M1) and the "good" (M2) states, which are still used by the neuroscientist community. However, evidences from ex vivo genome-wide expression profiling of microglia clearly failed to demonstrate the M1/M2 dichotomy in mouse models of ALS, TBI, and experimental autoimmune encephalomyelitis (EAE) [Chiu et al., 2013; Hammond et al., 2019; Morganti et al., 2016; Wes et al., 2016; Yamasaki et al., 2014]. In addition, single-cell RNAseq showed that microglial response to injury such as demyelination is more complex than simply two
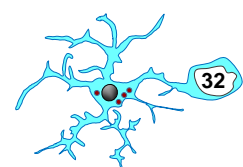
states M1 and M2 [Hammond et al., 2019; Keren-Shaul et al., 2017; Safaiyan et al., 2021]. Therefore, M1/M2 should be consider as an obsolete terminology since this simplistic view of microglial phenotype does not describe either the physiology or, more importantly, the function of microglial cells [Ransohoff, 2016].

Finally, the last pair of concepts that are emerged to define microglia are "homeostatic/surveillance" versus "reactive" **(Fig. 4)**. The concept of homeostatic microglia arises thanks to the new era of RNA-seq, quantitative proteomics, epigenetics, and bioinformatics, which allowed to identify unique gene in adult murine microglia under physiological or homeostatic conditions [Butovsky et al., 2014; Chiu et al., 2013; Gautiar et al., 2012; Hickman et al., 2013]. However, microglia change their transcriptional profile in murine models of neurodegenerative diseases such as AD, ALS, and/or aging [Holtman et al., 2015; Jordão et al., 2019; Keren-Shaul et al., 2017; Mathys et al., 2017]. Recently, it was proposed that the up-regulation of these homeostatic gene on microglia leads to the appearance of a reactive state, characterized by common disease-associated microglia (DAM) or neurodegenerative phenotype [Friedman et al., 2018; Keren-Shaul et al., 2017; Krasemann et al., 2017]. Nonetheless, this nomenclature is only focused on transcriptional changes and does not really explore the function of microglia. Undoubtedly, the alterations of these genes allow us to understand part of the puzzle but we need to comprehend the role of microglia first in physiological conditions to then be able to explore pathological situations.
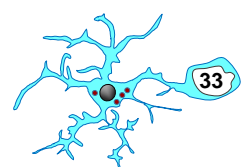
CURRENT VIEW OF MICROGLIAL NOMENCLATURE
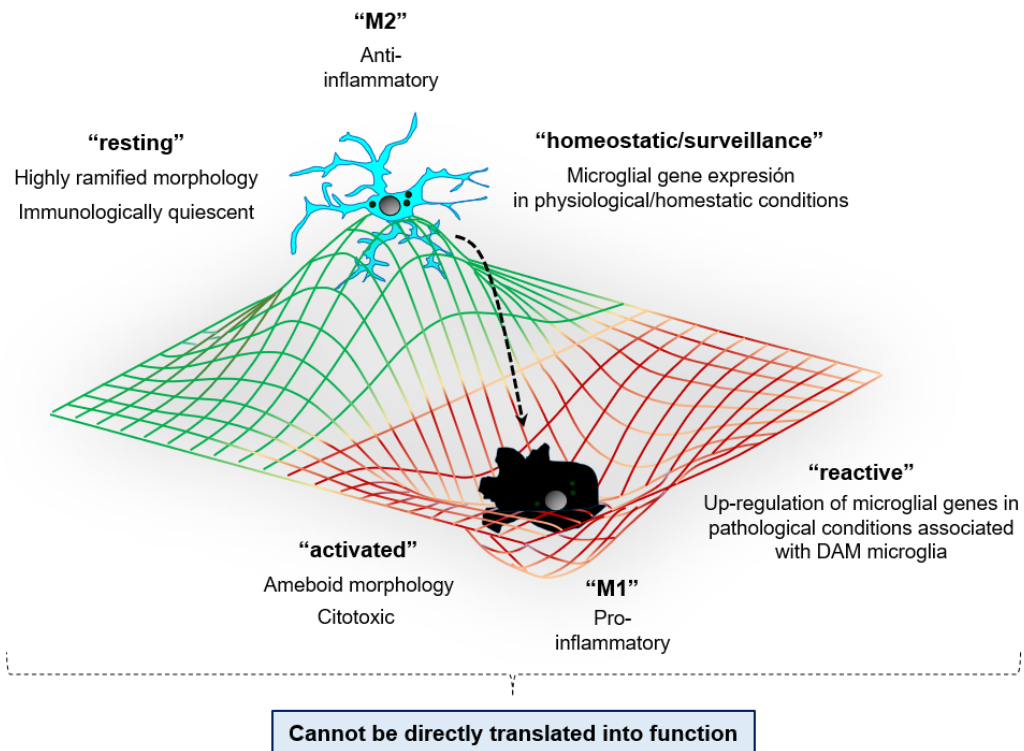
NEW INTERPRETATION
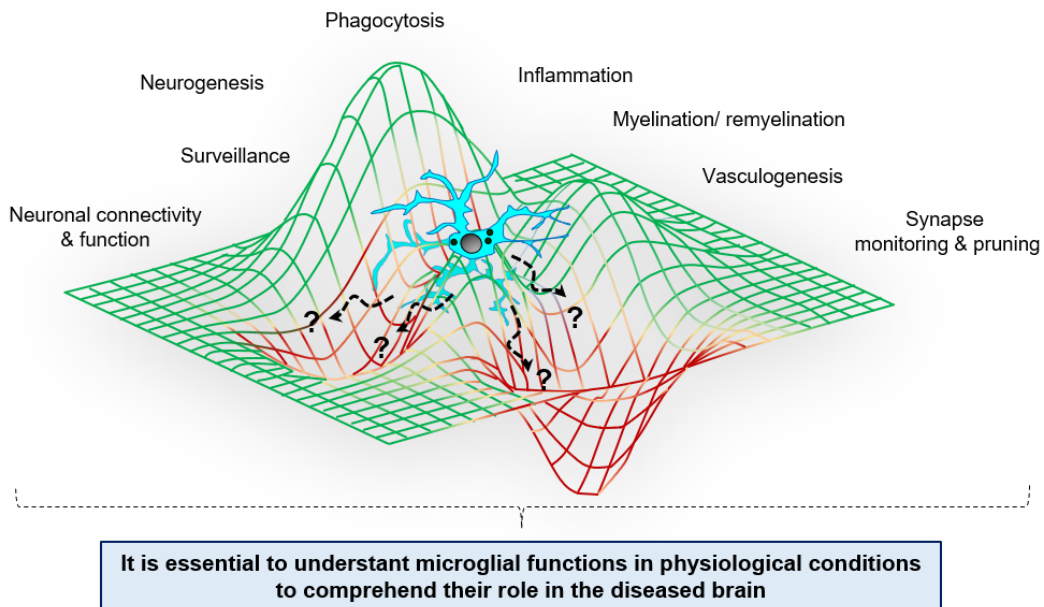
Figure 4. Microglial nomenclature. *Traditionally, microglia were designated based on their morphology: "resting" state, characterized by a ramified morphology and immunologically quiescent under physiological conditions; or "activated" state, marked by a morphological transformation from ramified to ameboid and a cytotoxic behavior. Another commonly classification used is derived from inflammatory response of macrophages: "M1 or classical", which is considered a pro-inflammatory and neurotoxic microglial phenotype; and "M2 or alternative", which is assumed an anti-inflammatory and neuroprotective phenotype. The last current nomenclature is based on RNA-seq, quantitative proteomics, epigenetics, and*
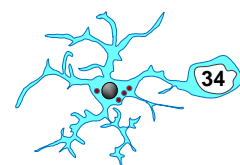
bioinformatics studies, which identify unique microglial genes in physiological conditions and leads to classify microglia in "homeostatic/surveillance". Under pathological conditions, microglia change their transcriptional profile and triggers the appearance of a reactive microglial state, characterized by common disease-associated microglia (DAM). The main issue with these classifications is the fact that they simplify our conception of microglial cells in "white" or "black" without a clear evidence about how these changes impact on microglial functions. Therefore, a new interpretation of microglial research is needed. We first should need to understand the role of microglia in physiological conditions, in which these brain sentinels perform several functions, including phagocytosis, inflammation, neurogenesis, among others, to finally comprehend their function in the diseased brain.

Over the years, these classifications were recurrently used by neuroscientist to refer to microglia in different neuropathological conditions such as epilepsy and stroke, AD, ALS, PD, MS, aging, among many other scenarios. In this PhD Thesis, we focus on the function of microglia in order to comprehend the efficiency of these cell as phagocyte in Hypoxia-Ischemia encephalopathies (HIE), stroke, and epilepsy.

3.5 PHAGOCYTOSIS

The term "phagocytosis" derives from the Greek words "phagein" & "kytos," which can be translated as "devour cell". This process involves the recognition, engulfment, and degradation of particles larger than 0.5μm, specially microorganisms, foreign substances, and apoptotic cells [Mukherjee et al., 1997; Uribe-Querol and Rosales, 2020]. Therefore, phagocytosis, in parallel to inflammation, composes the first line of defense against pathogens by the innate immune system.

Phagocytosis can be performed by most cell types, including unicellular organisms. Nonetheless, only specialized cells termed professional phagocytes execute this process with high efficiency: macrophages, dendritic cells, and neutrophils [Sierra et al., 2013; Uribe-Querol and Rosales, 2020]. In the CNS, microglia are the expert phagocytes. In addition, other cell types have the ability to phagocytose such as astrocytes [Magnus et al., 2002] and/or neuroblasts [Lu et al., 2011; Sierra et al., 2010], although they are not as efficient as microglia [Magnus et al., 2002; Parnaik et al., 2000].

Many elegant studies demonstrated that microglia phagocytose different types of cargo in both physiological and pathological scenarios. Among these targets are included microbes, axonal and myelin debris, pathogenic proteins (such as Amyloid β (Aβ)), synapses and spines, living cells (mediated a process called "phagoptosis") and/or apoptotic cells [Diaz-Aparicio et al., 2016; Jana et al., 2008; Meyer-Luehmann et al.,
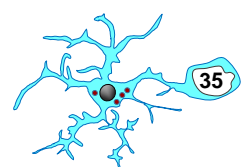
2008; Pomilio et al., 2016; Sierra et al., 2013; Tahara et al., 2006]. All of them will be covered in more detail in the following section.

3.5.1 Types of cargo

Microbes. Microglia rapidly respond to entry of pathogens microbes such as bacteria, fungi, parasites, and viruses into CNS [Dando et al., 2014]. Although the brain is rarely invaded by microbes since it is well protected by the BBB [Pardridge, 2005], some pathogens microbes make their way to the CNS and cause infections.

Several studies showed the phagocytic role of microglia in the clearance of microglial targets such as fungi or bacteria. For instance, the BV-2 microglial cell line can remove a filamentous fungi named *Lomentospora prolificans*, although in a minor proportion compared to J774A.1, a macrophage-like cell line [Pellon et al., 2018]. Moreover, microglia also phagocytose other species of fungus related to CNS infections as *Candida albicans* [Maneu et al., 2011; Neglia et al., 2006; Pellon et al., 2018] or *Cryptococcus neoformans* [Blasi et al., 1995]. Similarly, BV-2 and/or primary microglial cultures remove bacterial targets, such as *Staphylococcus aureus* [Baldwin and Kielian, 2004; Kochan et al., 2012] or *Escherichia coli* [Diesselberg et al., 2018; Ribes et al., 2009].

Axonal and myelin debris. Few reports showed that microglia remove neuronal components, such as axonal debris, promoting the axonal outgrowth during brain injury. For instance, microglia can phagocytose axonal debris in rat explants with sectioned neurites [Jin and Yamashita, 2016; Tanaka et al., 2009]. Similarly, in axonal degeneration co-culture models microglia eliminate axonal debris, allowing axonal regeneration [Hosmane et al., 2012].

In parallel to axonal fragments, myelin debris is also phagocytosed by microglia [Rawji and Yong, 2013]. While in physiological conditions, microglia remove myelin residues released from aging myelin sheaths [Safaiyan et al., 2016], with aging myelin fragments are increased and accumulate in microglial lysosomal compartments, contributing to microglial dysfunction [Safaiyan et al., 2016]. Moreover, the inefficient clearance of myelin fragments leads to an impaired remyelination process [Lampron et al., 2015]. Therefore, the correct clearance of myelin debris is critical, especially in demyelinating diseases such as MS and nerve or spinal cord injuries. Regarding these neuropathological scenarios, it was proposed that interferon beta (IFNβ) secreted by microglia mediate an enhanced removal of myelin debris [Kocur et al., 2015]. Overall, the successful myelin fragments clearance is critical for an efficient remyelination.
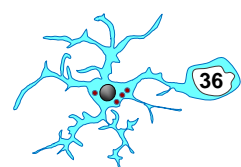
Amyloid β (Aβ). Several studies propose that microglia could remove Aβ plaques. Aβ is a small peptide produced by proteolytic cleavage from amyloid precursor protein (APP) by β- and γ-secretases [Hamley, 2012]. The accumulation of this peptide in the brain is believed to trigger a pathological cascade leading to AD [Selkoe and Hardy, 2016]. In addition, the progression of AD pathogenesis was suggested to be related to the deficiency in Aβ clearance [Mawuenyega et al., 2010; Zuroff et al., 2017].

Microglia are found surrounding amyloid plaques in both mouse models of amyloidosis as well as in AD patients [Dickson et al., 1988; Frautschy et al., 1998; Haga et al., 1989; Itagaki et al., 1989; Stalder et al., 1999; Wegiel and Wisniewski, 1990], albeit their role in Aβ clearance is still under debate. Some studies reported that microglia phagocytose Aβ in vitro [Chung et al., 1999; Koenigsknecht and Landreth, 2004; Majumdar et al., 2008; Mandrekar et al., 2009; Xu et al., 2020; Yang et al., 2011]. Nonetheless, the evidence supporting Aβ phagocytosis by microglia in vivo are unclear. While few studies suggest an Aβ internalization by microglia [Bolmont et al., 2008; Hellwig et al., 2015; Henjum et al., 2020; Zhao et al., 2018b], others report an incomplete degradation of the peptide [Grathwohl et al., 2009; Krabbe et al., 2013; Spangenberg and Green, 2017]. Therefore, microglial function related to Aβ clearance in vivo is yet to be uncovered.

Synapses and spines. Numerous studies propose that microglia have an important role in remodeling of neuronal circuit though the phagocytosis of synaptic materials such as pre- and -post-synaptic proteins [Paolicelli et al., 2011; Weinhard et al., 2018] or synaptic debris [Tremblay et al., 2010] in the developing brain. Nonetheless, there is no clear evidence supporting phagocytosis of entire synapses. Moreover, it was observed that microglia from organotypic hippocampal slices remove synapses by a process named trogocytosis, a partial elimination or nibbling [Weinhard et al., 2018], however, there are no evidence of this phenomenon in vivo.

Many studied also reported the interaction between microglia and synapses under neuropathological conditions. In ischemic-stroke mouse model, microglia showed prolonged contacts with presynaptic boutons, although only a minority of these disappeared after the microglial contact and phagocytosis was not observed [Wake et al., 2009]. Similar observations were also reported after laser-induced focal injury into the brain [Cangalaya et al., 2020]. In addition, there was a reduction in the number of synapses in AD mouse models, which was mediated by a combination of microglia and the complement protein C1q [Hong et al., 2016]. In parallel to ischemia-stroke and/or AD, other neurodegenerative diseases including Huntington´s disease, glaucoma,
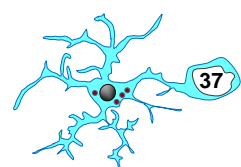
neuropathies, among others are characterized by synapse loss [McGonigal et al., 2016; Perry et al., 2010; Williams et al., 2016], albeit the role of microglia to remove synapse is still under debate.

Living cells. Years ago, it was proposed a new form of cell death caused by phagocytosis of viable or non-apoptotic cells, resulting in their destruction. This phenomenon is known as "phagoptosis" and is triggered by inflammation [Brown and Neher, 2014]. Living cells phagocytosis is initiated by exposure of "eat-me" signals such as phosphatidylserine (PS), among others (**more details in section 3.5.2 "Stages of apoptotic cells phagocytosis"**) on the surface of a viable cell, evoking its engulfment by phagocytes [Neher et al., 2011; Brown and Neher, 2012; Butler et al., 2021].

Several in vitro studies reported that viable or non-apoptotic neurons are phagocytosed by microglia after treatment with bacterial lipopolysaccharides (LPS), TNF-α, and/or Aβ [Fricker et al., 2012b, 2012a; Neher et al., 2011; Neniskyte and Brown, 2013; Neniskyte et al., 2011]. This process can be mediated via several microglial receptors and opsonins. For instance, under inflammatory conditions, microglia release increased levels of milk fat globule EGF factor 8 (MFG-E8), which tightly binds to exposed PS on viable cells and to microglial vitronectin receptors (VNRs), promoting phagocytosis of non-apoptotic cells [Fricker et al., 2012b; Neniskyte and Brown, 2013]. In addition, it was proposed that non-apoptotic cells are phagocytosed by microglia/peripheral macrophages in in vivo models of neurodegenerative diseases, such as focal ischemia [Neher et al., 2013]. Moreover, our group also identified phagoptosis executed by microglia in a murine model of Mesial Temporal Lobe Epilepsy (MTLE) induced by intrahippocampal administration of kainic acid (KA) [Abiega et al., 2016].

In this PhD Thesis, we will focus on apoptotic cells and their phagocytosis, and we will cover this mechanism in more detail in the next sections.

Apoptotic cells. Apoptosis or programmed cells death is a ubiquitous biological process that occurs in the brain under both physiological (development and adult neurogenesis) and pathological conditions (neurodegenerative diseases) [Madden and Cotter, 2008].

The mechanisms controlling apoptosis are highly complex and sophisticated, involving an energy-dependent cascade of molecular events. There are two main apoptotic pathways: the extrinsic pathway, initiated by surface receptors; and the intrinsic pathway, characterized by cellular death and mitochondrial damage [Barber,
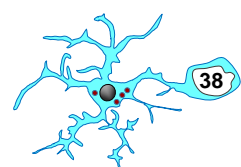
2001; Reubold and Eschenburg, 2012; Taylor et al., 2008; Xu et al., 2019]. Each pathway activates its own initiator caspase, which in turn will activate the executioner caspase 3 [Elmore, 2007], and ultimately will induce the morphological and biochemical changes related to apoptosis. These changes include cell blebbing and shrinkage, nuclear fragmentation (karyorrhexis), irreversible condensation of the chromatin (pyknosis), and formation of small vesicles known as apoptotic bodied [Xu et al., 2019]. One important aspect of apoptosis is that the integrity of the plasma membrane is preserved until the final stages of the apoptotic process, in contrast to necrosis, another form of cell death characterized by the loss of plasma membrane integrity [D'Arcy, 2019]. The lack of membrane permeability during apoptotic cell death is particularly relevant since the clearance of dead cells avoids the release of toxic intracellular contents into the surrounding tissue, which can evoke an exacerbated inflammatory response and cellular stress. Therefore, apoptosis and phagocytosis must be tightly coupled to ensure the successful elimination of dead cells, and ultimately, to maintain the tissue homeostasis.

In the next section, we will cover the narrow communication between apoptosis and phagocytosis executed by microglia.

3.5.2 Stages of apoptotic cells phagocytosis: "Find-me", "Eat-me", and "Digest-me"

The mechanical process of apoptotic cells phagocytosis is summarized in three phases: "find-me", "eat-me", and "digest-me" **(Fig. 5)**. First, in the "find-me" step, dead cells release signals to attract microglia [Peter et al., 2010; Sierra et al., 2013]. Second, in the "eat-me" step, microglia recognize their targets through specific ligands present in apoptotic cells [Gardai et al., 2006; Sierra et al., 2013]. Finally, in the "digest-me" step, microglia engulf and completely degrade dead cells in the lysosomal compartment [Arandjelovic and Ravichandran, 2015; Diaz-Aparicio et al., 2016; Gardai et al., 2006; Sierra et al., 2013]. Each step of phagocytosis is carefully regulated by molecules, such as ligands and receptors present on apoptotic cell and microglia, which guarantee the correct functioning of the phagocytic process.

FIND-ME   EAT-ME   DIGEST-ME
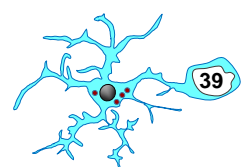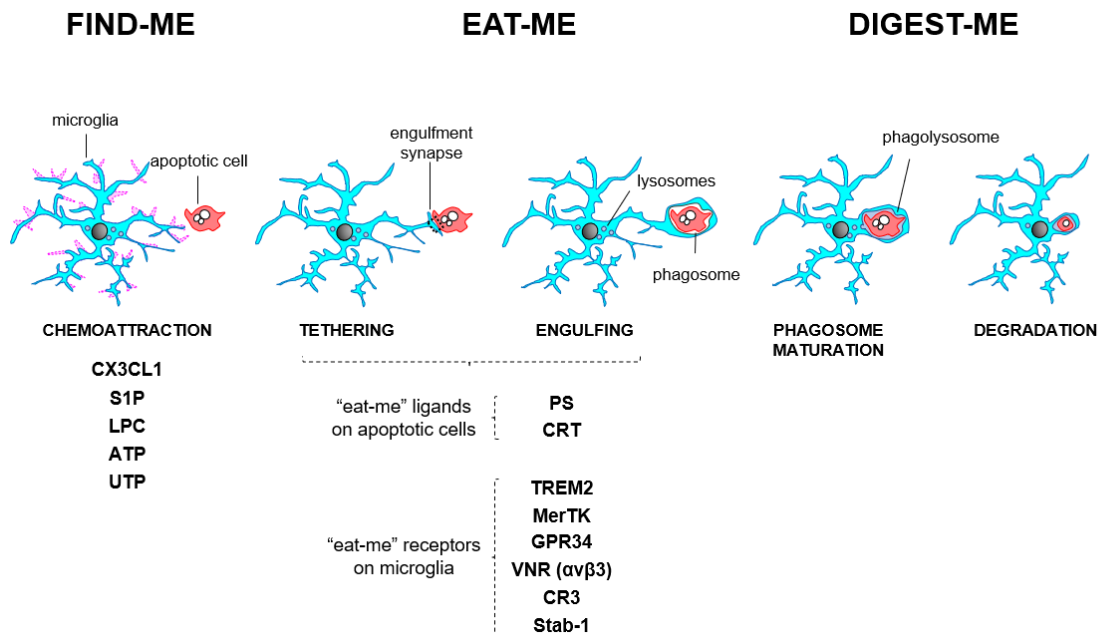
Figure 5. Microglial phagocytosis of apoptotic cells. *Phagocytosis comprises three different phases: "find-me", "eat-me", and "digest-me". First, in the "find-me" stage, apoptotic cells release signals to attract phagocytes, such as fractalkine and the extracellular nucleotide adenosine triphosphate (ATP). Second, in the "eat-me stage", an engulfment synapse is formed between a series of microglial receptors, such as triggering receptor expressed on myeloid cells-2 (TREM2), and their ligands present in apoptotic cells such as phosphatidylserine (PS), leading to the tethering and engulfing of the apoptotic cell in a phagosome. Finally, in the "digest-me" stage, the phagosome becomes mature by fusing with lysosomes and other organelles, and the apoptotic cell is fully degraded in the phagolysosome within microglia.*

3.5.2.1 "Find-me" step

Dead cells can release several "find-me" signals to recruit microglia towards them. These molecules include the chemokine fractalkine (CX3CL1), the lipids sphingosine-1-phosphate (S1P) and lysophosphatidylcholine (LPC), and extracellular nucleotides adenosine triphosphate (ATP) and uridine 5´-triphosphate (UDP) [Arandjelovic and Ravichandran, 2015; Elliott et al., 2009; Gude et al., 2008; Lauber et al., 2003; Sierra et al., 2013; Truman et al., 2008].

Fractalkine (CX3CL1). In the CNS, CX3CL1 is expressed by neurons, while its receptors are only expressed by microglia under physiological conditions. After neuronal stress, fractalkine is cleaved by matrix metalloproteases to release a soluble fragment, which act as a chemotactic signal to microglia [Sokolowski et al., 2014; Truman et al., 2008], promoting the migration of the phagocyte [Eyo et al., 2016; Jung et al., 2000; Mizutani et al., 2012].
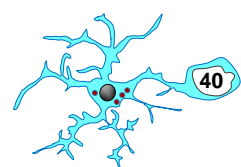
Sphingosine-1-phosphate (S1P). S1P is secreted by apoptotic cells and binds to S1P receptor expressed by phagocytes, promoting its migration toward dead cells [Gude et al., 2008]. Recently, it was demonstrated the expression of S1PR on microglia [O'Sullivan et al., 2018], although its possible influence in phagocyte recruitment is still unknown.

Lysophosphatidylcholine (LPC). LPC is released by dead cells and binds to G2A receptor expressed on microglia [Lauber et al., 2003; Peter et al., 2008], which, for instance, leads to the colonization of phagocytes in the developing brain zebrafish [Xu et al., 2016a].

Extracellular nucleotides (ATP and UTP). ATP and UDP are released by apoptotic cells, which act on purinergic receptors expressed by microglia, leading to the recruitment of microglia towards dead cells [Domercq et al., 2013; Elliott et al., 2009]. One of the mechanisms that explain the release of these nucleotides by apoptotic cells occurs via pannexin 1 channels [Chekeni et al., 2010].

Once apoptotic cells release "find-me" signals and microglia recognize them and chemotactically approach them, the "eat-me" step is started, in which physical contact between microglia and apoptotic targets occurs to perform recognition and tethering of the apoptotic cell [Sierra et al., 2013].

3.5.2.2 "Eat-me" step

The recognition and engulfment of apoptotic cells is the most critical step in phagocytosis [Sierra et al., 2013]. Apoptotic cells also express a variety of ligands in their membrane that are recognized as "eat-me" signals by phagocytes. In parallel to dead cells, microglia are also equipped with a plethora of surface receptors that enable to detect "eat-me" signals released by apoptotic cells.

➢ "Eat-me" ligands present on apoptotic cells

Dead cells express "eat-me" signals on the cell surface to indicate that they should be removed by microglia. These "eat-me" signals include the expression of PS and calreticulin (CRT) [Park and Kim, 2017].

PS. Phosphatidylserine is the best characterized "eat-me" signal express on the cell surface. PS is a phospholipid that resides on the inner leaflet of the plasma membrane bilayer in healthy cells, but it is externalized on the cell surface in response to apoptotic stimuli [Fadok et al., 1992; Ravichandran and Lorenz, 2007]. This
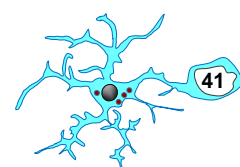
externalization occurs via activation of the Xk-related protein 8 (Xkr8) in a caspase-3-dependent manner [Suzuki et al., 2016].

Calreticulin (CRT). CRT is a protein localized in the endoplasmic/sarcoplasmic reticulum (ER/SR) membranes [Ostwald and MacLennan, 1974] and, probably, in the nucleus [Burns et al., 1994]. ER stress and/or apoptotic signaling can lead to expression of CRT on surface of dead cells, which is sensed by low-density lipoprotein receptor-related protein on phagocytes to promote engulfment [Gardai et al., 2005]. Moreover, it was recently showed that CRT binds to phosphatidylserine via its C-terminal acidic region, leading to apoptotic cell phagocytosis [Wijeyesakere et al., 2016].

➤ **"Eat-me" receptors present on microglia**

Different phagocytic receptors localized in the cellular membrane of the microglia allow to bind diverse "eat-me" ligands on apoptotic cell. The most conspicuous phagocytosis receptors expressed on microglia are the triggering receptor expressed on myeloid cells-2 (TREM2), Mer tyrosine kinase (MerTK), G protein-coupled receptor 34 (GPR34), vitronectin receptor (VNR or αvβ3), complement receptor 3 (CR3), and stabilin-1 (Stab-1).

Triggering receptor expressed on myeloid cells-2 (TREM2). TREM2 is an immunoglobulin-like receptor expressed by macrophages, dendritic cells (DCs), and microglia [Neumann and Takahashi, 2007]. This receptor is associated with the immunoreceptor tyrosine-based activation motif (ITAM)-containing signaling adapter molecule DAP12. Loss of function mutations in either TREM2 or DAP12 cause a rare a fatal neurodegenerative disease named Nasu-Hakola [Paloneva et al., 2000, 2002]. Although the mechanisms underlying this disorder are unknown, it was suggested that the lack of TREM2 and/or DAP12 disturb the elimination of apoptotic neurons by microglia, leading to their accumulation [Thrash et al., 2009]. TREM2 is also involved in the recognition of extracellular amyloid β deposits in AD [Parhizkar et al., 2019].

Mer tyrosine kinase (MerTK). MerTK is a member of the Tyro2, Axl, and MerTK (TAM) family of receptors [Lemke, 2013], which is expressed on macrophages and DCs [Behrens et al., 2003]. MerTK ligands, the arrest-specific protein 6 (GAS6) and Protein S (ProS) [Nagata et al., 1996; Wu et al., 2005], both bind to PS expressed on the surface of apoptotic cells and to TAM receptors on the surface of phagocytes [Lemke, 2013; Zizzo et al., 2012]. Another MerTK ligand is the galectin-3 (Gal-3), which is also implicated in the elimination of dead cells [Caberoy et al., 2012].
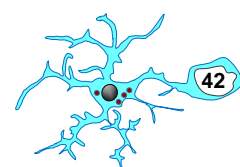
G protein-coupled receptor 34 (GPR34). GPR34 is a P2Y family member receptor highly expressed by microglia [Bédard et al., 2007; Butovsky et al., 2014; Hickman et al., 2013], although can be found in other populations such as monocytes, DCs, natural killer cells, and/or B cells [Ikubo et al., 2015; Schöneberg et al., 2018]. In vitro experiments showed that GPR34 deficient microglia decrease their capacity to phagocytose latex beads and myelin, suggesting that this receptor could play a critical role in phagocytosis of apoptotic cells [Preissler et al., 2015].

Vitronectin receptor (VNR or αvβ3). VNR is a member of the integrin superfamily of adhesion molecules expressed by macrophages [Lauber et al., 2004]. The clearance of apoptotic cells is mediated via VNR, which binds to the opsonin MFG-E8 [Hanayama et al., 2002]. The activation of VNRs stimulate phagocytosis remodeling of the microglial actin cytoskeleton [Arcuri et al., 2017; Yanuck, 2019].

Complement receptor 3 (CR3). CR3 belongs to the family of beta-2 (CD18) integrins [Vorup-Jensen and Jensen, 2018], and is expressed by microglia in the CNS [Ehlers, 2000]. CR3 binds to C1q and/or C3b, both component of the complement cascade [Linnartz et al., 2012], but also is involved in the cellular adhesion and phagocytosis of apoptotic cell by microglia in vitro [Trouw et al., 2008].

Stabilin-1 (Stab-1). Stab-1 is a transmembrane receptor expressed on the cell surface of macrophages [Kzhyshkowska et al., 2006], which mediates apoptotic cell engulfment through phosphatidylserine recognition [Park et al., 2009; Park and Kim, 2017].

Once the "eat-me" signals and their respective receptors contact each other, microglia undergo cytoskeletal rearrangements, which lead to the formation of a tridimensional pouch, usually located in the terminal or en passant branches of microglia, completely surrounding an apoptotic cell [Sierra et al., 2010]. After the internalization, the "digest-me" step of phagocytosis starts, in which the apoptotic target is degraded in the lysosomal compartment of phagocytes [Arandjelovic and Ravichandran, 2015].

3.5.2.3 "Digest-me" step

The internalization of apoptotic cells within microglia occurs through the formation of a phagosome. To perform the degradation of dead cells, phagosomes undergo a process of maturation, becoming increasingly acidic and fusing with lysosomes, which contain digestive enzymes required for degradation [Kinchen and Ravichandran, 2008].
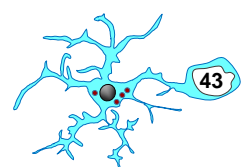
It was proposed that the signaling cascade triggered after internalization could regulate the phagocytic capacity of phagocytes to engulf additional targets [Park et al., 2011; Wu et al., 2000]. Nonetheless, the process of phagosome formation and cargo degradation is poorly explored in microglia, and therefore, further studies are required to uncover the mechanisms of degradation of dead cell by microglia.

Therefore, microglial phagocytosis of apoptotic cells can be regulated at three different steps: "find-me", "eat-me", and "digest-me", and more importantly, changes in any of these steps could potentially affect phagocytic efficiency.

3.6 METHODS FOR ASSESING MICROGLIAL PHAGOCYTOSIS OF APOPTOTIC CELLS

Microglial phagocytosis is a critical process to maintain brain homeostasis, however, its efficiency in the living brain has long been overlooked or assessed using indirect methods [Diaz-Aparicio et al., 2016; Sierra et al., 2013]**(Fig. 6)**.

One of the classical strategies to measure phagocytosis both in vitro and in vivo is based on microglial adopting an ameboid morphology. However, contrary to the traditional assumption that phagocytosis is performed only by ameboid-shaped microglia [Kettenmann, 2007], our lab observed that phagocytosis is effectively executed by either ramified microglia (in physiological conditions) or a more hypertrophic microglia (in acute inflammation induced by LPS). Therefore, changes in microglial morphology are not associated with their capacity to phagocytose [Sierra et al., 2013]. Another method used to determine phagocytosis is the analysis of classical microglial "activation markers", such as macrosialin or ED1 (CD68) [Ekdahl et al., 2003; Da Silva and Gordon, 1999], a lysosomal and membrane protein overexpressed during inflammation. The localization of this protein suggested its involvement in phagocytosis, however, macrophages from deficient CD68 mice have no defects in phagocytosis [Song et al., 2011], indicating that there is no correlation between the expression of CD68 and phagocytosis [Sierra et al., 2013]. Thus, the use of "activation markers" as a substitute for direct measurements of phagocytosis can lead to incorrect conclusions. Moreover, phagocytic efficiency is also estimated based on the quantification of engulfed artificial targets, such as latex beads. These types of target are widely used, especially in vitro, although can be also found in several in vivo studies. The main limitations of these targets are that they do not release chemoattractant, do not express any ligands that could interact with microglial phagocytic receptors, and cannot be degraded. Therefore, the use of these synthetic phagocytic
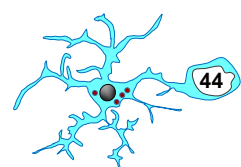
beads is highly artificial since they cannot mimic the different steps of phagocytosis [Diaz-Aparicio et al., 2016]. Overall, microglial phagocytosis analysis must always be based on the direct observation of 1, the phagocytic pouch, and 2, the presence of cargo inside the pouch, which allows us to confirm that phagocytosis indeed occurs.

Importantly, advances in imaging techniques have also become powerful tools to visualize microglial phagocytosis, albeit with limitations. For instance, light microscopy in combination with immunostaining allows identifying phagocytic pouches [Perez-Pouchoulen et al., 2015] but does not ensure that they contain apoptotic cells [Diaz-Aparicio et al., 2016]. Another strategy is the use of electron microscopy, which represents an excellent method to confirm apoptosis [Savill et al., 2002], although it is time-consuming and analyzes only small regions. The last two critical techniques are 2-photon and confocal microscopy, which are considered the most reliable methods to directly assess microglial phagocytosis in vivo. Both techniques offer quantitative data of the process of phagocytosis performed by an individual microglial cell in real time (2-photon microscopy) or by the microglial population in fixed tissue (confocal microscopy).

How to assess microglial phagocytosis?
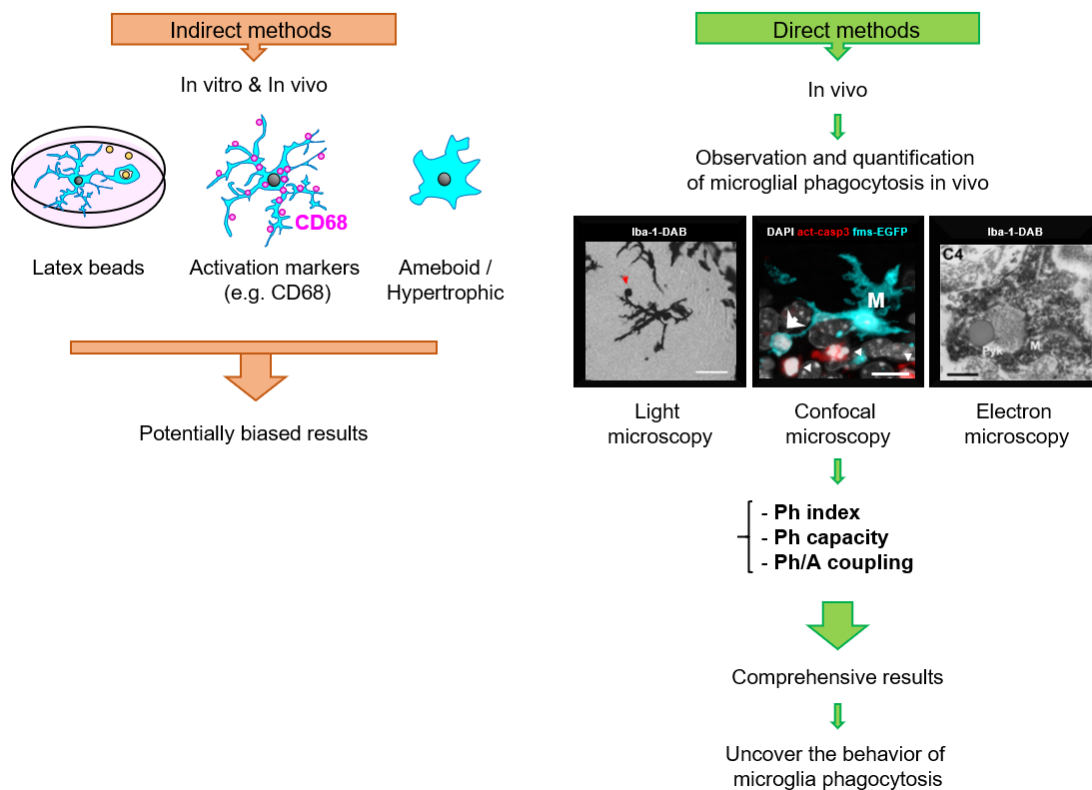
Figure 6. Quantification of microglial phagocytosis. *Microglial phagocytosis is an essential mechanism to remove apoptotic cells from the tissue. However, this critical process has long been either overlooked or assessed using indirect methods based on: 1, engulfment of artificial phagocytic targets such as latex beads;*
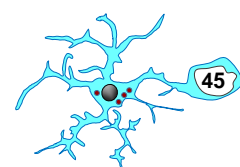
2, expression of classical phagocytic markers such as CD68; or 3, morphological changes, including ameboid or hypertrophic. These methods are inconclusive and offer potentially biased results since they do not reliably represent the efficiency of microglial phagocytosis. Importantly, there are some studies that have developed different strategies to directly quantify phagocytosis in vivo, such as light microscopy, confocal microscopy, or electron microscopy. To obtain a comprehensive understanding of the dynamics of microglial phagocytosis we have developed a novel set of parameters based on confocal imaging of microglia: Ph index (i.e., proportion of apoptotic cells completely engulfed by microglia), Ph capacity (i.e., proportion of microglia with one or more phagocytic pouches, each containing one apoptotic cell), and Ph/A coupling (i.e., net phagocytosis (number of microglia multiplied by their phagocytic capacity) divided by the number of apoptotic cells. These parameters have allowed us to uncover the modus operandi of microglia in the healthy and diseased brain. Adapted from [Diaz-Aparicio et al., 2016].

In this PhD Thesis, we analyzed microglial phagocytosis of apoptotic cells in different brain tissue from mice, monkeys, and human patients. For this purpose, we used confocal microscopy in combination with immunofluorescence in order to identify the tiny microglial process that create the phagocytic pouch, and also to test the presence of apoptotic cell inside the pouch, which allow us to confirm that phagocytosis indeed occurs.

3.7 FUNCTIONAL CONSEQUENCES OF THE PHAGOCYTOSIS OF APOPTOTIC CELLS

The generation of the apoptotic cells in both physiological and pathological scenarios needs to be counteracted by an active and efficient clean-up system. Dead cells must rapidly phagocytose from the brain parenchyma, otherwise, they could transform into secondary necrotic cells, losing their cell membrane permeability and leading to the spillover of intracellular contents [Poon et al., 2014; Roth et al., 2021]. This event would lead to the leakage of toxic cell components, which might evoke an inflammatory response or autoimmune diseases [Nagata et al., 2010; Poon et al., 2014]. Thus, failure to efficiently phagocytose apoptotic cells might be harmful to the brain parenchyma. Importantly, phagocytosis also exerts an anti-inflammatory role, at least in vitro [Fadok et al., 1998; Stern et al., 1996; Voll et al., 1997]**(Fig. 7)**. A few studies reported that ingestion of apoptotic cells by macrophages induces the production of TGF-β and PGE_2, and the suppression of TNF-α [Byrne and Reen, 2002; Fadok et al., 1998; Voll et al., 1997]. A similar anti-inflammatory response was also observed in cultured phagocytic microglia, which increased the release of TGF-β and NGF, and reduced the secretion of TNF-α compared to microglia challenged with LPS [Fraser et al., 2010; Magnus et al., 2001; De Simone et al., 2003]. Although further studies are needed to
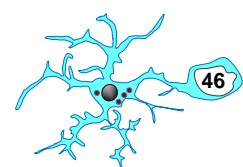
determine the inflammatory response after microglial phagocytosis in vivo, these in vitro data are promising since the anti-inflammatory characteristics of microglia might facilitate the functional recovery of the surrounding compromised neurons in a diseased brain. In addition, these results also suggest that an impairment of phagocytosis would correlate with an inflammatory response **(Fig. 7)**. In line with this assumption, our group discovered that microglial phagocytosis impairment is directly related to development of an inflammatory response during epilepsy [Abiega et al., 2016]**(Fig. 7)**, although the signal/s which initiate this response in the epileptic brain are still unknown. Overall, microglial phagocytosis of apoptotic cells is a vital process to maintain the tissue homeostasis.
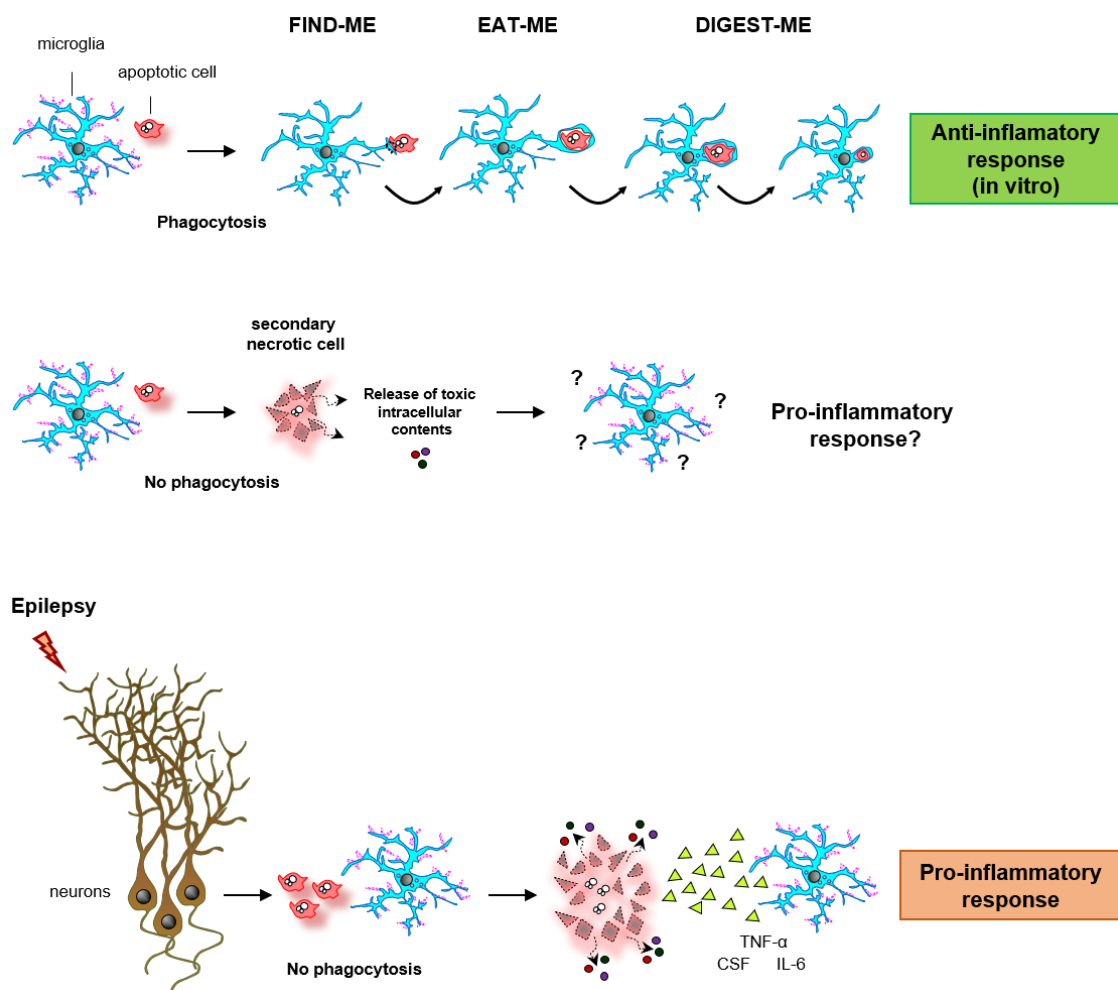
Figure 7. Functional consequences of apoptotic cells phagocytosis. Microglial phagocytosis is a vital process for tissue homeostasis for two reasons: 1, the clearance of apoptotic cells by phagocytes is actively anti-inflammatory, at least in vitro; and 2, phagocytosis prevents the apoptotic cells from losing membrane integrity and leak potentially toxic intracellular contents into the surrounding parenchyma, a process that could also trigger an inflammatory response. Therefore, the efficient clearance of the dead cells is crucial for the maintenance of healthy brain tissue. However, in some pathological conditions, such as epilepsy,
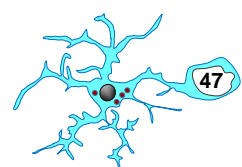
microglial phagocytosis is rapidly and chronically impaired, correlating with the development of a pro-inflammatory response.

In the next sections, we will cover microglial phagocytosis of apoptotic cells in physiological conditions, where we establish the baseline of phagocytosis, and then we will describe what is known about its efficiency under pathological conditions induced by LPS, ethanol (EtOH), Hypoxia-Ischemia encephalopathies (HIE), cranial irradiation (CIR), stroke, and epilepsy.

3.8 MICROGLIAL PHAGOCYTOSIS OF APOPTOTIC CELLS IN PHYSIOLOGICAL CONDITIONS

To study the efficiency of microglial phagocytosis in pathological conditions we first needed to determine how much they could eat in physiological conditions. To establish the baseline of microglial phagocytosis efficiency, we focused our attention in the hippocampal neurogenic cascade, where there is ongoing production of newborn neurons, many of which undergo apoptosis and are subsequently phagocytosed by microglia [Sierra et al., 2010]. In this section, we will first describe the hippocampal neurogenic niche, the survival of the newborn cells, and the phagocytosis of apoptotic cells by microglia.

3.8.1 Adult hippocampal neurogenesis as a model of microglial phagocytosis of apoptotic cells

Neurogenesis, or the generation of new neurons, is a complex process that occurs throughout adulthood in two regions of the mammalian brain, the subventricular zone, which generates new neurons destined to the olfactory bulb [Obernier and Alvarez-Buylla, 2019], and the SGZ of the hippocampus, which gives rise to newborn cells that are locally integrated as mature granule cells in the DG [Obernier and Alvarez-Buylla, 2019]. This process comprises different steps in which neural stem cell proliferate, differentiate and migrate until they eventually integrate into the existing circuitry and gradually acquire physiological neuronal properties [Kempermann et al., 2004].

The hippocampal neurogenic cascade is initiated by the neural stem cells (NSCs), which reside in the SGZ of the DG, between the hilus and the granule cell layer **(Fig. 8)**. Adult NSCs are normally maintained in mitotic quiescence, with a low rate of division [Encinas et al., 2006]. Nonetheless, after their activation, these cells divide
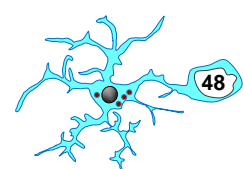
asymmetrically and give rise to astrocytes and amplifying neuroprogenitors (ANPs) [Encinas et al., 2011], which divide several times before they differentiate into neuroblasts [Encinas and Sierra, 2012]. Afterwards, neuroblasts eventually go through a stage of immature neuron until they differentiate into mature granule neurons. During this multistep neurogenic process, many newborn cells naturally undergo apoptosis in two periods: 1, a main early critical period, in which 56% of cells are lost in the first 1-4 days after cell birth, and 2, a secondary late critical period, in which other 25% of newborn cells die from 4-8 days of cell life [Sierra et al., 2010]**(Fig. 8)**. This natural apoptotic event allowed us to establish, for the first time, the baseline of microglial phagocytosis in physiological condition in the adult hippocampal niche [Sierra et al., 2010]. In this PhD Thesis, we will use this baseline to assess the changes in the efficiency of phagocytosis under pathological conditions.
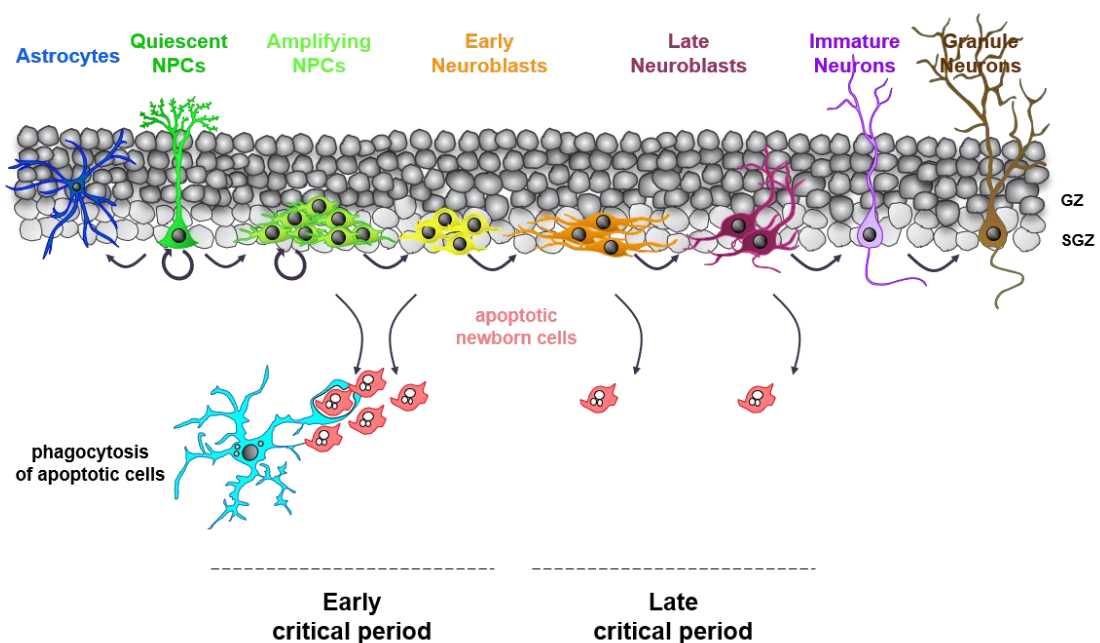
Figure 8. Microglial phagocytosis of apoptotic cells in physiological conditions. In the adult hippocampal neurogenic cascade, neuroprogenitors (NSCs and ANPs) in the subgranular zone (SGZ) of the dentate gyrus (DG) proliferate and differentiate into neuroblasts. During this process, the majority of the newborn neuroblasts naturally undergo apoptosis in two periods: 1, a main early critical period, in which cells are lost in the first 1-4d of cell life, and 2, a later critical period, in which other percentage of newborn cells die from 4-8d after cell birth. Importantly, these apoptotic cells are efficiently removed by microglia, as shown by Ph index, which is around 90%, and occurs very rapidly, in under 1.5h. Adapted from [Sierra et al., 2010].

3.8.2 Microglial phagocytosis of apoptotic cells in the adult hippocampus

Microglia are physically part of the hippocampal neurogenic niche and intermingle with all cell types. This proximity allows them to recognize and engulf the newborn cells that undergo apoptosis. A few years ago, our group assessed the efficiency of microglia
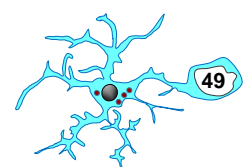
in the adult brain and found that the phagocytic index (Ph index), which is the proportion of dead cells phagocytosed by microglia, is around 90% [Sierra et al., 2010]. The remaining 10% of cells not engulfed by microglia represents cells that are in the earliest stages of apoptosis, indicating that the phagocytosis process has not yet started [Sierra et al., 2010]. Moreover, we also determined that phagocytosis occurs very rapidly (under 1.5h per apoptotic cell) [Sierra et al., 2010]**(Fig. 8)**, which is in agreement with a general 1-2h that need macrophages to phagocytose [Henson and Hume, 2006]. Therefore, the number of apoptotic cells observed in particular time point represents only a small proportion of the actual number of apoptotic cells generated (or total number of cells which disappear). For instance, if 800 cells die in 24h, a clearance time of 1.5h leads us to observe only 50 dead cells at any time point (more details about the estimation of clearance can be found in [Barres et al., 1992; Sierra et al., 2010]). Therefore, microglia are a very efficient phagocyte in the healthy and adult DG.

In the young hippocampus only a small proportion of microglia are in the process of phagocytosing at a given time [Sierra et al., 2010]. Under apoptotic challenge induced by excitotoxicity or inflammation, microglia uncover their phagocytic potential to cope apoptosis throughout three strategies: 1, recruit more phagocytic cells; 2, increase their phagocytic capacity; and 3, increase the number of microglia [Abiega et al., 2016]**(Fig. 9)**. The combination of these adaptation strategies allowed microglia to boost their phagocytosis efficiency and cope with increased apoptosis, maintaining phagocytosis and apoptosis tightly coupled. However, these strategies are only defined in adult microglia [Abiega et al., 2016; Sierra et al., 2010] but whether these cells utilize the same tactics to confront the number of dead cells in the developing brain is still unexplored. In this PhD Thesis, we will analyze postnatal microglial response to face different phagocytic challenges.
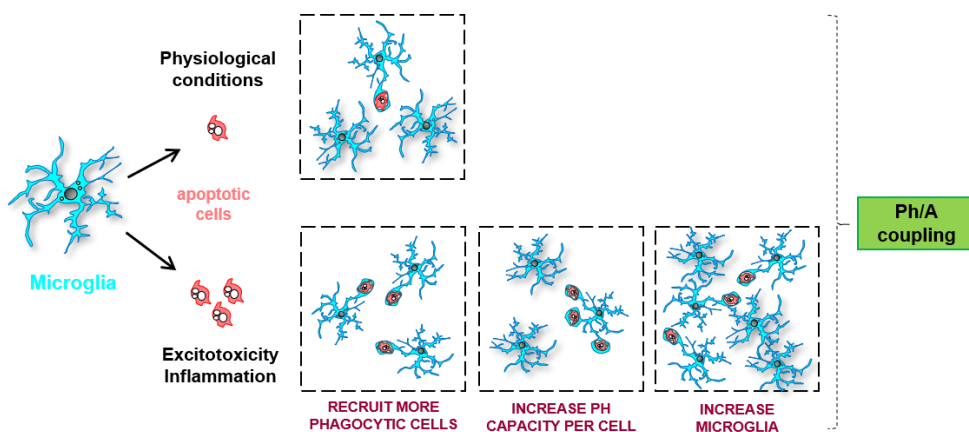
Figure 9. Microglial phagocytic strategies. *In physiological conditions in the adult hippocampus, microglia are an efficient phagocyte. Under apoptotic challenge induced by excitotoxicity and/or inflammation,*
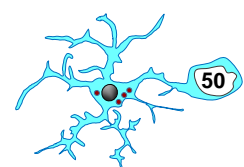
microglia boost their phagocytic efficiency to counterbalance the increase number of dead cells by combining three different strategies: 1, recruiting more phagocytic microglia; 2, increasing the phagocytic capacity of each microglia; and 3, increasing the number of microglial cells. The combination of these adaptation tactics allows microglia to cope with increased apoptosis, maintaining phagocytosis and apoptosis tightly coupled.

3.8.3 Microglial phagocytosis of apoptotic cells in the developing hippocampus

Once they invade the brain parenchyma, microglia undergo a maturation process [Hammond et al., 2019; Masuda et al., 2019]. Several transcriptome analyses of the development of microglia from yolk sac progenitors to adult microglia have shown the degree to which these cells change during this interval and revealed marked differences in gene expression between early postnatal periods and adulthood [Hagemeyer et al., 2017; Hammond et al., 2019; Kierdorf et al., 2013a; Masuda et al., 2019; Matcovitch-Natan et al., 2016]. The process of microglial maturation might affect not only the transcriptional profile but also their functions, including phagocytosis. In line with this premise, our group found that while the Ph index of adult microglia is around 90% [Sierra et al., 2010], it is around 60-70% at postnatal days 7 and 14 (P7-P14) [Abiega et al., 2016]. These data suggest that the efficiency of phagocytosis also experience a maturation and could causally related to microglial response to different phagocytic challenges.

Microglial phagocytosis of apoptotic cells has been reported in different regions of developing CNS such as hippocampus [Abiega et al., 2016; Dalmau et al., 2003][Diaz-Aparicio et al., 2016], amygdala [VanRyzin et al., 2019], cerebral cortex [Ayata et al., 2018; Cunningham et al., 2013a; Dalmau et al., 2003; Ferrer et al., 1990], corpus callosum [Kaur et al., 1985; Ling, 1976], striatum [Ayata et al., 2018], and/or white matter [Dalmau et al., 2003]. Nonetheless, little is known about the tactics that developing microglia display to confront apoptotic challenges. In this PhD Thesis, we will assess the efficiency of microglia to cope the increased number of dead cells in pathological conditions induced by LPS and EtOH at postnatal days P9 and P14, and HIE at P9.

3.9 MICROGLIAL PHAGOCYTOSIS OF APOPTOTIC CELLS IN PATHOLOGICAL CONDITIONS IN THE DEVELOPING HIPPOCAMPUS
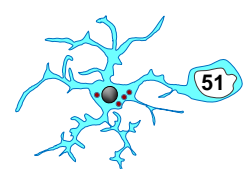
In this PhD Thesis, one of our objectives has been to analyze the efficiency of microglia to phagocytose dead cells in developing brain under different pathological conditions. For this purpose, we will explore the response of postnatal microglia to phagocytic challenge evoked by LPS, EtOH, and HIE. We have chosen these models because all of them induce apoptotic events in different brain areas, including DG of the hippocampus, where we established the baseline of microglial phagocytosis.

In the next sections, we will explain in more detail the impact of LPS, EtOH, and HIE on microglial phagocytosis **(Fig. 10)**.

3.9.1 LPS as a model of neuroinflammation

LPS (also termed endotoxin) is the major component of the outer membrane of Gram-negative bacteria [Alexander and Rietschel, 2001; Raetz and Whitfield, 2002]. This microbial mediator can trigger a variety of systemic inflammatory reactions, such as the release of pro-inflammatory cytokines and other soluble factors, which lead to tissue injuries and finally multiorgan failure, the clinical hallmarks of septic shock in humans [Rietschel et al., 1994; Schletter et al., 1995].

Peripheral administration of LPS is a widely used model to induce an inflammatory response by microglia, which recognize the endotoxin via toll-like receptor 4 (TLR4) [Lehnard et al., 2002]. Microglia propagate inflammatory signals initiated in the periphery by the release of pro-inflammatory cytokines, such as IL-1β, IL-6 and TNF-α [Cunha et al., 2016; Liu et al., 2001; Nakamura et al., 1999; Sierra et al., 2007]. While it is generally accepted that cytokines released in periphery do not diffuse across the BBB [Elmquist et al., 1997; Lacroix and Rivest, 1998; Vallières and Rivest, 1997], it was observed that high levels of systemic TNF-α can cross the BBB, stimulating microglia to secrete more systemic TNF-α as well as other pro-inflammatory factors [Qin et al., 2007]. In parallel to inducing an inflammatory response, LPS also evokes apoptosis in different brain regions, including hippocampus, cortex, cerebellum, and striatum [Czapski et al., 2010; Semmler et al., 2005; You et al., 2017]. In agreement with these data, we found that intraperitoneal injection of LPS stimulated microglia to express pro-inflammatory cytokines [Sierra et al., 2007] and induced apoptosis in the adult DG [Sierra et al., 2010]. Therefore, in this PhD Thesis, we will use LPS stimuli to analyze microglial phagocytosis of apoptotic cells in the developing hippocampus.

3.9.2 Microglia and LPS

Microglial response to LPS stimuli is associated to both morphological and molecular changes **(Fig. 10)**. Many in vitro and in vivo studies reported that LPS induces a
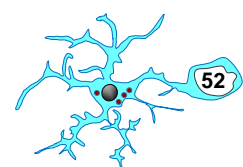
phenotypic microglial transformation from ramified to ameboid accompanied by a reduced number of microglial branches [Cunha et al., 2016; Hines et al., 2013; Ifuku et al., 2012; Jin et al., 2014; Kloss et al., 2001; Kondo et al., 2011; Nakamura et al., 1999; Perry and Andersson, 1992; Qin et al., 2007; Savage et al., 2019]. Regarding molecular changes, microglia upregulate the expression pattern of classical markers, cytokines, integrin proteins, and fractalkine receptors [Cunha et al., 2016; Kloss et al., 2001; Liu et al., 2001; Lund et al., 2006; Nair et al., 2019; Nakamura et al., 1999; Sierra et al., 2007]. In addition, LPS evokes the microglial release of NO, ROS, and matrix metallopeptidases [Cunha et al., 2016; Nair et al., 2019]. In parallel to these observations, some reports also suggested that LPS increases the number of microglia compared to control [Cunha et al., 2016; Ifuku et al., 2012; Jin et al., 2014; Okuyama et al., 2013] although can also induce microglial apoptosis [Liu et al., 2001]. Recently, [Nair et al., 2019] proposed that microglia treated with LPS show an excessive mitochondrial fragmentation and a switch from oxidative phosphorylation to glycolysis, which is dose and time dependent. Together, these studies show that microglia undergo both morphological and molecular changes following LPS, nonetheless, little is known how these events impact on phagocytic capacity of postnatal microglia.

3.9.3 Microglial phagocytosis and LPS

The efficiency of microglial phagocytosis after LPS has been poorly explored. Many years ago, [Abd-El-Basset and Fedoroff, 1995] observed that microglia culture phagocytosed a higher number of Ig-G-coated sheep erythrocytes following LPS compared to untreated microglia. More recently, [Gaikwad and Agrawal-Rajput, 2015] showed that BV2 microglia cell line engulfed a significant number of bacterial *E.coli* DH5α after LPS compared to control microglia. Another study also observed that LPS increased the proportion of fluorescent latex beads phagocytosed by N9 microglia cell line [Cunha et al., 2016]. In addition, [Mizobuchi et al., 2020] found that C8-B4 murine microglial cell increased the number of latex beads removed following LPS. However, none of these studies directly assess the phagocytosis of apoptotic cells in the living brain. Regarding this assumption, our group demonstrated that adult hippocampal microglia increased their phagocytic capacity to face the increased number of apoptotic cells at 8h after intraperitoneal LPS injection [Abiega et al., 2016; Sierra et al., 2010]. Based on our previous result, in this PhD Thesis we will analyze the microglial phagocytic response in the DG at postnatal day 9 (P9) and 14 (P14) after systemic administration of LPS.
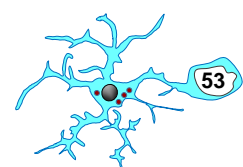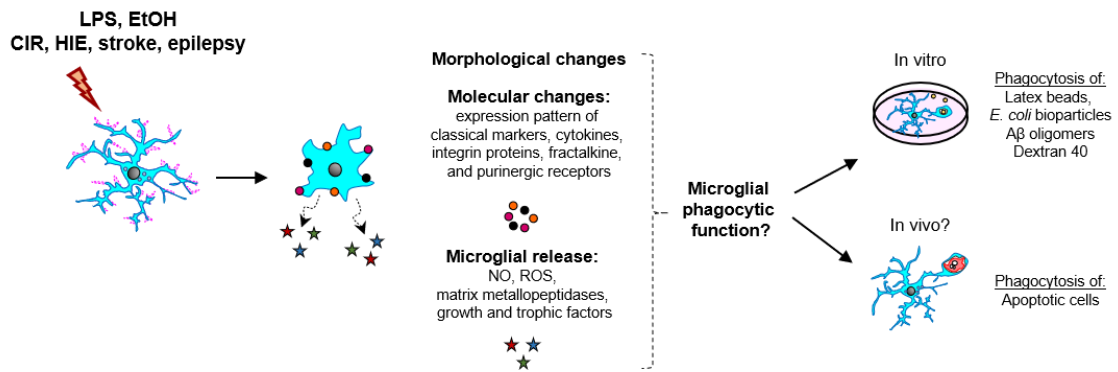
Figure 10. Microglial phagocytosis in pathological conditions. Microglial response to pathological conditions induced by LPS and EtOH stimuli is associated to both morphological and molecular changes as well as release of different molecules. Similar changes are also observed in CIR, HIE, stroke, and epilepsy. Importantly, little is known how these events impact on microglial phagocytosis. Several in vitro assays were performed to study phagocytosis under these pathological conditions, but the efficiency of microglia to phagocytose apoptotic cells in vivo is still unexplored.

3.9.4 EtOH as a model of neuropathology

EtOH (or ethyl alcohol) is a member of a class of organic chemical compounds that are classified as alcohols [PubChem, 2021]. It has several roles as antiseptic drug, neurotoxic, disinfectant, and metabolite [PubChem, 2021]. In addition, ethanol is a potent CNS depressant, an NMDA receptor antagonist, and a protein kinase C agonist [Costardi et al., 2015; Gilpin and Koob, 2008; Hicklin et al., 2011; Mohamed et al., 2018; Möykkynen and Korpi, 2012]. As the most widely abused drug in the world, EtOH has many negative effects on human health, such as a decreased motor function, loss of consciousness, hypothermia, hypotension, coma, and death from respiratory depression, and cardiovascular collapse [Brumback et al., 2007; Granberg, 1991; Guzzo-Merello et al., 2014; Kivimäki et al., 2020; Oscar-Berman and Marinković, 2007; Thakur et al., 2009].

Ethanol induces both systemic and CNS inflammation [Wang et al., 2010], which is associated with the diffusion of cytokines from the periphery through leaky regions of the blood brain barrier, such as the circumventricular organs and/or by transport of cytokines across the blood brain barrier to the brain [Qin et al., 2007]. In the CNS, the inflammatory response is mainly mediated by microglia through TLR4 [Alfonso-Loeches et al., 2010]. This response implies the release of pro-inflammatory cytokines, such as TNF-α, IL-6 and IL-1β [Li et al., 2019; Marshall et al., 2013; McClain et al., 2011]. In parallel to inflammation, EtOH also causes neurodegeneration [Crews and Nixon, 2009]. Post-mortem studies by [Harper et al., 1985; de la Monte, 1988] showed a reduction in brain volume related to a loss of white matter in chronic alcoholic patients compared to control.
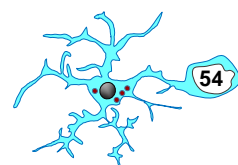
Ethanol exposure during adolescence (ages 12-16) is associated with alterations in both gray- and white matter brain structures, and aberrations in brain activity. These differences in structure and function are related to poorer neurocognitive performance on test of attention, working memory, spatial functioning, verbal and visual memory, and executive functioning [Squeglia et al., 2014]. In vivo murine (mouse and rat) and monkey models reported several changes after EtOH. For instance, using different routes of ethanol administration (by intraperitoneal (i.p), intragastric gavage, and/or ethanol in drinking water) and doses (5mg-5g/kg), it was found that EtOH causes an impairment of adult hippocampal neurogenesis, reducing NSCs proliferation and newborn cell survival [Morris et al., 2010; Nixon and Crews, 2002; Richardson et al., 2009; Taffe et al., 2010]. Moreover, this organic compound also causes neuronal cell death in different areas of developing brain. For example, EtOH injection in postnatal day 7 mice (by intraperitoneal injection (i.p); 5g/kg) induces apoptotic neurodegeneration in many specific regions of the forebrain, including specific layers of the frontal, parietal, temporal, occipital and cingulate cortices, nucleus accumbens, dorsolateral amygdala, and hippocampus [Ieraci and Herrera, 2006; Olney et al., 2002]. In adult rats, EtOH exposure (i.p; 5g/kg) evokes neuronal death in limbic association regions, such as agranular insular cortex, anterior piriform cortex, entorhinal cortex, and DG of the hippocampus [Obernier et al., 2002]. In this PhD Thesis, we will use EtOH stimuli to analyze microglial phagocytosis of apoptotic cells in the DG at P9 and P14.

3.9.5 Microglia and EtOH

Microglia undergo morphological changes following EtOH stimulus in both in vitro and in vivo [Drew et al., 2015; Fernandez-Lizarbe et al., 2009; Grifasi et al., 2019; Hu et al., 2020; Marshall et al., 2013, 2020; McClain et al., 2011; Siemsen et al., 2020; Zhao et al., 2013]**(Fig. 10)**. Contrary to these reports, [Stowell and Majewska, 2020] showed that adult microglial morphology in the primary visual cortex remained unaltered by EtOH exposure, although it reduced process motility and parenchyma surveillance. In addition, microglia also experience molecular changes after EtOH stimulus, which include upregulation of the microglial expression pattern of classical markers, complement receptors, cytokines, fractalkine and purinergic receptors [Asatryan et al., 2018; Boyadjieva and Sarkar, 2010; Crews et al., 2021; Erickson et al., 2019; Fernandez-Lizarbe et al., 2009; Guergues et al., 2020; Li et al., 2019; Peng et al., 2017; Sanchez-Alavez et al., 2019]**(Fig. 10)**. In parallel to morphological and molecular changes, there are controversial reports in the literature about the impact of EtOH on microglial survival. On the one hand, several in vivo studies proposed that the number of adult microglia, identified by Iba1 expression, dramatically decreased in the cortex and hippocampus
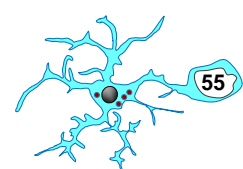
[Barton et al., 2017; Grifasi et al., 2019; Hu et al., 2020; Marshall et al., 2020; Siemsen et al., 2020], which could be explained by the fact that EtOH induces apoptosis in microglia cells [Hu et al., 2020]. On the other hand, others report showed that adult microglia increased their population in the cortex, amygdala, hippocampus, substantia nigra, and cerebellum [Li et al., 2019; Marshall et al., 2013; Riikonen et al., 2002; Sanchez-Alavez et al., 2019]. Regarding clinical analysis in human, [Beynon and Walker, 2012] observed hypertrophic microglial morphology in post-mortem human tissue from alcoholic patients compared to control brains as well as a downregulation of classical microglial markers [He and Crews, 2008]. Therefore, EtOH evokes morphological and molecular changes in microglia, however, it is not clear how these changes can directly affect microglial phagocytic function in postnatal brain.

3.9.6 Microglial phagocytosis and EtOH

Few laboratories have explored microglial phagocytosis after EtOH. Preliminary data published by [Colton et al., 1998] suggested that EtOH-treated primary hamster microglia culture increased the number of fluorescent latex beads compared to untreated microglia. Moreover, [Fernandez-Lizarbe et al., 2009] proposed that primary rat and mouse microglial culture phagocytosed more fluorescein-labeled latex beads vs control, however, this assumption is only based on observations and not accompanied by quantifications. In contrast to these results, [Gofman et al., 2014] showed that embryonic stem cell derived microglia reduced their phagocytic capacity to engulf *E. coli* bioparticles following EtOH treatment. More recently, [Kalinin et al., 2018] found that EtOH-treated rat primary microglia decreased the number of fluorescent Aβ oligomers phagocytosed compared to control. Nevertheless, none of these reports directly assessed the engulfment of apoptotic cells, therefore, the phagocytic efficiency of microglia after EtOH is still unknown. In this PhD Thesis, we will quantify phagocytosis in the DG in postnatal P9 and P14 after EtOH.

In parallel to the analysis of the role of phagocytosis after LPS and EtOH, in this PhD Thesis we will also explore the postnatal microglial response to a major neurological disorder: brain infarction resulting in HIE. In the next section, we will introduce in more detail the concept and origin of HIE, the current animal models to mimic it, and the role of microglia in these pathological conditions.

3.9.7 Introduction to HIE

HIE is a syndrome of acute global brain injury resulting from critical reduction or loss of blood flow (ischemia) and supply of oxygen (hypoxia) to the brain [Nalivaeva and
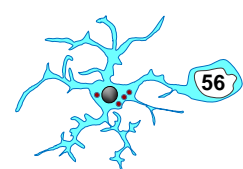
Rybnikova, 2019]. HIE is one of the most reported injuries among neonates, with an incidence between 1.5-2 per 1000 live births in developed countries, although the number affected increases to 26 per 1000 in resource-limited settings [Black et al., 2010; Oorschot et al., 2020]. Patients that suffer from this syndrome develop long-term severe and chronic neurophysiological impairments, including cerebral palsy, epilepsy, and motor and cognitive deficits [Al-Macki et al., 2009; Driscoll et al., 2018; Fernández-López et al., 2014; Gonzales-Portillo et al., 2014]. Annually, HIE causes one million neonatal deaths worldwide [Pauliah et al., 2013]. Therefore, HIE is a public health event of international concern.

The common reason for neonatal HIE is related to oxygen deprivation evoked by asphyxia that happens in the perinatal period due to circulatory problems, including placental abruption, placental arterial clotting, and inflammatory processes. It usually occurs in the weeks leading up to birth or during labor and delivery [Fatemi et al., 2009]. The standard treatment for HIE is to apply moderate hypothermia (HT; a temperature decreases of 2-5ºC) that maintains a core body temperature of 33.5ºC for 72h commenced within the first 6h for life [Perlman et al., 2010; Rossouw et al., 2015; Sabir et al., 2016]. This therapy decreases the metabolic activity of the brain, which modulates some of the harmful metabolic pathways triggered by asphyxia such as excitotoxicity, inflammation, and oxidative stress, and cell death (apoptosis and necrosis) [Cánovas-Ahedo and Alonso-Alconada, 2019]. However, hypothermia is not effective in half of the cases, and therefore, current researchers are focused on the development of treatments that may be used in combination with hypothermia [Cánovas-Ahedo and Alonso-Alconada, 2019].

3.9.8 Rodent models of HIE

In efforts to comprehend human neonatal HIE and develop potential therapeutics, several animal models have been developed to mimic its pathophysiology. Although the most widely used models are carried out in rodents, other animal have been studied such as sheep, piglets, and non-human primates. The main rodent method to study HIE is the Rice-Vanucci technique (also known as the Vanucci method) [Hamdy et al., 2020].

The Rice-Vanucci model. This technique was originally developed in adult rats [Levine, 1960], and then, it was modified for neonatal application in both rats [Rice et al., 1981; Vannucci and Vannucci, 1997] and mice [Albertsson et al., 2014]. HIE is induced through permanent unilateral ligation of the common carotid artery (CCA) followed by exposure to mild global hypoxia in a hypoxia chamber. CCA ligation alone does not cause brain damage since the circle of Willis compensates the cerebral blood flow (CBF).
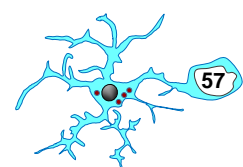
However, hypoxia lowers oxygen tension and reduces blood flow in the ipsilateral hemisphere, which promotes brain damage. Several factors affect the consistency and reliability of the resulting brain injury such as oxygen saturation, duration of hypoxia and reoxygenation, as well as the age of animal. The standard percentage of oxygen saturation used in this method is 8% for 60 to 12mins. Moreover, some groups also employ oxygen rates as low as 4% O_2 in nitrogen (N_2) or up to 12% O_2 in N_2 [Faustino-Mendes et al., 2018]. Animals subjected to the Rice-Vanucci method develop behavioral phenotypes similar to those observed in human neonates exposed to HI including motor deficits [Tomimatsu et al., 2002], cognitive dysfunction [Miguel et al., 2015], impaired learning and memory [Balduini et al., 2000], and sensory processing [Alexander et al., 2014]. These behavioral impairments correlate to brain injury in the ipsilateral cerebral cortex, white matter, hippocampus, striatum, and thalamus [Millar et al., 2017; Rice et al., 1981; Selip et al., 2012; Umekawa et al., 2015]. The Rice-Vanucci method successfully replicates the pathophysiology of human neonate HIE injury [Rice et al., 1981; Rumajogee et al., 2016]. In this PhD Thesis, we will use this model to test microglial phagocytosis of apoptotic cells in postnatal (P9) DG. Furthermore, we will also use this method to explore phagocytosis in adult (3m, month old) DG after HIE.

3.9.9 Microglia and HIE

Microglial response to HIE is associated to both morphological and molecular changes **(Fig. 10A)**. Experimental animal models of HIE allowed to observe that microglia undergo a transition from ramified to ameboid morphology after HIE [Fisch et al., 2020]. Moreover, there is an upregulation in the microglial expression pattern of cytokines, complement protein, neurotrophic factors, classical markers, and purinergic as well as fractalkine receptors [Fisch et al., 2020; Hedtjärn et al., 2004]. In addition, microglia release ROS and NO under HIE [Cowell et al., 2002; Hagberg et al., 1996; Hedtjärn et al., 2002; Kaur et al., 2013; Rocha-Ferreira and Hristova, 2015]. In parallel to these changes, murine microglia proliferate after HIE in two well-known neurogenic areas such as SVZ [Fisch et al., 2020] and DG of the hippocampus [Umekawa et al., 2015] early after HIE. Regarding the response of human microglia to HIE, it was observed that these cells were distributed diffusely or in patches in the polymorphous layer and adjacent granule layer of the DG [Del Bigio and Becker, 1994]. This event is assumed as a pathological marker of HIE, although its functional implications are unclear. Altogether, these data show that microglial response to HIE is accompanied by morphological and molecular changes but their functional implications remain widely unexplored.
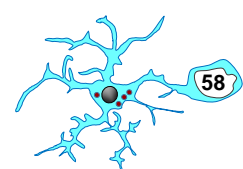
3.9.10 Microglial phagocytosis and HIE

Few laboratories have explored microglial phagocytosis in HIE. Recently, [Min et al., 2020] suggested that microglial cell line BV2 increased their ability to engulf dextran-40 under oxygen and glucose deprivation (OGD) conditions. In addition, [Min et al., 2020] observed an upregulated expression of toll-like receptor 2 (TLR2), a critical receptor in the initiation of the inflammatory response within the CNS [Helmut et al., 2011; Lehnardt, 2010] and downregulated expression of lysosome-associated membrane protein 1 (LAMP1), a well-known lysosomal marker [Cheng et al., 2018], which was interpreted as an increase in phagocytosis. Another study published by [Fisch et al., 2020] observed an increment in the number of microglial "ball-and-chain buds", defined as spherically shaped extensions at the terminal branch of microglial processes), but they did not assess what the content of these "buds" were. However, none of these studies directly assessed the engulfment of apoptotic cells and, in this PhD Thesis we will quantify phagocytosis in the DG at P9 and 3m after HIE.

3.10 MICROGLIAL PHAGOCYTOSIS OF APOPTOTIC CELLS IN PATHOLOGICAL CONDITIONS   IN ADULT HIPPOCAMPUS

Another major objective of this PhD Thesis is the analysis of adult microglial response to apoptotic challenges induced by CIR and neuropathological scenarios, such as HIE (**explained in more detail in previous section "3.9.7 Introduction to HIE**)**,** stroke, and epilepsy. We have selected these models because they evoke cell death in many regions of the brain such as DG, where we estimated the baseline of phagocytosis. In the next sections, we will explain in more detail the impact of CIR, stroke, and epilepsy on microglial phagocytosis **(Fig. 10)**.

3.10.1 Introduction to CIR

CIR constitutes a first-line treatment option for various primary or metastatic brain tumors, as well as head and neck cancer in both children and adults. The main aim of CIR is to destroy proliferative cancer cells while causing minimal damage to the surrounding healthy tissue. Nonetheless, the use of such therapy is not without devastating side effects to treated individuals, particularly in pediatric patients [Han et al., 2009; Makale et al., 2016], in which brain tumors constitute approximately one third of all childhood cancers [Girardi et al., 2019]. CIR is directly related to cognitive deficits in various degrees, including memory impairment, learning difficulties, declines flexibility in thinking and IQ performance, and, in extreme cases, full dementias [Greene-
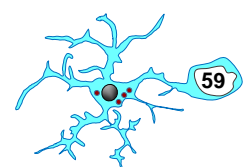
Schloesser et al., 2012]. These features reduce quality of life of surviving patients and their families [Makale et al., 2016; Marazziti et al., 2012].

The pathophysiology of cognitive dysfunction associated with cranial irradiation is poorly understood, albeit several studies suggest that depletion of neuroprogenitor cells (NSCs and ANPs) may be among the underlying mechanisms [Boström et al., 2013; Madsen et al., 2003; Makale et al., 2016; Mizumatsu et al., 2003; Monje et al., 2002; Rola et al., 2004; Roughton et al., 2012]. Neuroprogenitors, mainly ANPs, are highly proliferative cells [Encinas et al., 2011; Encinas and Sierra, 2012], and therefore, become susceptible to CIR-induced cell death resulting from DNA damage [Robbins and Zhao, 2004; Yu, 2012]. Brain damage derived from CIR is causally related to the radiation dosage, and volume of tissue irradiated.

Recently, [Yang et al., 2017] summarized the changes produced by this therapy in murine experimental models. The range of radiation dose used in in vivo analysis is around 5Gy-35Gy (in mice) and 5Gy-40Gy (in rats), which is mathematically estimated to represent equivalent doses delivered in patients with brain cancer [Fowler, 1989]. The main brain alterations evoked by this dosage of CIR in mice and rats include cognitive impairment, apoptosis, decreased neurogenesis, and/or an increased mRNA and protein expression levels of inflammatory mediators, such as TNF-α, IL-1β, and/or IL-6 [Gaber et al., 2003; Han et al., 2016b; Hwang et al., 2006; Kurita et al., 2001; Lee et al., 2010; Michaelidesová et al., 2019; Osman et al., 2020; Pineda et al., 2013; Tada et al., 2000]. The cellular response to CIR involves not only the NSCs population but also other cell types, including astrocytes, oligodendrocytes, endothelial cells, and microglia, which initiate and respond to inflammatory cascades. In this PhD Thesis, we will explore the microglial phagocytic response of apoptotic cells induced by CIR in the adult DG.

3.10.2 Microglia and CIR

Several studies reported that microglial response to CIR includes morphological and molecular changes **(Fig. 10)**. The microglial cell line BV2 and organotypic hippocampal slices subjected to irradiation showed morphological alterations on microglia, such as changes in their soma size, process length, and complexity of processes [Dong et al., 2015; Menzel et al., 2018; Xu et al., 2015; Xue et al., 2014b]. Similar to in vitro findings, in vivo analysis in rodents (mice and rats) allowed to observe that microglia undergo a transition from ramified to ameboid morphology following CIR [Dong et al., 2015; Kalm et al., 2009; Osman et al., 2020; Xu et al., 2015], although [Menzel et al., 2018] showed an increased microglial soma size and process length after whole brain irradiation. Regarding molecular changes, CIR induces changes in the expression pattern of
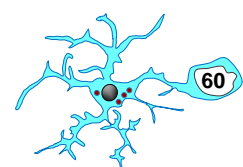
classical microglial markers, cytokines, and purinergic receptors [Acharya et al., 2016; Dong et al., 2015; Han et al., 2016b; Li et al., 2015; Morganti et al., 2014; Osman et al., 2020; Schnegg et al., 2012; Xu et al., 2015, 2016b; Xue et al., 2014b], and phosphorylated γ-histone 2A, member X (γ-H2AX) [Xue et al., 2014b], a marker of DNA damage [Mah et al., 2010]. In parallel to morphological and molecular alterations, some reports found that CIR reduced microglial population, particularly in those areas where cell death occurred, such as SGZ of the DG. For instance, organotypic hippocampal slices subjected to 7Gy and 30Gy of CIR showed a decreased number of microglia at 5d and maintained up to 90d after irradiation [Menzel et al., 2018]. Moreover, in vivo studies also found that microglia cells decreased in the SGZ, GZ, and ML at 7d and was still evident 6 weeks after 80Gy of CIR [Osman et al., 2020; Umekawa et al., 2015]. Therefore, these data describe morphological and molecular alterations evoked in microglia by CIR, nonetheless, is still unknown how these changes impact on phagocytosis.

3.10.3 Microglial phagocytosis and CIR

The efficiency of microglial phagocytosis under CIR is poorly analyzed. Initial work performed by [Huo et al., 2012; Kalm et al., 2009] showed microglial cells containing multiple, condensed, chromatin fragments stained with TUNEL (a marker of DNA strand breaks, [Crowley et al., 2016]) and presumably indicated phagocytic events in CIR-treated mice. On the contrary, [Xu et al., 2016b] suggested that primary microglia culture increased the proportion of latex beads phagocytosed after irradiation. Another in vitro study published by [Xu et al., 2016b], which injected fluorescent microspheres into the hippocampus, proposed an increment in the number of particles phagocytosed or attached to microglia after CIR. In line with [Huo et al., 2012; Kalm et al., 2009] findings, [Osman et al., 2020] recently reported that hippocampal microglia showed a single or multiple microglial pouches containing positive cells to activated-caspase 3 (act-casp 3; an apoptosis marker, [Choudhary et al., 2015]) with condensed chromatin, which were interpreted as apoptotic microglia, following CIR treatment. Nonetheless, these studies did not directly assess microglial phagocytosis of dead cells and, in this PhD Thesis, we will quantify phagocytosis in the DG at 3m after CIR.

Additionally, in this PhD Thesis, we will analyze adult microglial response to HIE and stroke. Both are, in essence, injuries caused by lack of oxygenated blood flow to the brain. However, the causes that originate them are different. As we mentioned in the previous section (**"3.9.7 Introduction to HIE"**), HIE usually occurs as a result of
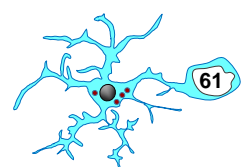
perinatal asphyxia in the period immediately before, during, or after the birth process [Fatemi et al., 2009; Millar et al., 2017]. In contrast, stroke is the result of either clot formation, which reduces the flow of oxygenated blood (ischemia), or hemorrhage, which disrupts normal blood circulation [Campbell et al., 2019; Donnan et al., 2008] and may occur both in neonates as well as in adults. HIE and stroke share common symptoms such as abnormalities in muscle tone, posturing, seizures, among others (https://hiehelpcenter.org/). The main aspects of HIE were covered in the previous sections (**"3.9.7 Introduction to HIE", "3.9.8 Rodent models of HIE", "3.9.9 Microglial and HIE", and "3.9.10 Microglial phagocytosis and HIE"**).

3.10.4 Introduction to Stroke

Stroke, also known as a cerebrovascular accident, is a complex pathology caused by a disturbance of the brain´s blood supply [Campbell et al., 2019; Donnan et al., 2008], and affects 13.7 million people globally per year [Johnson et al., 2019; World Stroke Organization, 2019]. Depending on the brain region affected by stroke insult, patients typically experience varying degrees of motor and neurophysiological deficits, and therefore memory, language, attention, and motor abilities are compromised. The clinical situation of stroke patients is complicated because of emotional deficits and mood disorders such as depression, which complicate their rehabilitation [Chen et al., 2013; Cumming et al., 2013]. Stroke is the second leading cause of death, which claims the lives of 5.5 million people every year [Johnson et al., 2019; World Stroke Organization, 2019]. Thus, this disease is a devastating global health concern.

A stroke occurs when blood flow to a part of the brain is interrupted as a result of a broken or blocked blood vessel [Moskowitz et al., 2010; Mozaffarian et al., 2016]. There are non-modifiable risk factors for stroke including age, gender, and genetic factors. Apart from these, several modifiable risk factors were also identified such as hypertension, atherosclerosis, diabetes, hypercholesterolemia, and high alcohol consumption [Campbell et al., 2019]. The two major types of stroke are divided in hemorrhagic or ischemic, with different incidence and treatments.

Hemorrhagic stroke

Less frequently (<15%), hemorrhagic stroke occurs when a brain artery becomes leaky or ruptures (breaks open) [Dirnagl et al., 1999; Krafft et al., 2012; Moskowitz et al., 2010]. There are two categories of hemorrhagic strokes: intracerebral and subarachnoid [Smith and Eskey, 2011]. The first one occurs when an artery in the brain bursts, flooding the surrounding tissue with blood, while the second one refers to bleeding in the area
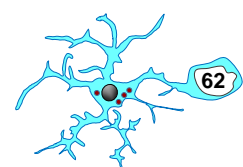
between the brain and the leptomeninges [Krafft et al., 2012]. Hemorrhagic stroke is the least treatable type [Hwang et al., 2011] and surgery is usually needed to reduced hematoma and repair the source of bleeding [Michelozzi and Cognard, 2019]. Among palliative treatments there are corticosteroids or diuretics to reduce swelling, painkillers, and anti-hypertensive drugs. In spite of that, current treatments are limited in efficacy and the prognosis is still poor [Arai et al., 2011; Krafft et al., 2012; Morotti and Goldstein, 2016].

Ischemic stroke

Up to 85% of all strokes are of ischemic origin [Mozaffarian et al., 2016]. They occur as a consequence of blood-clotting, affecting one or more cerebral arteries and drastically reducing or blocking CBF in the territory irrigated by arteries affected. There are two types of ischemic strokes: global and focal [Lee et al., 1999]. Global ischemia occurs when CBF is reduced throughout most or all of the brain [Traystman, 2003]. In contrast, focal ischemia is represented by a reduction in blood flow to a very distinct, specific brain region [Traystman, 2003]. Indeed, most focal cerebral ischemia in humans involve occlusion of one major cerebral blood vessel such as the middle cerebral artery (MCA) [Green, 2008]. Nowadays, the treatment available for ischemic stroke patients is thrombolysis (i. e., the dissolution of the blood clot) with recombinant tissue plasminogen activator (rt-PA), which promotes reperfusion and restores normal CBF. However, the main limitation of rt-PA is the short therapeutic window (<4.5h) and a higher risk of symptomatic hemorrhagic issues [Peña et al., 2017].

Middle cerebral artery occlusion (MCAo)

The majority of ischemic stroke in humans occurs in the vascular territory of the MCA [Bogousslavsky et al., 1988; del Zoppo et al., 1992], a terminal branch of the internal carotid artery (ICA). The MCA supplies specific regions of the brain parenchyma such as frontal, parietal, and temporal lobes [Navarro-Orozco and Sánchez-Manso, 2018]. Depending on the location and severity of the MCA occlusion, patients experiment different symptoms such as weakness, dizziness, numbness, issues with speech, or visual changes [Nogles and Galuska, 2020]. Distal blockages tend to produce milder deficits due to more extensive branching of the MCA and less ischemic response. In contrast, proximal occlusions result in widespread effects that can lead to significant cerebral damage, increased intracranial pressure, loss of consciousness, and could even result in the death of the patient [O'Sullivan, 2007].

3.10.5 Animal models of MCAo
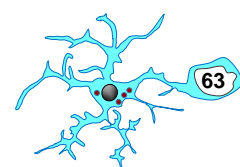
In order to identify the mechanisms that underlie MCAo and develop new avenues for effective therapies, different types of animal models are used to simulate the complex pathophysiology of human MCAo. The most widely used models are carried out in small animals (e.g., mice, rats, rabbits), as well as large animals (e.g., pigs, sheep, monkeys) [Fluri et al., 2015; Traystman, 2003]. However, rodents (especially mice) are commonly chosen to perform MCAo model since they are the most appropriate animals in which genetic modifications can be developed and therefore, these animals provide an excellent approach to determine potential mechanisms of injury and neuroprotection [Göb et al., 2015; Kraft et al., 2013]. There are five rodent stroke models: craniotomy, photothrombotic, embolic, endothelin-I, and intraluminal filament method [Fluri et al., 2015].

Craniotomy. The MCA is exposed after craniectomy and sectioning of the dura mater. The occlusion of the artery can be performed following two strategies. In the first one, the MCA is occluded by electrocoagulation and additional transection, leading to a permanent occlusion [Tamura et al., 1981], or by a clip, hooks, ligatures, or photochemical MCAo in mice [Buchan et al., 1992; Popa-Wagner et al., 1999; Shigeno et al., 2009; Sugimori et al., 2004]. The second strategy involves not only the MCA occlusion but also bilateral CCA blockage, which induces a reduction of the collateral blood flow, and thus consolidates the ischemic damage [McAuley, 1995]. The brain areas most compromised by craniotomy are the frontal, parietal, temporal, and rostral occipital cortices, the underlying white matter, and a marginal part of the striatum [Buchan et al., 1992; Tamura et al., 1981]. This technique evokes reproducible infarct size and neurological deficits, induces low mortality, and allows subsequent reperfusion of ischemic tissue. However, the main disadvantage is the craniotomy itself, which may lead to damage of the underlying cortex or rupture of blood vessels by drilling or electrocoagulation as well as inflammation. Due to the opening of the dura, the brain is exposed to the atmosphere, the intracranial pressure is affected and changes in regional brain temperature may occur [Dirnagl, 2010].

Photothrombosis. This technic also requires performing a craniectomy but the dura mater remains intact. The occlusion of the MCA is based on intravascular photo-oxidation, in which a photoactive dye (such as Rose Bengal or erythrosin D) is administered intraperitoneally (in mice; [Kleinschnitz et al., 2008]) or intravenously (in rats; [Watson et al., 1985]). Next, the intact skull is irradiated by a light beam at a specific wavelength [Watson et al., 1985]. This procedure induces localized oxidative lesion of endothelial membranes, platelet aggregation, and occlusion of microvessels, followed by CBF interruption [Watson et al., 1985]. The main areas affected by photothrombosis are
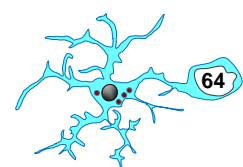
cortex [Watson et al., 1985] and striatum [Kuroiwa et al., 2009]. Moreover, the technique allows high reproducibility of ischemic lesions, and causes a low mortality. However, focal stroke induced by photothrombosis does not mimic well all aspects of acute human stroke. While the latter is characterized by a primarily accumulation of fluid (edema) in the intracellular spaces of the brain [Scalzo et al., 2015], photothrombosis induces a nearly simultaneous development of both intracellular and extracellular edema with rapid breakdown of the BBB. In addition, only a little or no salvageable ischemic penumbra and local collateral flow/reperfusion occur with this technique [Liu et al., 2017].

Embolism. Embolic stroke models are divided in two categories: micro/macrosphere-induced stroke models and thromboembolic clot models. The first one involves injecting the spheres into the MCA or the ICA via ECA using a microcatheter. In contrast, the second model is based on the application of spontaneously formed clots or thrombin-induced clots from autologous blood [Niessen et al., 2003; Overgaard et al., 1992] as well as thrombin injection into the intracranial area of the ICA or into the MCA [Ansar et al., 2014; Orset et al., 2007]. The micro/macrosphere model induces multifocal and heterogeneous brain areas infarcted [Gerriets et al., 2003]. Moreover, the volume and localization of infarcts in the thromboembolic clot method depend on the size of the clot [Ren et al., 2012] and the infarct volume is smaller and more variable compared to lesion evoked by intraluminal filament technique [Beech et al., 2001].

Endothelin-1 administration. ET-1 is a potent and long-acting vasoconstrictive peptide [Yanagisawa et al., 1988], which is directly administered onto the exposed MCA [Robinson et al., 1990] or onto the cortical surface [Fuxe et al., 1997], or by an intracerebral (stereotactic) injection [Hughes et al., 2003]. The brain areas damaged by ET-1 are cortex, striatum, thalamus, and cortical layers [Fuxe et al., 1997; Tamura et al., 1981]. This technique causes low mortality and offers the possibility of inducing direct focal ischemia in deep and superficial brain regions. Nonetheless, it induces variable ischemic volume [Braeuninger and Kleinschnitz, 2009]. In addition, it was described that ET-1 evokes astrocytosis and allows axonal sprouting [Uesugi et al., 1998], which could interfere with the interpretation of neural repair data after stroke [Carmichael, 2005].

Intraluminal filament insertion. The first version of this technique involved a permanently occluding the CCA by introducing a filament directly into the internal carotid artery (ICA), and advancing the filament until it blocked the blood supply to the MCA [Koizumi et al., 1986]. In a modified version developed by [Longa et al., 1989], the CCA is temporarily occluded and the filament is inserted into the transected external carotid
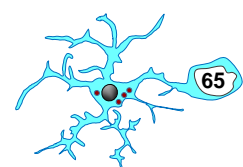
artery (ECA), using the ECA trunk as a path to advance a filament through the ICA, which allows either permanent or transient occlusion followed by reperfusion. The technique developed by [Longa et al., 1989] is a better choice than the Koizumi method for transient MCAo because it maintains the anatomic integrity required for reperfusion [Liu et al., 2009b; Morris et al., 2016a]. The filament occlusion can be permanent [Liu et al., 2009b] or transient (60min, 90min, and 120min). In the latter, Laser Doppler flowmetry is a useful tool to check complete occlusion and posterior reperfusion of the MCA. The brain areas damaged after MCAo include most of the cortex, striatum, thalamus, and SVZ [Maeda et al., 1999; McColl et al., 2004]. Reproducibility of infarcted region in the brain is affected by different factors, such as filament diameter and material [Shimamura et al., 2006; Tsuchiya et al., 2003], strain of animal [Bardutzky et al., 2005; Cheng et al., 2012; Maeda et al., 1999; Ström et al., 2013; Walberer et al., 2006], rat vs mice [Carmichael, 2005], variations in cerebrovasculature [McColl et al., 2004; Yang et al., 1997], gender [Alkayed et al., 1998], weight [Hata et al., 1998; Spratt et al., 2006], anesthesia [Michenfelder et al., 1976], among many others. Despite all these critical factors, the intraluminal filament technique is suitable for reproducing ischemic stroke and subsequent neuronal cell death, cerebral inflammation, and BBB damage, as well as producing replicate results in behavior tests [Howells et al., 2010]. The intraluminal filament technique is less invasive than other focal stroke methods that require craniotomy, and therefore, avoids damage to cranial structures.

These five models represent useful methods for human MCAo replication in rodents. However, the intraluminal filament technique to induce focal MCAo is one of the methods that most closely simulate human ischemic stroke [Ansari et al., 2011; Morris et al., 2016b]. For this reason, in this PhD Thesis we will use this method to evoke transient MCAo and study microglial phagocytosis in adult (2m) mouse brain.

3.10.6 Microglia in stroke

As occurs in other neuropathological diseases, microglia experience morphological transformations after stroke [Ito et al., 2001; Kato et al., 1996; Morrison and Filosa, 2013; Otxoa-de-Amezaga et al., 2019; Rupalla et al., 1998; Thored et al., 2009]**(Fig. 10)**. In addition, microglia undergoes several molecular changes, including the expression of surface receptors, such as purinergic receptors [Franke et al., 2004; Melani et al., 2006], fractalkine receptors [Fumagalli et al., 2013; Tarozzo et al., 2002], Toll-like receptors (TLRs) [Anttila et al., 2017], and TREM2 [Heldmann et al., 2011; Sugimoto et al., 2014]. Moreover, stroke alters the release of several mediators produced by microglia including cytokines [Hu et al., 2012; Iadecola and Anrather, 2011; Lambertsen et al., 2009; Lan et
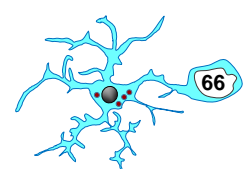
al., 2017; Ritzel et al., 2015; Zhang et al., 2017; Zhao et al., 2017], ROS [Cherry et al., 2014; Wu et al., 2012], NO [Gibson et al., 2005; Nakashima et al., 1995], and growth and trophic factors [Elkabes et al., 1996; Lai and Todd, 2006]. In parallel to these changes, microglia undergo cell death in the necrotic core (the brain region irrigated by the occluded artery) whereas they proliferate in the penumbra (the area surrounding the core) [Denes et al., 2007; Lalancette-Hébert et al., 2007; Li et al., 2013; Moraga et al., 2015; Otxoa-de-Amezaga et al., 2019; Thored et al., 2009]. Clinical studies found morphological changes in microglia after human ischemic stroke [Gulyás et al., 2012; Krupiński et al., 1996; Price et al., 2006; Tomimoto et al., 1996]. In addition, it was also observed an increased expression of translocator protein (TSPO), previously known as peripheral benzodiazepine receptor (PBR) in stroke patients using positron emission tomography (PET). TSPO is used as a target to image neuroinflammation as its expression is upregulated in glial cells (microglia and astrocytes) during CNS pathologies [Beckers et al., 2018; Yao et al., 2020]. Despite the relevance of these findings, it is still unknown how these molecular and morphological changes translate into microglial functional changes.

3.10.7 Microglial phagocytosis in stroke

Microglial phagocytic activity after stroke was explored by several laboratories around the world using different approaches. Initially, [Schilling et al., 2003] suggested that phagocytosis, defined as the colocalization of neuronal material identified by NeuN (mature neuron marker; [Gusel'nikova and Korzhevskiy, 2015]) signal into microglia, increased at 1d and 2d in the striatum after tMCAo. Years later, [Ritzel et al., 2015] analyzed the capacity of isolated microglia to engulf fluorescent latex beads and proposed that this type of cargo was significantly phagocytosed at 1d after tMCAo and peaked up to 3d. In parallel to mouse models, [Yeo et al., 2019] described that rhesus monkeys subjected to tMCAo showed an increased expression of CD68 on microglia/macrophages, identified by Iba-1, indirectly suggesting increased phagocytosis. Recently, it was also reported that microglia phagocytose neutrophils using in vitro and in vivo models of stroke [Neumann et al., 2018; Otxoa-de-Amezaga et al., 2019]. However, none of these studies directly quantified phagocytosis of apoptotic cells in situ and therefore, the efficiency of microglia in stroke is still uncovered. In this PhD Thesis, we will analyze the microglial phagocytic response in the DG at 2m after tMCAo.

3.10.8 Introduction to epilepsy
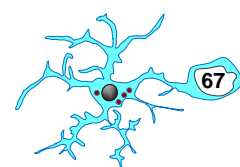
Epilepsy is a chronic neurological disorder characterized by seizures, which are defined as transient occurrence of signs and/or symptoms due to abnormally excessive or synchronous neuronal activity in the brain [Fisher et al., 2014; Savage, 2014]. Globally, more than 50 million people suffer from epilepsy [Thurman et al., 2011]. Apart from seizures, the quality of life of epileptic patients is significantly conditioned by the development of psychiatric comorbidities, such as mood disorders and anxiety [Quintas et al., 2012]; and cognitive impairment, including deficits in attention, memory, language, and executive functions [Holmes, 2015]. These features have a profoundly negative effect on an individual's wellbeing and the perceived quality of life [Lehrner et al., 1999; Szemere and Jokeit, 2015], possibly more so than the seizures themselves [Boylan et al., 2004]. In addition, people with epilepsy have a mortality rate 2-3 times higher than in the general population [Forsgren et al., 2005; Gaitatzis and Sander, 2004]. Therefore, epilepsy is a public health problem that concerns us all as a society.

Epilepsy has many possible causes, including genetic factors, developmental brain abnormalities, infection, traumatic brain injury, stroke, and/or brain tumors [Ahl et al., 2016; Temkin, 2009], however, for up to half of epileptic patients epilepsy is idiopathic. Importantly, this neurological disorder cannot be "cured" but seizures can be "controlled or stopped" with antiepileptic drugs, which are anticonvulsant agents that suppress the excessive rapid firing of neurons during seizures and prevent their spread [Sankaraneni and Lachhwani, 2015]. Nonetheless, around 70% of patients are pharmacoresistant and, therefore, surgery is usually the best chance to stop the seizures. Thus, there is a critical need for the development of new appropriate strategies to ameliorate the progression and/or limit the detrimental consequences of the disease.

Depending on where in the brain seizures are generated, they are classified in two categories: focal or generalized [Fisher et al., 2017]. Most seizures, at least at the onset, are focal or partial, which means that abnormal activity begins in one part of the brain, and often without outward (movement or "motor") signs [Ahl et al., 2016]. The most common type of focal-onset seizure disorder is temporal lobe epilepsy (TLE), in which the epileptic foci are located in the limbic system and temporal lobes, substrates for emotion and memory. In contrast, generalized seizures arise when uncontrolled neural activity spreads throughout the brain. In this case, the patient loses consciousness and has violent muscle contractions (convulsions) [Ahl et al., 2016]. In this PhD Thesis, we will focus on Mesial Temporal Lobe Epilepsy (MTLE), the most frequent form of human epilepsy [Tatum, 2012].

3.10.9 Mesial temporal lobe epilepsy (MTLE)
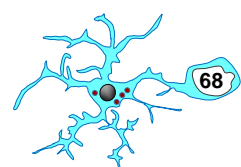
Mesial temporal lobe epilepsy (MTLE) is the most common and the best-characterized form of TLE [Tatum, 2012], a group of disorders that predominately involves dysregulation of hippocampal function caused by neuronal hyperexcitability [Schwartzkroin, 1986]. MTLE also represents the most common form of drug-resistant epilepsy [Duveau et al., 2016], for which the resection of the epileptic hippocampus is the only treatment available to control seizures [Lee, 2014; Mathon et al., 2015]. The pathophysiology of this disorder includes unprovoked seizures and histological changes in the hippocampus, including neuronal loss, inflammation, dispersion of the granule cell layer (GCL), and lesions in Cornus Ammonis (CA) [Bae et al., 2010; De Lanerolle et al., 2003; Sharma et al., 2007], as well as gliosis with reactive astrocytes [O'Dell et al., 2012; Sierra et al., 2015]. These alterations are known as hippocampal sclerosis and its severity usually correlates with an increased loss of the cognitive functions related to the hippocampus [Wieser, 2004].

3.10.10 Rodent models of MTLE

To fully understand MTLE pathophysiology and to develop new therapeutic approaches, several animal models are extensively used to reproduce the electroencephalographic, behavioral, and neuropathological features of MTLE [Kandratavicius et al., 2014; Lévesque et al., 2016]. The most widely used models are based on the administration of pilocarpine [Vezzani, 2009]) or kainic acid (KA; [Ben-Ari and Lagowska, 1978]. Both are two potent chemoconvulsants that induce hippocampal sclerosis and mimic human MTLE features.

Pilocarpine induces seizures by acting as an agonist of muscarinic acetylcholine receptor receptor 1 (M_1) [Hamilton et al., 1997]. It can be administered systemically [Arida et al., 1999; Cavalheiro et al., 1996; Goffin et al., 2007; Parent et al., 1997, 2006] or intrahippocampally (De Furtado et al., 2002). After pilocarpine administration animals develop *status epilepticus* (SE), an acute and prolonged seizure typically related to convulsions and loss of consciousness [Betjemann and Lowenstein, 2015]. The main areas affected by pilocarpine are the olfactory cortex, amygdala, thalamus, neocortex, hippocampus, and the substantia nigra [Turski et al., 1989]. Approximately 2 weeks after the initial SE, animals suffer spontaneous seizures that continue for the rest of the animal's life [Turski et al., 1983].

KA evokes seizures by acting as an agonist of the KA glutamate receptor [Ben-Ari and Cossart, 2000] and as a partial agonist of AMPA receptors [Fritsch et al., 2014]. It can be administered either systemically or intracerebrally by injection into the amygdala or the hippocampus [Lévesque and Avoli, 2013; Muro-García et al., 2019].
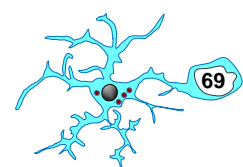
Intrahippocampal KA is a well-characterized preclinical epilepsy model that mimics major aspects of human MTLE such as SE, hippocampal sclerosis, and electroencephalographic (EEG) pattern [Bouilleret et al., 1999; Sierra et al., 2015]. In addition, this method shows a low mortality compared to other different administration models [Lévesque and Avoli, 2013].

Both models (pilocarpine and KA) and their different experimental applications (intraperitoneal, intraamygdaloid or intrahippocampal) represent valid methods for human MTLE replication in rodents. However, the KA intrahippocampal injection model was described to be the one that more reliably reproduces human MTLE, mimicking the effect of hippocampal focal seizures and their extended damage over related healthy tissue [Lévesque and Avoli, 2013]. For this reason, in this PhD Thesis we will use an intrahippocampal KA injection to model MTLE and study microglial phagocytosis of apoptotic cells in the DG of hippocampus.

3.10.11 Microglia in epilepsy

Microglial response to seizures or epilepsy implicates morphological and molecular changes in both animal models and humans **(Fig. 10)**. In rodent experimental models of epilepsy, the most notable morphological alterations on microglia include changes in their cell body size, process length, process numbers, and complexity of branching [Avignone et al., 2008; Borges et al., 2003; Eyo et al., 2014; Jung et al., 2009; Kang et al., 2006; Rappold et al., 2006; Rosell et al., 2003; Shapiro et al., 2008]. Regarding molecular aspects, microglia in epileptic brains change the expression pattern of classical microglial markers, purinergic receptors, fractalkine receptors and cytokines [Akahoshi et al., 2007; Ali et al., 2015; Avignone et al., 2008; Banerjee et al., 2015; Eriksson et al., 2000; Hughes et al., 2002; Morgan et al., 1993; Rappold et al., 2006; Turrin and Rivest, 2004; Vezzani, 2009; Yeo et al., 2011]. Moreover, microglia release ROS and NO following seizures [Helmut et al., 2011; Kalozoumi et al., 2018; Rettenbeck et al., 2015; Ryan et al., 2014]. The microglial response in MTLE patients is similar to that of epileptic animal models, [Morin-Brureau et al., 2018], including an ameboid morphology with few processes, particularly in those brain areas affected by temporal lobe epilepsy such as CA3, CA1, and DG. Moreover, these authors observed an up-regulation of pro-inflammatory cytokines on epileptic microglia. Together, these studies show that microglia change at both morphological and molecular levels following seizures, however, little is known how these events affect microglial function, and ultimately, whether they are beneficial or harmful to the brain.

3.10.12 Microglial phagocytosis and epilepsy
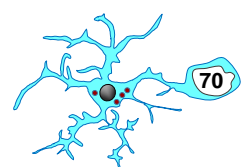
Only a few papers analyzed the efficiency of microglial phagocytosis in epilepsy. Initial work by [Koizumi et al., 2013] suggested that microglial phagocytosis of exogenously administered latex microbeads in the cortex was increased after KA treatment. More recently, [Morin-Brureau et al., 2018] reported an increased expression of CD68 and the immunoglobulin Fc receptor CD16/32a, as an indirect measurement of phagocytosis in tissue resected from MTLE patients. In contrast, our group performed a more direct assessment of phagocytosis of apoptotic cells in the cortex and hippocampus after KA injection and showed a dramatic reduction from 6h to 24h (PhD Thesis O. Abiega, 2017; [Abiega et al., 2016]). This impairment was a complex phenomenon triggered by the overlap of different mechanisms: 1, seizures decreased the expression of phagocytosis receptors in microglia such as TREM2, MerTK, CR3, and GPR34, which lead to an impairment in the recognition of apoptotic cells and phagocytosis initiation; and 2, seizures impaired the motility of microglial process, which reduced surveillance and/or targeting of dead cells. At the molecular level, the impairment of phagocytosis resulted from the massive release of ATP, a well-known neurotransmitter, during seizures. ATP blinded microglia to the local microgradients of ATP released by apoptotic cells as a "find-me" signal and prevented their targeting [Abiega et al., 2016]. In order to evaluate whether the impairment of microglial phagocytosis was maintained over time and related to the chronic damage in MTLE patients, in this PhD Thesis we will assess phagocytosis in chronic stages of in mice injected with KA, and human hippocampal MTLE tissue.

3.11 PATHOPHYSIOLOGY OF HIE, STROKE, AND EPILEPSY

HIE, stroke, and epilepsy have very different etiology but nonetheless share cardinal pathophysiological features; 1, cell death by excitotoxicity; 2, excessive extracellular ATP release; and 3, inflammation **(Fig. 11)**. Therefore, it is possible that they may impact on microglial function (and more specifically, phagocytosis), in a similar manner. In this section, we will first describe the common pathological features and then, we will focus on particular aspects in each disease.
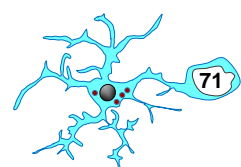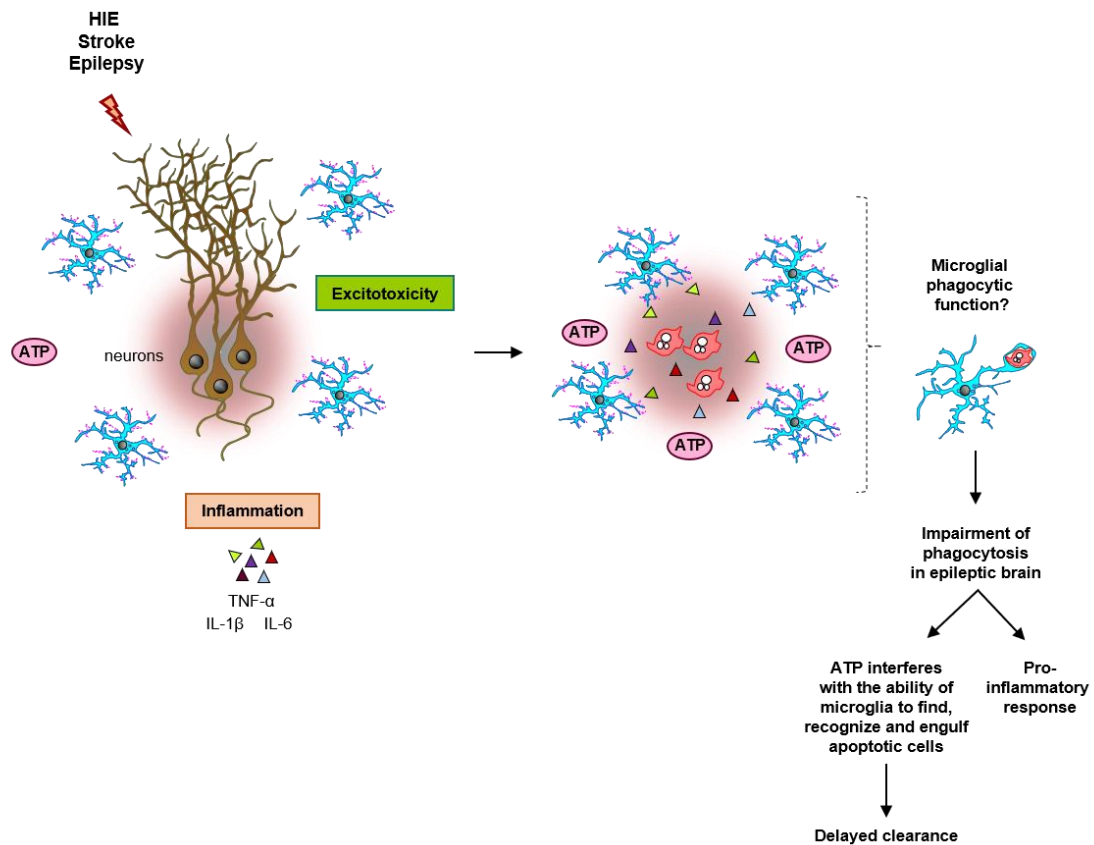
Figure 11. Pathophysiology of HIE, stroke, and epilepsy. *These diseases share cardinal pathophysiological features: cell death by excitotoxicity, excessive extracellular ATP release, and inflammation. These phenomena may impact on microglial phagocytosis in a similar manner. In the epileptic brain, seizures led to a widespread release of ATP, among other possible signals, and interfered with the ability of microglia to find, recognize and engulf apoptotic cells, resulting in their delayed clearance* [Abiega et al., 2016]. *Moreover, the impairment of phagocytosis was associated with the production of pro-inflammatory, epileptogenic cytokines. This scenario could also occur in other diseases, such as stroke, TBI, AD, and/or PD.*

3.11.1 Excitotoxicity

Excitotoxicity refers to the process by which excessive stimulation of glutamate receptors induces neuronal cell death. This phenomenon is implicated in several neurodegenerative diseases including epilepsy, stroke, traumatic brain injury, Alzheimer's Disease, Parkinson's Disease, Huntington's Disease and many others [Wang and Qin, 2010], and evokes cell death by apoptosis or necrosis, depending on its intensity [Bonfoco et al., 1995]. Excitotoxicity is initiated by activation of glutamatergic ionotropic channels, NMDA, AMPA and KA through endogenous excitotoxins (i.e., high concentrations of glutamate); or exogenous excitotoxins (i.e., glutamate agonists NMDA and KA). The continuous stimulation of glutamate receptors results in high accumulation of calcium ions (Ca^{2+}) into the cell, which activate enzymes that damage the
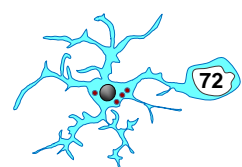
cytoskeleton, the cell membrane, and the DNA, resulting in neuronal death [Orrenius et al., 2003]. These dead neurons need to be swiftly removed by microglial phagocytosis to prevent the spillover of intracellular contents that would result in further damage in neighbor cells.

The mechanism of excitotoxicity in HIE and stroke is relatively simple. As we described in previous sections (**"3.9.7 Introduction to HIE and 3.10.4 Introduction to stroke"**), HIE and stroke are characterized by a reduced supply of oxygen and blood flow. These two events cause an impairment of glutamate transporters [Belov Kirdajova et al., 2020; Woodruff et al., 2011; Yang and Lai, 2011], which results in neuronal depolarization and leads to an unregulated accumulation of glutamate in the synaptic cleft. Excess glutamate released during stroke over-activates NMDA receptors, which cause an influx of Ca^{2+}, the production of reactive nitrogen species (RNS), mitochondrial dysfunction, and the generation of ROS, all of which contribute to cell death [Barker-Haliski and Steve White, 2015; Lai et al., 2014; Yang and Lai, 2011].

Similar to HIE and stroke, the mechanism of excitotoxicity in epilepsy is primarily attributed to dysfunction in the homeostasis of glutamate. As we mentioned in previous section (**"3.10.8 Introduction to epilepsy"**), epilepsy is associated with unpredictable seizures due to abnormal electrical activity. Glutamate that is released from synapses act on ionotropic and metabotropic receptors, which afterwards leads to the initiation and transmission of the seizures [Chapman, 2000]. The excess of glutamate leads to repeated depolarization-repolarization cycles in glutamate terminals, until this amino acid reaches toxic concentration and, finally, the excitotoxic degeneration of post-synaptic neurons occurs [Eid et al., 2008].

3.11.2 Inflammation

In the brain, microglia are the main orchestrators of the inflammatory response [Sierra et al., 2013]. In the presence of an inflammatory insult, microglia produce an array of inflammatory mediators, among which cytokines have a critical role [Akira et al., 2001; Nguyen et al., 2002]. Along these years, an increasing data of experimental and clinical observations describe that many neurodegenerative diseases including epilepsy, ischemia/stroke, Alzheimer´s disease, Parkinson´s disease, Multiple Sclerosis, among others, share a ubiquitous feature: chronic inflammation.

In HIE and stroke, most of the analysis of inflammatory response is focused on production of IL-1β, IL-6, and TNF-α [Han and Yenari, 2003]. Findings from rat models of HIE showed an increased mRNA expression of IL-1β, IL-6, and TNF-α in the neonatal
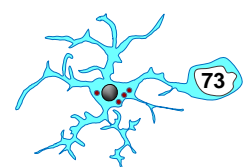
brain after insult [Bonestroo et al., 2013; Hagberg et al., 1996; Jaworska et al., 2017; Sun et al., 2005; Szaflarski et al., 1995]. Moreover, microglia and astrocytes also response to these detrimental conditions producing excess amount of IL-1β, IL-6, TNF-α, among others [Bona et al., 1999; Cowell et al., 2002; Ivacko et al., 1996; Lau and Yu, 2001; McRae et al., 1995; Orzyłowska et al., 1999; Tuttolomondo et al., 2008]. Similar findings are observed in human HIE, including an increased level of pro-inflammatory cytokines (IL-1β, IL-6 and TNF-α) mRNA expression in the CBF, umbilical artery blood, and peripheral venous blood from HIE patients compared to healthy newborns at birth and/or control samples [Chalak et al., 2014; Chaparro-Huerta et al., 2017; Jenkins et al., 2012; Liu and Feng, 2009; Perrone et al., 2018]. In addition to HIE, several studies described an increased level of mRNA and protein expression of these three pro-inflammatory cytokines (IL-1β, IL-6 and TNF-α) in rodent (rats and mouse) after stroke [Berti et al., 2002; Buttini et al., 1996; Clausen et al., 2008; Haglid et al., 1994; Hill et al., 1999; Liu et al., 1993, 1994; Loddick et al., 1998; Suzuki et al., 1999; Walberer et al., 2010]. In addition, it was observed by immunohistochemistry a positive colocalization between microglia and IL-1β antibody in the cortex of rats subjected to stroke [Berti et al., 2002; Liu et al., 1993; Wang et al., 1994]. Regarding human, postmortem brain tissue showed the presence of TNF-α^{+} cells up to 3m following injury, which were identified most of them as microglia/macrophages, astrocytes, and neurons [Dziewulska and Mossakowski, 2003; Sairanen et al., 2001; Tarkowski et al., 1997]. In parallel to these data, there are many reports that found an increased IL-1β, IL-6 and TNF-α levels in CSF, serum, and plasma of stroke patients [Beridze et al., 2011; Castellanos et al., 2002; Tarkowski et al., 1997; Vila et al., 2000; Waje-Andreassen et al., 2005; Zaremba and Losy, 2001], which are associated with larger infarct size, neurological deterioration, and poor outcome independently of the stroke subtype.

In epilepsy, data from experimental studies on rodents (rats and mouse) demonstrated that seizures induce high levels of inflammatory mediators in brain regions involved in the generation and propagation of epileptic activity [Fabene et al., 2010; Ravizza et al., 2010; Vezzani et al., 2008; Yoshikawa et al., 2006]. At tissue level, mRNA expression of pro-inflammatory cytokines including IL-1β, IL-6, TNF-α, and macrophage colony stimulating factor (CSF) are upregulated in epileptic hippocampus [Abiega et al., 2016; Han et al., 2016a; Plata-Salamán et al., 2000; Scorza et al., 2018]. In addition, several studies also demonstrated that microglia and astrocytes from murine epileptic brain express high levels of IL-1β, IL-6, and TNF-α [Abiega et al., 2016; Vezzani and Granata, 2005] as well as upregulated expression of cytokines receptor in both microglia and astrocytes, but also in neurons [Vezzani and Granata, 2005]. In human epilepsy,
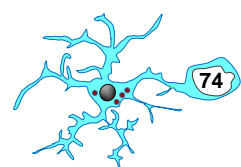
increased levels of pro-inflammatory cytokines including IL-1β, IL-6, and TNF-α in cerebrospinal fluid from drug-refractory epileptic patients [Scorza et al., 2018] and an upregulation of IL-1β and their receptors in glial cells (microglia and astrocytes) and neurons in epileptic brain tissue [Ravizza et al., 2008]. These data evidence the critical role of inflammatory response in epileptic brain. In fact, pro-inflammatory cytokines IL-1β, IL-6, and TNF-α contribute to the epileptic pathophysiology in several aspects: modulation of glutamatergic transmission [Młodzikowska-Albrecht et al., 2007], altering GABAergic neurotransmission [Roseti et al., 2015], and/or potentiating NMDA receptor function through activation of Src tyrosine kinase [Viviani et al., 2003]. Importantly, several animal models have demonstrated that specific anti-inflammatory treatments can be effective at both suppressing chronic seizures and interfering with the process of epileptogenesis [Marchi et al., 2011; French et al., 2017;; Radu et al., 2017].

The relationship between inflammation and phagocytosis is not well understood. Traditionally, it was believed that removal of cellular debris by phagocytosis was a neutral immune event since it does not initiate an inflammatory response [Savill et al., 2002]. Nonetheless, in the last 20 years, in vitro data on macrophages and microglia have shown that phagocytosis of apoptotic cells triggers an active anti-inflammatory response [Fadok et al., 1998; Fraser et al., 2010; De Simone et al., 2003]. Therefore, a dysfunctional phagocytic process might correlate with the development of an inflammatory response. In line with this assumption, our group discovered that microglial phagocytosis was rapidly impaired in a mouse model of MTLE, and this impairment led to the accumulation of apoptotic cells in the DG [Abiega et al., 2016]. The presence of non-phagocytosed cells in the parenchyma correlated with the expression of both pro- and anti-inflammatory cytokines in hippocampal tissue. In addition, microglial population that exhibited impaired phagocytosis also had a strong pro-inflammatory profile (PhD Thesis Abiega. O; [Abiega et al., 2016]). Thus, these results showed that microglial phagocytic impairment led a delayed clearance of apoptotic cells and contributed to the development of an inflammatory response in the brain tissue.

More recently, our lab observed that the anti-inflammatory role of microglia phagocytosis is a more complex mechanisms that we initially believed. We performed a gene-wide expression analysis of primary phagocytic microglia (at 3h and 24h) and found that these cells overexpressed several pro-inflammatory cytokines, such as CSF3, IL-1β, IL-6, and TNF-α, whereas in agreement with previous studies, there was an increase in the anti-inflammatory TGF-β [Diaz-Aparicio et al., 2020]. This cytokine profile triggered in phagocytic microglia was similar to cytokine expression after inflammatory stimuli induced by LPS. We found that microglia increased expression of pro-inflammatory
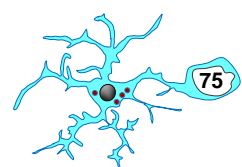
cytokines IL-1β, IL-6, and TNF-α as well as other immunomodulators, including IFN-β, IL-10, IL-12, IL-18, NO, and chemokines such as macrophage-inflammatory protein (MIP)-1a, monocyte chemotactic protein (MCP)-1, and chemokine ligand 5 (RANTES) [Diaz-Aparicio et al., 2020]. These results suggested a complex immunomodulatory effect of phagocytosis on microglia that deserves further testing, although it is not the goal of this PhD Thesis.

3.11.3 ATP release

The nucleotide ATP is a pleiotropic molecule. Intracellularly, ATP is the universal energy currency in living cells for supporting the energy needs of various cellular activities and functions. In the brain, a majority of ATP is formed in the mitochondria [Boyer, 1999] and its energy is used in cytosol to pump sodium and potassium across the cellular membrane for maintaining transmembrane ion gradients and to support neurotransmitters cycling, sustaining electrophysiological activity and cell signaling. In addition to its metabolic roles, ATP is a major neuromodulator, released from neurons and glial cells into the extracellular space after brain injury, via exocytosis of secretory granules, vesicular transport and membrane channels [Lazarowski et al., 2011]. Additional mechanisms were proposed to contribute to the release of ATP including ATP-binding cassette transporters [Naumann et al., 2005], connexin and pannexin hemichannels [Montero and Orellana, 2015; Shan et al., 2020], and/or mitochondrial porins [Crompton, 1999]. In the extracellular space, ATP is rapidly degraded by ectonucleotidases into ADP, AMP, and adenosine [Boison, 2013; Burnstock, 2016; Zimmermann, 1996], which signal to target cells, including microglia, through a plethora of receptors: P2X receptors (ionotropic, activated by ATP), P2Y receptors (metabotropic, activated by ATP and ADP), and P1 receptors (metabotropic, activated by adenosine. However, several studies demonstrated an increased extracellular ATP after brain insult, including seizures [Doná et al., 2016; Frenguelli and Wall, 2016; Lietsche et al., 2016; Wu and Phillis, 1978], stroke [Frenguelli et al., 2007; Melani et al., 2005], among others.

In HIE and stroke, the interruption of oxygen and blood supply to the brain induces an increase ATP concentration into the extracellular space [Frenguelli et al., 2007; Jurányi et al., 1999; M. Morais-Lima et al., 2020; Melani et al., 2005, 2012; Schock et al., 2007]. Multiple sources of ATP are described in the HIE and stroke context, including vesicular release from neurons [Orlando et al., 2014] and astrocytes [Hamilton and Attwell, 2010], by exocytosis from microglia [Imura et al., 2013], along an electrochemical gradient through membrane channels of glial cells [Ballerini et al., 2002], by P2X7 receptors expressed on astrocytes [North, 2002; Yan et al., 2010], by pannexins present
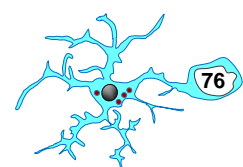
on glial cells [Montero and Orellana, 2015], and pyramidal neurons [Schock et al., 2007]. The massive release of ATP aggravates cerebral damage after HIE and stroke, since high ATP concentrations induce cell death [Cisneros-Mejorado et al., 2014].

Regarding epilepsy, high levels of neuronal activity and metabolic stress associated with seizures evoke the release of ATP into the extracellular space [Frenguelli and Wall, 2016], in part from astrocytes [Cotrina et al., 1998; Guthrie et al., 1999]. Moreover, the activity of ectonucleotidases is altered in experimental epilepsy models [Bonan et al., 2000]. In addition, ATP-derived adenosine is implicated in hyperexcitability and seizure generation [Boison, 2013, 2016; Masino et al., 2014]. The massive extracellular ATP activates purinergic P2 receptors [Engel et al., 2016], which mediate processes associated with the exacerbation of seizures [Jimenez-Pacheco et al., 2016], initiation of long-term changes in network excitability, underlying epileptogenesis [Engel et al., 2012; Jimenez-Pacheco et al., 2016], and resistance to anti-convulsant drugs [Beamer et al., 2017].

The massive release of ATP into extracellular space not only has a critical impact on neuronal cell death but also on microglial phagocytosis since this molecule is a well-known "find-me" signal released by apoptotic cells to attract microglia and promote phagocytic clearance [Elliott et al., 2009; Sierra et al., 2013]. Our lab recently discovered that this chemistry communication between dead cells and microglia is dramatically affected in the epileptic brain **(Fig. 11)**. We found that the release of ATP by neurons and/or astrocytes during seizures interferes with the ATP release as "find-me" signal by apoptotic cells, disrupting the local microgradients of ATP and turn microglia "blind" to dead cells (PhD Thesis O. Abiega; [Abiega et al., 2016]). This mechanism could also occur in other diseases with uncontrolled release, including TBI, stroke, AD, and/or PD.
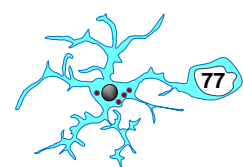
4. HYPOTHESYS AND OBJECTIVES

4. HYPOTHESIS AND OBJECTIVES

Microglial phagocytosis is very rapid and efficient in physiological conditions in the adult brain, as we have observed using as a model the hippocampal neurogenic cascade, where newborn cells naturally undergo apoptosis [Sierra et al., 2010]. In response to apoptotic challenge induced by excitotoxicity or inflammation, adult microglia utilize a combination of three strategies to counteract the increased number of apoptosis: 1, recruit more phagocytic cells; 2, increase the phagocytic capacity per cell; and/or 3, increase the number of microglial cells [Abiega et al., 2016]. Thus, in the adult brain there is a general mechanism of phagocytic response, in which microglial phagocytosis is efficiently coupled to apoptosis. Nonetheless, this coupling is rapidly disturbed in pathological conditions such as epilepsy, a neurological disorder characterized by seizures, excitotoxicity, and inflammation. Based on these observations, we hypothesize that microglial phagocytosis is impaired in other neurodegenerative diseases where apoptosis, excitotoxicity and/or inflammation also occur.

In this PhD Thesis project, we explored apoptosis and microglial phagocytosis from postnatal development to adulthood using as a model the adult hippocampal neurogenic cascade. We analyzed the phagocytic response at different in vivo models: inflammation, ethanol (EtOH) addition, Hypoxia-Ischemia encephalopathies (HIE), cranial irradiation (CIR), transient Middle Cerebral Artery occlusion (tMCAo), and intrahippocampal kainic acid (KA) administration. The results are structured in three sections:

In the first section, we analyzed the microglial phagocytic response in the hippocampus during early postnatal development (P9 and P14). We first analyzed the microglial strategies to apoptotic challenge induced by bacterial *Lipopolysaccharides* (LPS) and ethanol (EtOH) injection. We then tested a model of Hypoxia-Ischemia encephalopathies (HIE).

In the second section, we focused on microglial phagocytic response in the hippocampus to apoptotic challenge induced by four in vivo models in adult mice (2-3m): cranial irradiation (CIR), transient Middle Cerebral Artery occlusion (tMCAo), Hypoxia-Ischemia encephalopathies (HIE), and intrahippocampal KA.

In the third section, we studied another issue related to hippocampal phagocytosis through adulthood: newborn cell survival in the adult hippocampal neurogenic cascade.
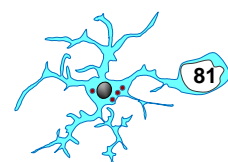
In young mice (1m), the majority of apoptotic cells found in the hippocampus are newborn cells that undergo apoptosis in the first 1-4d of cell life [Sierra et al., 2010]. To determine whether this critical period of survival was maintained through adulthood, and therefore whether the adult neurogenic cascade could be used as a model to analyze phagocytosis in older mice, we performed a systematical analysis of newborn cell survival. We used bromo-deoxyuridine (BrdU) to trace newborn cells longitudinally (from 2h to 30d of cell life) and transversally (at 1m to 12m). In addition, we generated a Marsaglia simulation model to predict newborn cell dynamics across ages.

Aim 1. To analyze microglial phagocytosis efficiency in early postnatal mice under apoptotic challenge.

Aim 1.1 LPS. We evoked apoptotic challenge by LPS injection (5mg/kg) in P9 and P14 fms-EGFP mice, in which microglia express the green fluorescent protein GFP. The study of phagocytosis was performed at 8h after LPS. Quantitative analysis of apoptosis and phagocytosis was performed by immunofluorescence in sections imaged by confocal microscopy.

Aim 1.2 EtOH. We evoked apoptotic challenge by EtOH injection (6g/kg) in P9 and P14 fms-EGFP mice. The study of phagocytosis was performed at 8h after EtOH. Quantitative analysis of apoptosis and phagocytosis was performed by immunofluorescence in sections imaged by confocal microscopy.

Aim 1.3 Hypoxia-Ischemia encephalopathies (HIE). Surgeries related to this part were performed by Takashi Umekawa (postdoctoral researcher in Klas Blomgren´s laboratory, Karolinska Institute, Sweden). HIE conditions were evoked by ligation of the right common carotid artery (CCA) and exposed to gas mixture (10% oxygen in nitrogen) in P9 CX3CR1$^{GFP/+}$ CCR2$^{RFP/+}$ mice, in which microglia express the green fluorescent protein GFP and monocytes express the red fluorescent protein RFP. These double transgenic mice allowed us to discriminate between both populations of macrophages (microglia and peripheral monocytes). The study of phagocytosis was performed at different time points after HIE: 1d and 3d. Quantitative analysis of apoptosis and phagocytosis was performed by immunofluorescence in sections imaged by confocal microscopy.
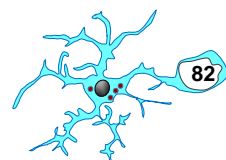
Aim 2. To analyze microglial phagocytosis efficiency in the adult mice under neurodegenerative conditions.

Aim 2.1 Cranial irradiation (CIR). Surgeries related to this part were performed by Wei Han (postdoctoral researcher in Klas Blomgren´s laboratory, Karolinska Institute, Sweden). He induced CIR conditions in 2m CX3CR1$^{GFP/+}$ CCR2$^{RFP/+}$ mice. The study of phagocytosis was performed at different time points after CIR: 6h, 1d, 3d, 7d and 30d. Quantitative analysis of apoptosis and phagocytosis was performed by immunofluorescence in sections imaged by confocal microscopy.

Aim 2.2 Hypoxia-Ischemia encephalopathies (HIE). Surgeries related to this part were performed by Takashi Umekawa (postdoctoral researcher in Klas Blomgren´s laboratory, Karolinska Institute, Sweden). He evoked HIE conditions in 3m CX3CR1$^{GFP/+}$ CCR2$^{RFP/+}$ mice. The study of phagocytosis was performed at different time points after HIE: 1d and 3d. Quantitative analysis of apoptosis and phagocytosis was performed by immunofluorescence in sections imaged by confocal microscopy.

Aim 2.3 transient Middle Cerebral Artery occlusion (tMCAo). We evoked tMCAo in both 2-3m fms-EGFP and fms-EGFP/CCR2$^{RFP/+}$ mice. The study of phagocytosis was performed at different time points after tMCAo: 6h and 1d. In addition, we analyzed non-human primate tissue (marmoset) under tMCAo conditions. Quantitative analysis of apoptosis, phagocytosis, and hypoxic areas was performed by immunofluorescence in sections imaged by confocal microscopy. Evolution of the brain infarct was studied with cresyl violet staining in section imaged by automated digital slide scanner. Moreover, we analyzed neurological impairments induced by tMCAo using two behavioral test: Pole test and Adhesive removal test.

Aim 2.4 Intrahippocampal KA administration. We used intrahippocampal KA injection as a model of MTLE in 2m fms-EGFP and CCR2$^{-/-}$ mice, the latter of which lacked circulating monocytes. The study of phagocytosis was performed at different time points after KA: 3d, 7d and 4m. In addition, we analyzed freshly hippocampal tissue resected from drug-resistant MTLE patients as well as autopsy hippocampal tissue from epilepsy patients. Quantitative analysis of apoptosis and phagocytosis was performed by immunofluorescence in sections imaged by confocal microscopy.

Aim 3. To analyze hippocampal newborn cell survival in the neurogenic niche across adulthood. We used a BrdU pulse-and-chase paradigm to analyze newborn cell decay both longitudinally (from 2h to 30d of their cell life) and transversally (from 1m to 12m of age) in C57BL/6 mice. Quantitative analysis of the BrdU$^+$ cell population was
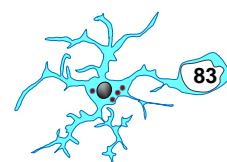
performed by immunofluorescence in tissue sections imaged by epifluorescence and confocal microscopy. With these experimental data, Jorge Valero (Senior Research in our group) generated a Marsaglia simulation model to predict newborn cell dynamics across ages.
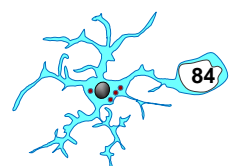
5. EXPERIMENTAL PROCEDURES

5. EXPERIMENTAL PROCEDURES

Further details about reagents and/or resources used in this Thesis are specified in **Table 1**.

5.1 SUBJECTS

5.1.1 Animal tissue

5.1.1.1 Mice

All animals used were on a C57BL/6 background. Mice were housed in 12:12h light cycle with ad libitum access to food and water. Both males and females were used and pooled together, unless otherwise noted. The analysis of neurogenesis across adulthood was performed in C57BL/6 mice. Analysis of microglial and blood-derived macrophages phagocytosis was measured under the following experimental conditions: bacterial *Lipopolysaccharides* (LPS) and ethanol (EtOH) injection, Hypoxia-Ischemia encephalopathies (HIE), Cranial Irradiation (CIR), transient Middle Cerebral Artery occlusion (tMCAo), and intrahippocampal kainic acid (KA) injection. The experiments were carried out in fms-EGFP (MacGreen), CX3CR1$^{GFP/+}$ CCR2 $^{RFP/+}$ mice and/or fms-EGFP CCR2 $^{RFP/+}$, as indicated in the text. In both fms-EGFP and CX3CR1$^{GFP/+}$ CCR2 $^{RFP/+}$ mice resident microglia express the green fluorescent protein GFP [Jung et al., 2010] and in CCR2 $^{RFP/+}$ mice peripheral monocytes express the red fluorescent protein RFP [Saederup et al., 2010]. Analysis of the effect of infiltrating monocytes after KA was performed in CCR2$^{-/-}$ mice [Serbina and Pamer, 2006]. All procedures followed the European Directive 2010/63/EU, NIH guidelines and were approved by the Ethics Committees of the University of the Basque Country EHU/UPV (Leioa, Spain; CEBA/205/2011, CEBA/206/2011, CEIAB/82/2011, CEIAB/105/2012), Karolinska Institute (Stockholm, Sweden; protocol number N249/13), and Southampton University (in accordance with U.K. Home Office licensing; project license 30/3056).

5.1.1.2 Non-Human Primates

Analysis of microglial phagocytosis in non-human primate species under transient Middle Cerebral Artery occlusion (tMCAo) conditions was performed in common marmoset (*Callithrix jacchus*). Brain samples were provided by Omar Touzani (University of Caen, France). Animals were housed in a 12h light-dark cycle. All
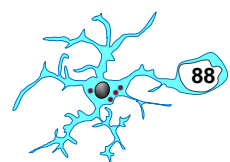
procedures were approval by the Conseil Régional de Normandie and the French National Agency for Research (ANR MAESTRO 15-CE18-0029-01).

5.1.2 Human tissue

Analysis of microglial phagocytosis in freshly brain tissue from adult drug-resistant Mesial Temporal Lobe Epilepsy (MTLE) patients, whose anonymity was preserved. The tissue was obtained from the Basque Biobank at the Cruces University Hospital (Bilbao, Spain). Paraffin-embedded hippocampal tissue from epileptic patients as well as non-demented controls was obtained from the Netherlands Brain Bank (NBB) (Amsterdam). All tissue was collected from donors with a written informed consent for a brain autopsy and the use of the material and clinical information for research purposes had been obtained by the NBB. All procedures were approval by the University of the Basque Country Ethics committee (CEISH/154/2012).

5.2 INTRAPERITONEAL INJECTIONS

5.2.1 BrdU (5-bromo-2'-deoxyuridine) injections

1, 2, 6, and 12m C57BL/6 mice were received four intraperitoneal injections of BrdU (150mg/kg, diluted in 0.1% NaOH and PBS), every 2h (4x) and were sacrificed 2 hours (h), 2d, 4d, 10d, or 30d later.

5.2.2 LPS and Ethanol injections

Postnatal day 9 (P9) and 14 (P14) fms-EGFP mice were received an intraperitoneal injection of bacterial lipopolysaccharides (LPS; 1mg and 5mg/kg) [Sierra et al., 2010] or ethanol (6g/kg; 40% in saline solution) [Lebedeva et al., 2017]. Animals were sacrificed 8h later. Sham mice were injected with saline solution (0.9% NaCl).

5.3 TAIL INJECTIONS

5.3.1 Pimonizadole injections

2m fms-EGFP mice were received one tail injection of Pimonidazole (60mg/kg, diluted in 0.9% NaCl) 30min before Middle Cerebral Artery (MCA) reperfusion and were sacrificed 30min later.
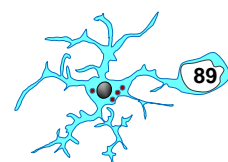
5.4 NEUROSURGERY

5.4.1 Cranial irradiation (CIR)

3m CX3CR1$^{GFP/+}$ CCR2 $^{RFP/+}$ mice were irradiated in X-ray irradiator [Han et al., 2016b]. Animals were anesthetized with isofluorane (5% for induction and 2% for maintenance) and the whole brain was irradiated with a single dose of 8Gy (0.72Gy/min). The acute exposure of 8Gy is equivalent to approximately 18Gy when delivered in repeated 2Gy fractions, which represents a clinically relevant dose used in treatment protocols such as the medulloblastoma study (PNET5 MB) designed for children (open access: https://clinicaltrials.gov/ct2/show/NCT02066220). Animals were sacrificed 6h, 1d, 3d, 7d or 30d after irradiation. Sham mice were anesthetized but did not receive any CIR. These experiments were performed at the Karolinska Institute (Sweden).

5.4.2 Mouse model of Mesial Temporal Lobe Epilepsy (MTLE)

2m fms-EGFP mice received an intrahippocampal injection of kainic acid (KA) [Bouilleret et al., 1999; Sierra et al., 2015]. Animals were anesthetized with ketamine/xylazine (10:1mg/kg) and received a single dose of the analgesic buprenorphine (1mg/kg) subcutaneously. After positioning in the stereotaxic apparatus, a 0.6mm whole was drilled at coordinates taken from Bregma: anteroposterior (AP) -1.7mm, laterolateral (LL) -1.6mm. A pooled glass microcapillary was inserted at -1.9mm dorsoventral (DV), and 50nL of saline or KA (20mM) were delivered into the right hippocampus using a Nanoject II microinjector. Animals were sacrificed 3d, 7d or 4m after injection. Control mice were injected with saline solution.

5.4.3 Mouse model of Hypoxia-ischemia encephalopathies (HIE)

P9 or 3m CX3CR1$^{GFP/+}$ CCR2 $^{RFP/+}$ mice were anesthetized with isoflurane (5% for induction and 2% for maintenance) and the right common carotid artery was ligated with a 6-0 silk suture according to the Rice-Vannucci model [Rice et al., 1981; Umekawa et al., 2015; Zhu et al., 2005]. After ligation, the animals were returned to the dam for 2h (P9) or the home cage for 1h (3m), and then placed in a chamber perfused with a humidified gas mixture (10% oxygen in nitrogen) for 50min (P9) or 75min (3m) at 36ºC. Animals were sacrificed 1d and 3d after injury. Control mice for both ages (P9 and 3m) were neither subjected to ligation nor hypoxia. These experiments were performed at the Karolinska Institute (Sweden).
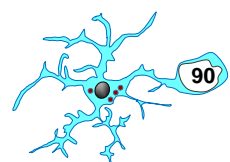
5.4.4 Mouse model of transient Middle Cerebral Artery occlusion (tMCAo)

2m fms-EGFP CCR2 [RFP/+] and fms-EGFP mice were anaesthetized with isofluorane (2% for induction and 1% for maintenance). tMCAo was induced using the intraluminal filament method as previously described [Longa et al., 1989]. Two different monofilaments were used in this Thesis. Filament 1 (F1) was 2 cm-long, nylon filament with a bulbous tip end of 20mm diameter, and filament 2 (F2) was 3cm-long, silicon coated silk with an extended tip of width of 9-10mm and 21mm diameter. Briefly, a midline-neck incision was performed to expose the left Common Carotid Artery (LCCA). The two bifurcation of the LCCA, the External and Internal Carotid Artery (LECA and LICA, respectively) were carefully isolated, and a monofilament was inserted into the LECA and advancing it via the LICA to the origin of the MCA. After embolization for 60min, the monofilament was removed to restore blood flow. The successful occlusion and reperfusion were confirmed by a Laser-Doppler flowmetry (LDF). The blood flow in the MCA area was continuously measured up to 10-15min after reperfusion. Mice that did not demonstrate a rapid restoration of the LDF signal during reperfusion were excluded. Body temperature was kept at 37±0.5°C throughout the experiment by an electrical blanket. Mice were sacrificed 6h, 1d or 3d after the damage. Sham animals were anesthetized but did not subjected to ligation.

5.4.5 Non-Human Primate model of transient Middle Cerebral Artery occlusion (tMCAo)

Adult (22-30m) common marmosets (*Callithrix jacchus*) were anaesthetized with isofluorane (5% for induction and 1.5% for maintenance). tMCAo conditions were induced using the intraluminal filament technique as described previously [Bihel et al., 2010, 2011; Freret et al., 2008]. A nylon monofilament was inserted into the ECA and gently advanced up to the origin of the MCA. After 3h the monofilament was removed, and the animals were sacrificed at 45d later. These experiments were performed at the University of Caen (France).

5.5 NEUROLOGICAL IMPAIRMENT ANALYSIS

Sensorimotor and cognitive impairments in tMCAo mice were evaluated by the Pole and Adhesive Removal Test [Ogawa et al., 1985, Matssura et al., 1997]. To achieve an optimal level of performance and minimize the inter-individual variations, animals were trained for five days (one trial per day) before the surgery and then tested at 1h before
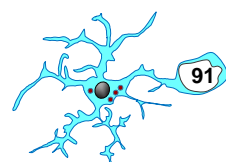
sacrifice. Mice were first undergone to Pole test and after 5min rest to Adhesive Removal test. In order to analyze the animal´s behavior in more detail video-recordings were performed.

5.5.1 Pole test

The apparatus consisted of a vertical wooden pole (50cm length, 8mm in diameter) mounted on a base and placed inside the home cage. Mice were positioned on top of the pole and two parameters were measured: the time to turn (TT), which is the time until the mouse completely turns from head-up to head-down; and the total time to descend and reach the floor (TD). When mice did not turn but descend in a lateral position, the value of the TD was attributed to both parameters (TT and TD). Maximum time of analysis was fixed in 120s [Bouët et al., 2007]. The apparatus was cleaned with 70% ethanol between animals to avoid odor cues.

5.5.2 Adhesive Removal test

Mice were placed into a transparent home cage for 1min habituation period. Animals were carefully removed from the testing cage and two adhesive tapes strips (0.3 x 0.2cm^2) were applied with equal pressure on each mouse paw. Two different colors were used and the order of placing them (right or left) was alternated between animal and session. Animals were replaced in the cage and the times to contact and to remove each adhesive tape were collected with a maximum of 120s [Bouet et al., 2009]. The home cage was cleaned with 70% ethanol between animals to avoid odor cues.

5.6 TISSUE PROCESSING, STAINING AND IMMUNOSTAINING

5.6.1. Mice tissue

Mice were transcardially perfused with 30ml of PBS followed by 30ml of 4% PFA. The brains were removed and post-fixed with the same fixative for 3h at RT, then washed in PBS and kept in cryoprotectant at -20°C. Six series of 50µm-thick sections of brain were cut using a Leica VT 1200S vibrating blade microtome (Leica Microsystems GmbH, Wetzlar, Germany).

Brains obtained from the Karolinska Institute were processed slightly differently. HIE-treated mice were anesthetized with 50mg/kg sodium pentobarbital and transcardially perfused-fixed with 6% formaldehyde solution. The tissue was immersion-

fixed in the same fixative for 24h at 4ºC after perfusion and then soaked overnight in graded concentrations of sucrose solution (10%, 20%, and 30%). The right hemisphere was cut into 40µm-thick sagittal sections in a series of 10 using a sliding microtome (Leica SM2010R, Wetzlar, Germany). The sections were stored in a cryoprotection solution at -20ºC for further use. CIR mice were anesthetized with 50mg/kg sodium pentobarbital and transcardially perfused with 4% paraformaldehyde (PFA). The brains were immersion-fixed in the same fixative for 3d at 4ºC after perfusion and then soaked overnight in graded concentrations of sucrose solution (10%, 20%, and 30% in 0.1M PB). One of the hemispheres was cut into 25µm-thick sagittal sections in a series of 12 using a sliding microtome (Leica SM2010R, Wetzlar, Germany). The sections were stored in a cryoprotection solution (25% ethylene glycol and 25% glycerin in 0.1M PB) at -20ºC for further use.
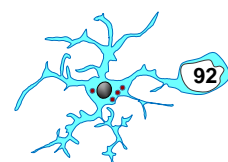
5.6.2 Non-Human primate tissue

Common marmosets (*Callithrix jacchus*) were deeply anesthetized with isoflurane (5% during 10min) and transcardially perfused with a heparinized solution of saline followed by a solution of 4% PFA. The brains were removed from the skull and post-fixed for 4h in the same fixative. Then the brains were cut in the coronal plane and sections (50µm) from the four anterioposterior levels (A4, A5.5 -for the MD, A8 -for the VPL/VPM and P3) were used for staining. The sections were stored in a cryoprotection solution at -20ºC for further use.

5.6.3 Human tissue

Freshly resected hippocampi from adult drug-resistant MTLE patients were immediately immersed in saline and maintained refrigerated until transported to the Pathology Unit of the Cruces Hospital (under 40min). Tissue was manually sectioned in 1-2mm thick coronal sections and transferred to 4% PFA in PBS, pH 7.4 for 30min, then washed in PBS and kept in cryoprotectant (30% sucrose, 30% ethylene glycol in PBS) at -20ºC until use. Six series of 50µm-thick coronal sections were cut using a Leica VT 1200S vibrating blade microtome (Leica Microsystems GmbH, Wetzlar, Germany).

Autopsy tissue from epileptic and non-demented control brains was immersed in 10% buffered formalin for 4 weeks. Then, hippocampi were dissected and embedded in paraffin. Coronal sections (8µm) were cut and mounted on slides, and kept at RT. All procedure was performed by Netherlands Brain Bank (NBB) (Amsterdam).
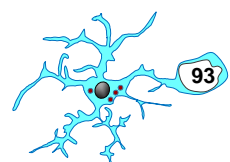
5.6.4 Cresyl violet staining

After sectioning, mouse coronal slices were mounted onto slides with Tespa (3-aminopropyl-triethoxysilane) to improve the adhesion of slices during ethanol dehydration. Slides were dipped in Tespa for 2min, in acetone three changes for 2min each time, allowed to dry, and stored at -4ºC. Mounted tissue was dipped in cresyl violet for 4-5min, then washed twice in 90% ethanol for 5min, in 96% ethanol for 3min, in 100% ethanol for 3min, and 100% xylene for 3min. Thereafter, the slides were mounted with Permount mounting media.

5.6.5 Immunofluorescence

Free-floating vibratome sections were incubated in permeabilization solution (0.3% Triton-X100, 0.5% BSA in PBS) for 2hr at RT, and then incubated overnight with the primary antibodies diluted in the permeabilization solution at 4ºC (a list of primary and secondary antibodies can be found in **Table 1**)[Beccari et al., 2018]. After thorough washing with PBS the sections were incubated with fluorochrome-conjugated secondary antibodies and DAPI (5mg/ml) diluted in the permeabilization solution for 2h at RT. After washing with PBS, the sections were mounted on glass slides with DakoCytomation Fluorescent Mounting Medium.

Tissue pretreatment was used in some experiments. For BrdU and act-casp 3 staining, sections were pretreated with 2M HCl for 15min at 37ºC and washed with 0.1M sodium tetraborate for 10min at RT prior to staining with the primary antibodies. Paraffin-embedded hippocampal tissue from epileptic (8µm) and non-demented controls (8µm) were immersed in xylene (5min, twice), followed by alcohol content solutions (100º, 95º, 70º and 50º, 5min), and deionized water (4min, twice). After deparaffinization, antigen retrieval was performed under a steam atmosphere, using R-Universal epitope recovery buffer (Aptum, Kassel, Germany) or Sodium Citrate buffer in a pressure cooker (Retriever 2100, Prestige Medical, Aptum, Southampton, UK) for 1h before incubating with the primary antibody.

5.7 IMAGE ANALYSIS

Fluorescence immunostaining images were collected using a Carl Zeiss ApoTome2 epifluorescence 20X objective and a Leica TCS STED CW SP8 laser scanning microscope using 40X or 63X oil-immersion objective and a z-step of 0.7µm. All images were imported into Adobe Photoshop 7.0 (Adobe Systems Incorporated, San Jose, CA) in tiff format. Brightness, contrast, and background were adjusted equally for the entire
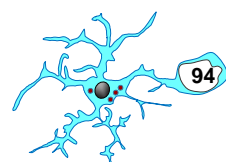
image using the "brightness and contrast" and "levels" controls from the "image/adjustment" set of options without any further modification. For mouse tissue sections, 2-5 20µm-thick z-stacks located at random positions containing the DG were collected per hippocampal section, and a minimum of 6 (sagittal) and 4-5 (coronal) sections per series were analyzed. For human and common marmoset tissue, 2-3 coronal sections were fully scanned under the microscope to find all apoptotic cells.

5.7.1 Hypoxia levels in vivo

The percentage of hypoxic area was estimated in confocal tiled image of coronal slices from sham and tMCAo-treated animals. First, hypoxic areas were manually selected in each image using the "Threshold" tool (Fiji) to mask only the pixels of the image with pimonidazole+ staining. Then, the percentage of pixels occupied by pimonidazole was calculated using the Area Fraction parameter of the "Measure" tool (Fiji). All commands were automated in an ImageJ macro (Fiji). The average Area Fraction from a minimum of 4-5 tiled images per animal was calculated. It was analyzed a minimum of 4-5 sections per series.

5.7.2 Infarct area

Cerebral infarct area was evaluated by cresyl violet staining, as routinely used in ischemic-stroke models [Türeyen et al., 2004].

5.8 QUANTITATIVE ANALYSIS OF CELLS

Cell BrdU$^+$ population, apoptosis and phagocytosis was performed using unbiased stereology methods as previously described [Beccari et al., 2018; Encinas and Enikolopov, 2008].

5.8.1 BrdU$^+$ cells

Total BrdU$^+$ cells were counted in 1-6 of the six series in a Zeiss Axiovert epifluorescent microscopy under a 20X objective. To avoid overestimation, cells whose nuclei were contained in the uppermost focal plane were disregarded. Only cells in the SGZ or the granule cell layer were counted, whereas cells in the hilus or the molecular layer were excluded. Individual BrdU$^+$ cells were identified based on DAPI nuclear staining. A 40X objective was used to unequivocally identify single BrdU$^+$ nuclei in highly dense cell clusters. Total BrdU$^+$ cells counted were extrapolated to the whole or the septal hippocampus (spanning from -1mm to -2.5mm in the AP axes, from Bregma;
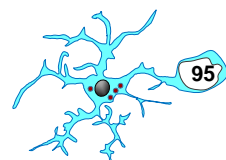
approximately six slices in each of the six series). Experiments involving marker expression of BrdU⁺ cells (minimum of 50 cells per animal, randomly selected) were performed in z-stacks obtained in a Leica TCS STED CW SP8 laser scanning microscope using a 63X oil-immersion objective and a z-step of 0.70 µm. Brightness and contrast were adjusted equally for the entire image in each channel (RGB format) using Adobe Photoshop 7.0 (Adobe Systems Incorporated, San Jose, CA).

5.8.2 Apoptosis and Phagocytosis

Apoptotic dead cells were determined by their nuclear morphology visualized with the DNA dye DAPI. These cells lost their chromatin structure (euchromatin and heterochromatin) and appeared condensed and/or fragmented (pyknosis/karyorrhexis). In addition to this, a well-known marker of apoptosis such as act-caspase-3 was used [Sierra et al., 2010]. Phagocytosis was defined as the formation of a three-dimensional pouch, usually located in the terminal or passant branches of microglia, completely surrounding an apoptotic cell [Sierra et al., 2010]. In tissue sections the number of apoptotic cells, phagocytosed cells, microglia, and/or blood-derived macrophages were estimated in the volume of the DG contained in the z-stack (determined by multiplying the thickness of the stack by the area of the DG at the center of the stack using ImageJ (Fiji)). To obtain the absolute numbers (cells per hippocampus), this density value was then multiplied by the volume of the septal hippocampus (spanning from -1mm to -2.5mm in the anteroposterior axes, from Bregma; approximately 6 slices in each of the 6 series), which was calculated using Fiji from a Zeiss Axiovert epifluorescent microscope images collected at 20X.

In the case of HIE and CIR experiments, a limited tissue and/or unrepresentative number of samples was provided by Karolinska Institute (Sweden). Due to this reason, the total volume of the septal hippocampus could not be calculated, and therefore the number of apoptotic, phagocytosed, microglial cells and peripheral monocytes was estimated as cell density (cells per mm^3).

The following formulae were used to estimate microglial phagocytic efficiency in tissue:

Ph index $= \frac{apo^{Ph}}{apo^{tot}}$

Ph capacity $= \frac{mg^{Ph1} + 2mg^{Ph2} + 3mg^{Ph3} \ldots + nmg^{Phn}}{mg}$
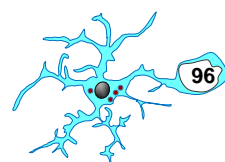
Ph/A coupling $= \frac{Ph\ capacity\ x\ microglia}{apo^{tot}}$

where apo^{Ph} is the number of apoptotic cells phagocytosed; apo^{tot} is the total number of apoptotic cells; and mg^{Phn} is the proportion of microglia with "n" phagocytic pouches.

5.8.3 Microglial area

The percentage of volume occupied by $Iba1^+$ microglia in mouse and human tissue was estimated in confocal z-stacks of the DG and hilus. First, microglia were manually selected in each z-stack using the "Threshold" tool (Fiji) to mask only the pixels of the image with $Iba1^+$ staining. Then, the percentage of pixels occupied by microglia was calculated using the Area Fraction parameter of the "Measure" tool (Fiji). All commands were automated in an ImageJ macro (Fiji). The average Area Fraction from a minimum of 10 images per z-stack was calculated. For mouse tissue, 2-3 20μm-thick z-stacks containing the DG and hilus were collected per hippocampal section and a minimum of 6 sections per series were analyzed. For human tissue, 3-4 12μm-thick z-stacks located at random positions containing the DG and hilus were analyzed.

5.9 STATISTICAL ANALYSIS

SigmaPlot (San Jose, CA, USA) was used for statistical analysis. Data was tested for normality and homoscedasticity. When the data did not comply with these assumptions, a logarithmic transformation was performed and the data was analyzed using parametric tests. Two-sample experiments were analyzed by Students´ t-Test and more than two sample experiments with ANOVA. Only $p < 0.05$ is reported to be significant. Data is shown as mean ± SEM (standard error of the mean).

5.10 GENERATION AND ANALYSIS OF PSEUDORANDOM SIMULATED DATA

Marsaglia simulation model. This model was developed by Dr. Jorge Valero. The Marsaglia polar method [Marsaglia and Bray, 1964] was implemented to generate pseudorandom and normally distributed populations of $BrdU^+$ cells and their progeny with mean and standard deviation corresponding to those experimentally determined in each age group. Each simulated cell value (v) was generated using the following formula:
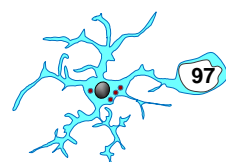
$$v = mean + (std.\,dev \times u_1 \times \sqrt{\frac{-2 \times Ln(s)}{s}})$$

Where mean and std. dev are the experimentally estimated mean and standard deviation of each age group; and u_1 is a random number between -1 and 1 that satisfies the condition:

$$s = u_1{}^2 + u_2{}^2 < 1$$

Where u_2 is a random number between -1 and 1 that is paired to u1 to satisfy the condition s < 1 [Marsaglia and Bray, 1964].

We first generated a population of 1,000 simulated BrdU$^+$ cells at 2h. For each one, we generated their progeny up to 30d using the Marsaglia polar method with the following biological-related restrictions:

$$2h \leq 2d \geq 4d \geq 10d \geq 30d \geq (NeuN^+ + GFAP^+)$$

Thus, each simulated BrdU$^+$ cell at 2h originated a string of linked simulated neurons and astrocytes up to 30d.

Two possible strategies were compared to satisfy that (NeuN$^+$ + GFAP$^+$) ≤ 30d: randomly determine percentage of GFAP$^+$ cells and condition the proportion of NeuN$^+$ to this value (GFAP-locked), or viceversa (NeuN-locked). In this supplementary text, we summarize the simulated NeuN-locked model and the main findings obtained with it: correlation between NeuN$^+$ and GFAP$^+$ at 30d with BrdU$^+$ at 2h; neuronal and astrocytic yield; and neuronal and astrocytic contribution to the increased 30d survival in 6 and 12m mice. The same trends and conclusions were reached using the GFAP-locked strategy reported in the main text and the NeuN-locked strategy shown here.

Data modelling. Curve fitting was used to model the longitudinal and transversal decay of BrdU$^+$, NeuN$^+$, GFAP$^+$, or human Dcx$^+$ cells. Data modeling was implemented using GraphPad Prism 5 (GraphPad Software, Incl, San Diego, CA) and optimal curve fitting was determined by Akaike's information criteria (AICc). We compared six alternative fitting curves: straight, semiLog, Log-Log, exponential decay, exponential decay with plateau, and second order polynomial. Optimal fitting for all data modeled was obtained with exponential curves (with or without plateau). The only exception was human Dcx data, which fit better with semiLog curves. However, we chose to model
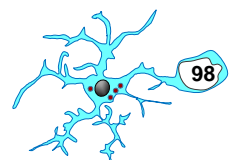
human Dcx data with exponential curves to compare the decay and half-life with those obtained with our own data.

Each exponential decay curve was defined by the following formula:

$$Y = (Y0 - Plateau) \times e^{(-K \times X)} + Plateau$$

Where K is the exponential decay constant and the half-life was calculated as:

$$Half\ life = \frac{Ln(2)}{K}$$

Neuronal:Astrocytic contribution to increased survival at 6 and 12m. To understand the survival of BrdU$^+$ cells (neurons + astrocytes) at 30d in 6 and 12m mice, we compared it with the basal survival at 1m. Thus, the number of BrdU$^+$ cells at 6 and 12m was modeled as the basal number of cells produced (using the survival and differentiation rates as in 1m) and a number of extra cells that could be calculated as the sum of extra neurons and extra astrocytes in different proportions. We explored different scenarios with different neuronal and astrocyte contributions. In addition, we performed an iterative algorithm to search for optimal contributions of neurons and astrocytes. We finally tested which scenario fit best with the experimentally determined and the Marsaglia simulation data comparing the neuron-to-astrocyte (N-to-A) ratios.

1. Basal number of neurons and astrocytes at 30d in 6 and 12m mice.
The basal number of neurons and astrocytes (basal N and basal A, respectively) at 6 and 12m was calculated using the basal survival (1m % survival) and differentiation rates (1m % NeuN and 1m % GFAP, respectively):

$$basal\ N_{6/12m} = BrdU2h_{6/12m} \times \frac{\%\ survival_{1m}}{100} \times \frac{\%\ NeuN_{1m}}{100}$$

$$basal\ A_{6/12m} = BrdU2h_{6/12m} \times \frac{\%\ survival_{1m}}{100} \times \frac{\%\ GFAP_{1m}}{100}$$

2. Extra number of neurons and astrocytes at 30d in 6 and 12m mice.
The extra number of neurons and astrocytes (extra N and extra A, respectively) at 6 and 12m was calculated using the extra survival and extra differentiation rates (extra % NeuN and % GFAP, respectively):

$$extra\ N_{6/12m} = BrdU2h_{6/12m} \times \frac{\%\ extra\ survival_{6/12m}}{100} \times \frac{\%\ extra\ NeuN_{6/12m}}{100}$$
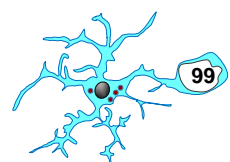
$$extra\ A_{6/12m} = BrdU2h_{6/12m} \times \frac{\%\ extra\ survival_{6/12m}}{100} \times \frac{\%\ extra\ GFAP_{6/12m}}{100}$$

Where the extra survival was calculated as a difference with the 1m % survival:

$$\%extra\ survival_{6/12m} = \%survival_{6/12m} - \%survival_{1m}$$

The extra differentiation rates were tested in different proportions (100N:0A, 50N:50A, and 0N:100A). The total number of neurons and astrocytes were calculated as the sum of basal + extra cells in each scenario. The N-to-A ratios were calculated and compared to the target ratios (obtained in experimentally estimated and Marsaglia simulation data)**(Fig. 48B)**.

<u>3. Optimization of neuronal and astrocyte contributions.</u>

We used a simple iterative parameter search algorithm to find the combination of neuronal and astrocytic contribution to the extra survival that resulted in the N-to-A ratio closest to the target ratios. The optimal neuron and astrocyte contributions were determined independently for the experimentally estimated and the Marsaglia simulation data. Initially, the algorithm tested two different combinations of neuronal and astrocyte contributions (C1=100N:0A and C2=0N:100A) and selected the optimal combination that rendered the smallest absolute difference to target N-to-A ratio. In the next step, the selected combination was compared with a newer combination calculated as:

$$C3 = optimal\ C \pm \frac{|C2 - C1|}{2}$$

Differences with opposite signs indicate that the optimal combination was in between the previous two combinations. In this case, the term $\frac{|C2-C1|}{2}$ was added to C1 or subtracted from C2 depending on which one was selected as optimal. In contrast, differences with identical signs indicate that the optimal combination was either below C1 or above C2. In this latter case, the term $\frac{|C2-C1|}{2}$ is added to C2 or subtracted from C1 depending on which one was selected as optimal. The algorithm was performed iteratively until the N-to-A ratios obtained reach the minimal possible absolute difference (0.001) with those obtained using experimentally estimated or ran Marsaglia simulation data.
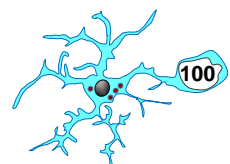
REAGENT and/or RESOURCE			
Antibodies			
Primary antibodies	**Dilution**	**Source**	**Cat. Number**
Bromodeoxyuridine (BrdU) (rat); clone BU1/75 (ICR1)	1:300	AbD Serotech	#MCA2060GA
CCR2 (rabbit)	1:300	Abcam	#ab203128
CD11b (rat); clone 5C6	1:200	BioRad	#MCA711
CD45.2 (mouse); clone 104	1:100	BD Pharmingen	#558702
CD68 (rat); cloneFA-11	1:200	Bio-Rad	#MCA1957GA
Cleaved Caspase-3 (Asp 175)(rabbit)	1:300	Cell Signaling	#9661
DsRed (rabbit)	1:1000	Clontech	#632496
Glial Fibrillary Acidic Protein (goat)	1:1000	Abcam	ab53554
Glial Fibrillary Acidic Protein (rabbit)	1:1000	DakoCytomation	#Z0334
Ionized calcium binding adaptor molecule 1 (Iba1) (rabbit)	1:1000	Wako Chemicals	#019-19741
Ki67 (rabbit); clone SP6	1:750	Abcam	#ab16667
Nestin (chicken)	1:1000	Aves Labs	#NES
NeuN (mouse), clone A60	1:750	Millipore	#MAB377
NeuN (rabbit)	1:1000	Abcam	#ab177487
P2Y12 (rabbit)	1:1000	Anasec	#AS-55043A
Phospho Histone 3 (PH3) (rabbit); clone Ser10	1:1000	Millipore	#06-570
Pimonidazole (mouse)	1:50	Hypoxyprobe	#HP1-100Kit
RFP (mouse); clone RF5R	1:100	Fisher (Spain)	##MA5-15257
TMEM119 (rabbit)	1:2000	Abcam	#ab209064
Green Fluorescent Protein (GFP) (chicken)	1:1000	Aves Labs	#GFP-1020
Secondary antibodies			
Goat anti-chicken (Alexa Fluor 488)	1:500	Life Technologies	#A11039
Goat anti-chicken (Alexa Fluor Rhodamine Red X, RRX)	1:500	Jackson Immunology Research	#103295155
Goat anti-mouse (Alexa Fluor Rhodamine Red X, RRX)	1:500	Jackson Immunology Research	#115295166
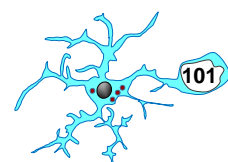
Goat anti-mouse (Alexa Fluor 647)	1:500	Jackson Immunology Research	#115605003
Goat anti-rabbit (Alexa Fluor 488)	1:500	Jackson Immunology Research	#111545144
Goat anti-rabbit (Alexa Fluor Rhodamine Red X, RRX)	1:500	Jackson Immunology Research	#111295144
Goat anti-rabbit (Alexa Fluor 647)	1:500	Jackson Immunology Research	#111605003
Goat anti-rat (Alexa Fluor Rhodamine Red X, RRX)	1:500	Jackson Immunology Research	#112295167
Donkey anti-goat (Alexa Fluor 568)	1:500	Fisher (Spain)	#A11057
Donkey anti-mouse (Alexa Fluor 568)	1:500	Fisher (Spain)	#A10037
Donkey anti-mouse (Alexa Fluor 647)	1:500	Fisher (Spain)	#A31571
DAPI	1:1000	Sigma-Aldrich (Spain)	#D9542-10mg

Biological Samples			
Freshly human hippocampal tissue affected by Mesial Temporal Lobe Epilepsy (MTLE)		Basque Biobank (Cruces University Hospital; Bilbao, Spain)	N/A
Paraffin-embedded human hippocampal tissue affected by Mesial Temporal Lobe Epilepsy (MTLE) and non-demented controls		Netherlands Brain Bank (Netherlands Institute for Neuroscience; Amsterdam)	N/A
Common marmoset (*Callithrix jacchus)*		Bred at University of Caen (France)	N/A

Chemicals			
5-Bromo-2′-deoxyuridine (BrdU)		Sigma-Aldrich (Spain)	#B5002-1G
2.2.2-tribromoethyl alcohol		Sigma-Aldrich (Spain)	#T48402
2-methyl-2-butanol		Sigma-Aldrich (Spain)	#240486
3-Aminopropyl-triethoxysilane (TESPA)		Sigma-Aldrich (Spain)	#440140
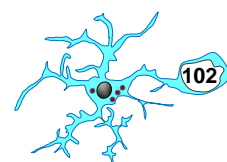
Absolute Ethanol	Panreac	#1310861211-1L
Acetone	Panreac	#141007.1611-1L
Bovine Serum Albumin (BSA)	Sigma-Aldrich (Spain)	#A7906-50G
Buprenorphine	Dechra	#582039.2
Cresyl Violet	Acros Organic	#405760100-10g
Ethylene glycol	Sigma-Aldrich (Spain)	#324558-2L
Fluorescent Mounting Medium	DAKO	#S302380-2
Isofluorane (Isovet)	S. Revet	#469860-250ml
Kainic acid (KA)	Sigma-Aldrich (Spain)	#K3375
Ketamine (Anesketin)	Dechra	#581140.6
Lipopolysaccharides from *Salmonella enterica* serotype typhimurium (LPS)	Sigma-Aldrich (Spain)	#L6143-1MG
Paraformaldehyde (PFA)	Sigma-Aldrich (Spain)	#441244-3Kg
Permount mounting media	Sigma-Aldrich (Spain)	#44581-500ml
Pimonidazole HCl	Hypoxyprobe (USA)	#Mouse-Mab
R-Universal epitope recovery buffer	Aptum	#AP0530-500ml
Triphenyltetrazolium chloride (TTC)	Alfa Aesar	#A10870
Triton™ X-100	Sigma-Aldrich (Spain)	#T8787-100ml
Xylazine	Sigma-Aldrich (Spain)	#X1126-1G
Experimental Models: Organisms/Strains		
Mouse C57BL/6 samples	The Jackson Laboratories	#000664
Mouse CCR2 $^{-/-}$ samples	The Jackson Laboratories	#017586
Mouse CX3CR1$^{GFP/+}$ CCR2 $^{RFP/+}$ samples	Bred at Karolinska Institute (Sweden)	N/A
Mouse fms-EGFP CCR2 $^{RFP/+}$ samples	Bred at UPV	N/A
Mouse fms-EGFP (MacGreen) samples	The Jackson Laboratories	#018549
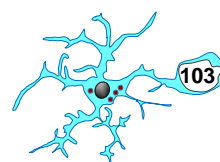
Software and Algorithms		
ImageJ (Fiji)	https://imagej.nih.gov/ij/	N/A
Adobe Photoshop 7.0	Adobe Systems Incorporated	N/A
Las AF Lite	https://www.leica-microsystems.com/products/microscope-software/p/leica-las-x-ls/	N/A
Marsaglia Polar Method	[Marsaglia and Bray, 1964]	N/A
SigmaPlot	http://sigmaplot.co.uk/index.php	N/A
Other		
PF5010, Laser Doppler Perfusion Monitoring (LDPM) Unit	Perimed Company	N/A
FACS Jazz (2B/4YG)	BD	N/A
Leica TCS STED CW SP8 laser scanning microscopy	Leica	N/A
Leica VT 1200S vibrating blade microtome	Leica	N/A
Zeiss Axiovert epifluorescent microscopy	Zeiss	N/A
Stereotactic model 51730	Stoelting Co.	N/A
Microinjector-Nanoject II	Drummond Scientific	#3-000-205A
Master Probe 418	Perimed Company	#91-00053
Filament 1 (F1)	BBraun	#C0936022
Filament 2 (F2)	Doccol corporation	#6021910PK10Re
6/0 silk suture	BBraun	#C0762067
6/0 silk suture	Ethicon Inc	#786G
X-ray irradiator	XRAD320, Precision X-Ray, North Branford, CT, US	N/A
Retriever 2100 (Pressure cooker)	Aptum, Southhsampton, UK	#R2100-EU

Table 1. *List of reagents and/or resources used in this Thesis.*
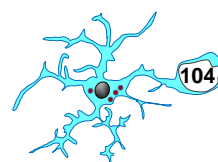
6. RESULTS

6. RESULTS

Microglial phagocytosis is very rapid and efficient in physiological conditions in the adult brain, using as a model the hippocampal neurogenic cascade, where newborn cells naturally undergo apoptosis [Sierra et al., 2010]. This natural apoptotic event allowed us to establish the baseline of phagocytosis and, thus, to assess the phagocytic response to different pathological conditions. Using this paradigm, we recently discovered that under apoptotic challenge induced by excitotoxicity and inflammation these brain sentinels proportionally boost their phagocytic efficiency to account for the increase in apoptosis, maintaining phagocytosis and apoptosis coupled [Abiega et al., 2016]. Nonetheless, these strategies were described only in the adult brain [Abiega et al., 2016; Sierra et al., 2010] and it is unclear how developing microglia face apoptotic challenges.

Microglia undergo a maturation process during early postnatal development [Hammond et al., 2019; Masuda et al., 2019]. This maturation may affect not only the transcriptional profile but also microglial functions, including phagocytosis. In fact, we observed that while the proportion of apoptotic cells engulfed by microglia (Ph index) is around 90% in the 1m hippocampus [Sierra et al., 2010], it is around 60-70% at postnatal days 7 and 14 (P7-P14) [Abiega et al., 2016]. These results suggested a maturation of the microglial phagocytosis efficiency and prompted us to test the response to postnatal microglia to different phagocytic challenges.

In the first part of this PhD Thesis, we explored microglial response during the early postnatal development of the hippocampus. The study was centered on postnatal days P9 and P14 because our preliminary data showed a microglial phagocytic disruption under chronic neuropathological conditions such as HIE at P9 and genetic progressive myoclonus epilepsy type 1 (EMP1) at P14 [Sierra-Torre et al., 2020]. In order to comprehend whether P9 and P14 microglia utilized the same strategies as adult microglia to confront apoptotic challenges [Abiega et al., 2016], we analyzed their phagocytosis under three different conditions: bacterial *Lipopolysaccharides* (LPS), Ethanol (EtOH), and HIE.

In the second part of this PhD Thesis, we expanded our analysis of microglial phagocytosis during adulthood. The study focused on 2-3m mice, in which we had established the baseline of phagocytosis [Sierra et al., 2010], and therefore, we were able to assess the microglial response to different pathological conditions. We explored phagocytosis under four different neuropathological scenarios: CIR, HIE, tMCAo, intrahippocampal KA injection.
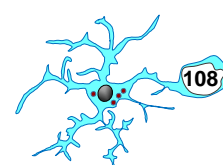
Finally, in the third part of this PhD Thesis, we focused on another issue related to hippocampal phagocytosis through adulthood up to 12mo: the survival of newborn cells in the adult hippocampal neurogenic cascade, which we use to determine the baseline of microglial phagocytosis. We used a BrdU pulse-and-chase paradigm to analyze newborn cell decay both longitudinally (from 2h to 30d of their cell life) and transversally (from 1m to 12m of age). This data allowed us to generate a Marsaglia simulation model to predict newborn cell dynamics across ages.

6.1 MICROGLIAL PHAGOCYTIC RESPONSE IN THE HIPPOCAMPUS DURING EARLY POSTNATAL DEVELOPMENT (P9 AND P14)

In this section we analyzed the postnatal microglial phagocytosis efficiency in the hippocampus under apoptotic challenge induced by LPS, EtOH, and HIE.

6.1.1 LPS exposure does not induce apoptotic changes in P9 and P14 mice

First, we explored whether postnatal phagocytosis was affected by inflammatory events such as LPS treatment, a great model to induce apoptosis and a proportional phagocytic response in adult mice [Sierra et al., 2007, 2010]. For this purpose, we evoked acute inflammation by peripheral administration of LPS (5mg/kg, 8h; [Sierra et al., 2007]) in both male and female (pooled) P9 and P14 mice **(Fig. 12)**. Apoptotic cells were identified by specific nuclear morphology such as pyknosis (DNA condensation) and karyorrhexis (nuclear fragmentation), both detected by condensed staining with DAPI, a DNA dye [Savill et al., 2002]. Microglia were identified by the expression of green fluorescent protein (GFP) in fms-EGFP mice [Sierra et al., 2007]**(Fig. 12A)**. Phagocytosis was defined as the formation of a three-dimensional pouch, usually located in the terminal or passant branches of microglia, completely surrounding an apoptotic cell [Sierra et al., 2010]. We found no significant changes either in the number of dead cells and Ph index (i. e., proportion of apoptotic cells engulfed by microglia) in the DG after LPS compared to saline at P9 **(Fig. 12B, C)**. A similar scenario was found when we expanded our analysis to P14 mice, in which there was no significant evidence of increasing apoptosis and/or phagocytosis after LPS **(Fig. 12D-F)**. One possible explanation is the relative low developmental level of Toll receptors, which recognize LPS and mediate some of its actions in the brain [Barak et al., 2014]. Taking together, these data showed that **LPS did not induce apoptosis, and, therefore, it was not a useful model to analyze the microglial phagocytic response in P9 and P14 mice**.

A

sal
LPS 5mg/kg

P9
fms-EGFP

8h

confocal

DAPI fms-EGFP

B Apoptosis

C Ph index

D

sal
LPS 5mg/kg

P14
fms-EGFP

8h

confocal

DAPI fms-EGFP

E Apoptosis

F Ph index
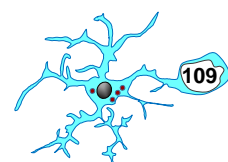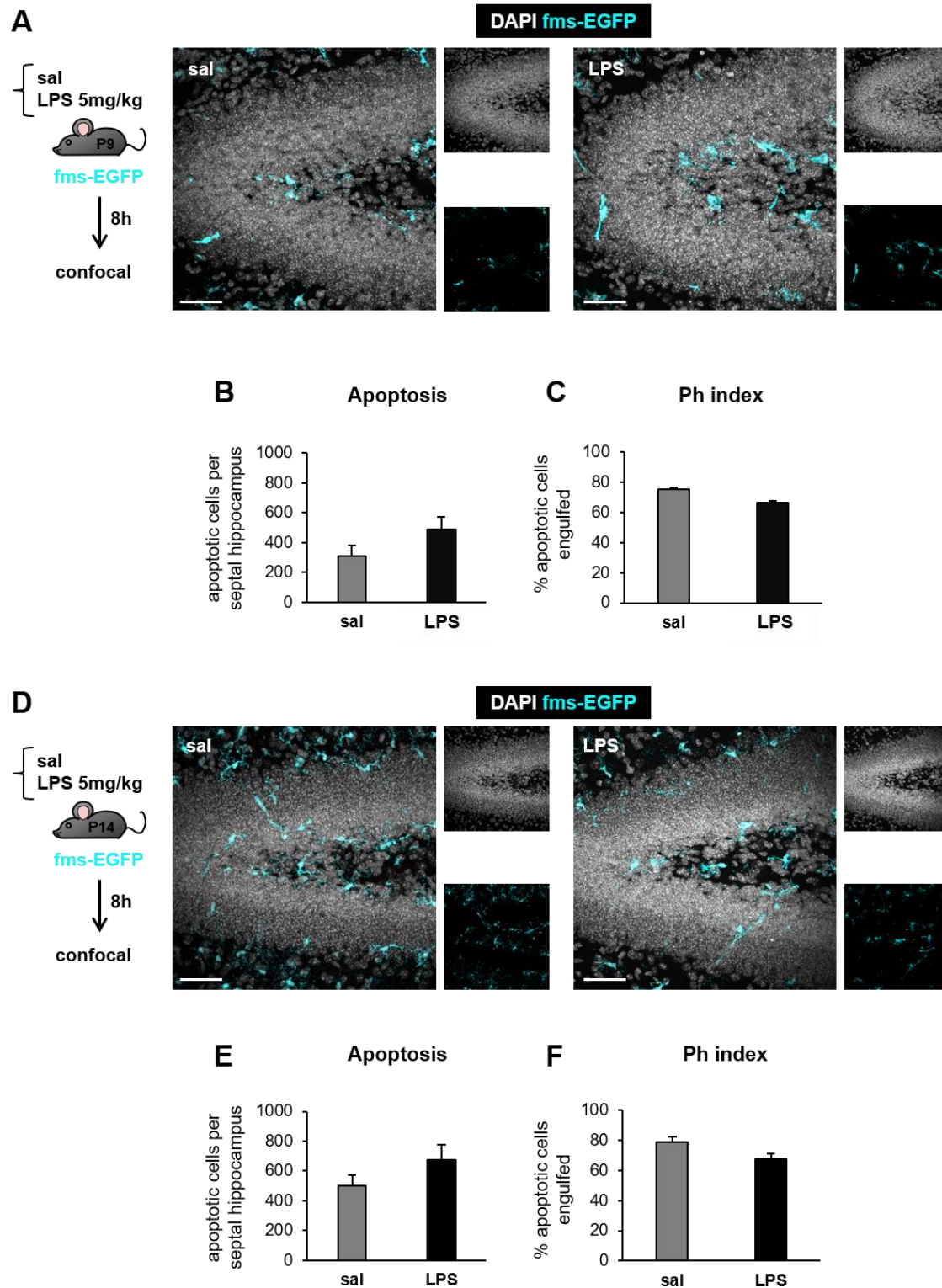
Figure 12. Postnatal microglial phagocytosis is not impaired during neuroinflammation induced by LPS. [A] *Experimental design and representative confocal z-stacks of the DG at P9 mice injected systemically with vehicle (saline) or LPS (5mg/kg) 8h prior to sacrifice. Apoptotic nuclei were detected by pyknosis/karyorrhexis (in white, DAPI) and microglia by the transgenic expression of fms-EGFP (in cyan).* **[B]** *Number of apoptotic cells (pyknotic/karyorrhectic) in the septal DG after saline and/or LPS injection.* **[C]** *Ph index in the septal DG (% of apoptotic cells engulfed by microglia).* **[D]** *Experimental design and representative confocal z-stacks of the DG at P14 in mice injected systemically with vehicle (saline) or LPS*
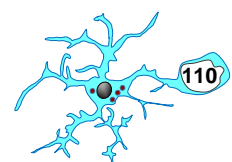
110

*(5mg/kg) 8h prior to sacrifice. Apoptotic nuclei were detected by pyknosis/karyorrhexis (in white, DAPI) and microglia by the transgenic expression of fms-EGFP (in cyan). **[E]** Number of apoptotic cells (pyknotic/karyorrhectic) in the septal DG after saline and/or LPS injection. **[F]** Ph index in the septal DG (% of apoptotic cells phagocytosed by microglia). Bars represent mean ± SEM. The effect of LPS on apoptosis **[B, E]** and Ph index **[C, F]** was analyzed using Student´s t test. To comply with homoscedasticity some data were Log_{10} transformed **[B]**. No significant effects were found in **[B, C, E, F]**. n=3 per group (saline and LPS at P9) and n=4 per group (saline and LPS at P14) per group. Scale bars=50µm [**A, D**]. z=20µm [saline at P9 and P14; **A, D**], 20µm [LPS at P9; **A**], 21µm [LPS at P14; **D**].*

6.1.2 EtOH exposure impairs microglial phagocytosis at P9 but induces an efficient phagocytic response at P14

We therefore moved to an alternative paradigm and explored microglial phagocytosis after ethanol administration, which triggers widespread apoptotic neurodegeneration in the developing brain [Schaffner et al., 2020; Subbanna et al., 2018]. To this aim, we administrated systemically EtOH (6g/kg, 8h; [Lebedeva et al., 2017]) in pooled male and female P9 mice **(Fig. 13)**. While in saline-treated mice apoptotic cells (determined by pyknosis/karyorrhexis and activated caspase-3) were mostly located in the SGZ, after the EtOH treatment dead cells were also observed in the GZ of the DG **(Fig. 13A)**. Therefore, we analyzed apoptosis and phagocytosis in the whole DG pooling together SGZ and GZ. We found that the number of dead cells significantly increased in the DG after EtOH treatment at P9, whereas the Ph index dramatically dropped compared to saline **(Fig. 13A-D)**. To further explore the phagocytic response, we analyzed the microglial Ph capacity (i.e., the proportion of microglia with one or more phagocytic pouches, each containing one apoptotic cell [Abiega et al., 2016]). After EtOH treatment, microglia responded to the increased number of apoptotic cells by rising their Ph capacity **(Fig. 13E)** and there were more phagocytic microglia overall, some of them with up to 4 pouches **(Fig. 13F),** while the number of microglia remained unchanged **(Fig. 13G).** Nevertheless, this strategy of increasing Ph capacity was insufficient to compensate the increased amount of apoptosis, leading to a reduction in the Phagocytosis/Apoptosis (Ph/A) coupling ratio (i.e., ratio between phagocytosis and total number of apoptotic cells)**(Fig. 13H). Therefore, our data showed that at P9, microglial phagocytosis was uncoupled to apoptosis after EtOH challenge**.
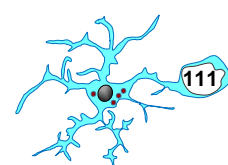
Figure 13. Postnatal microglial phagocytosis is impaired after EtOH administration. [A] *Experimental design and representative confocal z-stacks of the DG at P9 in mice injected systemically with vehicle (saline) or ethanol (EtOH, 6g/kg) 8h prior to sacrifice. Apoptotic nuclei were detected by pyknosis/karyorrhexis (in white, DAPI) and act-casp3+ (in red), and microglia by the transgenic expression of fms-EGFP (in cyan).* **[B]** *Orthogonal projection of a confocal z-stack from the DG of a saline and EtOH-treated mouse showing a microglia (fms-EGFP+, in cyan, M) phagocytosing an apoptotic cell (pyknotic by DAPI, in white and act-casp3+, in red).* **[C]** *Number of apoptotic cells (pyknotic/karyorrhectic and act-casp3+)*

*in the septal DG after saline and/or EtOH injection. **[D]** Ph index in the septal DG (% of apoptotic cells engulfed by microglia). **[E]** Weighted Ph capacity of microglia (parts per unit, ppu). **[F]** Histogram showing the Ph capacity of microglia (% of microglia with phagocytic pouches). **[G]** Total number of microglia (fms-EGFP+) in the septal DG. **[H]** Ph/A coupling (in fold change). Bars represent mean ± SEM. The effect of ethanol on apoptosis **[C]**, Ph index **[D]**, Ph capacity **[E]**, Ph capacity distribution **[F]**, microglia **[G]**, and Ph/A coupling **[H]** was analyzed using Student´s t test. To comply with homoscedasticity some data were Log$_{10}$ transformed **[D, G]**. Only significant effects are shown: * indicates p<0.05. In **[C, D, E, F, G, H]**, n=3 per group. Scale bars=50µm **[A]**, 20µm **[B]**. z=18µm **[A]**, 17µm **[B]**.*

We then explored the effect of EtOH at P14 (pooled male and female) and found a completely different phagocytic response **(Fig. 14).** The number of apoptotic cells (pyknosis/karyorrhexis and activated caspase-3) significantly increased in the DG after EtOH treatment, similar to P9, but at P14 the Ph index remained unaltered, indicating efficient phagocytosis **(Fig. 14A-D)**. In fact, microglia significantly increased their Ph capacity proportionally to the increase in apoptosis **(Fig. 14E**), with more phagocytic microglia, some of them up to 6 pouches **(Fig. 14F),** without increasing their cell numbers **(Fig. 14G).** As a result, the Ph/A coupling ratio was similar between EtOH and saline mice **(Fig. 14H). Thus, these results showed that at P14, microglial phagocytosis remained coupled to apoptosis after EtOH,** as it was proportional to the induction of apoptosis induced by EtOH, similar to adult responses to challenges such as LPS [Sierra et al., 2010] and diet deficiency in anti-inflammatory omega 3 polyunsaturated fatty acids [Abiega et al., 2016].
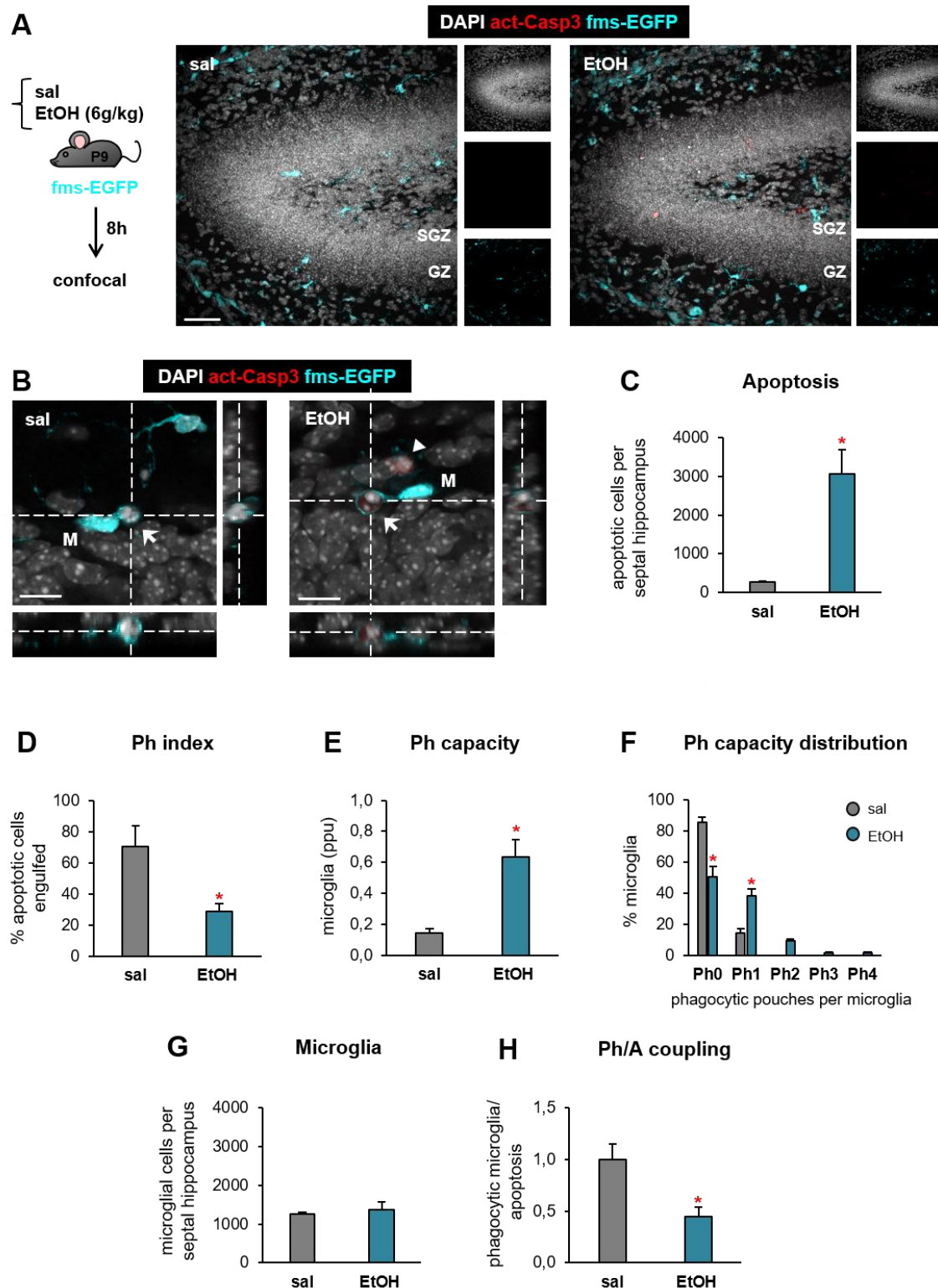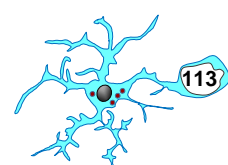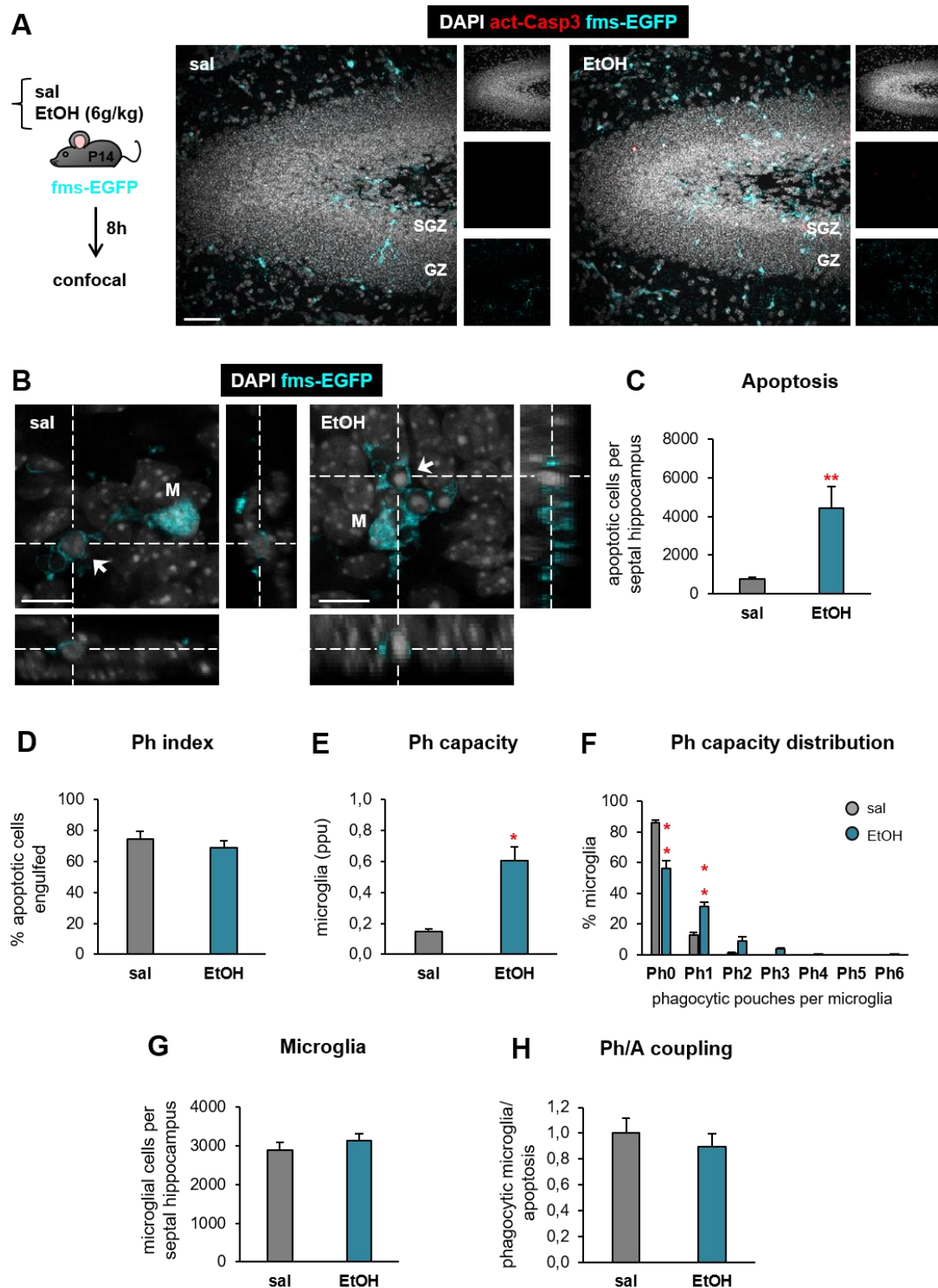
Figure 14. Postnatal microglial phagocytosis is not impaired during ethanol exposure. [A] *Experimental design and representative confocal z-stacks of the DG in P14 mice injected systemically with vehicle (saline) or ethanol (EtOH, 6g/kg) 8h prior to sacrifice. Apoptotic nuclei were detected by pyknosis/karyorrhexis (in white, DAPI) and activated-caspase 3 (act-casp3+, in red), and microglia by the transgenic expression of fms-EGFP (in cyan).* **[B]** *Orthogonal projection of a confocal z-stack from the DG of saline and EtOH-treated mice showing a microglia (fms-EGFP+, in cyan, M) phagocytosing an apoptotic*

*cell (pyknotic by DAPI, in white). **[C]** Number of apoptotic cells (pyknotic/karyorrhectic and act-casp3+) in the septal DG 8h after saline and/or EtOH injection. **[D]** Ph index in the septal DG (% of apoptotic cells engulfed by microglia). **[E]** Weighted Ph capacity of microglia (in parts per unit, ppu). **[F]** Histogram showing the Ph capacity of microglia (% of microglia with phagocytic pouches). **[G]** Total number of microglia (fms-EGFP+) in the septal DG. **[H]** Ph/A coupling (in fold change). Bars represent mean ± SEM. The effect of LPS on apoptosis **[C]**, Ph index **[D]**, Ph capacity **[E]**, Ph capacity distribution **[F]**, microglia **[G]** and/or Ph/A coupling **[H]** was analyzed using Student´s t test. To comply with homoscedasticity, some data were Log$_{10}$ transformed **[C]**. (*) One symbol indicates p < 0.05 and two for p < 0.01. Only significant effects are shown. In **[C, D, E, F, G, H]**, n=3 (saline) and n=6 (ethanol). Scale bars=50µm **[A]**, 20µm **[B]**. z=20µm **[A]**, 17µm **[B]**.*

6.1.3 Postnatal microglial phagocytic response is reduced after cerebral HIE, it is unrelated to peripheral monocyte invasion, and coincides with phagoptosis

To determine the phagocytic potential under pathological conditions, we challenged microglia to an in vivo model of neonatal cerebral HIE **(Fig. 15)**, characterized by a reduction in oxygen supply (hypoxia) combined with reduced blood flow (ischemia) to the brain. To mimic this scenario, P9 mice of both sexes were subjected to ligation of the right common carotid artery (CCA) and exposure to reduced oxygen (10% oxygen in nitrogen) for 50min to induce hypoxia. Animals were then sacrificed 1d and 3d later **(Fig. 15A)**. These surgeries were performed at the Karolinska Institute by Takashi Umekawa (postdoctoral researcher in Klas Blomgren´s laboratory)[Umekawa et al., 2015]. It should be mentioned that P14 mice were not subjected to cerebral HIE in this set of experiments. The combination of carotid ligation and hypoxia produced multifocal ischemic damage at different brain regions such as the cortex, hippocampus, striatum, and thalamus in the ipsilateral hemisphere [Rice et al., 1981; Vannucci et al., 1988], leaving the contralateral hemisphere uninjured and led to monocyte recruitment into the lesioned brain areas [Umekawa et al., 2015]. In order to discriminate between resident microglia and infiltrating monocytes and test their individual role under HIE, we used CX3CR1[GFP/+] CCR2 [RFP/+] double transgenic mice, in which resident microglia and monocytes express the fluorescent protein GFP and RFP, respectively [Chen et al., 2020; Saederup et al., 2010]. Both transgenic mouse models were developed using a knock-in technique [Doyle et al., 2012], in which the coding sequence for the fluorescent reporters replaced the endogenous CX3CR1 or CCR2 loci. Both models were used in heterozygosis to maintain the endogenous expression of both CX3CR1 and CCR2. In these experiments, we were provided a limited amount of tissue samples that prevented us to calculate the total volume of the septal hippocampus, and therefore in this experiment the number of
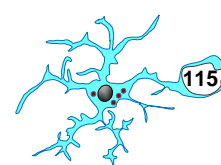
apoptotic, phagocytosed, microglial cells and peripheral monocytes was estimated as cell density (cells per mm^3).

First, we quantified apoptosis (pyknosis/karyorrhexis) and microglial phagocytosis in the DG. We found that the number of dead cells significantly increased 1d and 3d after HIE compared to control mice, whereas the Ph index significantly decreased as early as 1d after damage, as many apoptotic cells were not engulfed **(Fig. 15B-E)**. In addition, we observed that while in control conditions apoptotic cells were mostly engulfed by microglial terminal branches ("ball-and-chain" mechanism)**(Fig. 15F)**[Sierra et al., 2010], under HIE the few engulfed apoptotic cells were mostly phagocytosed by direct apposition to the soma ("apposition" mechanism)**(Fig. 15C)**. Interestingly, we found that many apoptotic cells were localized close to microglial process but were not phagocytosed **(Fig. 15B, C)**. This close proximity of apoptotic cells to microglial processes as well as phagocytosis by apposition in the context of phagocytosis failure were similar to that observed by our group in a model of epilepsy, where it was related to defects in microglial motility and apoptotic cell recognition [Abiega et al., 2016].

Next, we further analyzed the phagocytic response in the DG. We found an increased Ph capacity after HIE compared to controls, due to a higher proportion of phagocytic microglia (up to 10 pouches per cell) **(Fig. 15G, H)**, and an increase in the number of microglia **(Fig. 15I)**. In addition, we observed occasional events of multinucleated microglia at 3d after HIE **(Fig. 15J)**. However, the increment in the microglial phagocytic capacity was not enough to match the amount of apoptosis, and as a result, **the Ph/A coupling was lost (Fig. 15K)**.
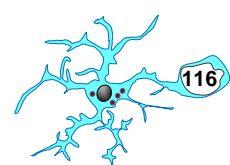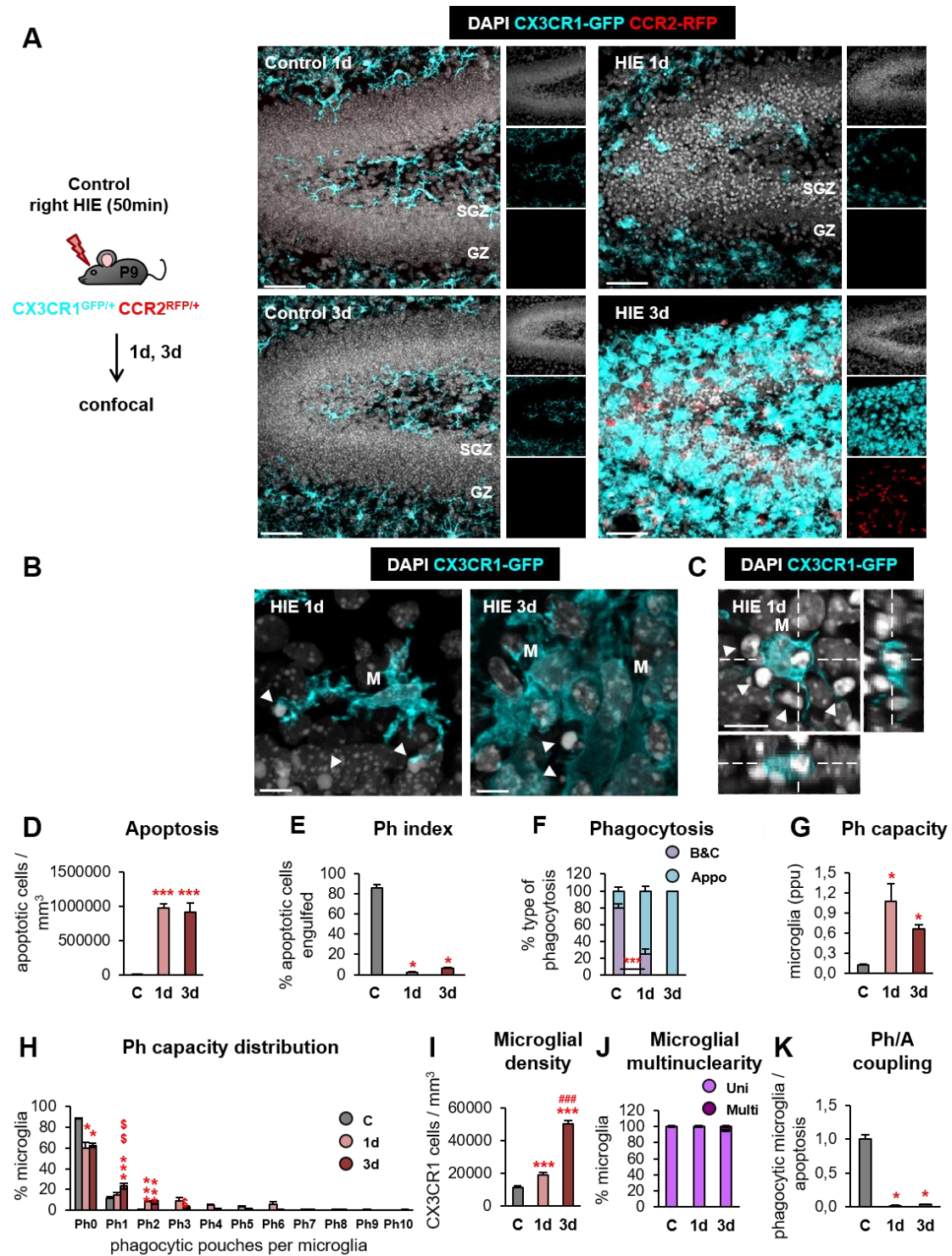
Figure 15. Microglial phagocytosis is impaired in a postnatal model of HIE. [A] *Experimental design and representative confocal z-stacks of the DG of postnatal day 9 (P9) CX3CR1-GFP CCR2-RFP mice at 1 and 3d under hypoxia-ischemia encephalopathies (HIE). Cell nuclei were visualized with DAPI (in white), microglia by CX3CR1-GFP1+ (in cyan) and monocytes by CCR2-RFP+ (in red).* **[B]** *Representative confocal z-stack from the DG of a HIE-treated mouse at 1 and 3d showing apoptotic cells non-phagocytosed by microglia (CX3CR1-GFP+, in cyan; M).* **[C]** *Orthogonal projection of a confocal z-stack from the septal DG of a HIE-treated mouse at 1d showing an apoptotic cell phagocytosed by microglia (CX3CR1-GFP+, in cyan; M).* **[D]** *Density of apoptotic cells (cells/mm3) in the septal DG in control and HIE mice.* **[E]** *Ph index in the*
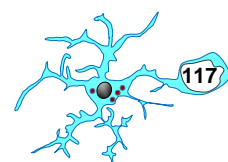
septal DG (% of apoptotic cells engulfed by microglia). [F] Type of microglial phagocytosis (% of microglia) by "ball-and-chain" (B&C) or "Apposition" (Appo) mechanism. [G] Weighted Ph capacity under control and HIE. [H] Histogram showing the Ph capacity of microglia (% of microglia with pouches). [I] Density of CX3CR1-GFP+ microglia (cells/mm³) in the septal DG. [J] Microglial multinuclearity. [K] Ph/A coupling (in fold change) in the septal DG. Bars represent mean ± SEM. The effect of HIE on apoptosis [D], Ph index [E], type of phagocytosis [F], Ph capacity [G], Ph capacity distribution [H], microglial density [I], microglial multinuclearity [J], and Ph/A coupling [K] was analyzed using 1-way ANOVA. Holm-Sidak was used as posthoc test. To comply with homoscedasticity, some data were Log_{10} [D, E, F] and/or Log_{10+1} [G, H, K] transformed. In the case that homoscedasticity was not achieved with a logarithmic transformation data were analyzed using a Kruskal-Wallis ranks test, followed by Dunn method as a posthoc test [E, F, G, K]. (* and $) One symbol indicates p<0.05, two p<0.01, and three p<0.001 (vs control and HIE at 1d, respectively). Only significant effects are shown. In [D, E, F, G, H, I, K], n=11 (control) and n=6 (at 1d and 3d). Scale bars=50µm [A], 10µm [B], 20µm [C]; z=22.4µm [Control 1d, A], 19.6µm [Control 3d, A], 16.8µm [HIE 1d, A], 16.1µm [HIE 3d, A], 14µm [HIE 1d, B], 9.1µm [HIE 3d, B], 14µm [HIE 1d, C].

We then asked whether this microglial phagocytosis impairment could be compensated by phagocytosis mediated by peripheral monocytes **(Fig. 16)**. Few monocytes (RFP+ cells) were found at 1d after HIE although their numbers significantly raised at 3d **(Fig. 16A, B)**, in agreement with previous reports [Umekawa et al., 2015]. In addition, we noticed that there were cells with double reporter expression (GFP and RFP), whose proportion increased from 1d to 3d following injury **(Fig. 16A, C)**. These GFP+/RFP+ cells were most likely peripheral monocytes, based on their elongated and smooth contour, whereas GFP+ microglia were characterized by a ramified morphology in control conditions **(Fig. 15A)** and a hypertrophic, seemingly ameboid morphology after HIE **(Fig. 15A-C)**.
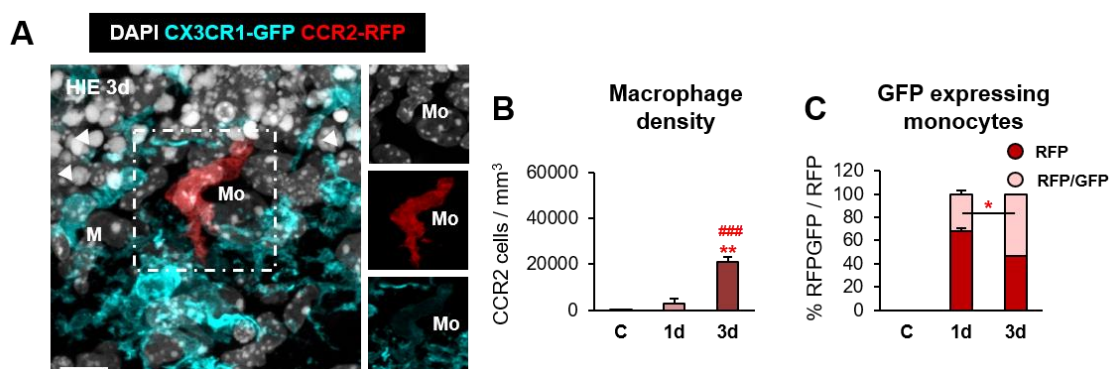
***Figure 16. Invading monocytes in postnatal model of HIE.** [A] Representative confocal z-stack of a CCR2-RFP+ cell (in red; Mo) expressing GFP signal (in cyan) at 3d after HIE. [B] Density of CCR2-RFP+ monocytes (cells/mm³) in the septal DG under control and HIE. [C] Percentage of CCR2-RFP+ monocytes expressing GFP in control and HIE. Bars represent mean ± SEM. The effect of HIE on macrophage density [B] was analyzed using 1-way ANOVA. Holm-Sidak was used as posthoc test. The effect of HIE on the % of GFP expressing monocytes [C] was analyzed using Student´s t test. (* and #) One symbol indicates*
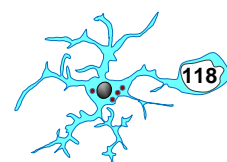
p<0.05, two p<0.01, and three p<0.001 (vs control and HIE at 1d, respectively). Only significant effects are shown. In [B, C], n=11 (control) and n=6 (at 1d and 3d). Scale bars=10μm [A]; z=13.3μm [A].

The origin of these double-positive cells could be explained by two alternative scenarios. One possibility is that CX3CR1 was induced in infiltrating monocytes, in agreement with data from experimental autoimmune EAE [Saederup et al., 2010]. A second possibility is that CCR2 was induced in parenchymal microglia, as suggested in a mouse model of ALS [Komiya et al., 2020]. To discriminate between the two alternatives, we used an antibody against P2Y12 (purinergic receptor type Y12), which was proposed as a specific marker to resident microglia [Haynes et al., 2006; Mildner et al., 2017]**(Fig. 17)**. We found a peculiar pattern of P2Y12 expression between both hemispheres **(Fig. 17A, B)**. While in the contralateral (CL) side to HIE all microglial cells (GFP+) co-localized with P2Y12 **(Fig. 17C)**, in the ipsilateral (IL) we did not observe a clear P2Y12 signal **(Fig. 17D)**, suggesting a possible downregulation of this receptor following an ischemic insult [Gelosa et al., 2014]. Therefore, **P2Y12 was not a useful tool to discriminate microglia from peripheral monocytes in the postnatal brain after HIE**. Although more analysis is required to clarify the identity of double-positive cells in postnatal cerebral HIE, our observations on the cells´ morphology suggested that CX3CR1 was induced in peripheral monocytes after their extravasation into the brain parenchyma.
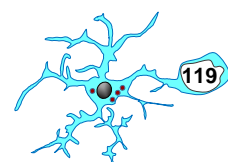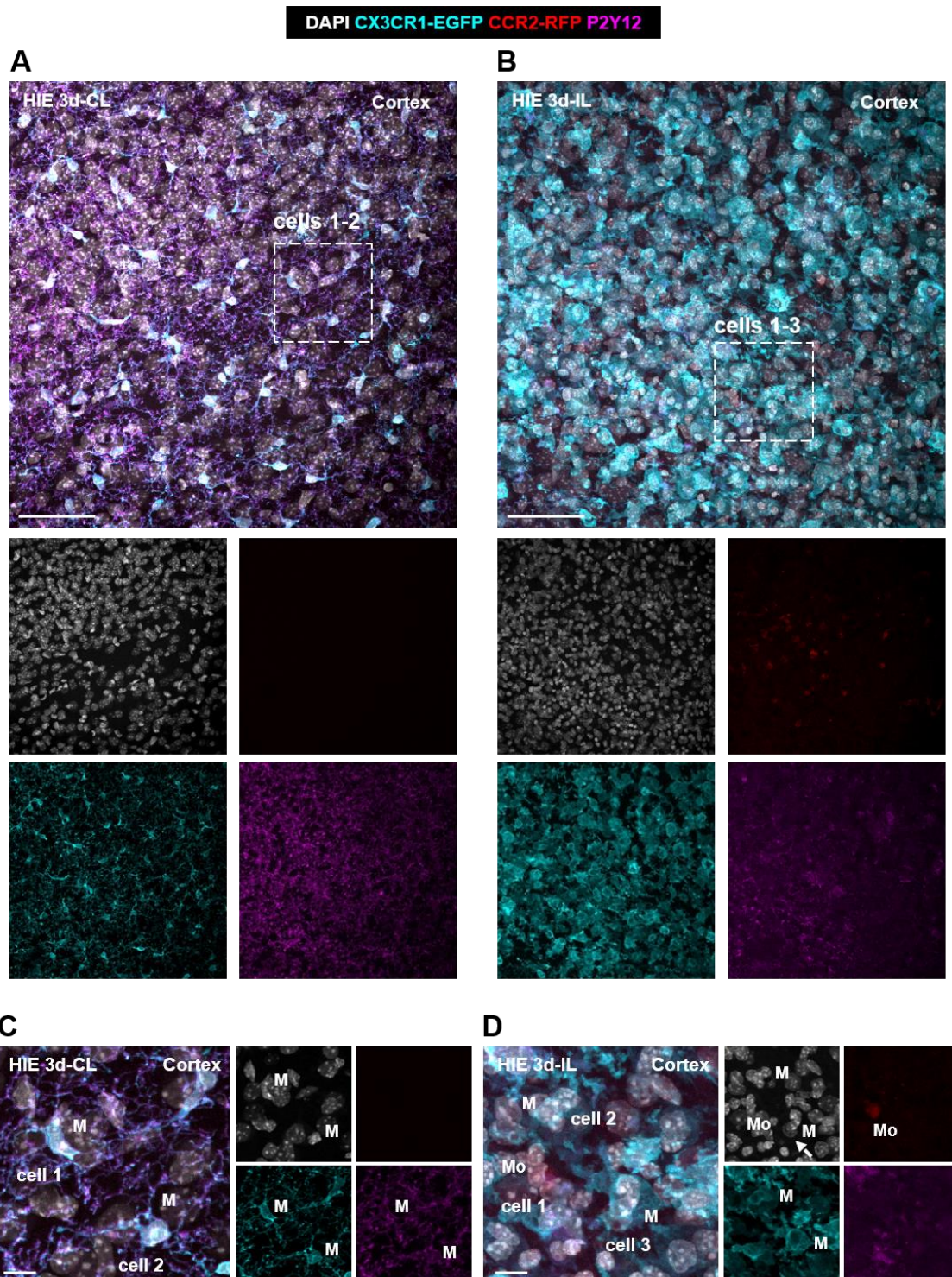
Figure 17. P2Y12 is not a useful tool to distinguish resident microglia from peripheral monocytes in the postnatal brain after HIE. [A] *Representative confocal z-stack of the contralateral (CL) cortex of a 3m CX3CR1-GFP CCR2-RFP mouse after HIE at 3d. Cell nuclei were visualized with DAPI (in white), microglia by CX3CR1-GFP1$^+$ (in cyan), and monocytes by CCR2-RFP$^+$ (in red). Expression of P2Y12 is shown in magenta.* **[B]** *Representative confocal z-stack of the ipsilateral (IL) cortex of a 3m CX3CR1-GFP CCR2-RFP mouse after HIE at 3d. Cell nuclei were visualized with DAPI (in white), microglia by CX3CR1-GFP1$^+$ (in cyan) and monocytes by CCR2-RFP$^+$ (in red). Expression of P2Y12 is shown in magenta.* **[C]** *Representative confocal z-stack from the contralateral (CL) cortex of a HIE-treated mouse at 3d showing microglia (GFP$^+$*
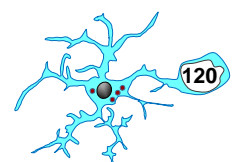
*RFP⁻, cell 1-2, M) co-labeled with P2Y12 (in magenta). **[D]** Representative confocal z-stack from the ipsilateral (IL) cortex of a HIE-treated mouse at 3d showing microglia (GFP⁺ RFP⁻, cell 2-3, M) and monocyte (GFP⁺ RFP⁺, cell 1, Mo) not co-labeled P2Y12 (in magenta). Scale bars=50μm [**A**, **B**], 20μm [**C**, **D**]; z=18.2μm [**A**], 16.8μm [**B**],13μm [**C**], 16μm [**D**].*

We next explored whether invading monocytes were phagocytic **(Fig. 18)**. We found that both RFP⁺ and RFP⁺/GFP⁺ monocytes were poor phagocytes because they engulfed a small number of apoptotic cells compared to microglia at 3d after HIE **(Fig. 18A, B)**. The proportion of apoptotic cells phagocytosed by microglia was 6.4±0.1% compared to 0.1±0.1% by RFP⁺ monocytes and 0.2±0.0% executed by RFP⁺/GFP⁺ monocytes **(Fig. 18C, D)**. Thus, our data showed that the **microglial phagocytosis response was reduced as early as 1d after HIE and was not compensated by peripheral monocyte invasion**.
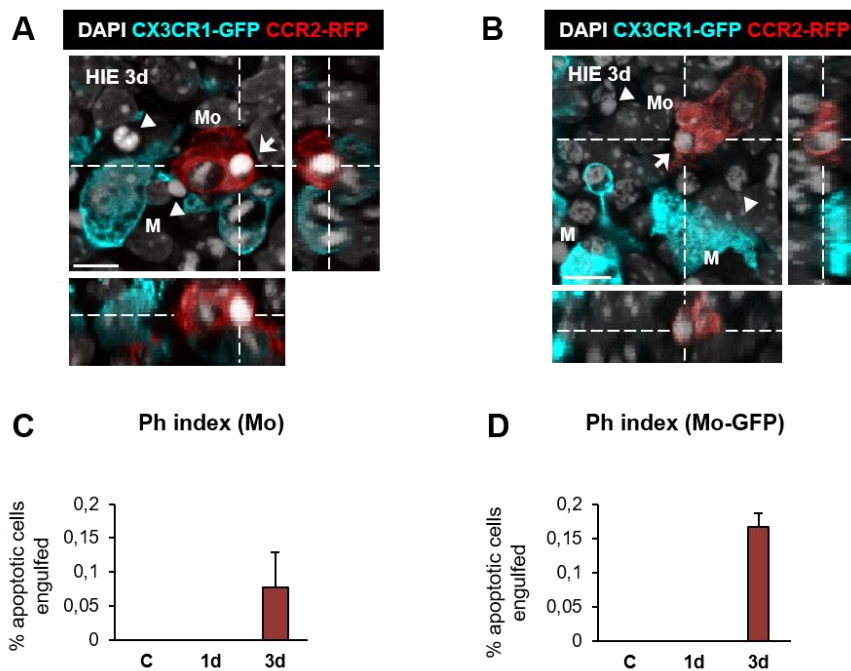
Figure 18. Postnatal microglial phagocytosis impairment is not compensated by monocytes phagocytosis. [A] *Orthogonal projection of a confocal z-stack from the DG of a HIE-treated mouse at 3d showing an apoptotic cell phagocytosed by CCR2-RFP+, monocyte (in red; Mo).* **[B]** *Orthogonal projection of a confocal z-stack from the DG of a HIE-treated mouse at 3d showing an apoptotic cell phagocytosed by monocytes expressing GFP signal (CX3CR1-GFP CCR2-RFP+, in light red; Mo).* **[C]** *Monocyte Ph index in the septal DG (% of apoptotic cells engulfed by monocytes).* **[D]** *Monocyte-GFP Ph index in the septal DG (% of apoptotic cells engulfed by monocytes). Bars represent mean ± SEM. Only significant effects are shown. In* **[C, D]**, *n=11 (control) and n=6 (at 1d and 3d). Scale bars=10μm [**A**, **B**]; z=19.6μm [**A**], 20μm [**B**].*
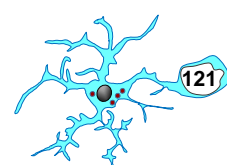
In parallel to the phagocytosis of apoptotic cells we also found some cases of phagoptosis (i.e., engulfment of non-apoptotic cells)**(Fig. 19)**, a process triggered by inflammation [Brown and Neher, 2014]. While in control conditions this phenomenon was not detected, we found some evidences of phagoptosis at 1d and 3d after HIE, and was predominantly executed by the microglial soma ("apposition" mechanism)**(Fig. 19A1)**. We also observed non-apoptotic cells engulfed by both RFP⁺ and RFP⁺/GFP⁺ monocytes **(Fig. 19A2, A3)**, although it occurred in a very low rate compared to microglial phagoptosis **(Fig. 19B)**.
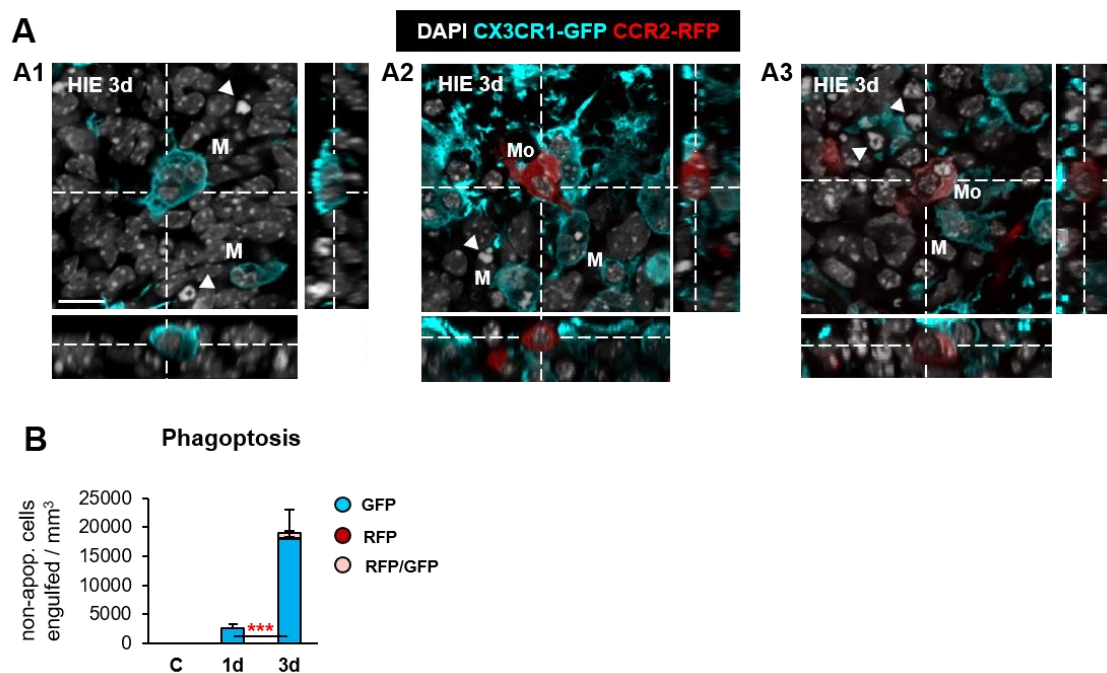
Figure 19. Postnatal microglial phagocytosis impairment is accompanied by phagoptosis. [A] *Orthogonal projection of non-apoptotic cell showing their complete engulfment by microglia (CX3CR1-GFP⁺, in cyan; M)[A1], peripheral monocytes (CCR2-RFP⁺, in red; Mo)[A2], and peripheral monocytes expressing GFP (CX3CR1-GFP CCR2-RFP⁺, in light red; Mo)[A3] at 3d after HIE. [B] Density of phagocytosed non-apoptotic cells in the septal DG (cells/mm³) in control and HIE treatment. Phagoptosis was not detected (nd) in control mice. Bars represent mean ± SEM. The effect of HIE on phagoptosis [B] was analyzed using Student´s t test. (*) One symbol indicates p<0.05, two p<0.01, and three p<0.001 (vs control and HIE at 1d, respectively). Only significant effects are shown. In [B], n=11 (control) and n=6 (at 1d and 3d). Scale bars=10μm [A]; z=16.1μm [A1], 17.5μm [A2], 15.4μm [A3].*

In summary, in the first part of this PhD thesis project we examined and quantified the phagocytic efficiency in the P9-P14 hippocampus under different phagocytic challenges induced by LPS, EtOH, and HIE **(Fig. 20)**. First, we observed that LPS stimulus did not induce apoptosis at any ages analyzed and consequently, it was not an appropriate model to study phagocytosis. In contrast, in the adult hippocampus, microglia
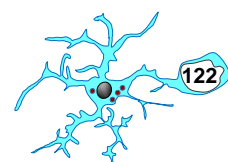
efficiently increased their phagocytic capacity to the brain damage evoked by LPS [Sierra et al., 2010]. Conversely, EtOH and HIE induced apoptosis at both P9 and P14 but the phagocytic response was different in each time point. At P9, microglia increased their phagocytic capacity in response to the apoptotic challenge induced by EtOH and HIE however, this strategy was not enough to compensate the number of apoptotic cells on the brain parenchyma and the A/Ph coupling was lost. On the contrary, under EtOH at P14 the increase in their phagocytic capacity matched the increase in apoptosis and allowed microglia to efficiently cope with the number of dead cells. Therefore, this data suggests maturation of the microglial phagocytic potential during brain development between P9 and P14.
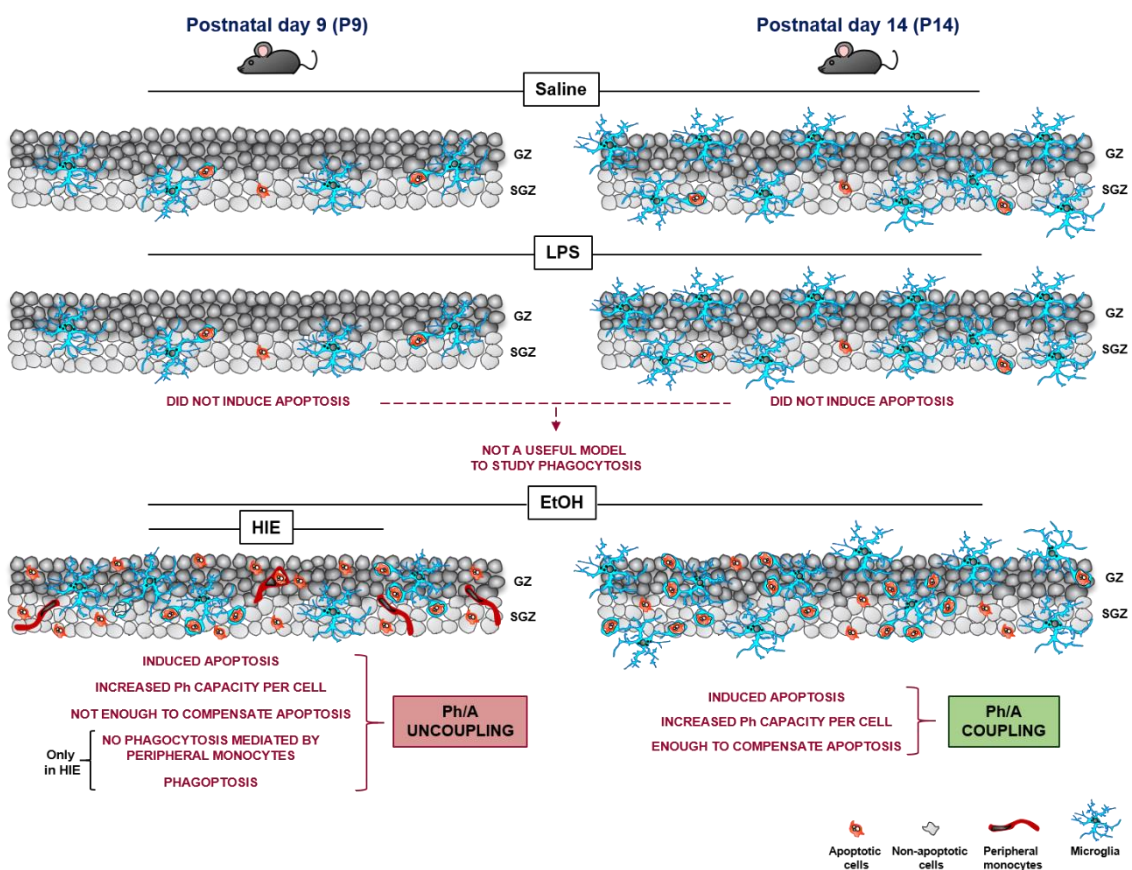
Figure 20. Postnatal microglial phagocytosis/apoptosis coupling in health and disease. *Microglia subjected to apoptotic challenge induced by LPS, EtOH, and HIE showed different phagocytic efficiency. LPS did not induce apoptosis at any ages analyzed and consequently, it was not a useful model to study phagocytosis. In contrast, EtOH and HIE evoked apoptosis at both P9 and P14 but the phagocytic response was different in each time point. At P9, microglia increased their phagocytic capacity in response to the apoptotic challenge induced by EtOH and HIE however, this strategy was not enough to compensate the number of apoptotic cells on the brain parenchyma and the Ph/A coupling was lost. In addition, the impairment of phagocytosis observed in HIE was not compensated by phagocytosis of infiltrating monocytes and was accompanied by phagoptosis. In contrast to P9, under EtOH at P14 the increase in their phagocytic*

capacity matched the increase in apoptosis and allowed microglia to efficiently cope with the number of dead cells, maintaining Ph/A coupling.

6.2 MICROGLIAL PHAGOCYTIC RESPONSE IN THE HIPPOCAMPUS UNDER NEUROPATHOLOGICAL CONDITIONS IN ADULT MICE (2-3m)

In this section we analyzed the adult phagocytosis efficiency in the hippocampus under apoptotic challenge induced by CIR, HIE, tMCAo, and KA.

6.2.1 Adult microglial phagocytosis is coupled to apoptosis after CIR

We explored the phagocytosis response under apoptotic challenge induced by CIR, an essential therapeutic treatment to combat malignant brain tumors [Shah and Kochar, 2018]. In order to evoke CIR, irradiation was delivered in the whole brain (8Gy; [Han et al., 2016b; Osman et al., 2020] and animals of both sexes were sacrificed at different time points: 6h, 1d, 3d, 7d, and 30d **(Fig. 21)**. The acute exposure of 8Gy is equivalent to approximately 18Gy when delivered in repeated 2Gy fractions, which represents a clinically relevant dose used in treatment protocols such as the medulloblastoma study (PNET5 MB) designed for children (https://clinicaltrials.gov/ct2/show/NCT02066220). These experimental procedures were performed at the Karolinska Institute by Wei Han (postdoctoral researcher in Klas Blomgren´s laboratory) [Han et al., 2016b]. Because blood-brain barrier (BBB) integrity is affected by CIR, implicating the infiltration of peripheral monocytes [Morganti et al., 2014], CX3CR1$^{GFP/+}$ CCR2 $^{RFP/+}$ mice were used to discriminate between microglia and monocytes [Chen et al., 2020; Saederup et al., 2010]. In these experiments, we were provided a limited amount of tissue samples that prevented us to calculate the total volume of the septal hippocampus, and therefore in this experiment the number of apoptotic, phagocytosed, microglial cells and peripheral monocytes was estimated as cell density (cells per mm^3).

We first analyzed apoptosis and determined that the number of dead cells (pyknotic/karyorrhectic nuclei visualized with Hoestch) significantly increased in the DG at 6h after CIR compared to sham mice. Importantly, apoptotic cells returned to basal levels 24h later, indicating that they were completely cleared from the brain parenchyma **(Fig. 21A, B)**. Furthermore, phagocytosis remained very efficient even in the face of such number of apoptotic cells, because the Ph index remained constant up to 30d after CIR **(Fig. 21C, D)**. We observed that the majority of microglia engulfed many apoptotic cells at 6h after CIR **(Fig. 21D)**, suggesting an increased Ph capacity. Nevertheless, we were not able to calculate the Ph capacity parameter because the thickness of the samples
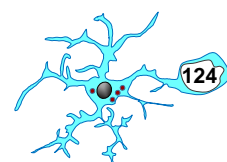
was very thin (25μm) to quantify whole microglial cells (soma and their processes) within the z-stack, and consequently, the Ph/A coupling ratio was not calculated either. In addition, we also analyzed the number of microglial cells and found that these cells significantly decreased at 30d after CIR compared to the previous time points studied (6h-7d)**(Fig. 21E)**. One possible explanation was that microglia undergo apoptosis in response to CIR, as it was suggested by [Han et al., 2016b]. However, we did not observe dead microglial cells throughout the time course (6h-30d), which could be due to the low level of this event and, therefore, the low probability of detecting it over time. In addition, we also analyzed the peripheral monocyte infiltration. No RFP+ cells were found in the brain parenchyma, suggesting that the blood-brain barrier permeability was not compromised after 8Gy irradiation [Han et al., 2016b]. Overall, our preliminary data showed an amazing microglial response to apoptotic challenge induced by CIR, in which these marvelous brain sentinels executed incredible labor of "superphagocytosis". In summary, **microglia become superphagocytic in CIR and apoptosis/phagocytosis remain coupled**.
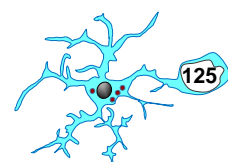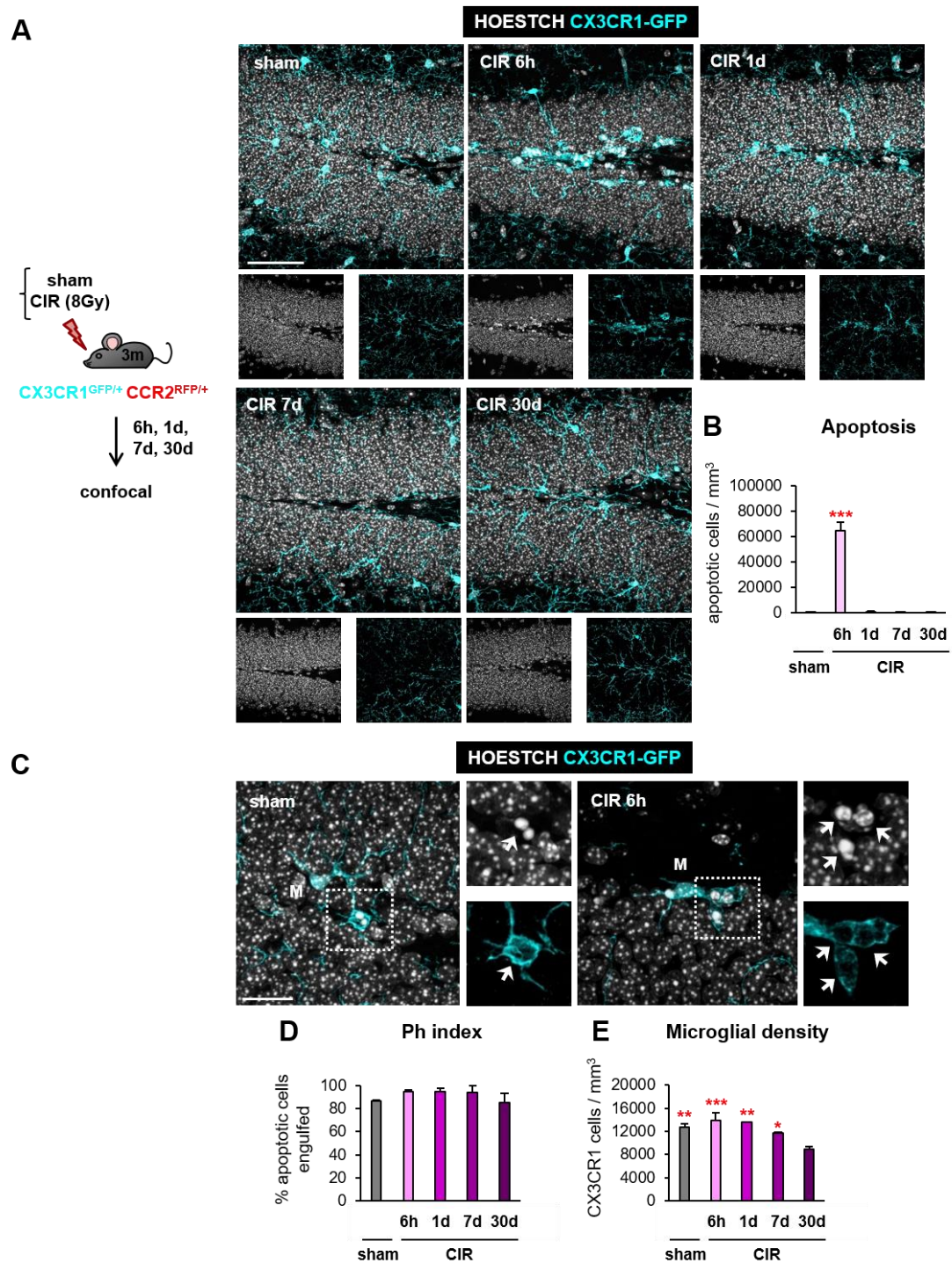
Figure 21. Microglial phagocytic response is increased after cranial irradiation (CIR) exposure. [A] Experimental design and representative confocal z-stacks of the DG of 3m CX3CR1-GFP/CCR2-RFP mice at 6h, 1d, 7d, and 30d after cranial irradiation (CIR, 8Gy). Apoptotic nuclei were detected by pyknosis/karyorrhexis (in white, Hoestch), microglia and blood-derived macrophages by the transgenic expression of CX3CR1-GFP (in cyan) and CCR2-RFP (in red), respectively. **[B]** Density of apoptotic cells (cells/mm^3) in the septal DG. **[C]** Representative confocal z-stack of apoptotic cells (pyknotic/karyorrhectic, Hoescht, in white, arrow) phagocytosed by microglia (CX3CR1-GFP$^+$, in cyan; M) in the septal DG of sham and CRI-treated mice. **[D]** Ph index (% of apoptotic cells engulfed by microglia) in the septal DG. **[E]** Density of CX3CR1$^+$ microglia (cells/mm^3) in the septal DG. Bars represent mean ± SEM. The effect of CIR on

126
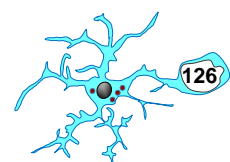
apoptosis [B], Ph index [D], and microglia [E] was analyzed using 1-way-ANOVA. Holm-Sidak was used as a posthoc test. To comply with homoscedasticity some data were Log_{10} transformed [B, E]. (*) One symbol indicates p<0.05, two p<0.01 and three p<0.001 (vs CIR at 30d). Only significant effects are shown. In [B, D, F], n=2 (sham) and n=3 (at 6h, 1d, 7d, and 30d). Scale bar=50µm [A], 20µm [D]; z=21µm [sham, 6h; A], 17.5µm [1d; A], 18.2µm [7d and 30d; A], 13.3µm [sham; D], 18.9µm [6h; D], 17.5µm [1d; D], 9.1µm [7d; D] and 10.5µm [30d; D].

6.2.2 Adult microglial phagocytic response is reduced after cerebral HIE, it is unrelated to peripheral monocyte invasion, and coincides with phagoptosis

The above results from CIR-treated mice were in agreement with previous data obtained in the lab, in which we discovered that adult microglia are efficiently coupled to apoptotic challenges induced by inflammatory conditions, such as LPS or dietary deficiency in omega 3 fatty acids [Abiega et al., 2016; Sierra et al., 2010]. To further test this phagocytic efficiency, we challenged microglia to an in vivo model of adult cerebral HIE **(Fig. 22)**. To evoke this condition, 3m mice of both sexes were subjected to ligation of the right CCA and exposure to reduced oxygen (10% oxygen in nitrogen) for 75min to induce hypoxia. Mice were then sacrificed 1d and 3d later **(Fig. 22A)**. These surgeries were also performed at the Karolinska Institute by Takashi Umekawa (postdoctoral researcher in Klas Blomgren´s laboratory)[Umekawa et al., 2015]. The brain areas affected by damage were mainly the cortex, hippocampus, striatum, and thalamus [Rice et al., 1981; Vannucci et al., 1988]. Because BBB integrity was compromised after HIE and it allowed peripheral monocytes invasion to the CNS, CX3CR1[GFP/+] CCR2 [RFP/+] double transgenic mice were used to discriminate resident microglia (GFP[+]) from monocytes (RFP[+])[Saederup et al., 2010]. In this set of experiments, our lab was provided a limited amount of tissue samples that prevented us to calculate the total volume of the septal hippocampus, and therefore in this experiment the number of apoptotic, phagocytosed, microglial cells and peripheral monocytes was estimated as cell density (cells per mm³).

First, we quantified apoptosis (pyknosis/karyorrhexis) and microglial phagocytosis in the DG. We found that the number of dead cells significantly increased after damage, whereas the Ph index dropped as early as 1d following HIE, as many apoptotic cells were not engulfed **(Fig. 22B-E)**. In addition, we observed that the proportion of apoptotic cells engulfed by direct apposition to the microglial soma ("apposition" mechanism) also increased after damage **(Fig. 22F)**. Moreover, many apoptotic cells were localized close to microglial process but were not phagocytosed, in contrast to what occurred in P9 mice
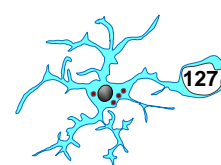
after HIE **(Fig. 22B)**, suggesting defects in apoptotic cell recognition and/or microglial motility [Abiega et al., 2016].
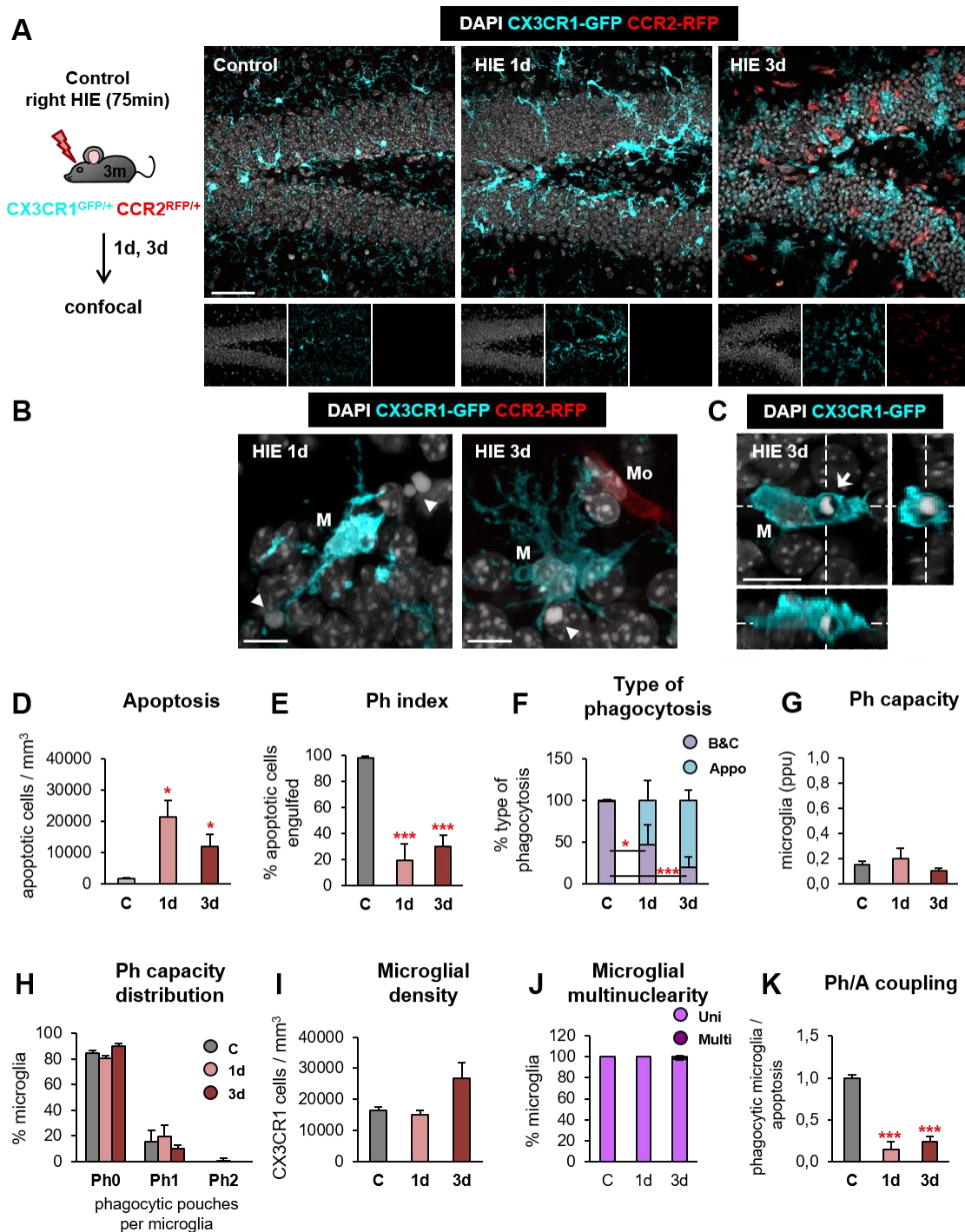
Figure 22. Microglial phagocytosis is impaired in an adult model of HIE. *[A]* *Experimental design and representative confocal z-stack of the DG of 3 month (3m) CX3CR1-GFP CCR2-RFP mice at 1 and 3d under hypoxia-ischemia encephalopathies (HIE). Cell nuclei were visualized with DAPI (in white), microglia (CX3CR1-GFP1+, in cyan) and monocytes (CCR2-RFP+, in red). [B] Representative confocal z-stack from*
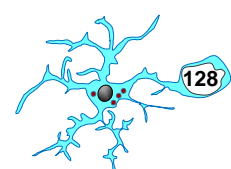
the DG of a HIE-treated mouse at 1 and 3d showing apoptotic cells non-phagocytosed by microglia (CX3CR1-GFP⁺, in cyan; M). **[C]** *Orthogonal projection of a confocal z-stack from the septal DG of a HIE-treated mouse at 3d showing an apoptotic cell phagocytosed by microglia (CX3CR1-GFP⁺, in cyan; M).* **[D]** *Density of apoptotic cells (cells/mm³) in the septal DG under control and HIE treatment.* **[E]** *Ph index in the septal DG (in % of apoptotic cells engulfed by microglia).* **[F]** *Type of microglial phagocytosis (in % of microglia) by "ball-and-chain" (B&C) or "Apposition" (Appo) mechanism.* **[G]** *Weighted Ph capacity under control and HIE conditions.* **[H]** *Histogram showing the Ph capacity of microglia (% of microglia with pouches).* **[I]** *Density of CX3CR1-GFP⁺ microglia(cells/mm³) in the septal DG.* **[J]** *Microglial multinuclearity.* **[K]** *Ph/A coupling (in fold change) in the septal DG. Bars represent mean ± SEM (standard error of the mean). The effect of HIE on apoptosis* **[C]**, *Ph index* **[D]**, *type of phagocytosis* **[E]**, *Ph capacity* **[F]**, *Ph capacity distribution* **[G]**, *microglial density* **[H]**, *microglial multinuclearity* **[J]** *and/or Ph/A coupling* **[K]** *was analyzed using 1-way ANOVA. Holm-Sidak was used as posthoc test. To comply with homoscedasticity, some data were Log₁₀* **[C, G]** *and/or Log₁₀₊₁* **[F]** *transformed. In the case that homoscedasticity was not achieved with a logarithmic transformation data were analyzed using a Kruskal-Wallis ranks test, followed by Dunn method as a posthoc test* **[C, F, G]**. *(*) One symbol indicates p<0.05, two p<0.01, and three p<0.001 (vs control). Only significant effects are shown. In* **[C, D, E, F, G, H, K]**, *n=5 (control), n=3 (at 1d) and n=6 (at 3d). Scale bars=50μm* **[A]**, *20μm* **[B]**, *10μm* **[C]**; *z=16μm* **[A]**, *15μm* **[B]**, *14μm* **[C]**.

Next, we analyzed the characteristics of this phagocytosis impairment in the DG. No significant changes were found in the Ph capacity **(Fig. 22G, H)** and/or number of microglial cells, although an increased tendency was observed at 3d after damage **(Fig. 22I)**. Moreover, we observed that microglia were mainly uninucleated in HIE-treated mice **(Fig. 22J)**. The increase in apoptosis was not compensated by an increased Ph capacity, and therefore, the Ph/A coupling ratio was dramatically lost **(Fig. 22J)**. Together, our data demonstrated that **microglial phagocytosis was disrupted after HIE**.

We then explored whether the impairment of microglia could be compensated by phagocytosis by peripheral monocytes **(Fig. 23)**. We first quantified the number of monocytes (RFP⁺ cells) and found few cells at 1d after HIE although their numbers peaked up 3d **(Fig. 22A, 23A, B)**, in agreement with previous reports [Umekawa et al., 2015]. Very rarely, an occasional RFP⁺ cell appeared in control animals, which might be located inside a blood vessel. Moreover, we also observed that some RFP⁺ cells also expressed GFP and the proportion of these GFP⁺/RFP⁺ cells increased across the time course **(Fig. 23A, C)**.
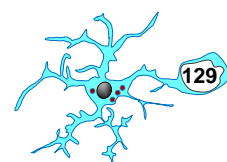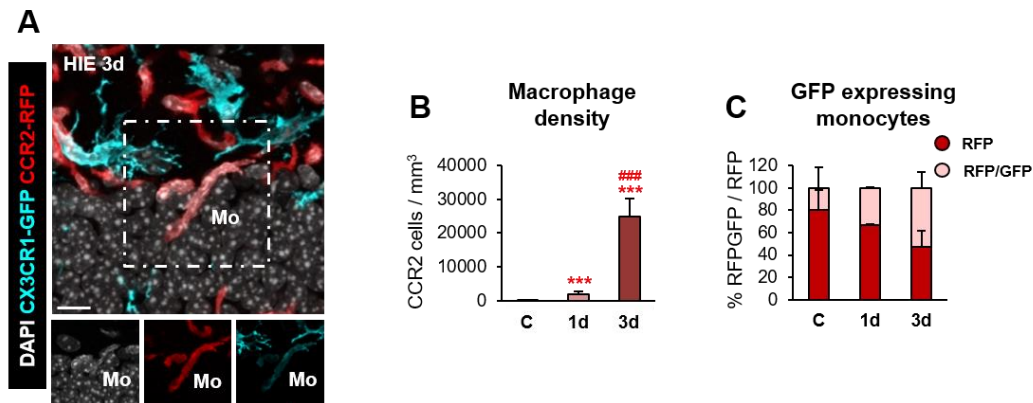
***Figure 23. Adult microglial phagocytosis impairment induced by HIE is not compensated by phagocytosis of monocytes. [A]** Representative confocal z-stack from the DG of a CCR2-RFP+ cell (in red; Mo) expressing GFP signal (in cyan) at 3d after HIE. **[B]** Density of monocytes (in CCR2-RFP+ cells/mm³) in the septal DG under control and HIE treatment. **[C]** Percentage of monocytes (CCR2-RFP+) expressing GFP in control and HIE conditions. Bars represent mean ± SEM. The effect of HIE on macrophage density **[B]**, percentage of RFP and RFP/GFP+ cells **[C]** was analyzed using 1-way ANOVA. Holm-Sidak was used as posthoc test. To comply with homoscedasticity, some data were Log_{10} **[C]** transformed. (* and #) One symbol indicates p<0.05, two p<0.01, and three p<0.001 (vs control and HIE at 1d, respectively). Only significant effects are shown. In **[B, C]**, n=5 (control), n=3 (at 1d) and n=6 (at 3d). Scale bars=50μm **[A]**; z=15μm **[A]**.*

As we previously explained in the postnatal HIE, there are two alternatives origin to these GFP+/RFP+ cells: 1, CX3CR1 was induced in infiltrating monocytes [Chen et al., 2020; Saederup et al., 2010] or 2, CCR2 was induced in parenchymal microglia [Komiya et al., 2020]. Based on our results, we suggested that CX3CR1 was induced in peripheral monocytes after their extravasation into the brain parenchyma, in agreement with [Chen et al., 2020; Saederup et al., 2010]. To identify both macrophage populations and prove our hypothesis, we used the P2Y12 antibody [Haynes et al., 2006; Mildner et al., 2017]. This analysis was performed in the penumbra cortex (CX), one of the main regions invaded by monocytes after the stroke insult. While in early postnatal mice P2Y12 was downregulated **(Fig. 6)**, in adult brains its expression was largely maintained after HIE **(Fig. 24)**. Remarkably, we observed that 100% of microglia (GFP+ RFP-; **Fig. 24B1-B2**) were P2Y12+, whereas 100% of monocytes (RFP+; **Fig. 24B1-B3**) were P2Y12- regardless of the GFP expression **(Fig. 24C)**. These data showed that **P2Y12 was a useful tool to discriminate microglia from peripheral monocytes in adult brain after HIE and that double-positive cells (RFP+/GFP+) were monocytes**.
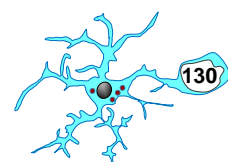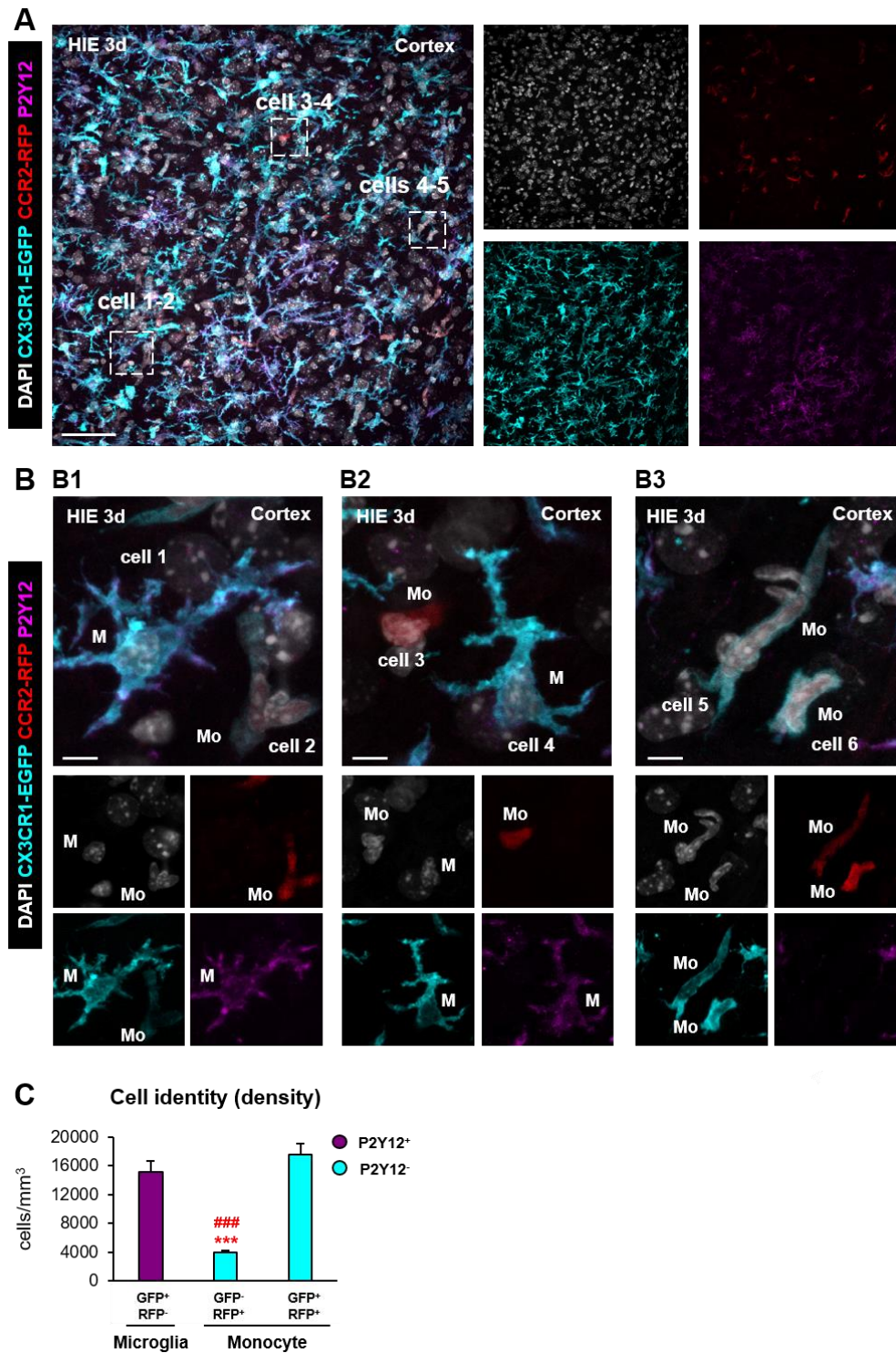
Figure 24. P2Y12 is a useful tool to discriminate microglia from peripheral monocytes in the adult brain after HIE. [A] Representative confocal z-stack of the DG of 3 month (3m) CX3CR1-GFP CCR2-RFP mice at 3d under hypoxia-ischemia conditions (HIE). Cell nuclei were visualized with DAPI (in white), microglia (CX3CR1-GFP1+, in cyan), and monocytes (CCR2-RFP+, in red). Expression of P2Y12 is shown in magenta. [B] Representative confocal z-stack from the septal DG of a HIE-treated mouse at 3d showing a P2Y12 expression (in magenta) in GFP+ microglia (cell 1 and cell 4, M)[B1, B2] and GFP- monocytes(cell 3, Mo)[B3]. [C] Density of microglia (GFP+ RFP-) and monocytes (GFP- RFP+ and GFP+ RFP+ cells/mm3) expressing P2Y12 in the cortex at 3d after HIE treatment. Bars represent mean ± SEM (standard error of
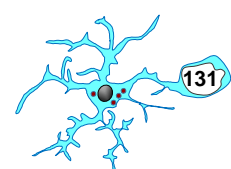
the mean). The expression of P2Y12R on microglia (GFP⁺ RFP⁻) and monocytes (GFP⁻ RFP⁺; GFP⁺ RFP⁺) **[C]** *was analyzed using 1-way ANOVA and Holm-Sidak was used as posthoc test. (* and #) One symbol indicates p<0.05, two p<0.01, and three p<0.001 (vs GFP⁺ RFP⁻ and GFP⁺ RFP⁺ cells, respectively). Only significant effects are shown. In* **[C]**, *n=3 per group (control and HIE at 1d and 3d). Scale bars=50μm* **[A]**, *10μm* **[B]**; *z=12μm* **[A]**, *10μm* **[B1-B2]**, *13μm* **[B3]**.

Next, we focused on phagocytosis executed by invading monocytes **(Fig. 25)**. We found that RFP⁺ monocytes engulfed a small proportion of apoptotic cells compared to microglia at 3d after HIE (10±8% by monocytes and 30±9% by microglia)**(Fig. 25A, B)**. Contrary to postnatal HIE, we did not observe dead cells phagocytosed by RFP⁺/GFP⁺ monocytes, in spite of the fact that the proportion of these double-positive cells were similar compared to P9 HIE **(Fig. 16)**. Thus, our data showed that the **microglial phagocytosis response was reduced as early as 1d after HIE and was not compensated by peripheral monocyte phagocytosis**.
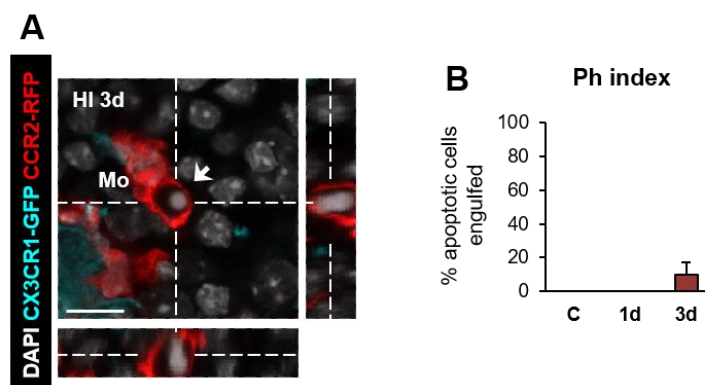
Figure 25. Adult microglial phagocytosis impairment is not compensated by monocytes. [A] Orthogonal projection of a confocal z-stack from the DG of a HIE-treated mouse at 3d showing an apoptotic cell phagocytosed by a monocyte (CCR2-RFP⁺, in red; Mo). [B] Monocyte Ph index in the septal DG (% of apoptotic cells engulfed by monocytes). Bars represent mean ± SEM. In [B], n=5 (control), n=3 (at 1d) and n=6 (at 3d). Scale bars=20μm [A]; z=12μm [A].

In parallel to the phagocytosis of apoptotic cells we also found some cases of phagoptosis **(Fig. 26)**. While in control conditions this phenomenon was not detected, we found some evidences of phagoptosis at 1 and 3d after HIE, and was predominantly executed by the microglial soma ("apposition" mechanism)**(Fig. 26A1)**. We observed few non-apoptotic cells engulfed by RFP⁺/GFP⁺ monocytes **(Fig. 26A2)**, although it occurred in a very low rate compared to microglial phagoptosis **(Fig. 26B)**. Interestingly, we also identified sporadic event of engulfment of viable in the cortex but also apoptotic monocytes in the hilus at 3d after HIE **(Fig. 26C, D)**. These observations might explain why the number of monocytes gradually decreased after 3d in HIE [Umekawa et al.,
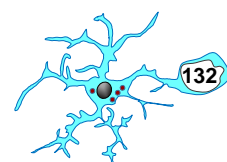
2015]. In fact, neutrophils can be phagocytosed by microglia after pMCAo [Otxoa-de-Amezaga et al., 2019], suggesting that microglia could contribute to elimination of several populations of myeloid cells from the brain parenchyma. Altogether, our results showed that **phagoptosis occurred in parallel to microglial phagocytosis impairment**.
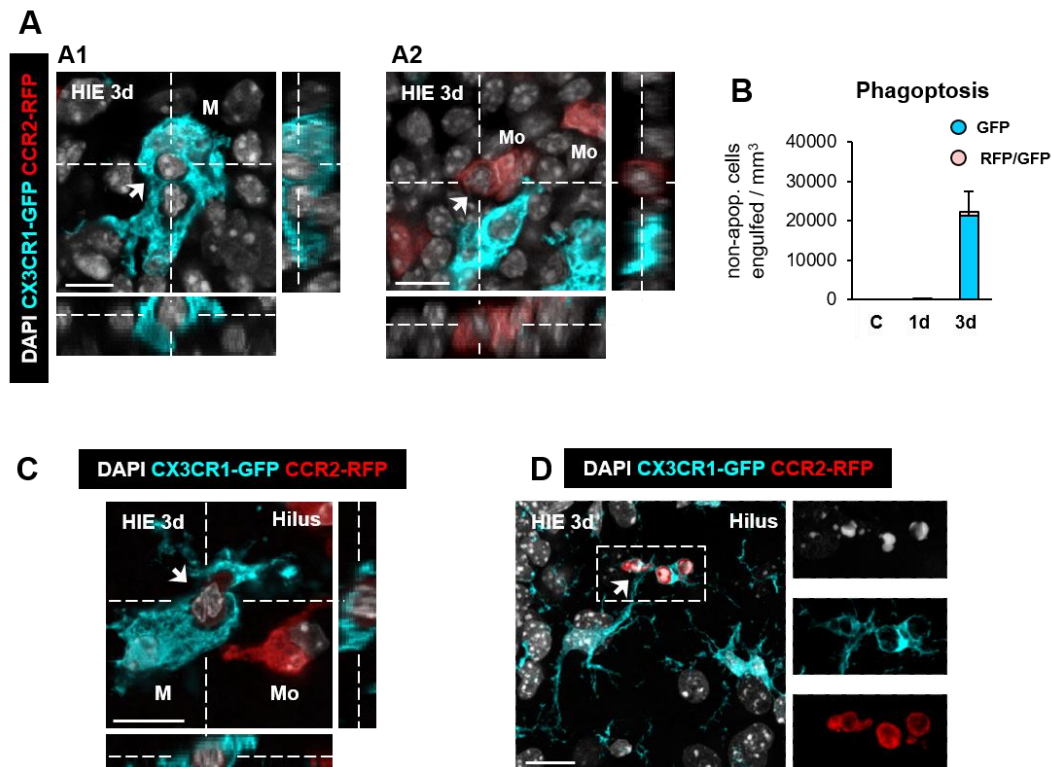
Figure 26. Adult microglial phagocytosis impairment is accompanied by phagoptosis. [A] *Orthogonal projection of non-apoptotic cell showing its complete engulfment by microglia (CX3CR1-GFP+, in cyan; M)[A1] or peripheral monocytes expressing GFP signal (CX3CR1-GFP CCR2-RFP+, in light red; Mo)[A2] at 3d after HIE. [B] Density of engulfed non-apoptotic cells in the septal DG (in cells/mm³) in control and HIE treatment. Phagoptosis was not detected (nd) in control mice. [C] Representative confocal z-stack from the hilus a HIE-treated mouse at 3d showing an apoptotic monocyte (arrow, Mo) engulfed by microglia (fms-EGFP+, in cyan; M). [D] Orthogonal projection of a confocal z-stack from the hilus a HIE-treated mouse at 3d showing a non-apoptotic monocyte (arrow, Mo) phagocytosed by microglia (fms-EGFP+, in cyan; M). Bars represent mean ± SEM (standard error of the mean). The effect of HIE on phagoptosis [B] was analyzed using Student´s t test. To comply with homoscedasticity, some data were Log_{10+1} [B] transformed. Only significant effects are shown. In [B], n=5 (control), n=3 (at 1d) and n=6 (at 3d). Scale bars=20µm [A], 20µm [C], 20µm [D]; z=10.5µm [A], 12µm [C], 15µm [D].*
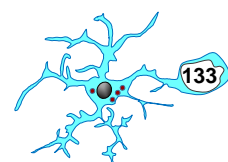
6.2.3 Optimization of a model of tMCAo to study the effect of stroke on microglial phagocytosis

The above results from HIE led us to wonder whether the efficiency of microglial phagocytosis was also impaired in other models of stroke. To this aim, we challenged microglia to an in vivo model of adult tMCAo, in which the Middle Cerebral Artery (MCA) is temporarily occluded. tMCAo is one of the models that most closely simulates the complex pathophysiology of human ischemic stroke. To evoke this detrimental scenario, we optimized and implemented in our lab the intraluminal filament technique [Koizumi et al., 1986; Longa et al., 1989]**(Fig. 27)**, in which a monofilament is advanced into the Internal Carotid Artery (ICA) until it occludes the origin of the MCA **(Fig. 27A, B)**. Although simple in theory, the MCAo technique required months of practice not only to master the surgical skills necessary to success but also to explore the many variables that impact the area and volume of the resulting ischemic injury to the brain. These include the physical properties of the chosen monofilament such as the diameter and material [Shimamura et al., 2006; Tsuchiya et al., 2003], occlusion and recovery time [Harada et al., 2005; Liu et al., 2009a], temperature during and post-surgery [Memezawa et al., 1992], mouse strain [Maeda et al., 1999], variation in cerebrovasculature between animals [McColl et al., 2004], sex [Alkayed et al., 1998], and age [Sutherland et al., 1996], among many others.

Taking into account these variables, we first focused on the type of monofilament **(Fig. 27C)**. Initially, we used a traditional 2 cm-long, nylon filament with a bulbous tip end of 20mm diameter (F1)**(Fig. 27C1)**. This filament occludes the MCA but not the Anterior choroidal Artery (AchA), which is the main artery irrigating the hippocampus [El Amki et al., 2015]. To obtain a more consistent hippocampal ischemia we used a second filament (F2), a 3cm-long, silicon coated silk with an extended tip of width of 9-10mm and 21mm diameter **(Fig. 27C2)**. This filament blocks not only the AchA but also the Lateral hypothalamic Artery (LHA) and Ventral thalamic Artery (VTA), which are small arteries originating from the ICA and irrigate the thalamus and hypothalamus [El Amki et al., 2015]**(Fig. 27B)**.

We also considered as an important point the mouse strain subjected to tMCAo **(Fig. 27D)**. Because MCAo conditions led to monocyte recruitment into the lesioned brain areas [Fang et al., 2018; Garcia-Bonilla et al., 2016; Wattananit et al., 2016], we explored the phagocytic contribution of these cells compared to resident microglia. For that purpose, we first used fms-EGFP CCR2$^{RFP/+}$ double transgenic mice (strain 1), in which microglia and peripheral monocytes expressed the GFP and RFP protein, respectively
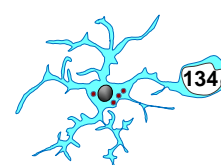
(Fig. 27D1). Additionally, we used fms-EGFP mice (strain 2), in which both macrophage populations (microglia and monocytes) express the GFP reporter [Sasmono et al., 2003; Sierra et al., 2007]**(Fig. 27D2)**. Furthermore, we took into account another crucial aspect to perform the tMCAo model such as animal sex. Because stroke is a sexually dimorphic pathology, and females show a less severe infarcts compared to males [Alkayed et al., 1998; Li et al., 1996], all surgeries were performed in adult male mice (2-3m).
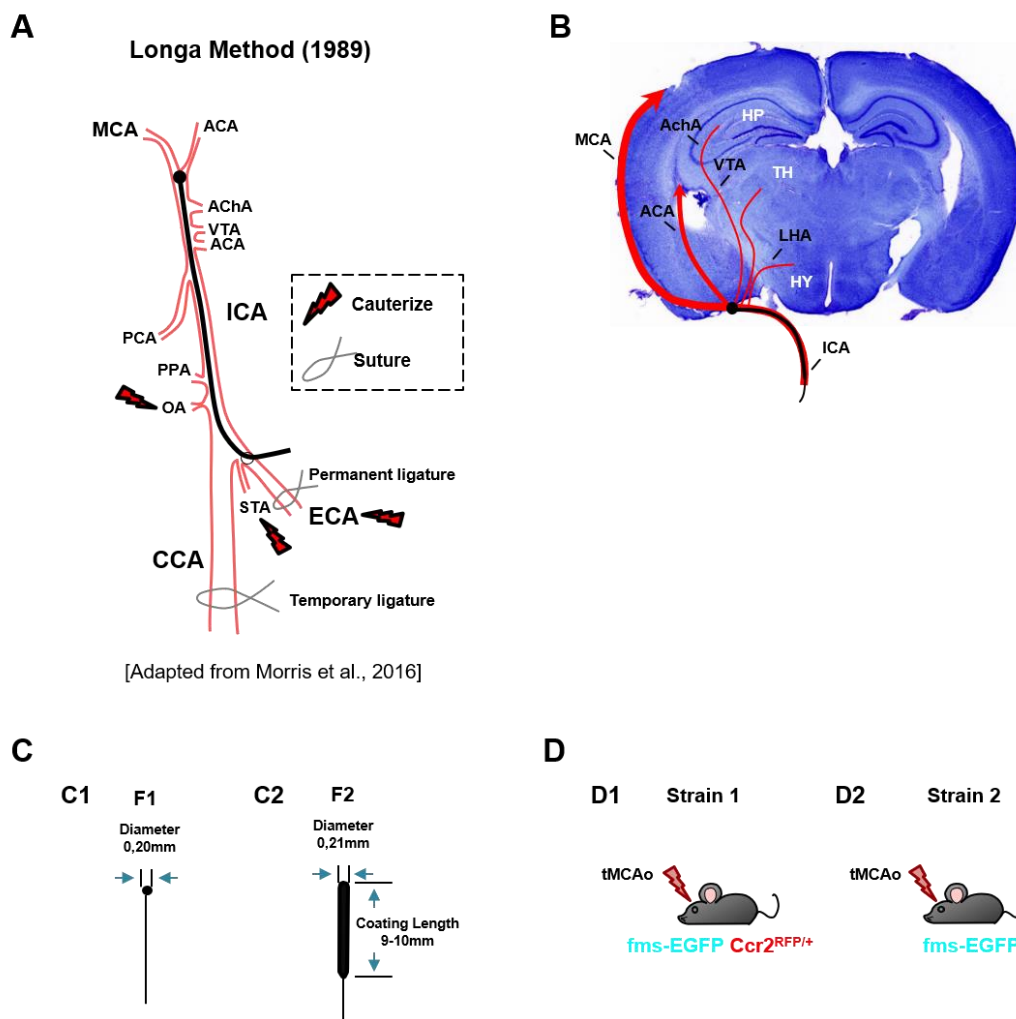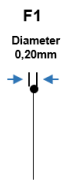
Figure 27. Mouse model of transient Middle Cerebral Artery occlusion (tMCAo) based on the Longa method. [A] *Method of the intraluminal filament into the MCA described by* [Longa et al., 1989]*. Common Carotid Artery [**CCA**], External Carotid Artery [**ECA**], Internal Carotid Artery [**ICA**], Middle Cerebral Artery [**MCA**], Anterior choroidal artery [**AChA**], Hypothalamic artery [**HTA**], Ventral thalamic artery [**VTA**], Anterior Carotid Artery [**ACA**], Superior thyroid artery [**STA**], Posterior Cerebral Artery [**PCA**], Pterygopalatine artery [**PPA**], Occipital artery [**OA**]. Drawing modified from* [Morris et al., 2016b]*. [B] Coronal slice with cresyl violet showing the areas irrigated by the MCA. [C] Filaments used to optimize our tMCAo model. The classical (F1)[C1] and (F2)[C2]. [D] Mouse strain subjected to tMCAo. Strain 1 (fms-EGFP CCR2$^{RFP/+}$)[D1] and strain 2 (fms-EGFP)[D2].*
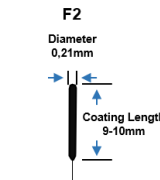
In addition to monofilament, mouse strain, and gender we also contemplated other details that could affect the optimization and reproducibility of our model: 1, age (in months, m); 2, proportion of mice with relative cerebral blood flow (CBF) drop of >70% and subsequent MCA reperfusion; 3, occlusion time (in min); 4, mortality and survival (% of mice); 5, existence of additional collateral branches of the arteries; 6, recovery time (h, d); 7, proportion of mice with macroscopic hippocampal damage; and 8, proportion of mice with microscopic hippocampal damage. In **Table 2** we summarize the results obtained after use F1 and F2 to occlude the MCA in fms-EGFP CCR2$^{RFP/+}$ and fms-EGFP mice.

Strain 1 — ♂ fms-EGFP / Ccr2$^{RFP/+}$ (tMCAo)
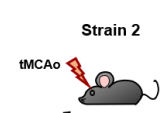
	F1		F2		
1. Age (month, m)	2-3m		2-3m		
2. Mice with a relative cerebral blood flow (CBF) drop of >70%, and reperfusion	n$_{Total}$=5/9 (56%); nMCAO=5		n$_{Total}$=10/17 (60%); nMCAo=10		
3. Occlusion time (min)	60min n=4	90min n=1	45min n=1	60min n=8	90min n=1
4. % Mortality (M); %Survival (S)	n$_M$=0/5 (0%); n$_S$=5/5 (100%)		n$_M$=6/10 (60%); n$_S$=4/10 (40%)		
5. Additional collateral branches of the arteries	n=3/5 (60%)		n=8/10 (80%)		
6. Recovery time (h, d)	1d n=4	3d n=1	6h n=1	1d n=2	3d n=1
7. Macroscopic hippocampal damage	1d	3d	6h-1d-3d n=0/4 (0%)		
8. Microscopic hippocampal damage	1d n=1/4 (25%)	3d n=0/1 (0%)	6h-1d n=0/3 (0%)	3d n=1/1 (100%)	

Strain 2 — ♂ fms-EGFP (tMCAo)

	F1		F2			
1. Age (month, m)	2-3m		2-3m			
2. Mice with a relative cerebral blood flow (CBF) drop of >70%, and reperfusion	n$_{Total}$=2/3 (67%); nMCAO=2		n$_{Total}$=16/17 (94%); nMCAo=16			
3. Occlusion time (min)	60min n=1	90min n=1	60min n=15		90min n=1	
4. % Mortality (M); %Survival (S)	n$_M$=0/2 (0%); n$_S$=2/2 (100%)		n$_M$=2/16 (12.5%); n$_S$=14/16 (87.5%)			
5. Additional collateral branches of the arteries	n=0/3 (0%)		n=0/16 (0%)			
6. Recovery time (h, d)	3d n=2		6h n=3/14 (21%)	1d n=5/14 (36%)	3d n=3/14 (21%)	7d n=3/14 (21%)
7. Macroscopic hippocampal damage	3d		6h n=2/3 (67%)	1d	3d	7d
8. Microscopic hippocampal damage	3d n=1/2 (50%)		6h n=3/3 (100%)	1d n=3/5 (60%)	3d n=3/3 (100%)	7d n=3/3 (100%)

Table 2. Optimization of transient Middle Cerebral Artery occlusion (tMCAo) model. Summary of variables in tMCAo model. Two different mouse strain (fms-EGFP CCR2-RFP vs fms-EGFP) and filaments (F1 vs F2) were used to optimize our model. This table summarizes: **1**, gender and age (month, m). **2**, "n" total and "n" MCAo (with a CBF flow>70% measured by Laser-Doppler. Animals in which MCA was occluded but not reperfused were removed from the analysis. *3, presence of additional collateral branches located in the external carotid artery (ECA) and/or internal carotid artery (ICA).* **4**, occlusion time (min): 45min (▢), 60min (▢) and 90min (▢). *5, mortality and survival rates.* **6**, *recovery time: 6h (▢), 1d (▢), 3d (▢) and 7d (▢)*. **7**, *macroscopic hippocampal damage (determined by cresyl violet staining).* **8**, *microscopic hippocampal damage (apoptosis determined by DAPI staining).*

In order to explain our results as clearly as possible, we divided results shown in **Table 2** in four parts:

Part I: F1 to occlude MCA in fms-EGFP / CCR2$^{RFP/+}$ mice

We subjected mice to tMCAo (n=9) and all of them showed a successful occlusion for 60min (n=4) and 90min (n=1). Nonetheless, only 56% of the animals had MCA reperfusion, determined by Laser-Doppler **(Fig. 28A)**. A possible interpretation of these observations could be that the filament induced the formation of thrombus in the MCA, ACA and/or ICA leading to failed reperfusion after tMCAo [Lin et al., 2013].

In addition, we noticed that all mice had problems to breathe (hyperventilation) after MCA reperfusion. The respiratory issue persisted for 30-45min during the post-operatory period and, then, animals slowly recovered from anesthesia (presence of urine) and started to move. This scenario could be related to the fact that the ischemic stroke conditions altered the respiratory pattern, inducing lung damage and inflammation [Samary et al., 2018]. Despite this problem, the mortality (M) rate was 0% in these experiments.

Moreover, we also observed that 60% of mice with MCA occluded had collateral circulation in anastomosis characterized by the presence of tiny branches in the ICA close to the CCA bifurcation **(Fig. 28B)**. We speculate that these alterations may contribute to altered blood flow in the arteries. But, nonetheless, an in-depth analysis should be done to understand the contribution of these additional branches to the cerebrovasculature system under tMCAo conditions.

After MCA reperfusion, animals were sacrificed at 1d (n=4) and 3d (n=1). At both time points, we observed that the brain areas affected were mainly the cortex and striatum, in agreement with previous studies [Carmichael, 2005; Morris et al., 2016b]. However, hippocampal damage was not consistent. We analyzed macroscopic damage by cresyl violet staining, a standard histological stain for neurons and common tool to measure infarct volume after stroke [Rousselet et al., 2012; Türeyen et al., 2004]**(Fig. 28C)**; and microscopic damage by presence of apoptotic cells (pyknotic/karyorrhectic nuclei, with DAPI). At both levels, we found that only 25% of tMCAo-treated mice presented hippocampal neuronal degeneration **(Fig. 28D)**. The hippocampus is in fact not supplied by the MCA, but some studies revealed that this brain area is damaged after stroke as well as thalamus and hypothalamus, even though they both are neither irrigated by MCA [Ansari et al., 2011; Hata et al., 1998; Kitagawa et al., 1998; Morris et al., 2016b]. Based on our data and studies previously published, the low efficiency to
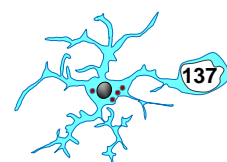
block the hippocampus could be related to the suture coating size, the filament insertion depth and/or in vivo formation of thrombus in the ICA [Lin et al., 2013].

Therefore, our results suggested that **F1 occluded the MCA with low mortality rate in fms-EGFP / CCR2$^{RFP/+}$ mice but only few animals had a successful reperfusion and it was not useful to induce injury in the hippocampus**.
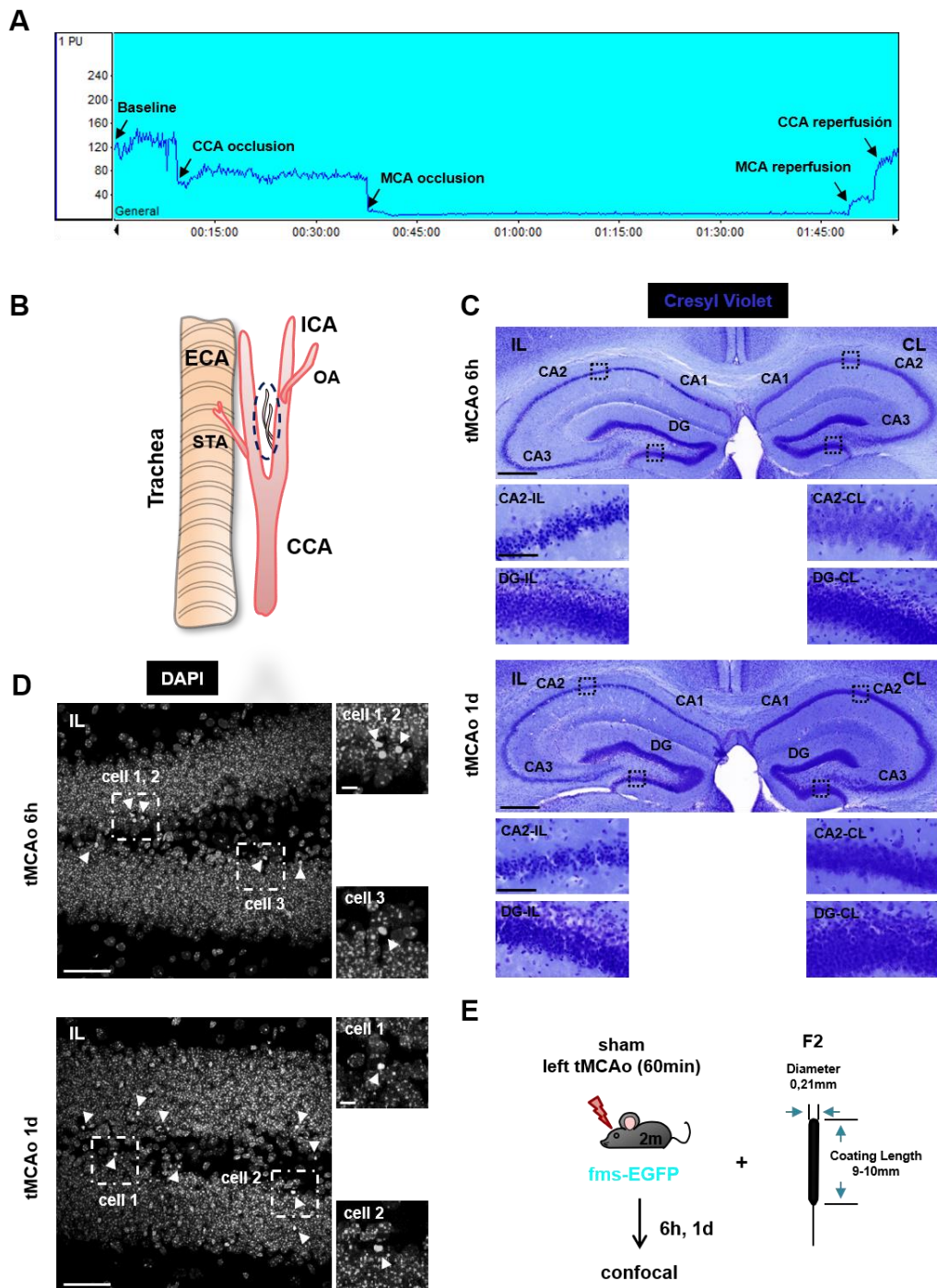
Figure 28. Analysis of the hippocampal damage after tMCAo. [A] *Laser Doppler signal graph showing CBF in the territory supplied by MCA during baseline, CCA and MCA occlusion, and reperfusion. Successful MCA occlusion, determined by CBF >70% drop from the baseline, recovers after reperfusion. The values*

*are expressed in arbitrary Perfusion Units (PU). **[B]** Cartoon representing the collateral branches in the ICA close to the CCA bifurcation observed in fms-EGFP / CCR2$^{RFP/+}$ mice. **[C]** Representative slide scanner image of cresyl-violet stained coronal hippocampi (ipsilateral (IL) and contralateral (CL)) in a 2m fms-EGFP mouse after tMCAo at 6h and 1d. The different hippocampal areas (DG, CA) are indicated. The inserts show representative images of CA2 and DG after tMCAo. **[D]** Representative confocal z-stack of the ipsilateral DG of a 2m fms-EGFP mice after tMCAo at 6h and 1d. Apoptotic nuclei were detected by pyknosis/karyorrhexis (in white, DAPI, arrowhead). **[E]** Final tMCAo experimental design selected to quantify microglial phagocytosis in mice. Scale bars=500μm [tMCAo 6h and 1d; **C**], 200μm [tMCAo 6h and 1d, down panel; **C**] 50μm [tMCAo 6h and 1d; **D**]; z=14.7μm [tMCAo 6h and 1d; **D**].*

Part II: F2 to occlude MCA in fms-EGFP / CCR2$^{RFP/+}$ mice

We performed a second set of experiments using filament F2, whose extended tip allowed to block not only the MCA but also three small deep arteries originating from the ICA such as AchA, Lateral hypothalamic Artery (LHA) and/or Ventral thalamic Artery (VTA), which supply the hippocampus, thalamus and hypothalamus, respectively [El Amki et al., 2015]**(Fig. 27B)**.

We found that 60% of fms-EGFP / CCR2$^{RFP/+}$ mice (n=10) showed a successful occlusion for 45min (n=1), 60min (n=8) and 90min (n=1), and posterior reperfusion of the MCA. Regarding the mortality (M) rate, we observed that 60% of mice did not survive the surgery. Moreover, we identified that 80% of mice with MCA occluded had variations in the cerebrovasculature system. After reperfusion, animals were sacrificed at 6h (n=1), 1d (n=2) and 3d (n=1). However, we observed that the only mouse subjected to tMCAo for 3d showed injury in the hippocampus. These results were not expected, as the physical properties of F2 were adapted to block the AchA, which irrigates the hippocampus. These observations could be related to unsuccessful occlusion of the AchA due to irrigation performed by compensatory collateral branches to the areas supplied by AchA.

These results suggested that **F2 effectively occluded the MCA but with higher mortality rate than F1 in fms-EGFP / CCR2$^{RFP/+}$, and was not useful to evoke injury in the hippocampus**.

Based on the data obtained from the fms-EGFP / CCR2$^{RFP/+}$ mice with F1 and F2, this mouse strain was not a great tool to induce hippocampal damage. To solve this issue, we performed the surgeries in our fms-EGFP mice and to be consistent with the previous data, we used both F1 and F2 monofilaments **(Table 2)**.
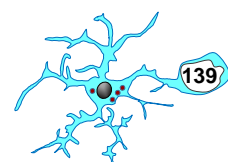
Part III: F1 to occlude MCA in fms-EGFP mice

We observed a similar percentage of mice (67%) with an efficient occlusion for 60min (n=1) and 90min (n=1), and posterior reperfusion of the MCA, compared to the previous mouse strain with both filaments. Importantly, these animals did not show respiratory problems and in fact they recovered faster (5-10min after MCA reperfusion) compared to fms-EGFP / CCR2$^{RFP/+}$ strain. In addition, the mortality rate (M) as well as presence of additional collateral branches in the arteries was 0%. Animals were sacrificed at 3d after damage and 50% of them had damage in the hippocampus. These results suggested that **F1 successfully occluded the MCA with low mortality rate in fms-EGFP but was not useful to induce injury in the hippocampus**. Due to that, we subjected mice to tMCAo using the F2.

Part IV: F2 to occlude MCA in fms-EGFP mice

In this model, we found that 94% of mice (n=16) showed a successful occlusion for 60min (n=15) and 90min (n=1) in fms-EGFP mice with F2. The mortality (M) rate was around 12.5%, the lowest value compared to the rest of the models. We did not find variations in the cerebrovasculature anatomy in any of mice operated in contrast to fms-EGFP / CCR2$^{RFP/+}$ mice. Animals were sacrificed at different time points: 6h (n=3); 1d (n=5); 3d (n=3), and 7d (n=3). Importantly, we observed that the proportion of mice with damage in the hippocampus increased compared to previous experiments. At macroscopic level, the proportion of injury was 67%, 60%, 100%, and 100% (at 6h, 1d, 3d, and 7d, respectively). Similar data was found at microscopic level: 100%, 60%, 100%, and 100% of animals with hippocampal damage (at 6h, 1d, respectively). These results showed **that F2 effectively occluded the MCA with low mortality rate in fms-EGFP mice, and induced damage in the hippocampus**. For this reason, we chose a 60 min occlusion with the F2 filament in fms-EGFP mice as a model of tMCAo and excluded from the analysis of phagocytosis efficiency those mice that did not have hippocampal damage **(Fig. 28E)**. In this PhD Thesis we only included the analysis of phagocytosis at 6h and 1d after tMCAo because tissue damage induced at later time points was very severe and samples could not be analyzed.

6.2.4 tMCAo leads to a sensory and motor coordination dysfunction

Sensorimotor neurological deficits are common sequelae of tMCAo and typically resolve, though at times incompletely [Bolognini et al., 2016]. To understand the magnitude of these neurological impairments evoked by our tMCAo model (F2, 60min occlusion, fms-EGFP mice), we subjected mice to the Pole test, one of the most
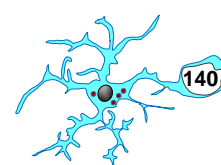
commonly used test to assess motor coordination dysfunction after stroke [Balkaya et al., 2013a; Linden et al., 2014]**(Fig. 29)**. In order to achieve an optimal level of performance and minimize the inter-individual, animals were trained for five days (one trial per day) before the surgery and then tested at 1h before sacrifice **(Fig. 29A)**. Briefly, animals were placed on top of a vertical pole and trained to turn around and descend the pole. Scoring started when the mice completely turned from head-up- to head-down (time to turn, TT) and descended to reach the floor (time to descend, TD)**(Fig. 29A)**.

During the training period, all mice achieved TT and TD before the maximum allowed time (120s) **(Fig. 29B-E)**. After surgery, no apparent issues were found in sham-treated animals to finish the test at any time points studied (6h-1d). However, mice subjected to tMCAo could not cling to the pole. As a consequence, none animals were not able to finish either the turn or the descend from the pole (TT and TD>120s)**(Fig. 29B-E)**. These data suggested that **tMCAo led to a motor coordination impairment**.
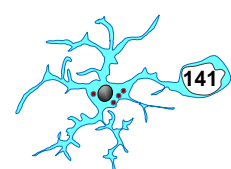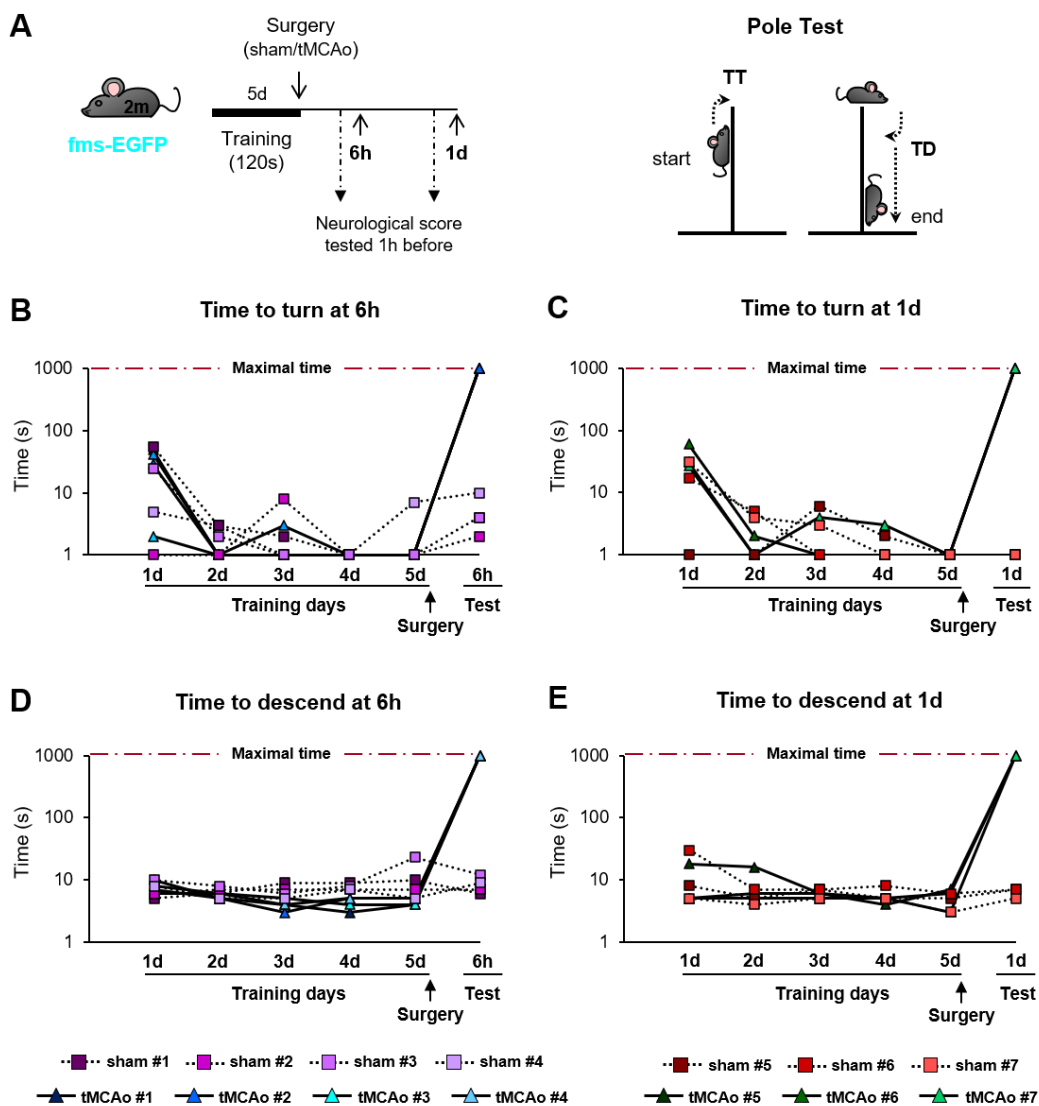
Figure 29. Pole test reveals motor coordination deficits after tMCAo. [A] Experimental design and schematic representation of pole test performance, representing the time to turn from head up to head down (TT) and time to descend and reach the floor (TD). [B, C] TT in sham and tMCAo-treated mice at 6h and 1d. [D, E] TD in sham and tMCAo-treated mice at 6h and 1d. Data represent the total time (in seconds, s) of each sham and tMCAo-treated mouse trained daily for 5 days (d) before surgery and 6h and 1d after surgery. The dashed dark red line indicates the maximal time (120s, in logarithmic scale) to perform the test. Sham mice are indicated by a square and dotted line (▪*), and tMCAo mice are indicated by a triangle and continuous line (▲). In [B, D], n=4 (sham and tMCAo at 6h). In [C, E], n=3 (sham and tMCAo at 1d).*

In order to confirm these data, we used the Adhesive Removal test, another routine strategy to assess sensorimotor dysfunction after stroke [Balkaya et al., 2013b; Bouet et al., 2009]**(Fig. 30)**. As above, mice were trained for five days (one trial per day) before surgery and then tested at 1h before sacrifice **(Fig. 30A)**. Basically, two adhesive tapes of defined size and different colors (blue and green) were applied with equal pressure in each mouse paw, which they naturally removed from their body by grooming. Tactile responses were measured by scoring the time to contact (TC) and remove (TR) tapes, which allowed us separated out sensory vs motor deficits [Montoya et al., 1991]**(Fig. 30A)**.

Prior to surgery, all animals performed the test under the maximum allowed time (120s) **(Fig. 30B-G)**. As an exception, a single mouse reached the maximum time to remove the tapes from the ipsilateral and contralateral paw on the third day of training, which could be related to a stressful situation due to the handling [Gouveia and Hurst, 2017]**(Fig. 30D, F)**. After surgery, sham-treated mice finished the test without issues at both time points studied (6h-1d)**(Fig. 30D, F)**. However, tMCAo led to a similar pattern of dysfunctional behavior previously described with the Pole test **(Fig. 29)**. This impairment was characterized by an inability to contact the tapes at 6h after damage **(Fig. 30D, F)**. Furthermore, some animals were not only able to contact but also removed one of the tapes from the ipsilateral or contralateral paw suggesting impairments in forelimb movement and coordination **(Fig. 30D, F)**. Overall, our results showed **a sensory and motor coordination deficit as early as 6h following tMCAo**.
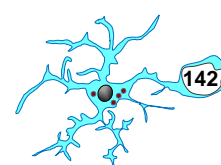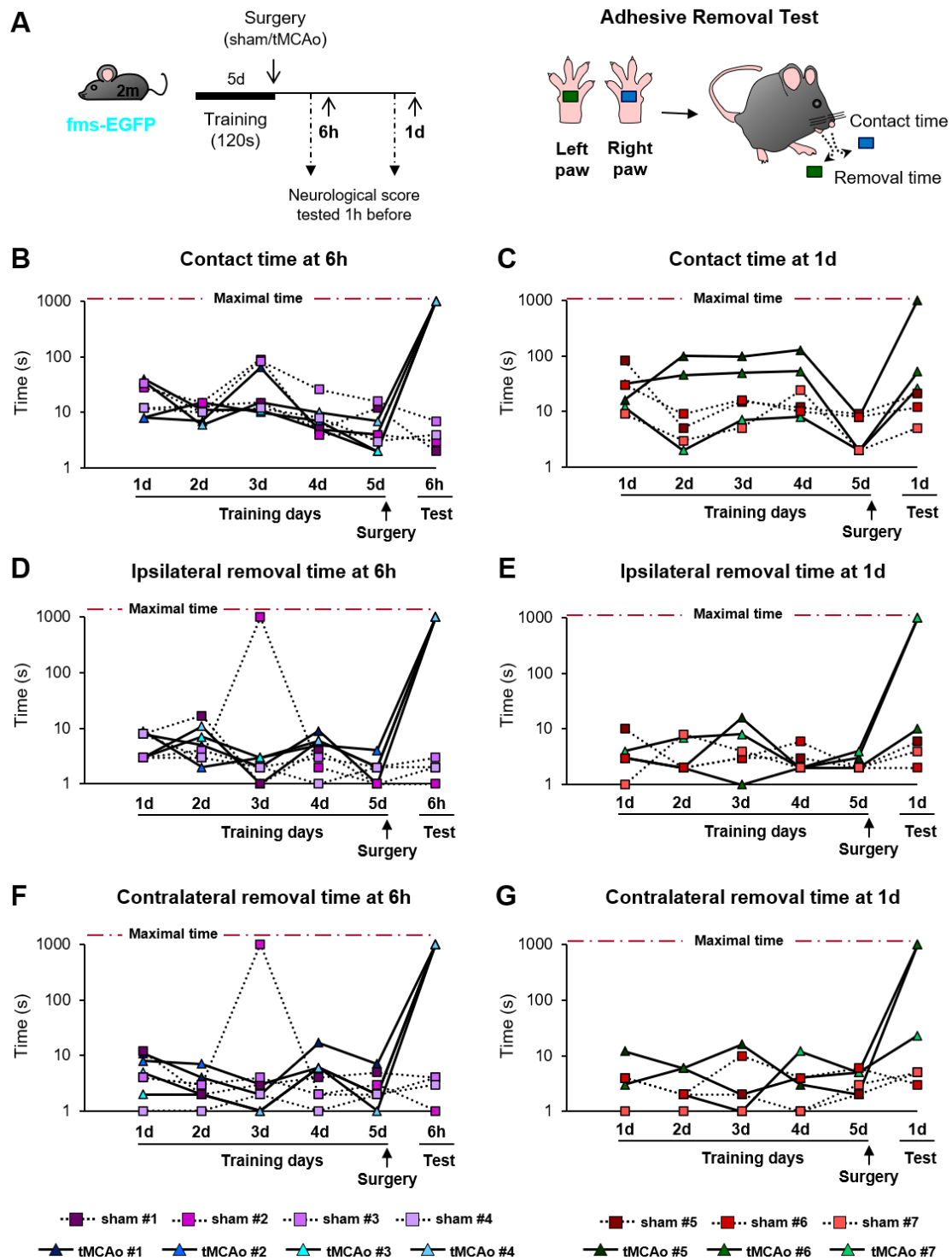
Figure 30. Adhesive removal test reveals somatosensory and motor coordination deficits after tMCAo. [A] Experimental design and schematic representation of adhesive removal test performance, representing the time to contact and remove each adhesive tape of each paw. **[B, C]** Contact time in sham and tMCAo-treated mice at 6h and 1d, respectively. **[D, E]** Ipsilateral removal time in sham and tMCAo-treated mice at 6h and 1d, respectively. **[F, G]** Contralateral removal time in sham and tMCAo-treated mice at 6h and 1d, respectively. Data represent the total time (in seconds, s) of each sham and tMCAo-treated mouse trained daily for 5 days (d) before surgery and 6h and 1d after surgery. The dashed dark red line indicates the maximal time (120s, in logarithmic scale) to perform the test. Sham mice are indicated by a

square and dotted line (▪▪▪), and tMCAo mice are indicated by a triangle and continuous line (▲). In [B, D], n=4 (sham and tMCAo at 6h). In [C, E], n=3 (sham and tMCAo at 1d).

6.2.5 Adult microglial phagocytosis disruption evoked by tMCAo conditions is not compensated by other resident cells with phagocytic potential, and is accompanied by phagoptosis

Once we had established our model and determined the impairment of sensory and motor coordination after tMCAo, we analyzed the phagocytic response at 6h and 1d following brain injury **(Fig. 31)**. First, we quantified the number of apoptotic cells (pyknosis/karyorrhexis) and microglial phagocytosis in the DG. We found that apoptosis significantly increased after tMCAo compared to sham, however, the Ph index dramatically decreased as early as 6h after damage **(Fig. 31A-D)**. Regarding phagocytosis, we also observed that the proportion of apoptotic cells engulfed by direct apposition to the microglial soma ("apposition" mechanism) were increased at 6h and 1d after tMCAo **(Fig. 31E)**. In addition, we found that many death cells were localized close to microglial processes but were not phagocytosed **(Fig. 31B)** suggesting defects in apoptotic cell recognition and/or microglial motility, similar to what we previously observed in KA-treated mice [Abiega et al., 2016]. Importantly, when we further explored the impairment of microglia in the DG, a decreased Ph capacity was observed after damage compared to sham mice, due to a reduced proportion of microglia with phagocytic pouches **(Fig. 31F, G)**, while the number of microglia remained unchanged **(Fig. 31H)**. As a result of the decreased Ph capacity, the Ph/A coupling ratio dramatically dropped **(Fig. 31I)**. Thus, these data showed that **microglial phagocytosis was uncoupled to apoptosis after tMCAo challenge**.
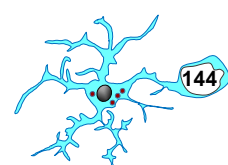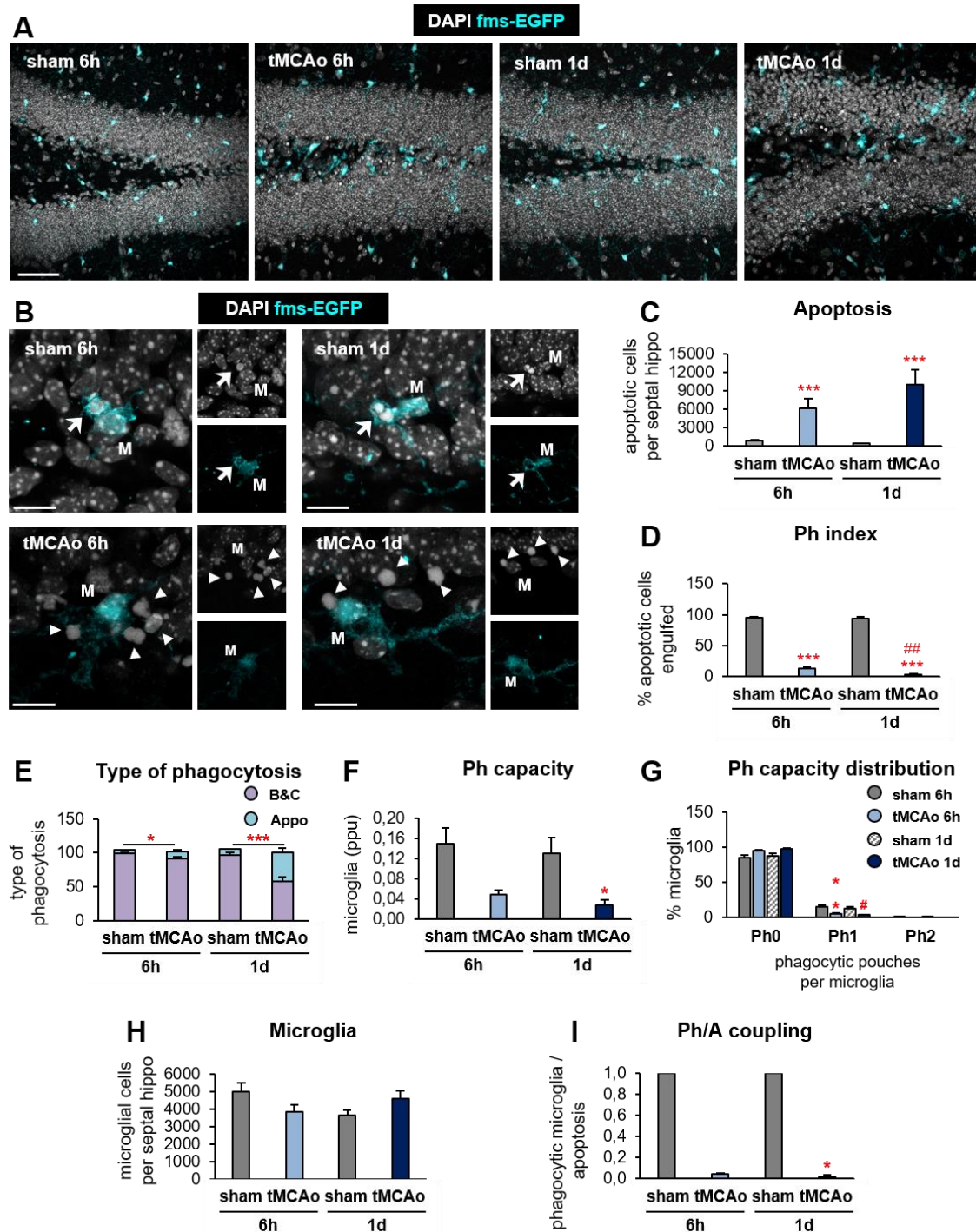
Figure 31. Microglial phagocytosis is impaired as early as 6h in an adult model of tMCAo. [A] *Representative confocal z-stacks of the DG of 2 month (2m) fms-EGFP mice at 6h and 1d after tMCAo. Cell nuclei were visualized with DAPI (in white) and microglia (fms-EGFP+, in cyan). [B] Representative confocal z-stacks from the septal DG of a sham and tMCAo-treated mice at 6h and 1d, showing an apoptotic cell phagocytosed by microglia (fms-EGFP+, in cyan; M). [C] Number of apoptotic cells per septal hippocampus in sham and tMCAo. [D] Ph index in the septal hippocampus (% of apoptotic cells engulfed by microglia). [E] Type of microglial phagocytosis (% of microglia) by "ball-and-chain" (B&C) or Apposition (Appo) mechanism. [F] Weighted Ph capacity (% of microglia with phagocytic pouches) in sham and tMCAo. [G] Histogram showing the Ph capacity of microglia (% of microglia with phagocytic pouches). [H] Number of*

*fms-EGFP+ microglia per septal hippocampus. **[I]** Ph/A coupling (in fold change) in the septal hippocampus. Bars show mean ± SEM. The effect of sham/tMCAo at 6h and 1d on apoptosis **[C]**, Ph index **[D]**, and microglia **[H]** was found using 2-way ANOVA. Significant interactions were found between the two factors (tMCAo treatment and time); therefore, data were split into two 1-way ANOVAs to analyze statistical differences due to the time after sham/ tMCAo at each time. Holm-Sidak was used as a posthoc test. To comply with homoscedasticity, some data were Log10$_{+1}$ transformed **[E, F, G, I]**. In the case that homoscedasticity was not achieved with a logarithmic transformation, data were analyzed using a Kruskal-Wallis ranks test, followed by Dunn method as a posthoc test **[E, F, G, I]**.* (* and #) represent significance compared to sham and/or tMCAo at 6h, respectively. *One symbol represents p<0.05, two p<0.01, and three p<0.001. Only significant effects are shown. In **[C, D, E, F, G, H, I]**, n=3 (sham at 6h), n=4 (sham at 1d), n=5 (tMCAo at 6h) and n=6 (tMCAo at 1d). Scale bars=50μm **[A]**, 14μm **[B]**; z=18.9μm **[A]**, 16μm **[B]**.*

Next, we analyzed whether the impairment of phagocytosis could be compensated by phagocytic peripheral monocytes **(Fig. 32)**. To discriminate between microglia and monocytes, we used a P2Y12 antibody [Haynes et al., 2006; Mildner et al., 2017]. We quantified the proportion of GFP+ cells expressing this receptor in the DG at 6h and 1d after tMCAO **(Fig. 32A)**. We found that the majority of cells were resident microglia (P2Y12+ GFP+; 96±2% and 96±1% at 6h and 1d after tMCAo, respectively)**(Fig. 32B, C)**, demonstrating that the presence of monocytes was remarkably low, at least in early time points after tMCAo.

A

B

C
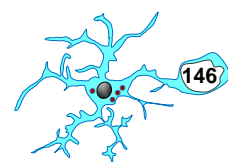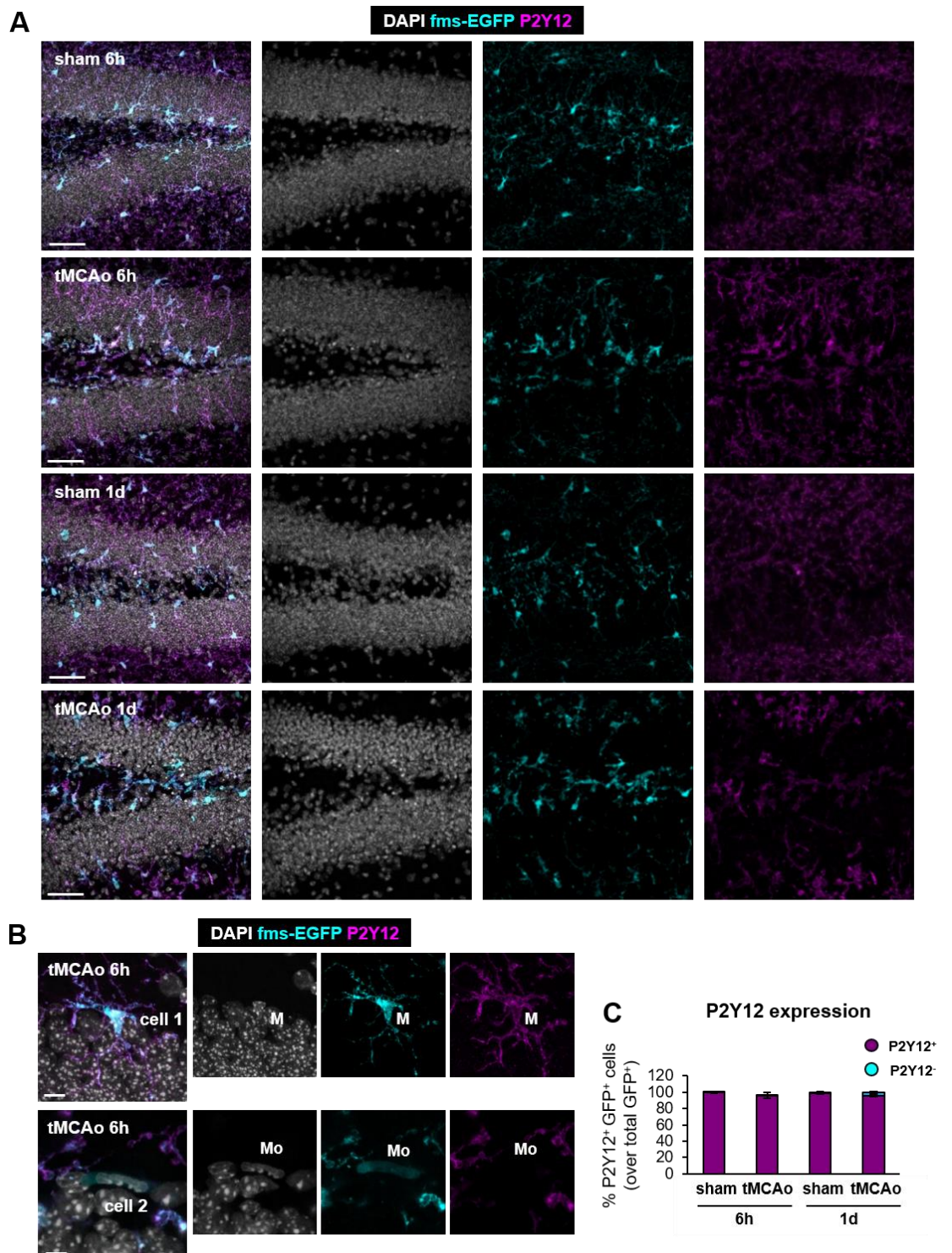
Figure 32. P2Y12 is a useful tool to distinguish microglia from peripheral monocytes in the adult brain after tMCAo. [A] *Representative confocal z-stacks of the DG of 2m fms-EGFP mice at 6h and 1d after sham and tMCAo. Cell nuclei were visualized with DAPI (in white) and microglia (fms-EGFP+, in cyan). Expression of P2Y12 is shown in magenta.* **[B]** *Representative confocal z-stack from the septal DG of a tMCAo-treated mouse at 6h and 1d showing P2Y12 expression in GFP+ microglia [cell 1, M] and not in presumptive monocytes [cell 2, Mo].* **[C]** *Percentage of GFP-labeled P2Y12 among the total number of GFP+ cells in the DG at 6h and 1d after sham and tMCAo treatment. Bars show mean ± SEM. The effect of tMCAo and time on P2Y12 expression* **[C]** *was analyzed using 2-way ANOVA. No significant interactions were found*
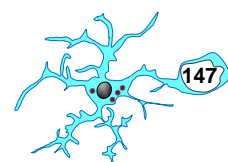
between the two factors. In [C], n=3 per group (sham/tMCAo at 6h and 1d). Scale bars=50μm [A], 10μm [B]; z=9.8μm [tMCAo at 6h, B], 6.3μm [tMCAo at 1d, B].

In addition, we used classical microglia/macrophages antibodies such as CD11b and CD45 as well as a recent specific microglial antibody named TMEM119 [Bennett et al., 2016](**Fig. 22**). As a strategy, we analyzed CD11b and CD45 expression together since it was described that microglia are CD11b$^+$/CD45^{low}, whereas peripheral macrophages are CD11b$^+$/CD45^{high} [Ford et al., 1995; Grabert et al., 2016; Zhang et al., 2002]. The pattern expression of these antibodies was not clear at 6h and 1d after tMCAo, and therefore, we could not use to discriminate microglia from peripheral macrophages (**Fig. 22A**). Regarding TMEM119 expression on microglia, we found that this antibody was downregulated as early as 6h after tMCAo (**Fig. 22B**), in agreement with previous reports [Honarpisheh et al., 2020]. Thus, our results proved that the **disruption of phagocytosis was not associated with peripheral monocytes**.
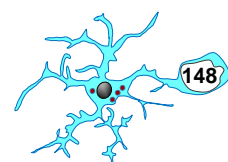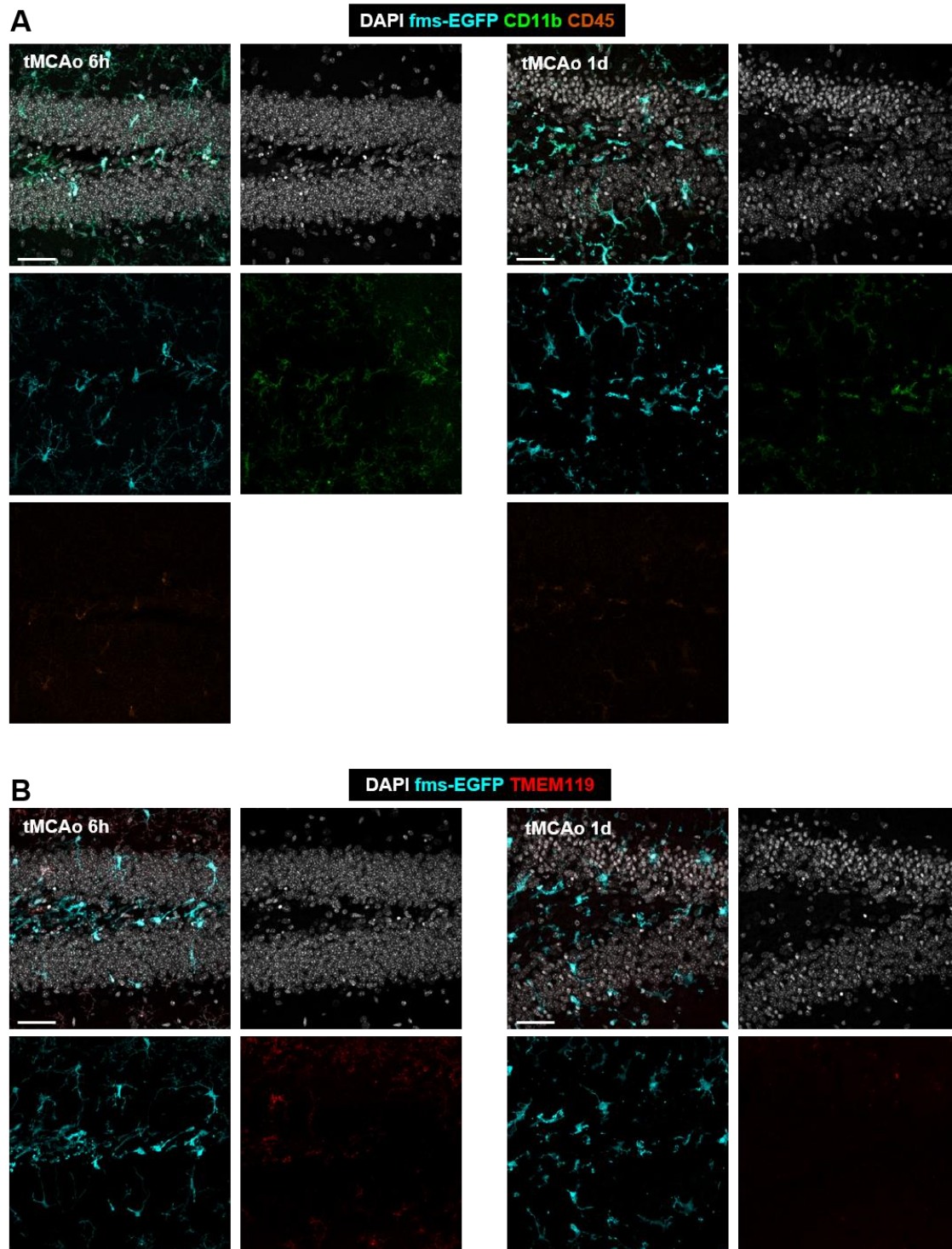
Figure 33. Expresion of TMEM119, CD11b, and CD45 after tMCAo. [A] *Representative confocal z-stacks of the DG of 2 month (2m) fms-EGFP at 6h and 1d after tMCAo. Cell nuclei were visualized with DAPI (white) and microglia (fms-EGFP⁺, in cyan) in combination with TMEM119 (in red). [B] Representative confocal z-stack of the DG of 2 month (2m) fms-EGFP at 6h and 1d after tMCAo. Cell nuclei were visualized with DAPI (in white), microglia (fms-EGFP⁺, in cyan), CD11b (in green), and CD45 (in orange). Scale bars=50μm [A, B]; z=25.9μm [tMCAo 6h, A], 23.8μm [tMCAo 1d, A], 30.1μm [tMCAo 6h, B], 23.8μm [tMCAo 1d, B].*

149

We then argued that microglial phagocytosis could be compensated by the recruitment of other resident cells with phagocytic potential, such as astrocytes [Magnus et al., 2002]**(Fig. 34)**. To test this hypothesis, we first identified astrocytes with glial fibrillary acid protein (GFAP), a well-known astrocytic marker [Middeldorp and Hol, 2011], and then quantified the proportion of apoptotic cells phagocytosed. Nonetheless, we did not find any dead cell engulfed by astrocytes, in spite of a study described that they become phagocytic after tMCAo [Morizawa et al., 2017]. This discrepancy between our data could be due to the authors analyzed phagocytosis at 3d compared to our study at 6h and 1d after tMCAo. Nonetheless, we found a few dead cells engulfed by neural stem cells (NSCs), who also express GFAP [Kronenberg et al., 2003] but are distinguished by a single apical process that expanded toward the molecular layer **(Fig. 34A)**. While this event was not either observed in sham or 6h after tMCAo, we found some dead cells engulfed by NSCs at 1d after damage, although the Ph index was remarkably lower compared to microglia (0.42±0.05% by NSCs vs 3.47%±1.10% by microglia)**(Fig. 34B)**. These results showed that **microglial phagocytosis impairment was not compensated by astrocytic or NSCs with phagocytic potential**.

Apart from phagocytosis of apoptotic cells, we also observed some cases of phagoptosis (i.e., engulfment of non-apoptotic cells)[Brown and Neher, 2014]. While in sham conditions this phenomenon was not detected, we found some evidences of phagoptosis at 6h and 1d after tMCAo, and was executed by both microglial "B&C" and "apposition" mechanisms **(Fig. 34C-E)**. Altogether, our data showed that **phagoptosis occurred in parallel to microglial phagocytosis impairment**.
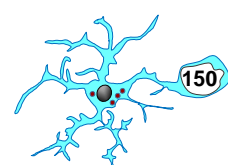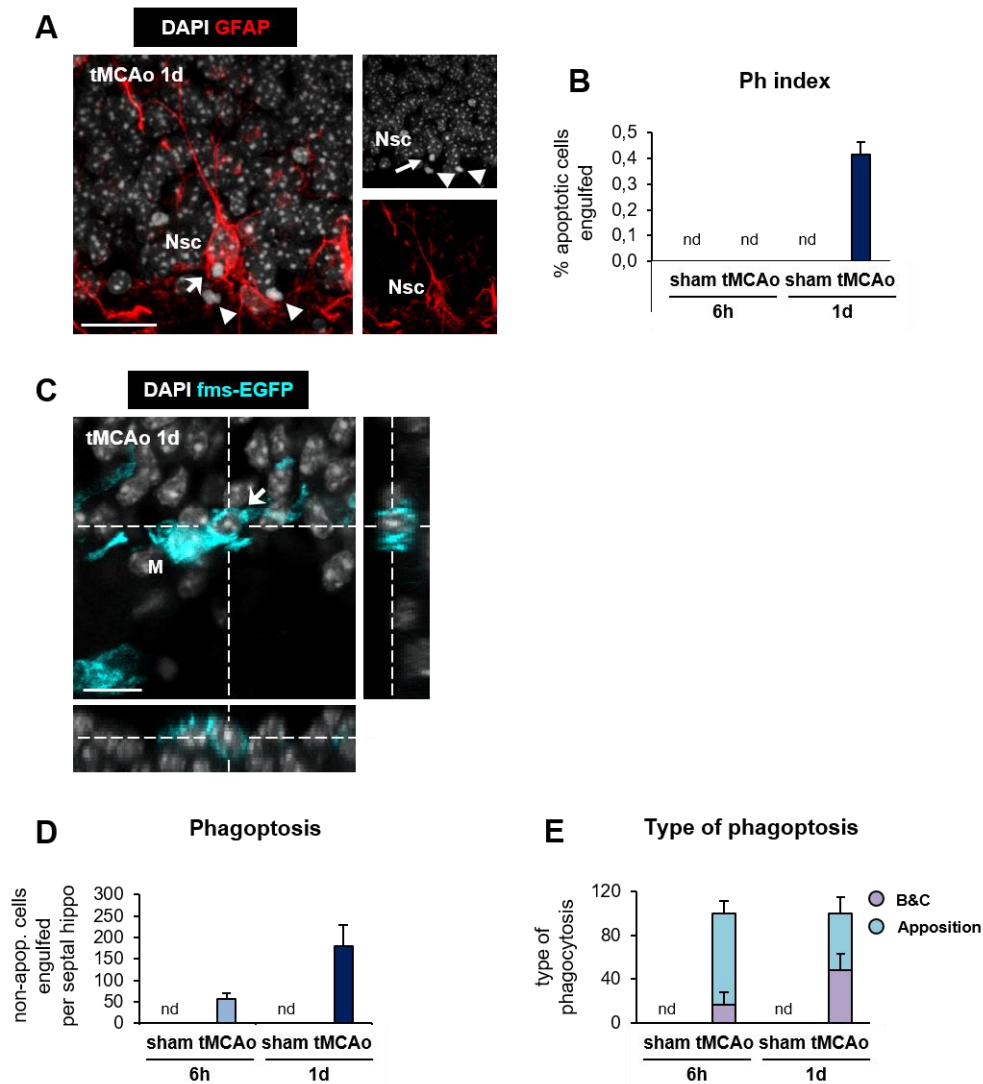
Figure 34. Adult microglial phagocytosis impairment induced by tMCAo is not compensated by phagocytosis of other cell types, and is accompanied by phagoptosis. [A] *Representative confocal z-stack of an apoptotic cell (pyknotic/karyorrhetic, with DAPI, in white) phagocytosed (arrow) or not (arrowhead) by neural stem cell (NSC) labeled with GFAP, (red in the DG of tMCAo-treated mice at 1d.* **[B]** *NSC Ph index in the septal hippocampus (% of apoptotic cells engulfed by NSC). Apoptotic cells engulfed were not found in sham mice. nd, not-detected.* **[C]** *Orthogonal projection of non-apoptotic cell showing its complete engulfment by microglia (fms-EGFP[+], in cyan; M) at 1d after tMCAo.* **[D]** *Density of engulfed non-apoptotic cells in the septal DG in sham and tMCAo. Phagoptosis events were not detected (nd) in sham mice.* **[E]** *Type of microglial phagoptosis (% of microglia) by "ball-and-chain" (B&C) or "Apposition" (Appo) mechanism. Bars show mean ± SEM. The effect of tMCAo on phagoptosis* **[D]** *and type of phagocytosis* **[E]** *at 6h and 1d was analyzed using Student´s t test. No statistical differences were found. In* **[B, D, E]**, *n=3 (sham at 6h), n=4 (sham at 1d), n=5 (tMCAo at 6h) and n=6 (tMCAo at 1d). Scale bars=20μm [A], 10μm [C]; z=10μm [A], 11.2μm [C].*

6.2.6 Adult microglial phagocytosis could be impaired in a monkey model of tMCAo

To validate our data and get a little closer to the pathology of human stroke, we analyzed phagocytosis in samples from non-human primates, in this case, common marmoset (*Callithrix jacchus*)**(Fig. 35)**. Animals were subjected to tMCAo for 3h, and sacrificed 45d later **(Fig. 35A)**. These surgeries were performed at the University of Normandie by researchers in Omar Touzani´s laboratory. It should be mentioned that in this set of experiments, we did not have control conditions. We scanned three independent brain samples from tMCAo-treated marmoset and noticed that microglia were morphologically more complex compared to human tissue (autopsy or biopsy) [Abiega et al., 2016]**(Fig. 35B, C)**. In addition, we found very few apoptotic cells (2-6 dead cells per whole section in cortex and hippocampus)**(Fig. 35D)**, which could be explained by the fact that we analyzed the tissue 45d after damage and maybe this period was enough to produce a partial recovery of the parenchyma. Although unfortunately we did not have control tissue, our quantifications revealed that few dead cells were phagocytosed, as shown by low Ph index **(Fig. 35D)**. These preliminary data suggested that microglial phagocytosis could be also impaired in a monkey model of tMCAo. To further validate these observations, we are currently analyzing apoptosis and phagocytosis in macaque (*Macaca fascicularis*) subjected to tMCAo and autopsy tissue from human stroke patients, in collaboration with Prof. Emmanuelle Canet (University of Lyon, France) and Prof. Isidre Ferrer (University of Barcelona, Spain), respectively.

A Left tMCAo (3h)

22-30m

WT
Callithrix jacchus

45d

confocal

DAPI Iba1 NeuN GFAP

B Cortex (CX)

C Dentate Gyrus (DG)

B1 tMCAo 45d

B2 tMCAo 45d

tMCAo 45d

DAPI Iba1 NeuN GFAP

M

M

M
SGZ

M
GZ

M

M

M

D

	Region	Total	Apo phago	Ph index (%)
Marmoset 1	CX	6	4	66,67%
	Hippo (DG)	/	/	/
Marmoset 2	CX	2	/	/
	Hippo (DG)	/	/	/
Marmoset 3	CX	5	3	60%
	Hippo (DG)	4	/	/
TOTAL		9	3	33,33%
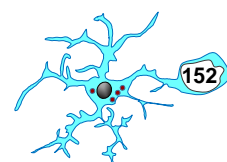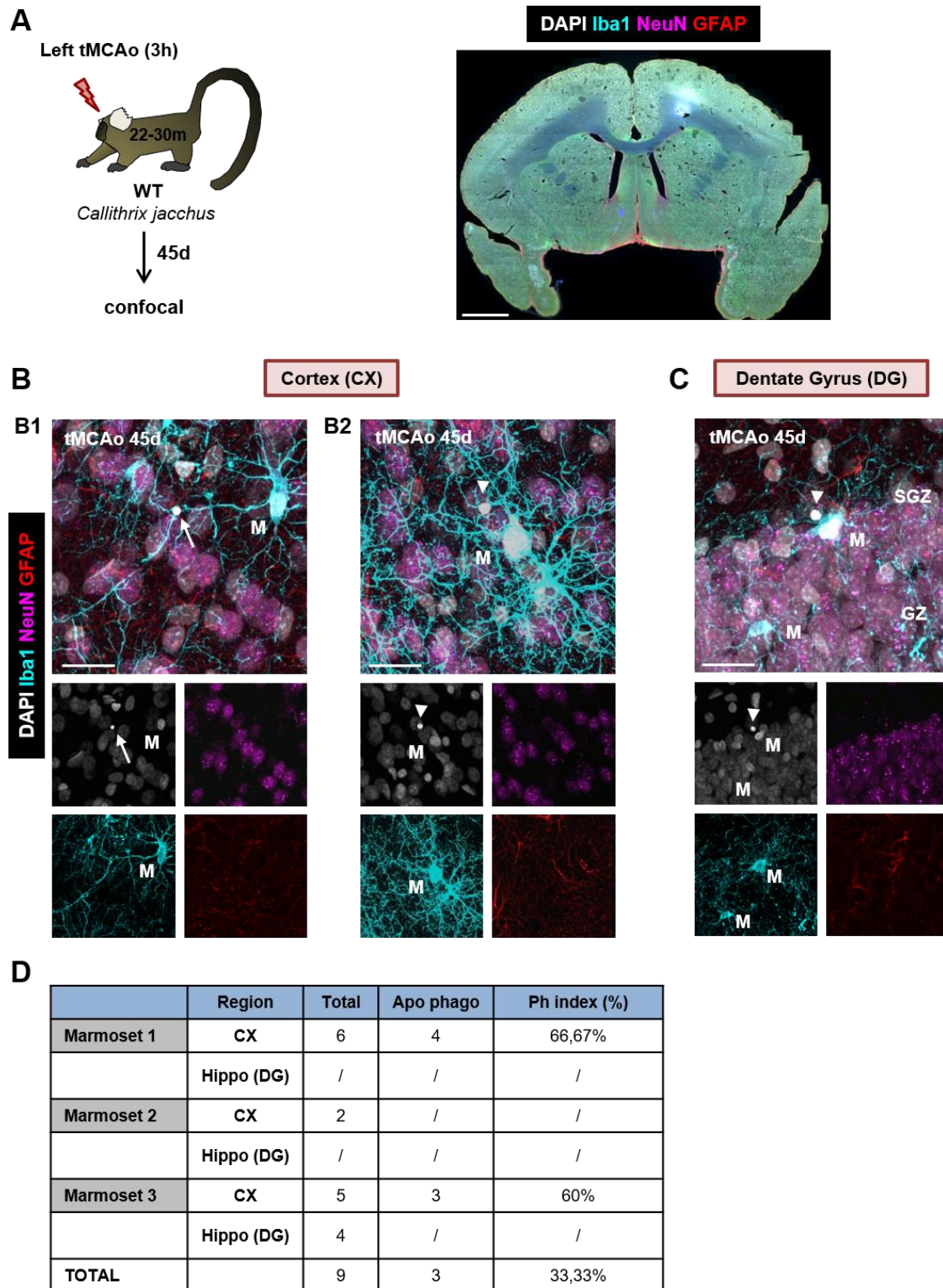
Figure 35. tMCAo in non-human primates. [A] *Experimental design and representative confocal z-stack of a brain slice of Callithrix jaccus at 45d after tMCAo. Cell nuclei were visualized with DAPI (in white), neuronal nuclei (NeuN[+], in magenta), astrocytes marker (GFAP[+], in red), and microglia (Iba1^{+}, in cyan).* **[B]** *Representative confocal z-stack of a phagocytosed* **[B1]** *and a non-phagocytosed apoptotic cell (pyknotic/karyorrhetic, with DAPI, in white; arrow)* **[B2]** *close to a microglial process (Iba1^{+}, in cyan; M) in the cortex (CX).* **[C]** *Representative confocal z-stack of a phagocytosed apoptotic cell (pyknotic/karyorrhetic, with DAPI, in white; arrow) by microglia (Iba1^{+}, in cyan; M) in the SGZ of the DG.* **[D]** *Summary of parameters*
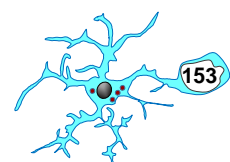
*in a marmoset model of tMCAo (n=3): brain region analyzed, total numbers of apoptotic cells quantified, apoptotic cells phagocytosed, and phagocytic index (Ph index). Scale bars=20μm [**B1-B3**]; z=19.6μm [**B1-B2**], 23.8μm [**B3**].*

6.2.7 Hippocampus is maintained hypoxic after reperfusion

A few years ago, our group analyzed biopsies and autopsies hippocampal samples from control patients and found that microglial phagocytosis was very low [Abiega et al., 2016]. These observations led us to wonder whether postmortem (PM) delay and oxygen and nutrient deprivation could affect phagocytosis. Indeed, it was described that microglial motility and damage response were strongly prevented in the spinal cord of mice as early as 3h PM, likely due to a depletion of energy sources in the dead tissue [Dibaj et al., 2010]. Because our model of tMCAo is a very good scenario of oxygen and nutrient deprivation, we asked whether the impairment of microglial phagocytosis could be partially explained by a permanent hypoxia of the hippocampus in spite of the reperfusion.

To test our hypothesis, we explored the presence of hypoxic areas in the brain tissue after tMCAo using a compound named pimonidazole **(Fig. 36)**. Pimonidazole or 2-nitroimidazole is reductively activated specifically in hypoxic cells and forms stable adducts with thiol groups in proteins, peptides, and amino acids [Raleigh and Koch, 1990; Raleigh et al., 1998; Arnold et al., 2010; Cenik et al., 2013; Aguilera and Brekken, 2014]. As a positive control, animals first were injected intravenously (tail injection) with pimonidazole (60mg/kg; [Aguilera and Brekken, 2014]) 30min before reperfusion since the plasma half-life of pimonidazole in mice is approximately 25min (Hypoxiprobe data analysis), and then animals were sacrificed 30min later, when the filament was removed **(Fig. 36A)**. In sham conditions, we detected a low signal of pimonidazole, which was associated with the choroid plexus **(Fig. 36B, C)**. In contrast, at the time of filament removal, there were small hypoxic areas in the infarcted hemisphere of tMCAo-treated mice, located in striatum (**Fig. 36A, B**). We next explored whether infarcted hemisphere was maintained hypoxic even though it was reperfused. Mice were injected intravenously (tail injection) with pimonidazole (60mg/kg; [Aguilera and Brekken, 2014]) 30min before being sacrificed at 6h and 1d after tMCAo **(Fig. 36A)**. The percentage of hypoxic areas in tMCAo-treated mice significantly increased at 6h and 1d compared to 1h, while no ischemic regions were detected in sham animals **(Fig. 36D, E)**. Several brain regions were maintained in hypoxia, such as CX, striatum, thalamus, hypothalamus, and hippocampus. These data indicated that tMCAo induced a permanent hypoxia in spite of the reperfusion. One possible explanation could be that pericytes die in rigor and
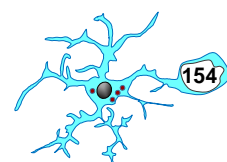
maintain vasoconstriction after reperfusion [Hall et al., 2014]. Together, our findings suggested that the impairment of microglial phagocytosis might be related to a continuous hypoxic level in the hippocampus.
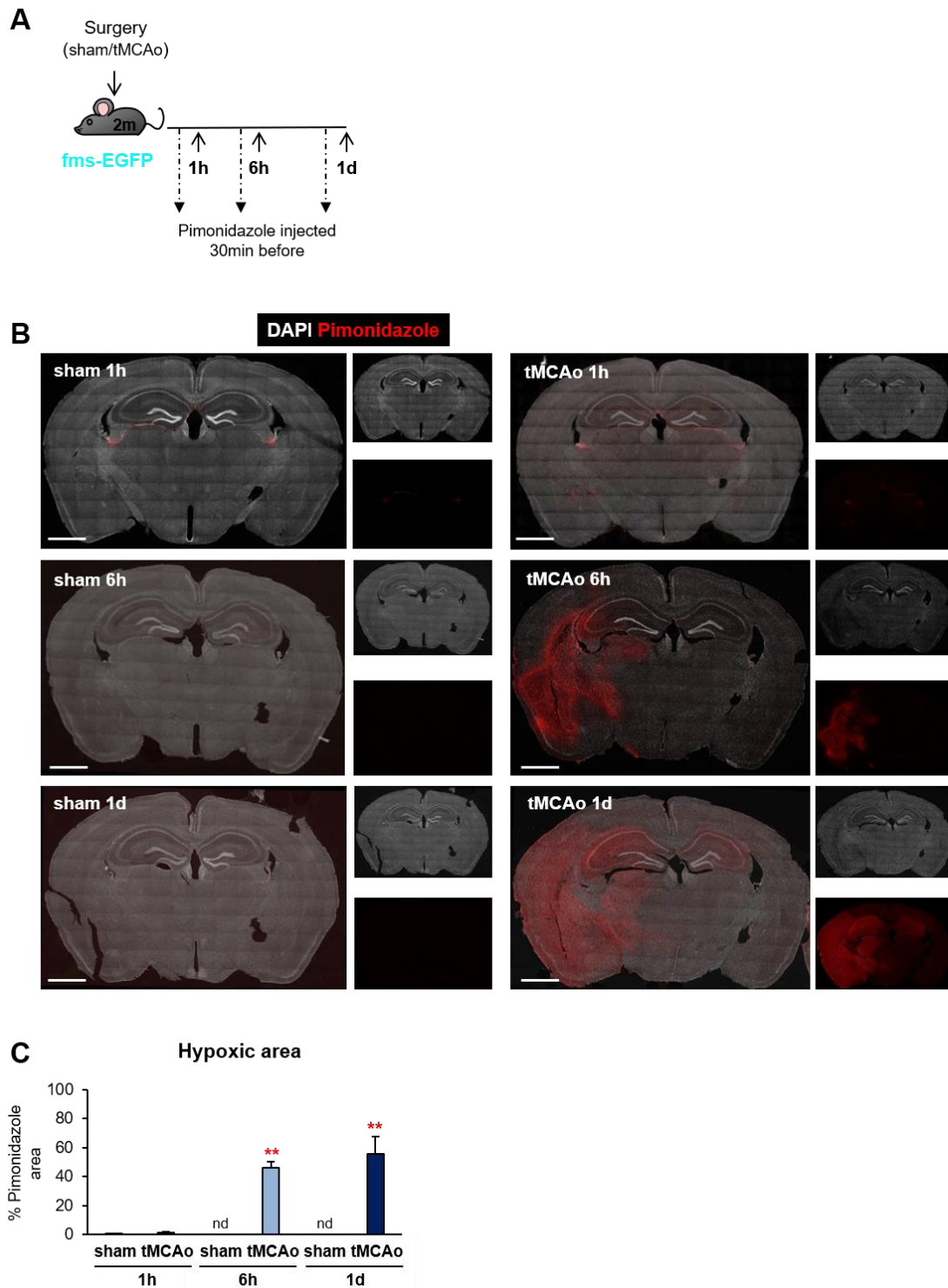
Figure 36. Hypoxic brain area associated to tMCAo. [A] *Experimental design of Pimonidazole treatment in 2m fms-EGFP mice after sham and tMCAo treatment at 1h, 6h, and 1d.* **[B]** *Representative tiled confocal images of coronal sections of the hippocampus showing cell nuclei (with DAPI, in white) and hypoxic areas*

*labeled with Pimonidazole (in red) after sham and tMCAo at 1h, 6h, and 1d. **[C]** Percentage of hypoxic brain area determined by pimonidazole hydrochloride after tMCAo at 1h, 6h, and 1d. In sham conditions at 6h and 1h was not detected (nd) signal of pimonidazole. Bars show mean ± SEM. The percentage of hypoxia area after tMCAo at 1h, 6h, and 1d was analyzed using 1-way ANOVA and Holm-Sidak was used as a posthoc test. (*) Two symbols represent p<0.01 (vs tMCAo at 1h). Only significant effects are shown. In **[C]**, n=2 (sham at 1h), n=3 (sham 6h and 1d), and n=3 (tMCAo at 1h, 6h, and 1d). Scale bars=500μm **[B]**.*

6.2.8 Adult microglial phagocytic efficiency is reduced after KA, it is accompanied by multinuclearity and phagoptosis, and is unrelated to peripheral monocyte invasion

The following data was published in the article titled "Neuronal Hyperactivity Disturbs ATP Microgradients, Impairs Microglial Motility, and Reduces Phagocytic Receptor Expression Triggering Apoptosis/Microglial Phagocytosis Uncoupling". Abiega O*, **Beccari S***, Diaz-Aparicio I* … Sierra A. *PLoS Biology* 14(5): e1002466. (2016). (*) These authors contributed equally to this work.

The microglial phagocytosis impairment obtained in the tMCAo scenario was similar to the impairment that we observed in the acute stages of a model of MTLE, characterized by seizures, excitotoxicity, and inflammation (PhD Thesis from Abiega O, 2017; [Abiega et al., 2016]). MTLE is the most common and well-defined human focal epilepsy syndrome, in which seizures originate in the hippocampus and/or related limbic areas [Bouilleret et al., 1999; Sharma et al., 2007]. To mimic this scenario, 2m mice (pooled male and female) were subjected to locally injection of the glutamate agonist kainic acid (KA) into the DG **(Fig. 37)**. Intrahippocampal KA administration is one of the models that most reproduce the pathophysiology features of human MTLE such as spontaneous seizures and hippocampal sclerosis [Babb et al., 1995; Bouilleret et al., 1999; Kralic et al., 2005; Nitta et al., 2008].

We initially reported that the microglial phagocytic response was dramatically reduced during acute stages of the MTLE model (at 6h post-injection (hpi) and 1dpi of KA)(PhD Thesis Abiega O, 2017) [Abiega et al., 2016], and in this PhD Thesis we further explored whether this impairment was maintained during later stages of MTLE (3 and 7dpi of KA)**(Fig. 37A)**. We first quantified apoptosis (pyknosis/karyorrhexis and activated caspase-3) and phagocytosis. The number of dead cells significantly increased after KA **(Fig. 37B)**, whereas the Ph index remained lower than in saline **(Fig. 37C, D)**. In spite of that, we observed a partial recovery of phagocytosis because the net phagocytosis significantly increased at 3pi and 7dpi **(Fig. 37E)**. Moreover, we noticed that microglia
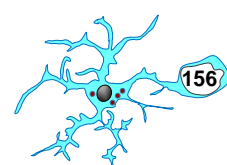
developed a hypertrophic, seemingly ameboid morphology, which was accompanied by an incomplete mitosis (nucleokinesis without cytokinesis), as determined by staining with the cell cycle marker phosphohistone 3 (PH3) **(Fig. 37C)**. We analyzed their proliferation level with the cell cycle marker Ki67 **(Fig. 37F)**, and found that microglia began to proliferate at 3dpi **(Fig. 37G)**, coincident with the proliferation of other cell types and a large activation of the proliferative molecular program induced by KA [Sierra et al., 2015]. While in saline conditions all microglia showed a single nucleus, KA treatment significantly increased multinuclearity **(Fig. 37G-I)**. When we analyzed the impairment of phagocytosis in more detail, we found that both uni- and multi-nucleated microglia executed phagocytosis similarly **(Fig. 37J)**. Nonetheless, we were not able to estimate the total number of microglia because the multinucleated cells frequently overlapped spatially, and consequently, the Ph/A coupling ratio was not either calculated. Taking together, our data showed that **microglial phagocytosis was partially recovered at 3d and 7d after KA, coincidental with multinuclearity**.
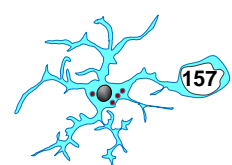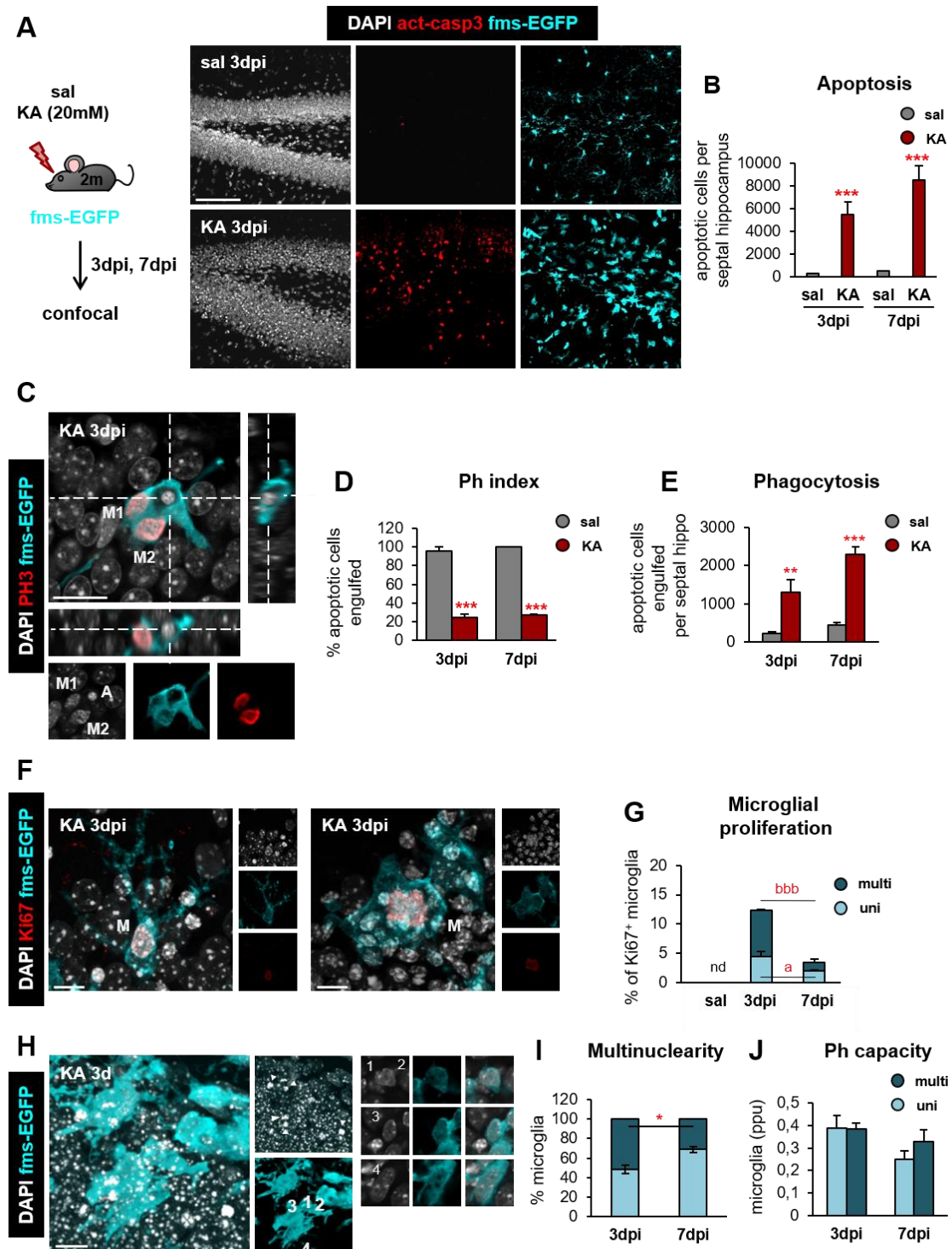
Figure 37. Microglial phagocytosis impairment in a model of MTLE at 3 and 7dpi occurs in parallel with multinuclearity and phagoptosis. [A] *Experimental design and representative confocal z-stack of the DG of 2m fms-EGFP mice at 3dpi (days postinjection) after saline and kainic acid (KA). Apoptotic cells (pyknotic/karyorrhectic) were visualized with DAPI (in white) and activated-caspase 3 (act-casp 3+, in red); and microglia (fms-EGFP, in cyan).* **[B]** *Number of apoptotic cells per septal hippocampus after treatment with saline and KA (3 and 7dpi).* **[C]** *Orthogonal projection of a confocal z-stack from the DG of a KA-treated mouse at 3dpi showing a bi-nucleated microglia cell (in cyan) undergoing mitosis (phosphohistone 3, PH3, in red) and phagocytosing an apoptotic cell (pyknotic/karyorrhectic with DAPI, in white; A). Note the*

condensed chromosomes in the microglial nuclei, typical of mitosis (M1, M2). [D] Ph index (% of apoptotic cells engulfed by microglia) in the septal DG at 3 and 7dpi after treatment with saline and KA. [E] Total number of phagocytosed apoptotic cells in the septal DG after treatment with saline and KA (3 and 7dpi). [F] Representative confocal z-stack of uni- [A1] and multinucleated [A2] microglia (in cyan) in the DG 3dpi after KA. Proliferating cells were labeled with Ki67 (in red) and nuclei with DAPI (in white). [G] Proportion (in % of cells) between uni- and multi-nucleated microglia labeled with Ki67 in the DG of KA-treated mice at 3 and 7dpi. [H] Representative confocal z-stack of a multinucleated microglia (in cyan) from the DG of a KA-treated mouse at 3d. [I] Proportion (in % of cells) between uni- and multi-nucleated microglia in the DG of KA-treated mice at 3 and 7dpi. [J] Weighted Ph capacity (in ppu) in the septal DG after treatment with saline and KA (3 and 7dpi). Bars show mean ± SEM (standard error of the mean). Significant interaction between the two factors (treatment x time: saline vs KA at 3 and 7dpi) in apoptosis [B], Ph index [D], and phagocytosis [E] was found using 2-way ANOVA. Therefore, data were split into 1-way ANOVA to analyze statistical differences due to the time after saline and/or KA injection at each time. Holm-Sidak was used as a posthoc test. The effect of KA on microglial proliferation [G] and multinuclearity [I] was analyzed using Student´s t test. The effect of KA on Ph capacity [J], was analyzed using 1-way ANOVA and Holm-Sidak was used as a posthoc test. (*) One symbol represents p<0.05, two p<0.01, and three p<0.001. Only significant effects are shown. In [B, D, E, G, I], n=3-9 per time point and treatment. Scale bars=50μm [A], 10μm [B, C]; z=25μm [A], 17μm [B], 10.5μm [C].

In parallel to phagocytosis of apoptotic cells, we also found some cases of phagoptosis **(Fig. 38)**. While this phenomenon was undetectable in saline, we observed some evidences of phagoptosis after KA treatment, mostly executed by multinucleated microglia at 3dpi, and similarly by uni and multi-nucleated cells at 7dpi **(Fig. 38A-C)**. Thus, these results showed that **phagoptosis occurred in parallel to microglial phagocytosis impairment**.
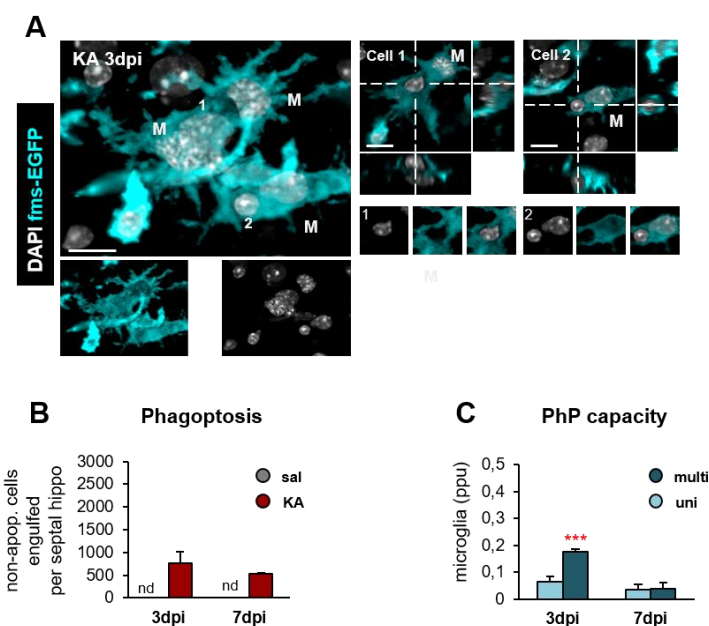
Figure 38. Microglial proliferation during MTLE. [A] *Representative confocal z-stack of a multinucleated and phagoptotic microglia (in cyan) from the DG of a KA-treated mouse at 3d. [C1] 3D-rendered image*
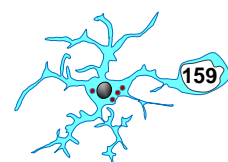
showing the continuum of EGFP through the microglial cytoplasm and within their nuclei. Up to 8 nuclei were contained. [C2] Individual images showing each nucleus: nuclei 2, 3, and 5 showed condensed chromosomes, characteristic of an ongoing division. Nuclei 4 and 7 were small but not pyknotic; they did not contain EGFP and thus were not microglial but rather surrounded by pouches of microglial cytoplasm. [C3] Orthogonal projections of nuclei 4 and 7 showing their complete engulfment by microglial processes (phagoptosis). [B] Total number of non-apoptotic cells phagocytosed by microglia (M, in cyan) in the septal DG after KA treatment (3 and 7dpi). [C] Weighted PhP (phagoptosis) capacity in the septal hippocampus at 3 and 7dpi. Bars represent mean ± SEM (standard error of the mean). The effect of KA on phagoptosis [B] was analyzed using Student´s t test. The effect of KA on PhP capacity [I], was analyzed using 1-way ANOVA and Holm-Sidak was used as a posthoc test. (*) Three symbols represent p<0.001. Only significant effects are shown. nd, not detectable in saline mice. In [B, C], n=3-9 per time point and treatment. Scale bars=10µm [A]. z=10.5µm [A].

We next argued that phagocytosis disruption might be related to the invasion of peripheral monocytes **(Fig. 39)**. Because this study was performed several years ago and published in 2016 [Abiega et al., 2016], we did not use P2Y12 to discriminate between both macrophages population. Instead, we analyzed the expression of CD45, a lymphocyte antigen with higher expression in circulating cells compared to resident microglia [Sierra et al., 2007]**(Fig. 39A)**. CD45 expression was undetectable in control but was evident in all fms-EGFP-expressing cells at 3dpi after KA. Flow cytometry analysis showed a transiently increased CD45 expression in the fms-EGFP population at 3dpi that returned to basal levels by 7dpi **(Fig. 39B, C)**. This observation could be interpreted as resulting from a transient overexpression of CD45 in microglia population, or from an invasion of CD45high monocytes that either died or down-regulated the antigen later on. To further explore the role of invading monocytes, we injected KA in *Ccr2* KO mice, characterized by a decreased population of circulating monocytes and recruitment into the brain parenchyma [Gómez-Nicola et al., 2014]. Then, animals were sacrificed at 3dpi **(Fig. 39D)**. This transgenic mouse was developed by knockout (KO) technique [Doyle et al., 2012], in which the *Ccr2* gene was deleted.

We first quantified the apoptosis and phagocytosis in the DG. No significant changes were found in the number of dead cells in WT compared to *Ccr2* KO **(Fig. 39E)**. Importantly, we observed that both genotypes showed a similar microglial impairment, determined by the Ph index **(Fig. 39F)**. As in KA-treated fms-EGFP mice, the number of microglial cells could not be accurately estimated because of their ameboid, multinucleated morphology, although no obvious differences were observed in *Ccr2* KO mice compared to WT. In fact, no significant changes were found in the proportion of multinucleated microglia and/or the average number of nuclei per cell **(Fig. 39G, H)**. Moreover, we also noticed that both uni- and multi-nucleated microglia executed phagocytosis and phagoptosis similarly **(Fig. 39I, J)**. Due to microglial multinuclearity,
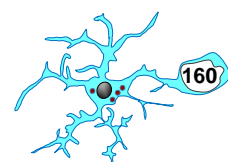
their total number was not calculated and, therefore, the Ph/A coupling ratio was not calculated in *Ccr2* KO mice. Thus, these results indicated that **invading peripheral monocytes was not contributed to microglial phagocytosis impairment after KA challenge**.
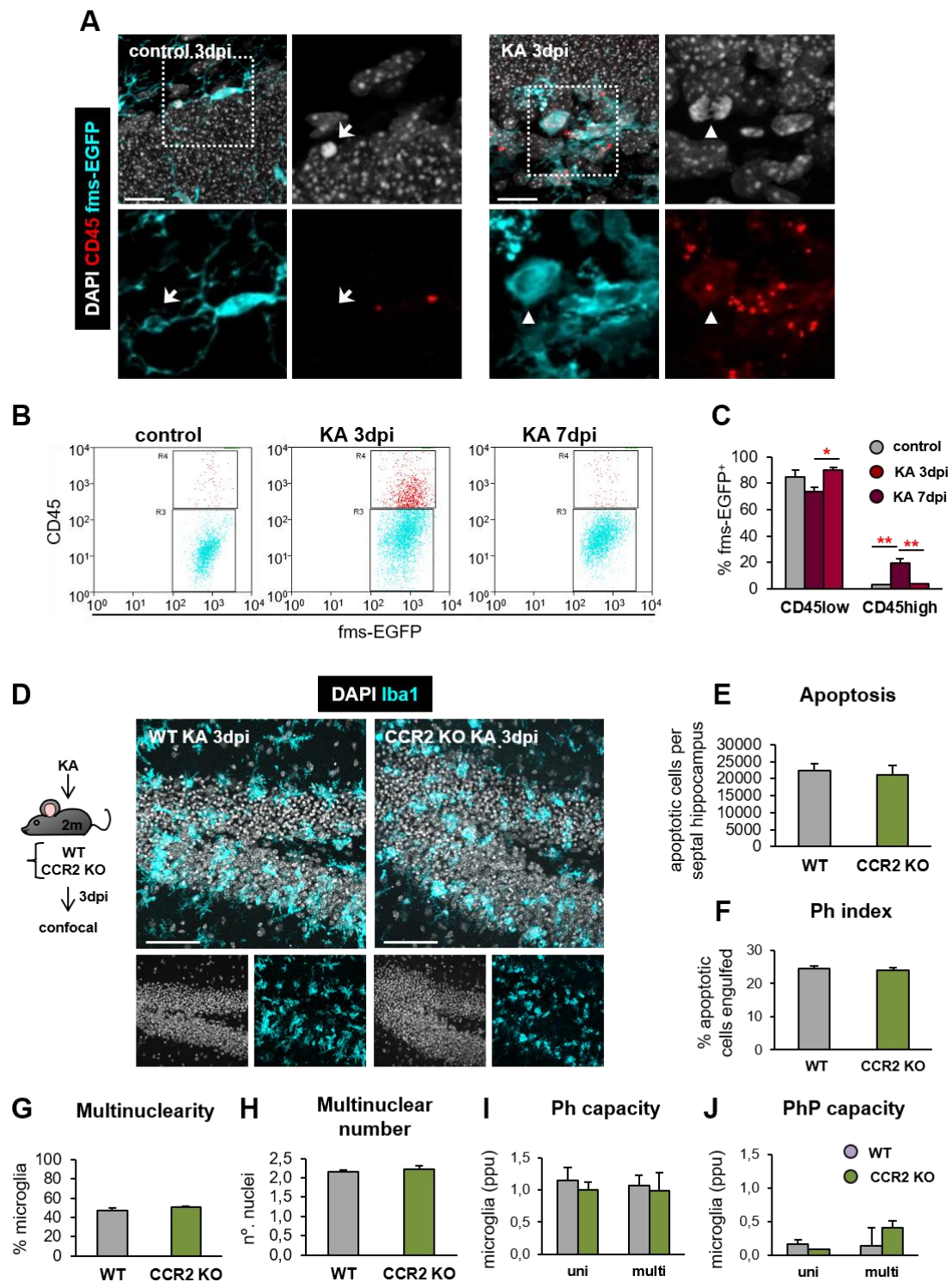
Figure 39. Microglial phagocytosis impairment during MTLE is not related to monocyte invasion. [A] *CD45 staining in saline and KA- injected mice at 3dpi. Cell nuclei are visualized with DAPI (in white),*
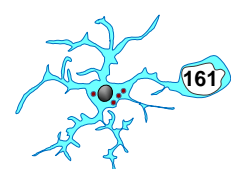
microglia with fms-EGFP (in cyan) and CD45 is shown in red. In control mice, the expression of CD45 was dim, showing diffuse cytoplasmic inclusions within microglia. A CD45⁺ cell is shown engulfing an apoptotic cell (arrow, enlarged). In KA mice, CD45 had a higher and more widespread expression in all microglial cells, including a dividing cell (arrowhead, enlarged). A clear distinction between CD45^{high} and CD45^{low} cells was not evident. [B] Flow cytometry analysis of the expression of CD45 in fms-EGFP⁺ hippocampal cells from control and KA-treated mice at 3 and 7dpi. Gates for CD45^{low} (in cyan) and CD45^{high} (in red) were defined based on the distribution of the fms-EGFP⁺ cells in control (not injected) mice. 3dpi after the KA injection, more cells were found in the CD45^{high} gate, although the fms-EGFP⁺ cells were in fact distributed along a continuum of CD45 expression, all of them with higher expression than in control mice. At 7dpi, the expression of CD45 returned to basal levels. [C] Percentage of fms-EGFP⁺ cells that expressed low or high levels of CD45 in control or KA-treated mice at 3 and 7dpi determined by flow cytometry. [D] Experimental design and representative confocal z-stacks of the DG of 2m CCR2⁻/⁻ (CCR2 KO) mice and control WTs (C57BL/6) at 3dpi after the KA injection. [E] Number of apoptotic (pyknotic/karyorrhectic) cells in the septal DG in WT and CCR2 KO mice. [F] Ph index (% of apoptotic cells engulfed by microglia) in the septal DG in WT and CCR2 KO mice. [G] Multinuclearity in WT and CCR2 KO mice. [H] Number of multinucleated cells in WT and CCR2 KO mice. [I] Weighted Ph capacity in WT and CCR2⁻/⁻ mice. [J] Weighted PhP (phagoptosis) capacity in the septal DG in WT and CCR2 KO mice. Bars show mean ± SEM. The effect of KA on CD45 expression level in microglia [C] was analyzed using 1-way ANOVA. Holm-Sidak was used as a posthoc test. The effect of KA on apoptosis [E], Ph index [F], multinuclearity [G], and multinuclear number [H] was analyzed using Student´s t test. The effect of KA on Ph capacity [I] and PhP capacity [J] was analyzed using 1-way ANOVA and Holm-Sidak was used as a posthoc test. Only significant effects are shown. In [C, E, F, G, H, I, J], n=4 per group. (*) One symbol indicates p<0.05 and two for p<0.01. Scale bars=20μm [A], 50μm [D]; z=14.7μm [A], 12.6μm [D].

6.2.9 Long-term impairment of adult microglial phagocytosis in mouse and human MTLE

The above results from KA-treated mice led us to propose that microglial phagocytosis was also impaired in human MTLE. Because in humans MTLE is a chronic disease, we first mimicked this detrimental scenario injecting intrahippocampal KA and sacrificed the animals 4m post-injection (mpi), when mice developed chronic epilepsy [Sierra et al., 2015] **(Fig. 40)**. An evident hippocampal sclerosis characterized by granule cell dispersion and the appearance of reactive, hypertrophic astrocytes was observed after 4mpi [Sofroniew and Vinters, 2010] **(Fig. 40A-E)**. While the number of apoptotic cells returned to basal level, the Ph index significantly decreased after KA treatment **(Fig. 40G)**, showing a continue impairment of microglia at 4mpi. Also, we observed a few dead cells engulfed by reactive astrocytes, although the frequency of this event was lower than phagocytosis executed by microglia (Ph index=5±3% (reactive astrocytes; **Fig. 40D**) vs Ph index=43±14 (microglia; **Fig. 40E**)). Importantly, we noticed that in KA mice over 80% of apoptotic cells were localized less than 0.5μm from a microglial process, and they were not phagocytosed **(Fig. 40C)**.
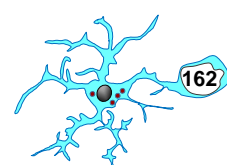
A similar scenario was observed in acute stages of the MTLE model (6hpi and 1dpi of KA), in which we discovered two mechanisms to explain the impairment of phagocytosis: 1, a defect in recognition and phagocytosis (resulting in apoptotic cells apposed to microglia but not phagocytosed) and 2, a defect in microglial surveillance and/or targeting of apoptotic cells (resulting in far-off apoptotic cells) [Abiega et al., 2016]. These findings lead us to wonder whether the impairment of phagocytosis at 4mpi was related to a decreased microglia surveillance. To test this hypothesis, we analyzed the density of microglial cells and the percentage of the parenchyma occupied by microglial processes (microglial volume). We found that both parameters significantly increased after 4mpi compared to saline, suggesting no defects in surveillance **(Fig. 40I, J)**. Together, our data showed that **microglial phagocytosis disfunction was maintained up to 4mpi following KA in spite of their increased density and the volume they occupied**.
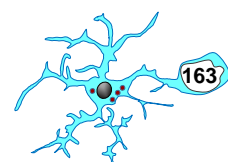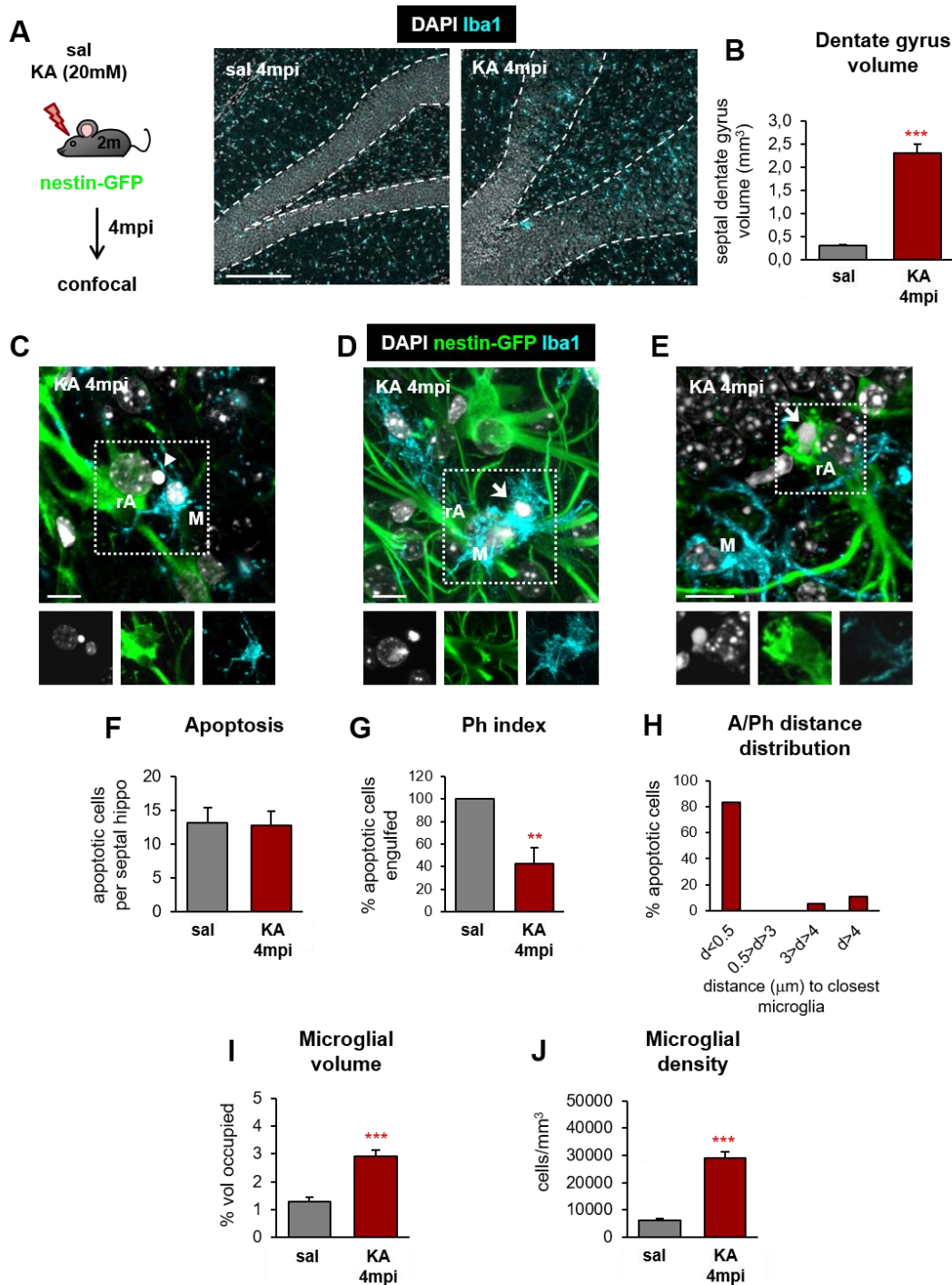
Figure 40. Impairment of microglial phagocytosis during MTLE is maintained up to 4mpi. [A]
Experimental design and representative confocal z-stack from the DG of 2m nestin-GFP mice at 4mpi after
the KA injection. Cell nuclei were visualized with DAPI (in white) and microglia with ionized calcium-binding
adapter molecule 1 (Iba1+, in cyan). [B] Septal dentate gyrus volume (mm³) at 4mpi after the saline and KA
injection. [C] Representative confocal z-stack of an apoptotic cell (pyknotic, with DAPI, in white; arrow)
located nearby a hypertrophic reactive astrocyte (rA; visualized with nestin-GFP+, in green) and a microglia
(Iba1+, in cyan; M) at 4mpi after the KA injection. [D] Representative confocal z-stack of an apoptotic cell
phagocytosed by microglia (M; Iba1+, in cyan) at 4mpi after the KA injection. [E] Representative confocal z-
stack of an apoptotic cell phagocytosed by a reactive astrocyte (rA; visualized with nestin-GFP+, in green)
at 4mpi after the KA. [F] Total number of apoptotic cells in the septal hippocampus in saline and KA-treated

164

mice. [G] Ph index in the DG (% of apoptotic cells engulfed by microglia). [H] Microglial volume (% of volume of DG occupied). [I] Histogram showing the distribution of the distance (in μm) of apoptotic cells to microglia (in %). [J] Density of microglia (cells/mm³). Bars represent mean ± SEM (standard error of the mean). The effect of KA on dentate gyrus volume [B], apoptosis [F], Ph index [G], microglial volume [H], and microglial density [J] was analyzed using Student´s t test. In [I], data represent the sum of cell in each distance slot. (*) Two and three symbols indicate p<0.05 and p<0.001, respectively. Only significant effects are shown. In [B, F, G, H, J], n=3-4 per group. Scale bars=50μm [A], 10μm [C, D, E]; z=58μm [A], 6.6μm [C], 12.7μm [D], 10μm [E].

Next, we investigated the phagocytic response in hippocampal tissue resected from drug-resistant MTLE patients, in which the hippocampal formation was removed to control the seizures **(Fig. 41)**. In order to preserve antigenicity and prevented further neuronal damage, the tissue had a minimal post-operative delay before it was fixed (under 40min) **(Fig. 41A)**. We quantified the apoptosis in three MTLE patients and found a very low level (typically 10-20 dead cells per slice). As in our mouse model of MTLE, many apoptotic cells were not phagocytosed in the hippocampus **(Fig. 41B)**. Regarding the small proportion of apoptotic cells phagocytosed, we observed that some of them were engulfed by microglial terminal branches ("ball-and-chain" mechanism)[Sierra et al., 2010]**(Fig. 41C)**. Surprisingly, we also noticed a unique type of microglial phagocytosis in human brain, in which several microglia formed a mesh surrounding the apoptotic cells, in an aster-like structure **(Fig. 41D)**. Furthermore, in all patients we found many events where several microglia directly projected their processes towards non-apoptotic neurons **(Fig. 41E)**, which could be interpreted as the initiation of a phagoptotic process or of the aster-shaped phagocytosis only found in the human tissue. When we analyzed the Ph index, our data reveled a low number of dead cells engulfed (on average, 49±4%; 26±3% "ball-and-chain" vs 23±4% "aster"; **Fig. 41F**), and a large proportion of apoptotic cells in close proximity to a microglial process (up to 67% of cells under 0.5µm; **Fig. 41B, G)**, similar to KA-treated mice at 4mpi. We also explored the density and the volume occupied by microglia and found that both parameters were consistent among patients **(Fig. 41H, I)** and remarkably similar to those in our mouse model of MTLE at 4mpi following KA **(Fig. 41I, J)**.

To further confirm these results, we obtained autopsy hippocampal tissue from epileptic patients (not MTLE) and non-demented controls from the Netherlands Brain Bank **(Fig. 41J, K)**. The long post-mortem (PM) delays (between 3-20h) hindered the interpretation of the data, as we found phagocytosis was mostly absent in the autopsy tissue. The low phagocytosis in autopsy human tissue is in agreement with results obtained from PM in spinal cord of mice, where the microglial motility and damage
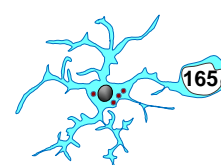
response were strongly prevented as early as 3h PM, probably due to a depletion of energy sources in the dead tissue [Dibaj et al., 2010]. Nevertheless, we found a significant decrease in the Ph index in the hippocampus of non-demented controls compared to epileptic patients (22±3% vs 1.3±1.3%, from 6 controls and 3 epileptic individuals, respectively). Thus, our data clearly demonstrated that **microglial phagocytosis was disrupted in human epilepsy**.
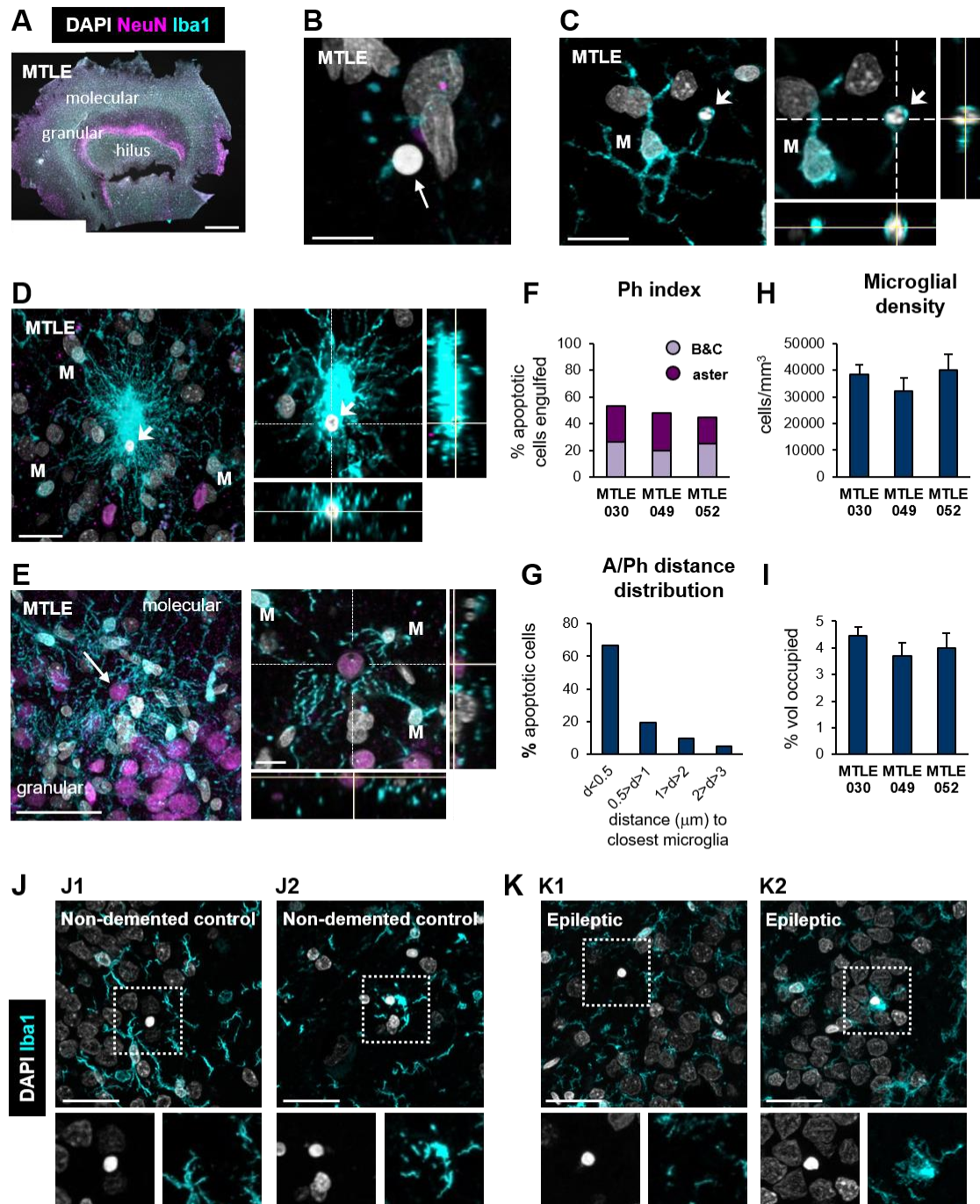
Figure 41. Chronic microglial phagocytosis impairment in human MTLE. [A] *Representative tiled confocal image of a slice of the human hippocampus from an MTLE patient showing cell nuclei (with DAPI, in white), neuronal nuclei (NeuN+, in magenta), and microglia (Iba1+, in cyan).* **[B]** *Representative confocal*

*z-stack of a non-phagocytosed apoptotic cell (pyknotic/karyorrhectic, with DAPI, in white; arrow) close to a microglial process (Iba1+, in cyan) in the hippocampus of an MTLE patient. **[C]** Representative confocal z-stack of phagocytosis by a "ball-and-chain" (B&C) mechanism in the hippocampus from an individual with MTLE. The apoptotic cell (pyknotic/karyorrhectic, with DAPI, in white; arrow) was engulfed by a terminal branch of a nearby microglia (Iba1+, in cyan; M). The right panel shows orthogonal projection of the same cell, where the 3D engulfment is evident. **[D]** Representative confocal z-stack of phagocytosis by an "aster" mechanism in the hippocampus from an individual with MTLE. The apoptotic cell (pyknotic/karyorrhectic, with DAPI, in white; arrow) was engulfed by a mesh of processes from many surrounding microglia (Iba1+, in cyan; M). The right panel shows an orthogonal projection of the same cell. **[E]** Representative confocal z-stack of a DG granule neuron (NeuN+, in magenta; arrow) targeted by the processes of several surrounding microglia (Iba1+, in cyan; M). Nuclei are shown with DAPI (in white). The right panel shows an orthogonal projection of the same neuron directly targeted the processes of up to three microglia (Iba1+, in cyan; M). **[F]** Ph index in the human DG (% of apoptotic cells engulfed by microglia). **[G]** Histogram showing the distribution of the distance of apoptotic cells (in %) to Iba1+ microglial processes in the DG of MTLE patients (n=21 cells from 3 patients). **[H]** Density of microglia (cells/mm^3) in the DG of three hippocampal samples from human MTLE patients. **[I]** Microglial volume (% of volume of DG occupied) in the three hippocampal samples from individuals with MTLE. **[J]** Representative confocal z-stack of apoptotic cells (pyknotic, DAPI, in white) not phagocytosed (J1, in the granular layer) and phagocytosed (J2, in the hilus) by microglia (Iba1+, in cyan) in the hippocampus of autopsy tissue from a non-demented control. **[K]** Representative confocal z-stack projections of apoptotic cells (pyknotic, DAPI, white) not phagocytosed (K1, in the hilus) and phagocytosed (K2, in the granular layer) by microglia (Iba1+, in cyan) in the hippocampus of autopsy tissue from an epileptic patient. Data represent the average values for measures in different z-stacks for each patient **[F, G]**, the individual values of all the pooled cells for each patient **[H]** or the sum of cells in each distance slot **[I]**. Scale bars=1mm **[A]**, 10μm **[B, C]**, 20μm **[D]**, 50μm **[E]**, 20μm **[J, K]**. z=2.8μm **[B]**, 2.6μm **[C]**, 5.2μm **[D]**, 12μm **[E]**, 3.5μm **[J1]**, 8.05μm **[J2]**, 4.55μm **[K1]**, 9.1μm **[K2]**.*

In summary, in the second part of this PhD thesis project we examined and quantified the phagocytic efficiency in the 2-3m hippocampus under different phagocytic challenges induced by CIR, HIE, tMCAo, and KA **(Fig. 42)**. First, we observed that the amount of apoptosis caused after CIR was surprisingly well cleaned from the parenchyma 24h later, showing a sublime labor of "superphagocytosis". Nonetheless, we found an opposite scenario in HIE, tMCAo, and KA, where microglial phagocytosis was impaired. In parallel to phagocytosis in mice, we discovered a dysfunctional response of microglia in human MTLE tissue, and a possible impairment of phagocytosis in marmosets after tMCAo, which we are currently validating in macaque and human tissue.
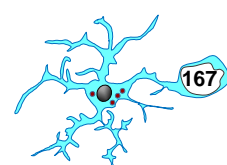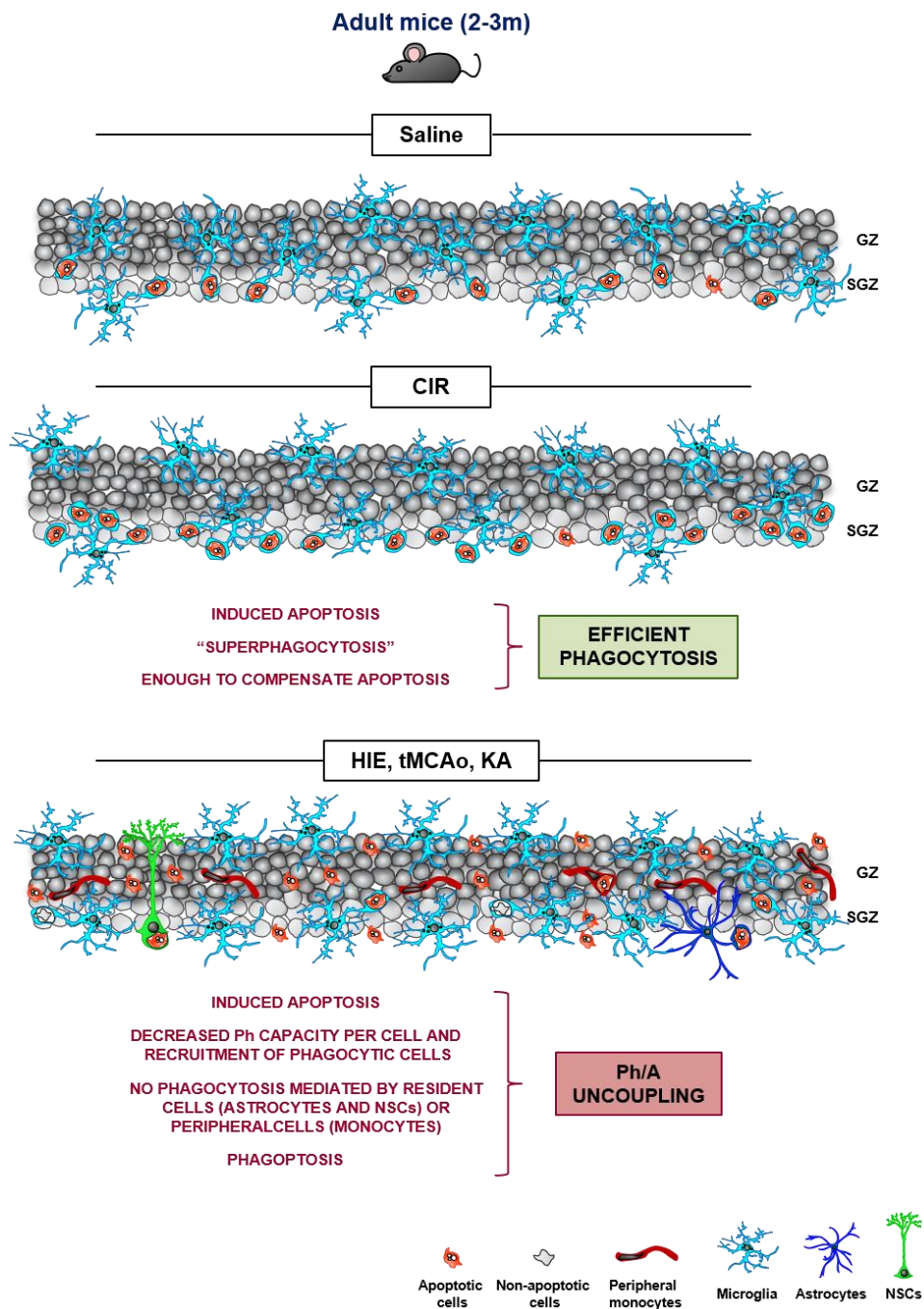
Figure 42. Adult microglial phagocytosis/apoptosis coupling in health and disease. *Microglia subjected to apoptotic challenge induced by CIR, HIE, tMCAo (as a model of stroke), and KA (as a model of MTLE) showed different phagocytic efficiency. First, the amount of apoptosis caused after CIR was rapidly removed from the parenchyma 24h later, indicating a "superphagocytic" capacity. Nonetheless, an opposite scenario occurred in HIE, tMCAo, and KA, where microglial phagocytosis reduced their phagocytic capacity and recruitment of phagocytic cells, leading to an uncoupling between phagocytosis and apoptosis. The impairment of microglial phagocytosis was not compensated by other resident cells (astrocytes and NSCs) or peripheral cells (monocytes) with phagocytic potential and was accompanied by phagoptosis.*
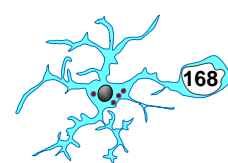
6.3 HIPPOCAMPAL NEWBORN CELLS SURVIVAL IN THE NEUROGENIC NICHE ACROSS ADULTHOOD

The following data was published in the article titled "A simulation model of neuroprogenitor proliferation dynamics predicts age-related loss of hippocampal neurogenesis but not astrogenesis". **Beccari S***, Valero J*, Maletic-Savatic M, Sierra A. *Scientific Reports* 7: 16528. (2017). (*) These authors contributed equally to this work.

In this section we analyzed another issue related to phagocytosis in the hippocampal neurogenic niche through adulthood: the survival of newborn cells, which we use to determine the baseline of microglial phagocytosis.

6.3.1. The dynamics of hippocampal newborn cell is similar throughout adulthood

To further investigate the dynamics of newborn cells survival, we performed a systematical analysis of the hippocampal cascade at two levels: 1, longitudinally (from 2h to 30d of cell life), and 2, transversally (from 1 month (1m) to 12m of age)**(Fig. 43)**. All experiments were performed in male mice to avoid possible differences related to animal gender. For our purpose, we used a semicumulative BrdU paradigm, in which BrdU was injected at 150mg/kg every 2h for 6h [Sierra et al., 2015](4x BrdU)**(Fig. 43A)**. This experimental strategy using a BrdU saturating dose prevents dilution of BrdU label over the time period studied [Sierra et al., 2010]. Moreover, a repeated injections paradigm increases the number of labeled cells and maximizes the probability of observing BrdU$^+$ cells in older mice, particularly at later stages of the neurogenic cascade. Another important point in this set of experiments is that we only quantified BrdU$^+$ cells localized in the SGZ as well as GZ of the hippocampus **(Fig. 43B)**, discarding those few cells found in the hilus or molecular layer (ML), which could complicate the interpretation of our data **(Fig. 43C)**.
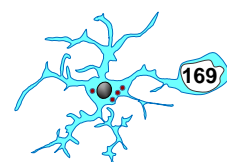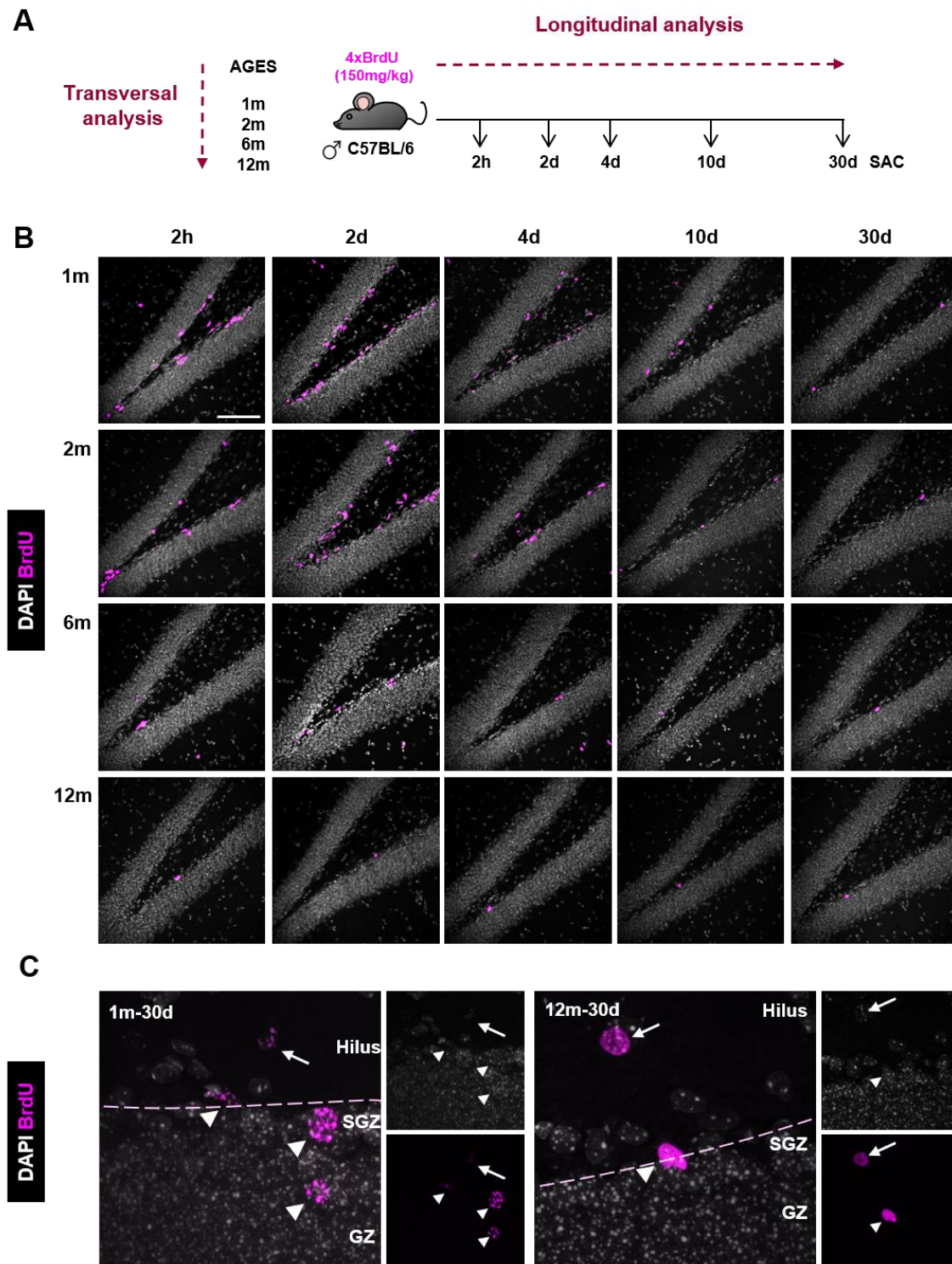
Figure 43. Systematical analysis of the hippocampal niche through adulthood. [A] *Experimental design used to analyze the murine hippocampal niche both longitudinally (from 2h to 30d of cell life) and transversally (from 1 month (1m) to 12m of age). Mice received an injection of BrdU every 2h for 6h (4x total) and were sacrificed (SAC) at different time points after the last injection.* **[B]** *Representative confocal z-stacks of the dentate gyrus (DG) of 1, 2, 6 and 12m C57BL/6 mice at 2h, 2d, 4d, 10d, and 30d after the BrdU injections (in magenta). Cell nuclei and the outline of the DG were determined with DAPI (in white).* **[C]** *High magnification confocal image of BrdU⁺ cells (in magenta) at 30d after BrdU injection in 1 and 12m mice. Nuclei were visualized with DAPI (in white). Arrowheads point to BrdU⁺ cells in the SGZ or the GZ (included*

170

in the analysis); arrows point to BrdU⁺ cells in the hilus (excluded from the analysis). Scale bar=100 µm; z=16.5µm.

We found that the number of BrdU⁺ cells in the whole hippocampus significantly declined with increased age at all time points analyzed (2h-30)**(Fig. 44A, B)**, in agreement with previous studies [Dayer et al., 2003; Encinas et al., 2011; Kempermann et al., 1998; Kuhn et al., 1996; Mandyam et al., 2007]. In all ages tested (1-12m), the maximum number of BrdU⁺ cells reached at 2d, suggesting a period of net proliferation between 2h and 2d **(Fig. 44A, B)**. The same scenario was observed in the septal portion of the hippocampus in spite of receiving different innervation and presenting cognitive functional differences compared to the temporal portion [Bannerman et al., 2002; Jinno, 2011; Strange et al., 2014]. It should be mentioned that the number of BrdU⁺ cells at 2d was to some extent smaller compared to other reports that used a single BrdU injection paradigm (1x BrdU)[Encinas et al., 2011; Kempermann et al., 2004; Mandyam et al., 2007; Sierra et al., 2010] and/or longer cumulative labeling paradigms (8x BrdU, injected every 3h for 24 h)[Sierra et al., 2010]. These data suggested that in multiple BrdU injection paradigms the overlap between the cell cycle progression and survival of the first labeled cohort as well as the continued labeling of subsequent cohorts of proliferating cells complicates the interpretation of the cell proliferation or BrdU peak detected at 2d. After this period of time, the absolute number of BrdU⁺ cells dramatically decreased up to 30d at all ages studied (1-12m)**(Fig. 44A, C)**. Moreover, no major differences were found when we normalized the time course for each age studied by the number of BrdU⁺ cells at 2d **(Fig. 44B, D)**. Thus, these data showed that the **dynamics pattern of hippocampal newborn cells was maintained across adulthood and largely depended on the initial number of proliferating neuroprogenitors**.

To further confirm this hypothesis, we next explored in more detail each step of the hippocampal neurogenic cascade focusing on proliferation, survival, and differentiation. First, we analyzed the period of net proliferation between 2h and 2d, where the maximum number of BrdU⁺ cells was found. No significant differences were found in the relative numbers of BrdU⁺ cells during this interval of time **(Fig. 44B, D)**, showing that the net proliferation between 2h and 2d is proportional to the initial number of proliferating cells throughout ages. To analyze the proliferation of BrdU⁺ cells at 2d, we analyzed the expression of Ki67, a well-known proliferation marker, which is expressed by cells during all active phases of the cell cycle [Scholzen and Gerdes, 2000]. We found no changes in the mitotic rates of newborn cells at 2d across adulthood **(Fig. 44E, F)**, suggesting that
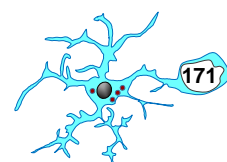
proliferation capacity of neuroprogenitors population is maintained largely constant up to 12m.
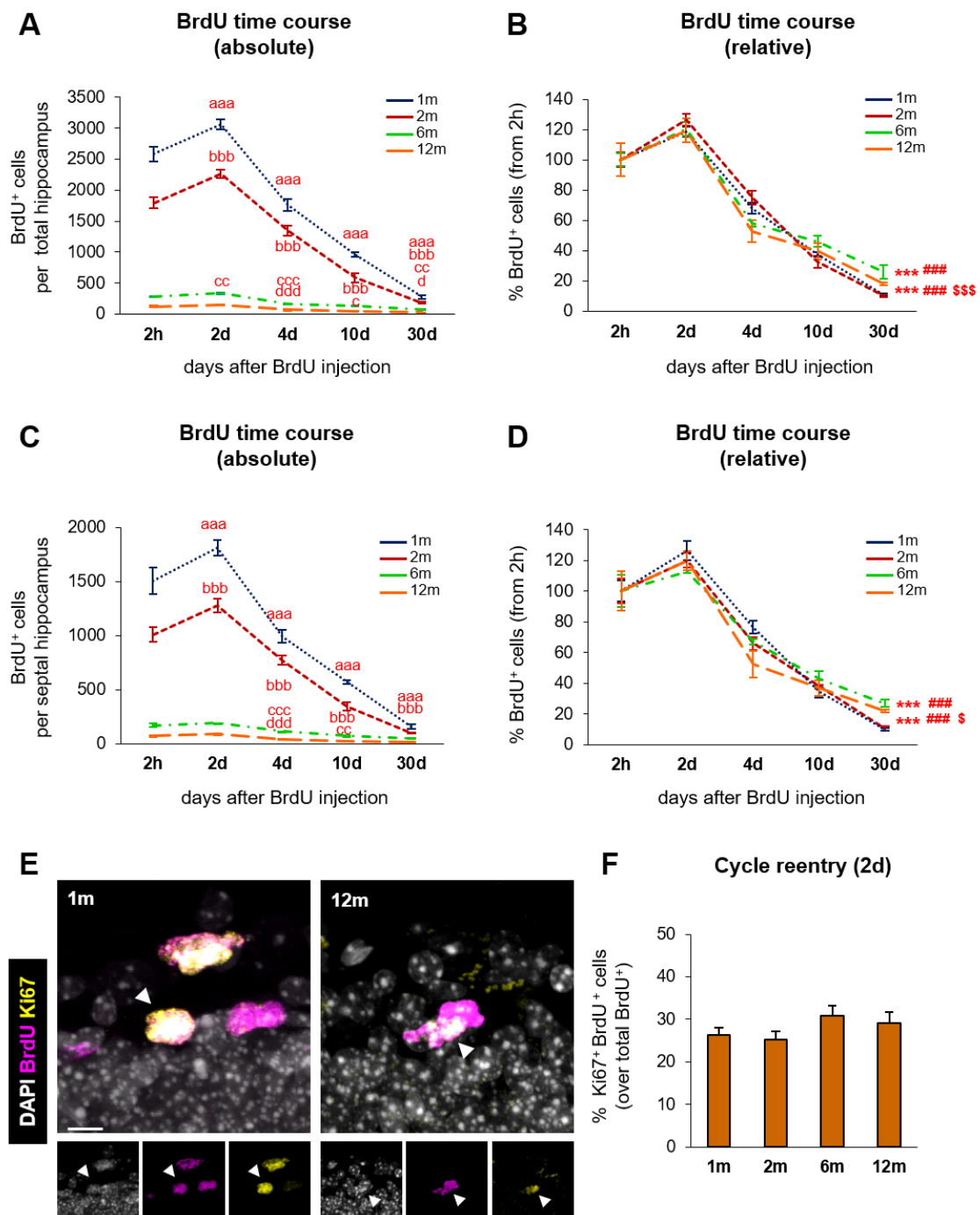
Figure 44. Hippocampal BrdU+ cells wane with age. [A] Absolute number of BrdU+ cells in the whole hippocampus along the BrdU time course. [B] Percentage of BrdU+ cells per whole hippocampus. Relative cell numbers were obtained from the normalization of the total BrdU+ cells found at 2h. [C] Absolute number of BrdU+ cells in the septal hippocampus along the BrdU time course. [D] Percentage of BrdU+ cells per septal hippocampus. Relative cell numbers were obtained from the normalization of the total BrdU+ cells found at 2h. [E] Representative confocal z-stacks of the DG of 1 and 12m mice at 2d after BrdU injection. [F] Percentage of BrdU+ cells that re-enter in cell cycle, assessed by their co-labeling with the proliferation
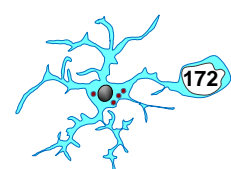
marker Ki67 (in yellow) 2d after BrdU injection. Bars represent mean $\pm$ SEM (standard error of the mean).
The effect of time after BrdU and age on the number of BrdU cells in the total [A] and septal [C] hippocampus
was analyzed using a 2-way ANOVA. Significant interaction between the two factors (time after BrdU
injection x age) was found, and therefore data were split into five 1-way ANOVAs to analyze statistical
differences due to the time after BrdU injection at each time. Holm-Sidak was used as a posthoc test. a, b,
c and d represent significance compared to the prior time point for 1m, 2m, 6m and 12m mice, respectively.
One symbol represents p<0.05, two: p<0.01, and three: p<0.001. In [B, D], no significant interaction was
found between the factors and effect of age but a significant effect of the time after BrdU injection. While no
overall effect of age was found, statistical differences due to the age at each time point was analyzed using
1-way ANOVA. Holm-Sidak was used as a posthoc test. Three symbols (*, #, \$) indicate p<0.001 between
1 and 2m vs 6m, 1 and 2m vs 12m, and 6m vs 12m at 30d, respectively. Only significant effects are shown.
In [A, B, C, D], n=5 for 1 and 2m mice at 2h, 2d, 4d, 10d and 30d; n=4 for 6m mice at 2h, 2d, 4d, 10d and
30d; n=7 for 12m mice at 2h, 2d, 4d and 10d, and n=10 for 12m mice at 30d. In [F], n=10 at 1m and 2m;
n=8 at 6m; n=14 at 12m. Scale bar=20µm [E]; z=22µm [E].

6.3.2. The critical periods of hippocampal newborn cell survival are maintained across adulthood

After the period of net proliferation at 2h-2d interval, the number of BrdU+ cells dramatically undergo death by apoptosis, at least in juvenile mice (1m)[Sierra et al., 2010]. Apoptotic cells are rapidly and efficiently cleared by resident microglia across adulthood [Sierra et al., 2010], and as a result they are very difficult to quantify, especially in older mice. Therefore, instead of directly quantifying apoptotic newborn cells, we quantified the total numbers of BrdU+ cells as a measure of net survival in three critical periods: 2d-4d, 4d-10d, and 10d-30d **(Fig. 45)**. At all ages, the largest BrdU+ cells loss per day occurred in the 2d-4d interval **(Fig. 45A)**. The decay of BrdU+ cells was smaller in the 4d-10d and 10d-30d intervals, indicating a late critical period of survival **(Fig. 45A)**. These results confirmed prior findings of our group showing that most of newborn cells undergo apoptosis in the first critical period of survival in juvenile mice (1m)[Sierra et al., 2010]. The similarity of BrdU+ cell decay at the different periods of survival was more evident when we normalized the data to the number of BrdU+ cells at 2d, because the largest decay rate also occurred in the first 2-4d, when 40 to 56% of the BrdU+ cells were lost **(Fig. 45B)**. Mature mice (6-12m) had a small but significant decrease in the cell loss rate in the 4-10d period (26%-34% in 1-2m vs 10-11% in 6-12m)**(Fig. 45B)**. Together, these results showed that 1, the **main critical period of survival (2d-4d) was maintained across adulthood** and 2, the **net survival of newborn cells at 30d was partially increased in mature mice (6-12m)**. This data also implies that newborn neurons undergo apoptosis at similar developmental stages throughout adulthood, and
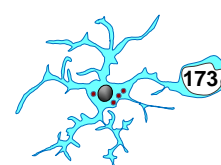
suggests that **the adult neurogenic niche can be used to analyze phagocytosis in mature mice.**

To further comprehend the longitudinal decay of BrdU+ cells after 2d peak, we fitted each age population to an exponential decay curve with plateau over the time course (2d-30d)**(Fig. 45C)**. The BrdU+ cell decay from 2d to 30d was notably similar at 1-2m mice, with a half-life of 2.7-2.8d and a survival plateau reached at 10.3-12.8% (of the 2d peak). A similar scenario was observed in a set of independent data previously published and obtained from 1m mice using either 1x BrdU or 8x BrdU paradigms [Sierra et al., 2010], which validated the results obtained **(Fig. 45D)**. Conversely, BrdU+ cells at 6-12m had a shorter half-life (1.1d) and the survival plateau was reached at 22.1-29.4% (of the 2d peak)**(Fig. 45C)**. These data suggested that **in mature mice the half-life of BrdU+ cell was shorter but more cells survived compared to younger mice**.
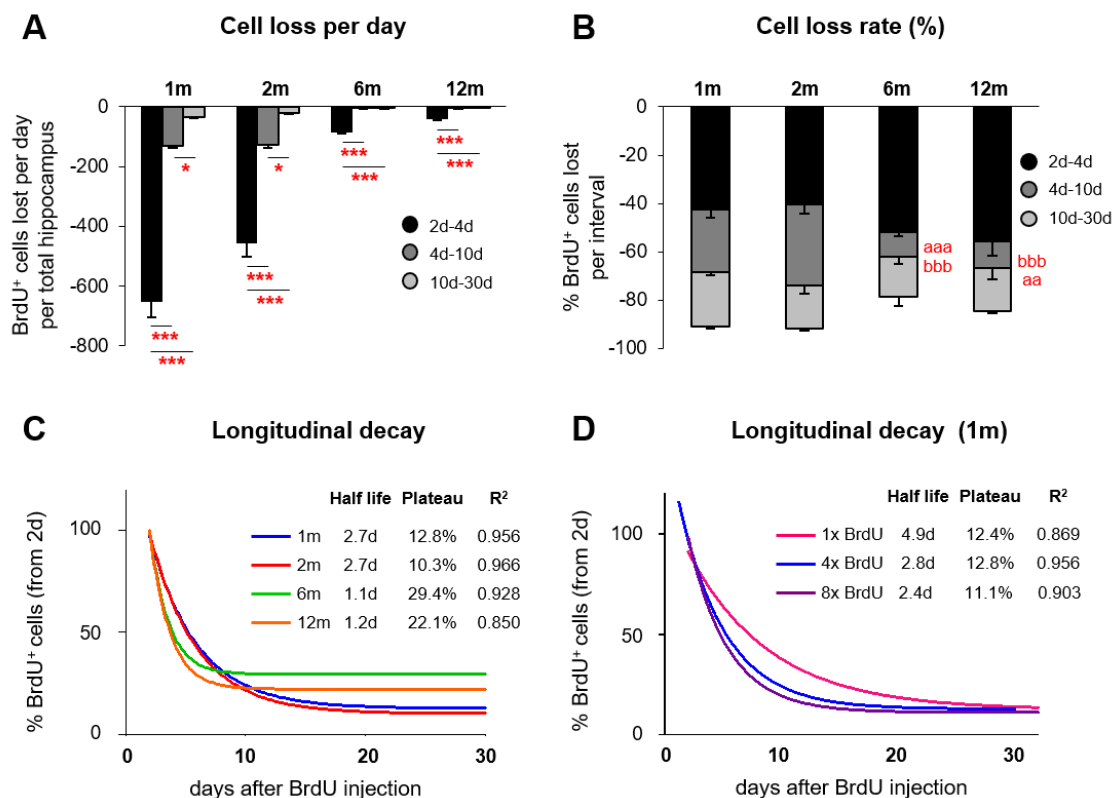
Figure 45. Longitudinal decay of hippocampal newborn cell populations. [A] *Total number of BrdU+ cells lost per day in the whole hippocampus during the intervals 2d-4d, 4d-10d, and 10d-30d.* **[B]** *Percentage of BrdU+ cells lost per interval (2d-4d, 4d-10d, and 10d-30d) from the number of BrdU+ cells at 2d at each interval in the whole hippocampus.* **[C]** *Longitudinal decay of BrdU+ cells from 2d to 30d after BrdU injection. These data were calculated as an exponential curve with plateau. Fitting curve, cell half-life, percentage of survival plateau, and R2 are indicated.* **[D]** *Longitudinal decay of 1m simulated BrdU+ cells from 2d to 30d after BrdU injection. These data were calculated as an exponential curve with plateau obtained with three BrdU administration protocols: 4x (shown in this Thesis), and 1x and 8x (from [Sierra et al., 2010]). From*
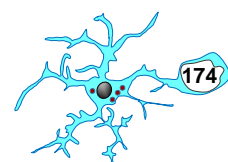
each population, the fitting curve, cell half-life, percentage of survival plateau, and R^2 are indicated. Bars represent mean ± SEM (standard error of the mean). The effect of the age in the loss of BrdU+ cells per period of time after injection [A], and the effect of the period in the loss of BrdU+ cells at each age [B] was analyzed using 1-way ANOVA. Holm-Sidak was used as a posthoc test. In [A]: one, two or three symbols (*) indicate p<0.05, two: p<0.01, and three: p<0.001 between periods for each age, respectively. In [B]: a, b, c and d represent significance compared to the prior time point for 1m, 2m and 6m; respectively. Two symbols are used to p<0.01 and three for p<0.001. Only significant effects are shown. In [A], n=5 for 1 and 2m mice at 2h, 2d, 4d, 10d and 30d; n=4 for 6m mice at 2h, 2d, 4d, 10d and 30d; n=7 for 12m mice at 2h, 2d, 4d and 10d, and n=10 for 12m mice at 30d.

6.3.3. Neuron and astrocyte generation are inversely regulated across adulthood

Finally, we explored whether the differentiation step of newborn cells was affected by increased age **(Fig. 46)**. For this purpose, we analyzed the expression of NeuN (neuronal marker) or GFAP (astrocytic marker) in BrdU+ cells at 30d. GFAP is expressed not only by astrocytes but also by neural stem cells (NSCs)[Kronenberg et al., 2003], therefore, to discriminate both populations we based on the ramified (i.e., non-radial) morphology of astrocytes. Because both NeuN and GFAP detecting antibodies were made in rabbit, we used them in adjacent section series and their combined number only roughly added to 100%. However, it is possible that BrdU labeled other cell types such us microglia, although their proliferative level in physiological conditions is very low [Lopez-Atalaya et al., 2018]. We observed that the newborn neurons ratio (NeuN-BrdU+) significantly decreased at 6-12m (51-56%) compared to 1-2m (79-87%). The opposite scenario was found when we quantified the percentage of newborn astrocytes (GFAP-BrdU+), which significantly increased at 6-12m (40-44%) compared to 1-2m (18-19%)**(Fig. 46A, B)**. In addition, the number of newborn neurons decreased from 1m to 12m, in a pattern reminiscent to that of proliferating neuroprogenitors found at 2h **(Fig. 44A)**. In contrast, the number of newborn astrocytes remained largely constant through adulthood and declined at very slow rate **(Fig. 46C)**. Thus, these results suggested that **neuron and astrocytes productions were inversely regulated across adulthood**.

Next, we compared the transversal decay of the three populations: proliferating neuroprogenitors (at 2h), newborn neurons (at 30d), and newborn astrocytes (at 30d) from 1m to 12m. To do that, we fitted each population to an exponential decay curve **(Fig. 46D)**. We observed that the decay occurred at different rates for each population. The decay of proliferating neuroprogenitors and newborn neurons was remarkably similar throughout adulthood, with a half-life of 53 and 49d, respectively. Excited by these findings, we performed a similar analysis of neuroblast samples (identified by
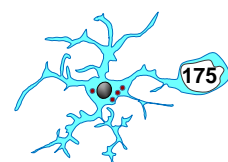
doublecortin, DCX$^+$) from human tissue, previously published [Knoth et al., 2010]. The optimal fitting was obtained when the samples were split into two populations, younger and older than 2 years of age (y) **(Fig. 46E, F)**. It should be mentioned that the 2y splitting point coincides with a previously identified maturation benchmark of the human brain, at 2-3y when it reaches 90-95% of adult brain weight [Semple et al., 2013]. Similarly, the human hippocampal volume increases sharply up to 2y and more slowly afterwards [Utsunomiya et al., 1999]. We observed that in infants under 2y, the neuroblast decayed exponentially with a half-life of 191d. The exponential decay of neuroblast density together with the roughly linear increase in hippocampal volume from birth up to 2y suggests an age-related decrease of neuroblast population. After the 2y benchmark and through adulthood the hippocampal volume is maintained largely constant and starts to decrease only in advanced age (over 70y) in healthy people [Šimić et al., 1997]. We found that in children over 2y and up to 100y the loss of neuroblast density decayed with a half-life of 25y **(Fig. 46E, F)**. Conversely, we discovered that the population of newborn astrocytes in the mouse hippocampus decayed at a slower rate and had a relatively long half-life of 161d compared to newborn neurons (half-life: 49d)**(Fig. 46D)**. Together, these data showed that **proliferating neuroprogenitors gave rise a differential production of neurons and astrocytes throughout adulthood**. Intrigued by these results, we next explored the neurogenic and astrogenic yield of the proliferating neuroprogenitors.
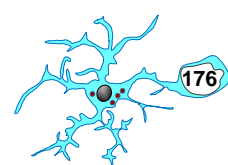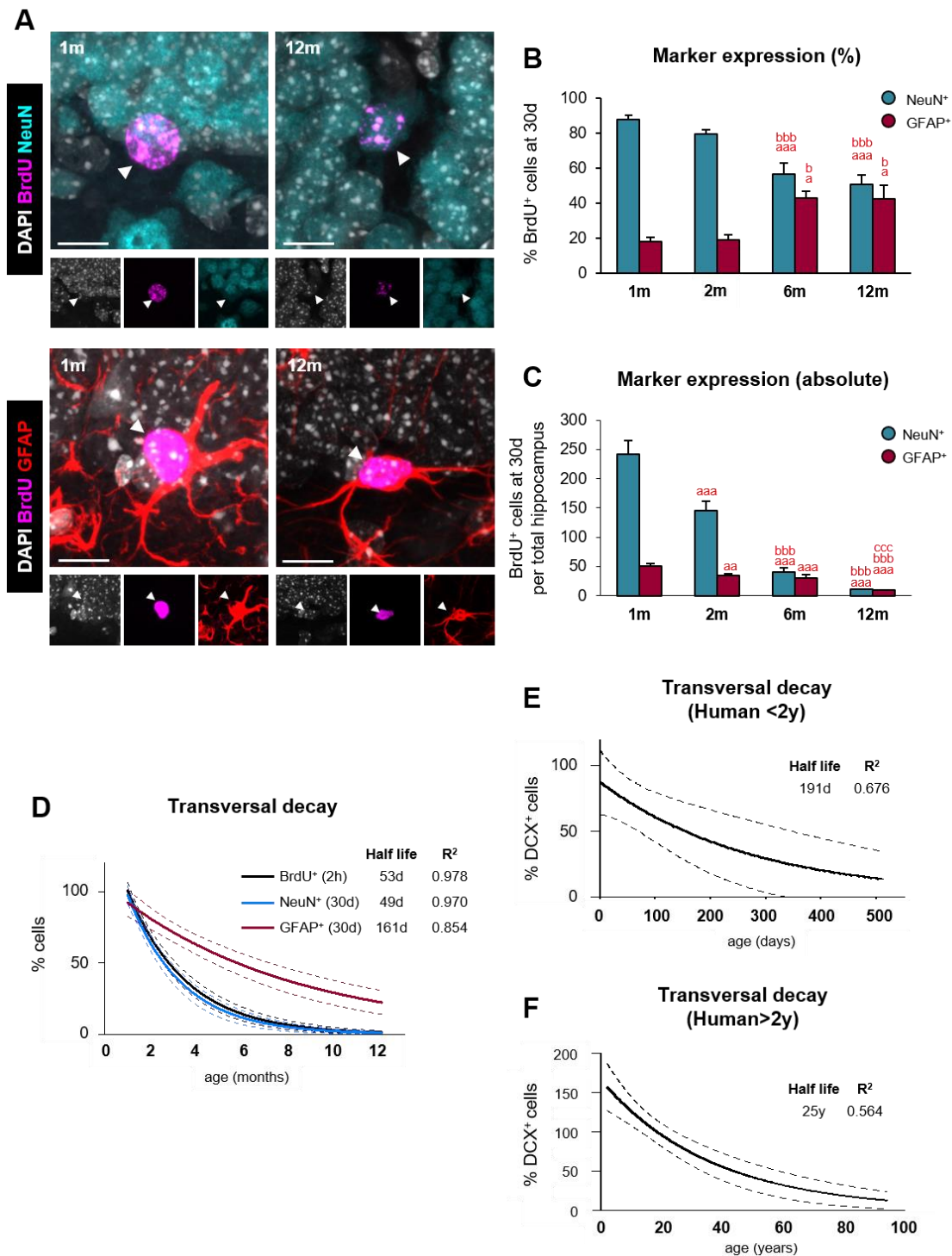
Figure 46. Transversal decay of hippocampal newborn cell populations. *[A] Representative confocal z-stacks of newborn neurons and astrocytes in the DG of 1 and 12m mice at 30d after the BrdU injections. BrdU+ cells (in magenta) were co-labeled with NeuN (mature neuronal marker, in cyan) or GFAP (mature astrocyte marker, in red). DAPI staining indicated cell nuclei (in white). [B] Percentage of BrdU-labeled neurons (NeuN) and astrocytes (GFAP) among the total number of BrdU+ cells in the DG at 30d. n=4 (at 1 and 2m), n=6 (at 6m), and n=5 (at 12m) for %NeuN+ BrdU+. n=9 (at 1 and 2m), n=10 (at 6m), and n=20 (at 12m) for %GFAP+ BrdU+. [C] Absolute number of BrdU-labeled neurons (NeuN) and astrocytes (GFAP) among the total number of BrdU+ cells in the DG at 30d. [D] Transversal decay of BrdU+ at 2h, BrdU+ NeuN+*

*at 30d and BrdU+ GFAP+ cells at 30d, is best fitted with an exponential curve. Fitting curve, cell half-life, and R² are indicated. **[E]** Transversal decay of DCX+ cells in infants under 2y (from [Manganas et al., 2007]). The fitting curve and 95% confidence Interval (dotted line), half-life, and R² are shown. **[F]** Transversal decay of DCX+ cells in children over 2y and adults (from [Manganas et al., 2007]). The fitting curve and 95% confidence Interval (dotted line), half-life, and R² are shown. Bars represent mean ± SEM (standard error of the mean). The effect of the age in the percentage **[B]** and absolute numbers **[C]** of newborn neurons (NeuN+ BrdU+) or astrocytes (GFAP+ BrdU+) at 30d was analyzed using 1-way ANOVA. Holm-Sidak was used as a posthoc test. a, b and c represent significance respect to 1m, 2m and 6m, respectively. Two symbols indicate p<0.01 and three for p<0.001. Only significant effects are shown. In **[C, D]**, n=5 (at 1 and 2m), n=4 (at 6m), and n=15 (at 12m) for NeuN+ and GFAP+ cells. Scale bars=10µm **[A]**; z=14µm **[A]**.*

6.3.4. The age-related decrease in neurogenesis is predicted by the proliferation of neuroprogenitors

Current methodology does not allow us to follow the fate of newborn cells in real time, but only in post-mortem tissue at different time points. Therefore, to analyze the relationship between proliferating neuroprogenitors and their offspring, we used a mathematical model. First, we extracted the mean survival of the BrdU+ cells (proliferating neuroprogenitors) at 2h and the differentiation rates experimentally estimated at 30d. Then, both data were used to estimate the number of simulated new neurons and new astrocytes produced at each age studied (1-12m)**(Fig. 47)**. We found that the initial number of BrdU+ cells at 2h was remarkably correlated with the numbers of simulated new neurons across ages (R^2=0.981)**(Fig. 47A)**. In contrast, the number of simulated new astrocytes was not predicted by the number of BrdU+ cells from 1 to 12m (R^2=0.444)**(Fig. 47B)**.

Nevertheless, this direct simulation was based only on the mean values and did not consider the biological variability of the populations. To solve this issue, we generated a pseudorandom simulation model suing a Marsaglia polar method that considered both the mean and standard deviation of the survival and differentiation rates estimated experimentally. Based on our BrdU data obtained along the study **(Fig. 44-46)**, we imposed two biological restrictions: 1, the maximum number of BrdU+ cells peaked at 2d; 2, the number of BrdU+ cells continuously decayed after 2d; and 3, the total number of BrdU+ cells at 30d was the sum of neurons and astrocytes **(Fig. 47C)**. Two models were possible from these imposed restrictions: 1, simulate the number of newborn astrocytes and calculate the number of newborn neurons as the total BrdU+ cells at 30d minus the number of newborn astrocytes (GFAP-locked model) and 2, simulate the number of newborn neurons and calculate the number of newborn astrocytes (NeuN-locked model). We found that the GFAP-locked model showed a smaller deviation from the
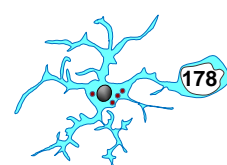
experimentally estimated data compared to the NeuN-locked model (4.7% vs 7.6%, respectively). Then, we generated pseudorandom populations of 1000 proliferating neuroprogenitors (BrdU$^+$ at 2h) and their fate at 2, 4, 10, and 30d for 1, 2, 6, and 12m mice based on GFAP-locked model.

Next, we compared the Marsaglia simulation model obtained from our experimentally estimated data (4x BrdU) with an independent set of data previously obtained in 1m mice using 1x BrdU and 8x BrdU paradigms at different time points (2, 3, 4, 8, 11, 15, 18, 22, and 32d)[Sierra et al., 2010]. To this end, we first generated the simulated longitudinal decay curve for 1m mice (R^2=0.951)**(Fig. 47D)**, which actually produced a similar cell half-life and survival plateau as the fitting curve obtained with our previous experimentally estimated data (R^2=0.956)**(Fig. 45C)**. After that, we compared the simulated 4x BrdU curve to the experimental 1x and 8x BrdU longitudinal decays by calculating the difference between the mean value of BrdU$^+$ cell number for each time point and the value predicted from the simulated longitudinal decay curve **(Fig. 47D)**. No significant differences were found between our Marsaglia simulation model and the data obtained with 1 and 8x BrdU paradigms (p=0.1124 and p=0.0822, respectively) or with the experimentally estimated 4x BrdU (p=0.9448), validating the use of our Marsaglia model to analyze BrdU$^+$ newborn cell dynamics. After confirming the *reliability* of the model, we used it to examine the relationship between proliferating neuroprogenitors (BrdU$^+$ at 2h) and their offspring (BrdU$^+$ at 30d). The number of simulated neuroprogenitors was remarkably correlated with the number of simulated new neurons (R^2=0.850)**(Fig. 47D)**. On the contrary, the number of simulated new astrocytes generated was not well predicted by the number of simulated neuroprogenitors (R^2=0.067)**(Fig. 47F)**. In parallel, we also found that in older mice (6-12m) the number of simulated astrocytes was largely above the fitting curve of the astrogenesis decline **(Fig. 47F)**. Thus, our data demonstrated that **astrocytes production was partially depended on the numbers of proliferating neuroprogenitors across adulthood**.

To further demonstrate the differences in the astrocytic production across ages, we calculated the neurogenic and astrogenic yield (i.e, ratio of the number of newborn neurons and newborn astrocytes at 30d divided by the number of proliferating neuroprogenitors at 2h) from both the experimentally estimated data and the Marsaglia simulated data. Experimentally, we observed that the neuronal yield was similar across ages, although we detected an increase at 6m but not at 12 m, which can be explained by the larger variability of the 6m group **(Fig. 47G)**. Computationally, we found a significantly smaller neuronal yield at 2, 6 and 12m compared to the experimentally estimated data, which is probably related to the use of the GFAP-locked model to
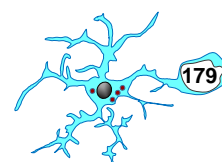
optimize the simulation newborn astrocytes. Additionally, we tested the NeuN-locked model using both experimentally estimated and the Marsaglia simulated data, however smaller differences in the neuronal yields were found. In contrast, we found that the production of newborn astrocytes was significantly smaller in 1-2 compared to 6-12m in both experimentally estimated and the Marsaglia simulated data using the GFAP-locked model **(Fig. 47H)** and the NeuN-locked model. Consequently, the neuron-to-astrocyte ratio (calculated as the ratio between the neuronal yield and the astrocytic yield) decreased from 4.8 at 1m to 1.2 at 12m in the experimental data, and from 4.4 at 1m to 0.8 at 12m in the Marsaglia simulated data. Taken together, these findings demonstrated that **in young mice (1-2m) the proliferating neuroprogenitors gave rise mainly neurons, while in mature mice (6-12m) they generated a similar yield of neurons and astrocytes**.

DIRECT SIMULATION

A Neurogenesis decline

R²=0.981
P<0.0001
○ 1m
○ 2m
○ 6m
○ 12m

B Astrogenesis decline

R²=0.444
P<0.0001
○ 1m
○ 2m
○ 6m
○ 12m

RANDOM SIMULATION

C

D Simulated longitudinal decay (1m)

	Half life	Plateau	R²
4x BrdU	2.7d	13.0%	0.951

○ 1x BrdU
○ 8x BrdU

E Neurogenesis decline

R²=0.850
P<0.0001
○ 1m
○ 2m
○ 6m
○ 12m

F Astrogenesis decline

R²=0.067
P<0.0001
○ 1m
○ 2m
○ 6m
○ 12m

G Neuronal yield

● exp. est. data
● r.sim. data

H Astrocytic yield

● exp. est. data
● r.sim. data
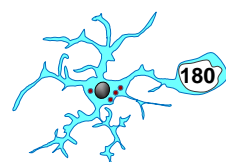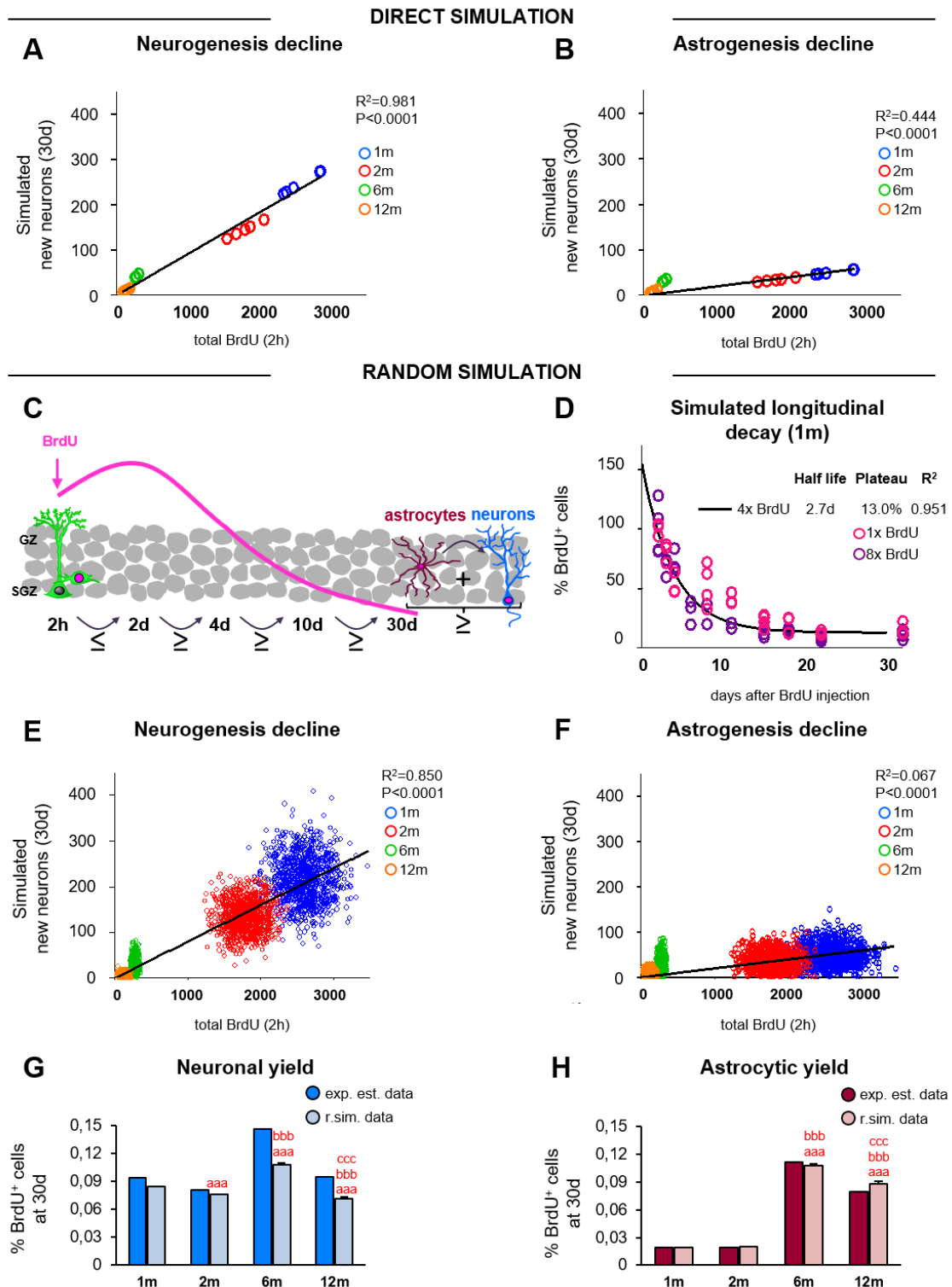
Figure 47. Neurogenesis but not astrogenesis decline is predicted by the reduction number of proliferating neuroprogenitors. [A] *Linear regression of the production of newborn neurons at 30d from proliferating progenitors at 2h across adulthood. Estimated number of BrdU+ cells at 2h obtained from **Fig. 44A** were correlated with simulated number of BrdU+ NeuN+ cells at 30d obtained by applying the estimated survival and differentiation rates (from **Fig. 44B** and **46C**, respectively). Each dot represents an individual value. The linear regression curve, R², and p-value are shown. **[B]** Linear regression of the production of newborn astrocytes at 30d from proliferating progenitors at 2h across adulthood. Estimated number of BrdU+ cells at 2h obtained from **Fig. 44A** were correlated with simulated number of BrdU+ GFAP+ cells at 30d*
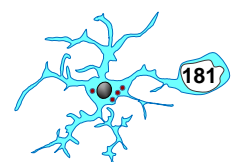
*obtained by applying the estimated survival and differentiation rates (from **Fig. 44B** and **46C**, respectively). Each dot represents an individual value. The linear regression curve, R², and p-value are shown. **[C]** Cartoon representing the random model simulation restrictions. In this model, the number of BrdU⁺ simulated cells at 2d must be equal or larger than at 2h. After 2d, each time point should have the same or fewer BrdU⁺ cells. At the end of the 30d period, the sum of neurons and astrocytes should be equal or smaller than the total BrdU⁺ at 30d. **[D]** Longitudinal decay of 1m simulated BrdU⁺ cells from 2d to 30d, calculated as an exponential curve with plateau. Fitting curve, cell half-life, survival plateau (in %), and R² are indicated. Individual dots represent two independent sets of BrdU data from single (1x) and cumulative (8x) BrdU injection paradigms (from* [Sierra et al., 2010]*). n=3 for 2, 3, 4, 11, 18, and 32d and n=4, 8, 15 and 22d in 1x BrdU; n=3, 6, 8, 11, 15, 22 and 32d; and n=4 for 2, 4, 18 for 8x BrdU. **[E]** Linear regression analysis of the simulated number of newborn neurons at 30d, generated from the proliferating progenitors at 2h across adulthood using the Marsaglia polar simulation model. Pseudorandom simulated numbers of BrdU⁺ cells at 2h and BrdU⁺ NeuN⁺ cells at 30d were obtained using the mean and standard deviation values (**Fig. 44A, B and 46D**). 1000 pseudorandom cells per age group for each population were generated. Each dot represents an individual value. The linear regression curve, R², and p-value are shown. **[F]** Linear regression analysis of the simulated number of newborn neurons at 30d, generated from the proliferating progenitors at 2h across adulthood using the Marsaglia polar simulation model. Pseudorandom simulated numbers of BrdU⁺ cells at 2h and BrdU⁺ GFAP⁺ cells at 30d were obtained using the mean and standard deviation values (**Fig. 44A, B and 46D**). 1000 pseudorandom cells per age group for each population were generated. Each dot represents an individual value. The linear regression curve, R², and p-value are shown. **[G]** Neuronal yield of proliferating neuroprecursors derived from the experimentally and the Marsaglia polar data. **[H]** Astrocytic yield of proliferating neuroprecursors derived from the experimentally and the Marsaglia polar data. Bars represent mean ± SEM (standard error of the mean). The effect of the age in neuronal **[G]** and astrocytic **[H]** generation was analyzed using Kruskal-Wallis. a, b and c represent significance compared to 1m, 2m and 6m, respectively. Two symbols indicate p<0.01 and three for p<0.001. Only significant effects are shown.*

6.3.5. The increased astrogenic yield across adulthood is explained by the increased BrdU⁺ cell survival during the late critical periods

Finally, we explored the possible mechanisms underlying the differential neuro/astrogenic duality of neuroprogenitors across ages. We noticed that in mature mice (6-12m): 1, the astrogenic yield was larger compared to young mice (1-2m)**(Fig. 47H)**; and 2, the net survival of BrdU⁺ cells at 30d was higher compared to 1-2 mice **(Fig. 45B, C)**. These two events led to us hypothesize that the increased BrdU⁺ cell net survival at 30d in mature mice could be explained by the increased production or survival of astrocytes. To address this hypothesis, we created a different computational scenario, in which we compared the effect of adding more newborn neurons and/or astrocytes to our basic model described above. The best scenario to analyzed the experimentally estimated data and the Marsaglia simulation was obtained from the neuron-to-astrocyte ratio (calculated as the ratio between the neuronal yield and the astrocytic yield)**(Fig. 47G, H)**. We first modeled the net survival at 30d in 6-12m mice as a sum of the baseline net survival and neuron/astrocyte production (as at 1m) and the extra net
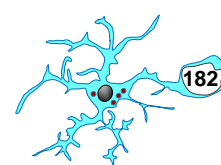
survival in 6-12m mice. This extra survival was modeled considering three different contributions of neurons (N) and astrocytes (A): 100N:0A (blue circle), 50N:50A (blue-dark red circle), and 0N:100A% (dark red circle), respectively **(Fig. 48A)**.

Next, we tested which scenario fit best with the experimentally determined and the Marsaglia simulation data **(Fig. 47G, H)** comparing the neuron-to-astrocyte (N-to-A) ratios. We analyzed the first option (100N:0A) and the ratios obtained were far away from the N-to-A ratio at 6m and 12m both in the experimentally estimated and the Marsaglia simulated data **(Fig. 48B)**, showing that neurons were not contributed to the increased net survival at 30d in mature mice (6-12m). Then, we tested the other two scenarios: 50N:50A and 0N:100A. In both we obtained a better fit of the N-to-A ratio compared to 100N:0A **(Fig. 48B)**. To determine the combination of neuronal and astrocytic contribution that rendered N-to-A ratios identical to the experimentally estimated and the Marsaglia simulation, we performed a simple iterative parameter search algorithm. To do this, we compared two scenarios (initially, 50N:50A and 0N:100A), determining a middle point in between (i.e.; 25N:75A), and comparing this third point with the best fitting of the initial pair. Firstly, the algorithm tested two different combinations of neuronal and astrocyte contributions (C) (C1=100N:0A and C2=0N:100A) and selected the optimal combination that rendered the smallest absolute difference to target N-to-A ratio. After, the selected combination was compared with a newer combination until the goal N-to-A ratio was reached. As a result, we found that at 6m the N-to-A ratio was 38N:62A (experimentally estimated) and 28N:72A (Marsaglia simulation). At 12m, the contribution of neurons to the increased net survival was smaller compared to 6m, as the N-to-A ratio was 2N:98A in the experimentally estimated data. Regarding the Marsaglia simulated N-to-A yield at 12m, these data could only be optimized when the baseline production of neurons was below the levels of 1m mice, resulting in -12N:112A ratio **(Fig. 48B)**. The negative proportion of neurons could either be explained by the variability of data, which in fact represents an optimal scenario of 0N:100A; or a reduced production of neurons a favor of astrocytes. Taking together, these data demonstrated that **the increased BrdU$^+$ cells net survival at 30d was due to increased production of astrocytes in mature mice (6-12m) compared to young mice (1-2m)**.
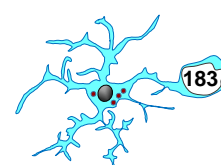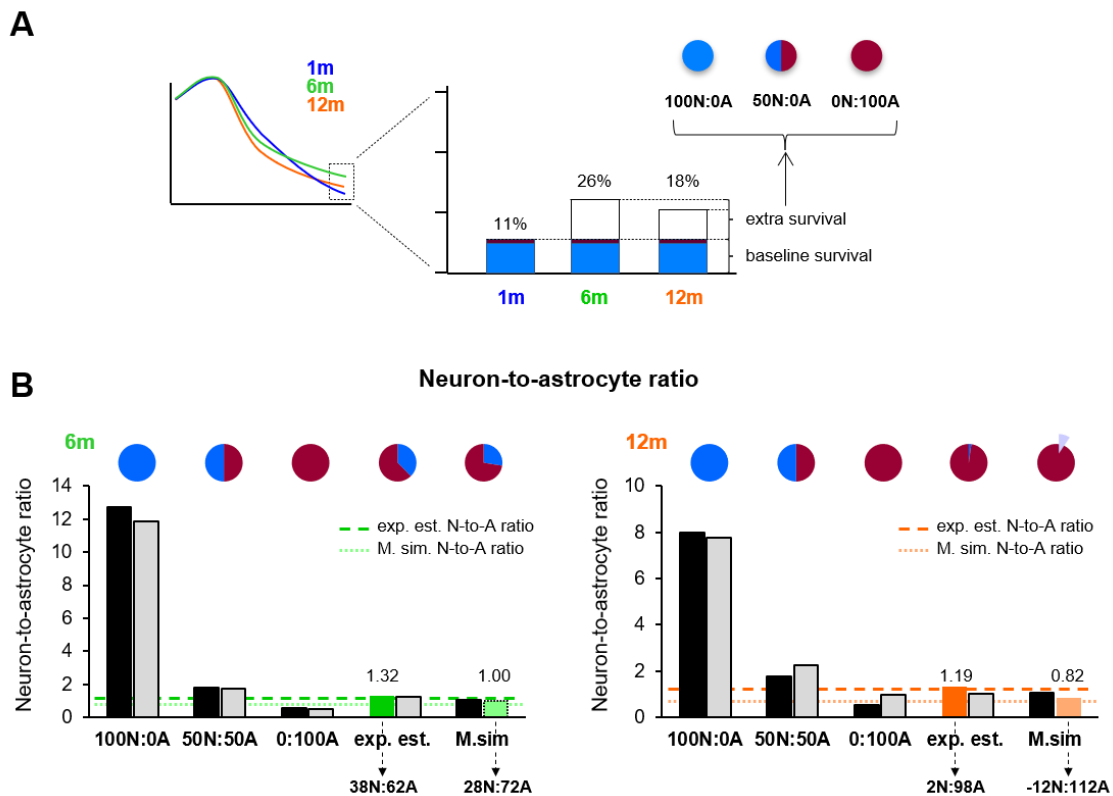
Figure 48. Hippocampal neuroprogenitors produce differential neurogenic and astrogenic outputs throughout adulthood. [A] *Cartoon representing the strategy used to recreate different scenarios of newborn neuronal and astrocyte survival (100:0, 50:50, and 0:100%) to account for the increased (extra-) survival found in 6m and 12m compared to 1m.* **[B]** *Neuron-to-astrocyte ratio from experimentally estimated and the Marsaglia simulated data in 6 and 12m mice was calculated for each of the scenarios of neuronal and astrocyte survival (100:0, 50:50, and 0:100% of the extra survival). Optimal proportions that allowed to reach the target ratios for the experimentally estimated and the Marsaglia simulated data are drown on the top. At 12m, the target ratio from the Marsaglia simulated data could only be reached with negative contributions of neurons (represented by a light purple pie slice).*

In summary, in the last part of this PhD thesis project we focused on another important point related to microglial phagocytosis in the hippocampal niche: the survival of newborn cells across ages **(Fig. 49)**. First, we performed a systematically analysis of the neurogenic niche both longitudinally (from 2h to 30d of cell life) and transversally (from 1m to 12m of age). This experimental strategy allowed us to uncover that 1, the dynamics pattern of newborn cells was maintained through adulthood and largely depended on the initial number of proliferating neuroprogenitors; 2, the main critical period of survival (2d-4d) was also maintained across ages, confirming previous data published by our group [Sierra et al., 2010]; 3, the net survival of newborn cells at 30d was partially increased in mature mice (6-12m); 4, the half-life of BrdU+ cell was shorter in mature mice but more cells survived compared to younger mice (1-2m); 5, neuron and astrocytes productions were inversely regulated across adulthood; and 6, proliferating
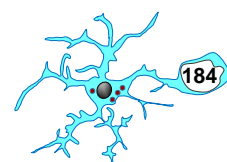
neuroprogenitors gave rise to a differential production of neurons and astrocytes across ages. We noticed that behind these findings there were still crucial aspects of newborn cell dynamics that remained to be uncovered. For that reason, we generated a simple but useful simulation model to predict the changes of newborn cell population with increased age. We discovered that 7, astrocytes production was partially depended on the numbers of proliferating neuroprogenitors across adulthood and 8, in young mice (1-2m) the neuroprogenitors produced mainly neurons, while in mature mice (6-12m) they generated a similar yield of neurons and astrocytes. Thus, our data demonstrated that the hippocampal cascade shifted towards a neuro-astrogenic phenotype with maturity.
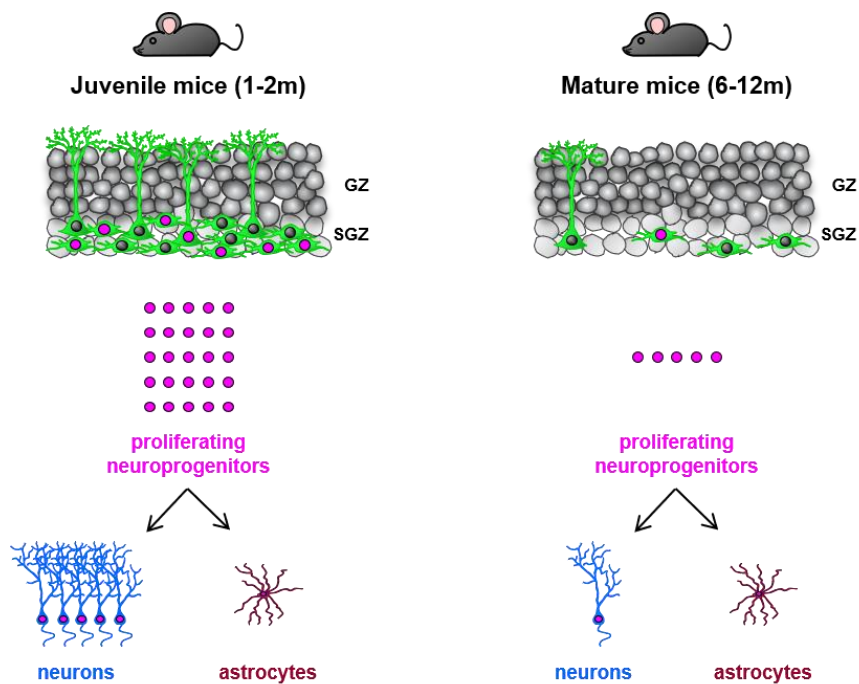
Figure 49. Proposed model to explain the major effect of age on the neuroprogenitor population and newborn neuronal and astrocytic yields. *The number of cells and dots are roughly proportional to the data from 1 and 12m mice (young and mature DG, respectively) shown in* **Figs. 44-47**.

7. DISCUSSION

7. DISCUSSION

Microglial phagocytosis is at the epicenter of the brain regenerative response in neurodegenerative diseases. First, it prevents the spillover of potentially toxic intracellular content that results from the cell death, and second, apoptotic cell clearance actively modulate the initiation of inflammatory and immune responses [Arandjelovic and Ravichandran, 2015; Sierra et al., 2013]. Despite these crucial roles, phagocytosis has been largely overlooked or indirectly assessed in both the healthy and diseased brain.

To uncover the modus operandi of phagocytic microglia, in this PhD Thesis project we addressed their phagocytic potential from different angles:

In the first part, we explored the postnatal microglial efficiency to face apoptotic challenge during early postnatal development evoked by LPS, EtOH, and HIE. We discovered that LPS was not an appropriate model to study phagocytosis at P9 or P14. In contrast, both EtOH and HIE induced apoptosis but the phagocytic response was different in each time point. At P9, microglia increased their Ph capacity in response to apoptosis induced by EtOH and HIE but this tactic was not enough to compensate apoptosis, leading to phagocytosis-apoptosis uncoupling. A different scenario was found at P14, where the increased Ph capacity matched the increase in apoptosis and, therefore, allowed microglia to efficiently cope with the number of dead cells, maintaining phagocytosis-apoptosis tightly coupled. Together, these results suggested a maturation of the microglial phagocytic potential during brain development between P9 and P14.

In the second part, we analyzed the adult microglial response to apoptotic challenge induced by CIR, HIE, tMCAo, and KA at 2-3m. We found that the amount of dead cells induced by CIR was cleaned from the brain parenchyma within 24h, showing an amazing labor of "superphagocytosis". To our surprise, we observed the opposite in HIE, tMCAo and KA, where microglial phagocytosis was rapidly impaired after damage. As a consequence, the phagocytosis-apoptosis coupling was lost, and was not compensated by recruiting other phagocytic cells such as peripheral monocytes and/or astrocytes. In addition, we also observed two phenomena that occurred in parallel to the impairment of phagocytosis: microglial multinucleation and phagoptosis. Together, these results showed that the pathological uncoupling between phagocytosis and apoptosis lead to the accumulation of dead cells in the brain parenchyma, which could exacerbate the pathology.
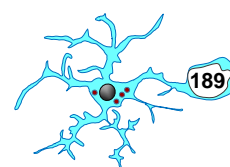
In the third part, we expanded our analysis to another issue related to phagocytosis in the hippocampal neurogenic niche through adulthood: the survival of newborn cells, which we used to establish the baseline of microglial phagocytosis. We performed a systematically analysis of the neurogenic niche both longitudinally (from 2h to 30d of cell life) and transversally (from 1m to 12m of age). We found that the dynamics of newborn cells was maintained through adulthood and largely depended on the initial number of proliferating neuroprogenitors. In addition, we observed that the main critical period of survival (2d-4d) was also maintained across ages, confirming previous data published by our group [Sierra et al., 2010]. Moreover, we used this data to study neurogenesis through adulthood and discovered that proliferating neuroprogenitors gave rise a differential production of neurons and astrocytes across ages. Together, these data allowed us to generate a Marsaglia polar random simulation model to predict newborn cell dynamics, and ultimately, understand the hippocampal neurogenic niche changes across adulthood.

In this section, we will discuss the key points that emerge from our data about microglial phagocytosis, building transversal connections between the different parts of this PhD Thesis project.

7.1 MICROGLIAL PHAGOCYTOSIS/APOPTOSIS COUPLING IN HEALTH AND DISEASE

7.1.1 Microglial responses to phagocytic challenge in the adult brain

Traditionally, the scientific community believed that phagocytosis was only executed by ameboid, activated microglia cells [Kettenmann, 2007]. In contrast our group demonstrated that in physiological conditions unchallenged, ramified, and surveillant microglia are efficient phagocytes [Sierra et al., 2010]. To analyze phagocytosis in brain tissue, we developed a set of quantitative parameters and used as a model the adult hippocampal neurogenic cascade, where newborn neurons naturally undergo apoptosis throughout adulthood [Sierra et al., 2010]. Using this set up we found that the majority of dead newborn cells were engulfed by microglia (Ph index > 90%) and eliminated from the brain parenchyma in a very short time (around 1.5h per apoptotic cell)[Sierra et al., 2010]. This strategic analysis allowed us to establish for the first time the baseline of microglial phagocytosis and, thus, to explore and comprehend the microglial response to phagocytic challenge in the adult brain.
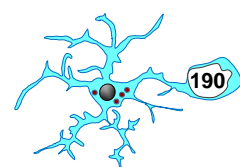
In this PhD Thesis, we explored the phagocytic potential of adult microglia in response to apoptosis evoked by CIR, an essential clinical practice in the treatment of brain tumors [Shah and Kochar, 2018]. Based on rodents models, this therapy induces a large increase in apoptosis in the SGZ of the hippocampus, and mostly affects neuroprogenitors, since they are highly proliferative and, hence, susceptible to DNA damage caused by CIR [Khanna and Jackson, 2001; Peißner et al., 1999; Robbins and Zhao, 2004]. Nonetheless, the effects of CIR on microglial phagocytosis are poorly explored. Prior data suggested that phagocytosis was increased after irradiation exposure in both in vitro and in vivo [Huo et al., 2012; Kalm et al., 2009; Xiao et al., 2015]. However, these studies should be carefully interpreted because the quantification of phagocytosis was assessed by indirect methods such as latex beads or fluorescent microsphere as an engulfment target, but these artificial targets cannot degraded within microglia, resulting in incomplete phagocytosis [Diaz-Aparicio et al., 2016]. More recently, [Osman et al., 2020] reported that adult microglia engulfed several apoptotic cells at the same time in the SGZ after CIR treatment although they did not quantify the proportion of dead cells phagocytosed (Ph index). We followed up on this observation and discovered that hippocampal microglia showed an enormous phagocytic potential to counteract the level of apoptosis induced by CIR.

Our data showed a "superphagocytosis" work executed by microglia, which allowed a fast cleaning of the brain parenchyma in the first 24h after irradiation without reducing the efficiency of phagocytosis, determined by the maintenance of the Ph index. These results suggested an increase in the microglial Ph capacity, which could not be estimated in our experiments because the thickness of the samples was very thin (25µm) to quantify whole microglial cells (soma and their processes), and therefore was not shown in this PhD Thesis. However, our group later optimized the CIR model in collaboration with Prof. Iñigo Casafont (University of Cantabria, Spain), and new results confirmed those suggested here (data from Mar Márquez´s PhD Thesis project; **Fig. 50**). Microglia responded to the increased number of dead cells by rising their Ph capacity, and there were more phagocytic microglia overall, some of them with up to five pouches at 6h after CIR. The fast and efficient phagocytic response allowed the majority of apoptotic cells be completely removed from the brain tissue 24h later.
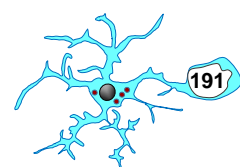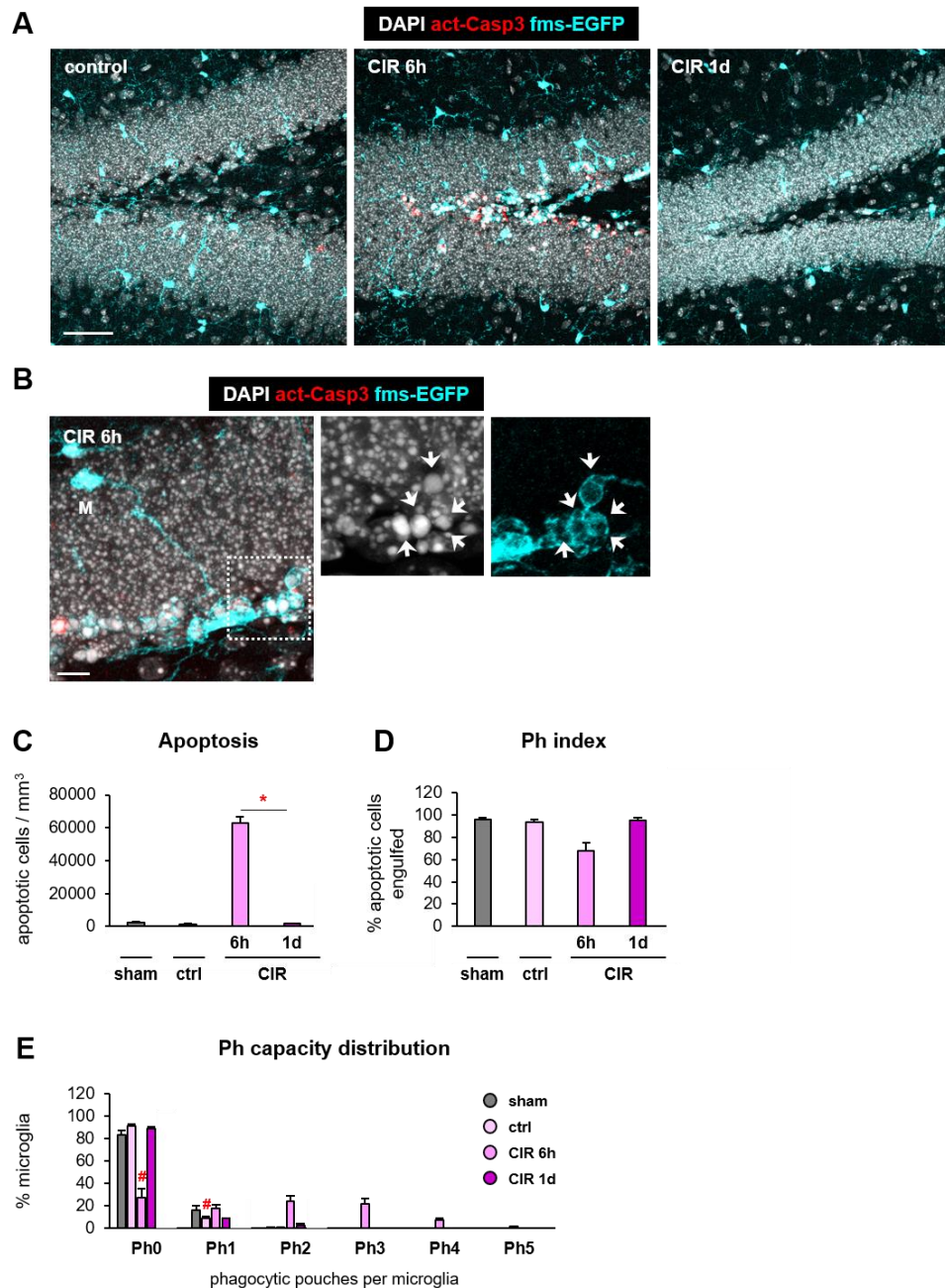
Figure 50. Microglial phagocytosis efficiency increased after CIR. [A] *Representative confocal z-stacks of the DG of 2m fms-EGFP mice at 6h and 1d after cranial irradiation (CIR, 2Gy). Apoptotic nuclei were detected by pyknosis/karyorrhexis (in white, DAPI), microglia by the transgenic expression of fms-EGFP (in cyan).* **[B]** *Representative confocal z-stack of apoptotic cells (pyknotic/karyorrhectic, DAPI, in white, arrow) phagocytosed by microglia (fms-EGFP+, in cyan; M) in the septal DG at 6h after CIR.* **[C]** *Density of apoptotic cells (cells/mm³) in the septal DG.* **[D]** *Ph index (% of apoptotic cells engulfed by microglia) in the septal DG.* **[E]** *Histogram showing the Ph capacity of microglia (% of microglia with pouches). Bars represent mean ± SEM. The effect of CIR on apoptosis **[C]**, Ph index **[D]**, and Ph capacity distribution **[E]** was analyzed using 1-way-ANOVA. Holm-Sidak was used as a posthoc test. (*) One symbol indicates p<0.05 (vs CIR at 6h), and (#) (vs control). Only significant effects are shown. In [**B, D, F**], n=3-4 (sham and control) and n=3-4 (at 6h, 1d). Scale bar=50µm [**A**], 10µm [**B**]; z=17.5µm [**A**], 18µm [**B**]. Data from Mar Márquez´s PhD Thesis project.*
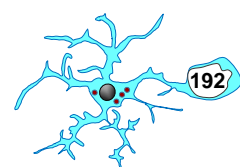
These results show that microglia possess a tremendous reservoir to counteract increased numbers of apoptotic cells, as we had observed in other models of apoptotic challenge induced by excitotoxicity (NMDA) and acute or chronic inflammation (LPS and Omega-3 deficiency) [Abiega et al., 2016]. When facing increased numbers of apoptotic cells, microglia proportionally increased their phagocytic capacity by 1, increasing the number of cells engaged in phagocytosis, and 2, increasing the number of phagocytic pouches per cell, as we have observed in CIR, NMDA, and LPS. In addition, in chronic conditions (Omega-3 deficiency) we have also observed an increased in the total number of microglia.

The combination of these three adaptation strategies (recruit more phagocytic cells, increase their phagocytic capacity, and increase microglial numbers) show that microglia have a large reservoir for phagocytosis, which could be reached by recruiting 100% of microglial cells to work at their maximum Ph capacity. As a result, phagocytosis is maintained coupled to apoptosis, ensuring the efficient removal of apoptotic cells, and limiting tissue damage. However, as we will discuss later on, this reservoir is not used in pathological conditions induced by KA, HIE, and tMCAo.

7.1.2 Maturation of microglial phagocytosis

In the section above, we have discussed the strategies used by microglia to face apoptotic challenges in the adult hippocampus. However, microglia go over a maturation period in the early postnatal days after their yolk sac progenitors infiltrate the brain parenchyma, during which they strongly remodel their transcriptional profile [Butovsky et al., 2014; Kierdorf et al., 2013b; Matcovitch-Natan et al., 2016; Thion et al., 2018]. These changes may also affect the efficiency of microglial phagocytosis, as it was proposed in in rats and monkeys, where the proportion of neuroprogenitors cells presumably phagocytosed by microglia increased during embryonic stages of cortical neurogenesis [Cunningham et al., 2013b]. Moreover, we also found an increased basal Ph index from P7 to P14 [Abiega et al., 2016]. In this PhD Thesis, we have assessed this hypothesis by confronting microglia to different pathological conditions induced by LPS, EtOH, and HIE at P9 and P14.

Treatment with LPS from *Salmonella enterica* serotype *typhimurium* did not result in increased hippocampal apoptosis at neither P9 nor P14, unexpectedly. This data is opposite to that has been observed in adult mice, in which LPS induces an increase level of dead cells in different brain regions, such as hippocampus, cortex, cerebellum, and/or striatum [Czapski et al., 2010; Semmler et al., 2005; Sierra et al., 2010; You et al., 2017]. One possible explanation to these different effects in postnatal versus adult could be the
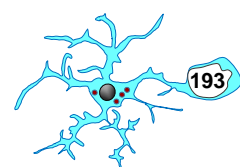
relatively low developmental level of Toll receptors, which recognize LPS and mediate some of its actions in the brain [Barak et al., 2014]. Therefore, LPS was not a useful model to induce apoptosis, and therefore, we could not use it to analyze changes in the efficiency of postnatal microglia.

In contrast to LPS, EtOH increased the number of apoptotic cells in DG, however, the phagocytic response to dead cells was completely different between P9 and P14, in parallel with the maturation of the SGZ of the hippocampus [Radic et al., 2017]. At P14, microglia proportionally raised their Ph capacity to the increase in apoptosis, a similar phagocytic strategy displayed by adult microglia to confront apoptosis induced by excitotoxicity and/or inflammation [Abiega et al., 2016]. This tactic allowed P14 microglia to maintain phagocytosis and apoptosis tightly coupled after EtOH.

However, at P9, the increment in the phagocytic capacity was not enough to face up to the amount of apoptosis induced by EtOH, leading to phagocytosis/apoptosis ratio uncoupling. These results suggested that microglia experience a development in their phagocytic efficiency between P9 and P14, in agreement with the increased basal Ph index we had initially observed between P7 and P14. These changes in phagocytic efficiency could be explained by the fact that microglia undergo a maturation process during early postnatal development [Hammond et al., 2019; Masuda et al., 2019], which implies alterations in their morphology and expression signatures throughout the CNS [Butovsky et al., 2014; Kierdorf et al., 2013b; Matcovitch-Natan et al., 2016; Thion et al., 2018]. Importantly, this maturation may affect not only their morphology and transcriptional profile but also affect microglial functions, including phagocytosis. In fact, the expression pattern of genes that encode microglial phagocytic receptors from matures embryonic to adult stages. For instance, gene expression of *Cx3cr1* and *P2ry12* is downregulated in embryonic microglia (E10.5-E14.5) and increases from postnatal (P3-P9) to adult (2m- ~1year) [Butovsky et al., 2014; Hammond et al., 2019; Matcovitch-Natan et al., 2016]. In addition, the same expression pattern is shown by other three important genes implicated in phagocytosis, such as *Trem2, Mertk,* and *Stab1* [Butovsky et al., 2014]. Therefore, these data suggested that microglial phagocytosis also experiences a maturation over the course of postnatal development in the hippocampus.

7.1.3 Microglial phagocytosis impairment in KA, tMCAo, and HIE

Once we had established the basal phagocytic efficiency in the hippocampus from P9 to adulthood, and the strategies used by microglia to cope with increased numbers of apoptotic cells, we studied whether this potential was in fact summoned in models of neurodegenerative diseases, where we found severe defects in microglial phagocytosis.
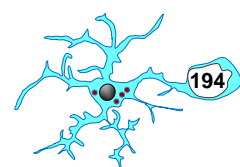
We had initially explored the phagocytic response of microglia in a mouse model of MTLE induced by intrahippocampal KA injection [Abiega et al., 2016]. In acute phase (6-24h) of the disease, the number of apoptotic cells significantly increased but, unexpectedly, phagocytosis was dramatically impaired both Ph index and Ph capacity decreased, contributing to phagocytosis uncoupling from apoptosis [Abiega et al., 2016]. In this PhD Thesis, we now evaluated whether microglial phagocytosis dysfunction was maintained over time in subacute (3d-7d) and chronic stages (4m) of MTLE.

The number of apoptotic cells continued to increase in subacute (3d-7d) phase of MTLE and the Ph index remained significantly lower compared to control mice, indicating a continued impairment of microglia. Nonetheless, there was a trend towards recovery of phagocytosis because the net phagocytosis, ie., the net number of phagocytic pouches, increased significantly. The dysfunction of microglia was not only restricted to acute and subacute stages of MTLE but extended into the chronic phase (4mpi) of the pathology [Abiega et al., 2016]. At this time, apoptosis returned to basal levels, but the Ph index was still maintained very low compared to control mice. We observed that the majority of apoptotic cells were close to microglial process but were not phagocytosed, which could be related to a decreased surveillance. However, our data showed that the density of microglial cells and the percentage of the parenchyma occupied by microglial processes increased in KA-treated mice versus controls. Thus, in spite of their increased density and volume occupied, the microglial phagocytosis impairment was long-lasting in our chronic MTLE experimental model.

The scenario was very similar in the early stages of tMCAo and HIE in adult mice, compared to KA. In tMCAo, the number of dead cells increased at 6h and 1d following the occlusion but apoptosis was not compensated by an increased Ph capacity. As a result, the Ph index dropped and the phagocytosis/apoptosis coupling was lost. We found a similar dysfunction of microglial phagocytosis after HIE. Apoptosis increased at 1d and 3d following the injury but was not compensated by an increased Ph capacity, which lead to an uncoupling between apoptosis and microglial phagocytosis. Interestingly, the effect of HIE in postnatal microglia was different since P9 microglia did increased their phagocytic capacity in response to dead cells following HIE, unlike adult microglia. Therefore, it is possible that P9 microglia, while less mature, may be more responsive to damage than adult microglia. However, it should be mentioned that the adult and postnatal HIE models are not directly comparable, because the amount of cell death induced was much larger in P9 mice. As a result, we cannot disregard a "threshold" effect, by which large amounts of apoptotic cells do summon microglial phagocytosis, as it happens at P9. Nonetheless, the microglial response at P9 was not enough to
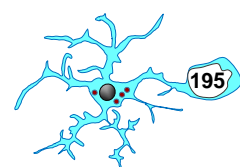
counterbalance the number of dead cells in the brain parenchyma, and as a result, phagocytosis was uncoupled from apoptosis. Overall, these data showed a similar impairment of microglial phagocytosis in tMCAo, tMCAo, and HIE. More importantly, this dysfunctional response of microglia could also occur in other neurological and neurodegenerative diseases, in which neuronal cell death is a hallmark, such as Alzheimer, Parkinson, or multiple sclerosis.

7.1.4 Microglial phagocytosis impairment is not compensated by other phagocytic cells after KA, tMCAo, and HIE

As we discussed in the previous section, microglial phagocytosis was not counteracted the amount of apoptosis evoked by KA, tMCAo, and HIE. However, additional phagocytosis mediated by other phagocytes could compensate the impairment of microglia. Because BBB integrity is affected by many neuropathological conditions, including KA, tMCAo, and HIE, peripheral monocytes with phagocytic capabilities easily access the CNS [Morganti et al., 2014].

To discriminate microglia from peripheral monocytes we have used different strategies. In our initial study of MTLE mouse model, we analyzed the expression of CD45, a lymphocyte antigen with higher expression in circulating cells compared to resident microglia [Sierra et al., 2007]. Data showed that CD45 transiently increased in all fms-EGFP population at 3d after KA and returned to basal levels at 7d. This finding could be interpreted as resulting from a transient overexpression of CD45 in resident microglia, or from an invasion of CD45^{high} monocytes that either died or downregulated the antigen later on. In fact, monocytes seem to reach the epileptic brain at a late time point, 3d after systemic and intracerebellar administration of KA [Feng et al., 2019; Tian et al., 2017; Varvel et al., 2016]. We have now used P2Y12 expression to assess monocyte infiltration in tMCAo and HIE. As in KA-treated mice, monocytes invade the brain parenchyma around 3d after the injury. In tMCAo, we observed remarkably few monocytes at 6h and 1d, although they have been reported at 3d [Garcia-Bonilla et al., 2016]. In HIE, occasional monocytes were observed 1d after the lesion and their numbers increased at 3d in both P9 and 3m mice, in agreement with previous reports [Umekawa et al., 2015]. This data showed that the invasion pattern of monocytes into the brain parenchyma was similar in mice subjected to KA, tMCAo, and HIE.

As macrophages, monocytes can also phagocytose [Garré and Yang, 2018] but we have found no evidence of their involvement in removal of apoptotic cells in the diseases studies. In KA-treated animals, we did not find any changes either in the seizures, apoptosis or microglial phagocytosis dysfunction in mice depleted of circulating
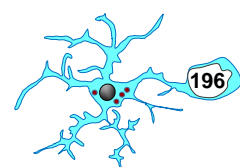
monocytes (CCR2 knock-out [Abiega et al., 2016]). In tMCAo only a few monocytes were observed at 6h and 1d, but none phagocytosed an apoptotic cell. In HIE, we found some cases of monocyte phagocytosis at 3d, but the proportion of apoptotic cells engulfed by them was remarkably low compared to microglia. Thus, our data showed that the impairment of microglia phagocytosis was not counterbalance by infiltrating monocytes with phagocytic potential.

In addition to invading monocytes, other resident cell types have the ability to phagocytose, such as astrocytes [Magnus et al., 2002] or neuroblasts [Lu et al., 2011]. Previous results of our group showed that these both populations were engaged in phagocytosis at early time points (6h and 1d) after KA, but they only engulfed a small proportion of the apoptotic cells compared to microglia [Abiega et al., 2016]. A recent report proposed that astrocytes become phagocytic in tMCAo [Morizawa et al., 2017] but, nonetheless, we did not find any phagocytic event executed by this glial population in our model of tMCAo. The discrepancy between data could be explained by the fact that we analyzed the number of apoptotic cells in the DG at 6h and 1d using confocal microscopy, while [Morizawa et al., 2017] explored the density of inclusions and cellular debris within astrocyte cytoplasm in the striatum at 3d using electron microscopy. Therefore, the phagocytic target, brain area, and time points studied after tMCAo could explain the conflictive results. In addition, we found that radial NSCs also participated in phagocytosis, but at a much lower rate compared to microglia. It should be indicated that we could not explore the phagocytic contribution of astrocytes, neuroblast, and/or radial NSCs after HIE because our lab was provided with a limited amount of tissue samples. In spite of the fact that these cells can engulf apoptotic cells after KA and/or tMCAo, it is still unknown their participation as phagocytes in HIE. Therefore, our data showed that the impairment of microglial phagocytosis was not compensated by recruiting astrocytes, neuroblast and/or radial NSCs. The importance of the microglial phagocytic dysfunction during these pathological scenarios induced phagocytosis-apoptosis uncoupling became critical to the brain parenchyma, as the impaired microglia remained by the most determinant phagocyte in the hippocampus following KA injection, tMCAo, and HIE.

7.1.5 Phagocytosis or phagoptosis?

In parallel to phagocytosis of dead cells, we found some potential cases of phagoptosis or engulfment of non-apoptotic cells [Neher et al., 2011; Brown and Neher, 2012; Butler et al., 2021]. This phenomenon has been primarily characterized in primary cerebellar culture subjected to inflammatory stimuli such as LPS and Aβ, which trigger the exposure of "eat-me" signals such as phosphatidylserine (PS), among others on the
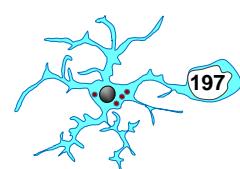
surface of viable cell, inducing its engulfment by phagocytes [Butler et al., 2021; Fricker et al., 2012b; Neher et al., 2011; Neniskyte et al., 2011]. In our mouse models of MTLE, tMCAo, and HIE, we observed potential engulfment of non-apoptotic cells by microglia, which was never observed in physiological conditions, nor in CIR, LPS, or EtOH models. In phagoptosis, the death of the cell is executed by microglia [Brown and Neher, 2014], however, we cannot be certain that cell death would be executed in our animal models of MTLE, tMCAo, and HIE because as it is a fixed tissue, we cannot ensure that cell death will be executed and that it is not a temporary "hug"

Phagoptosis occurred at lower frequency than phagocytosis of apoptotic cells after KA, tMCAo, and HIE treatment. It is possible that phagocytosis of stressed but viable cells requires more time to degrade the cargo since caspases are not activated in them. We observed engulfment of non-apoptotic cells at 3d and 7d after KA but not in chronic stages of this pathology 4m later. Moreover, we observed many instances where several microglia directly projected their processes towards non-apoptotic neurons in hippocampal tissue resected from MTLE patients, which can be interpreted either as the initiation of a phagoptotic process or of the aster-shaped phagocytosis. A similar scenario was found at 6h and 1d after tMCAo, where microglia phagocytosed a few non-apoptotic cells. In HIE, there were occasional events of phagoptosis at 1d and 3d after injury, and interestingly, this process was not only executed by microglia but also by invading monocytes. Thus, our findings showed that phagoptosis occurred in parallel to microglial phagocytosis impairment. The extent to which this process contributes or not to brain damage is still unknown and, therefore, it should be explored in detail in future studies.

Nonetheless, we did not observe phagoptosis in LPS, EtOH, and/or CIR, even though these conditions evoke an inflammatory response [Cunha et al., 2016; Osman et al., 2020; Wang et al., 2010], the trigger point for phagoptosis. These findings could indicate that the engulfment of non-apoptotic cells is not induced by all inflammatory situations, suggesting that the association between phagoptosis and inflammation is not universal.

7.1.6 Multinucleation

In addition to phagocytic dysfunction, we found that microglia developed an ameboid morphology and became multinucleated between 3d-7d after KA. Interestingly, we recently discovered a similar scenario in adult mouse model of genetic progressive myoclonus epilepsy 1 (EMP1) [Sierra-Torre et al., 2020] induced by biallelic loss-of-function mutations in the cystatin B gene (*CSTB*) [Joensuu et al., 2008; Lalioti et al., 1997; Pennacchio et al., 1996], although the number of multinucleated microglia in this
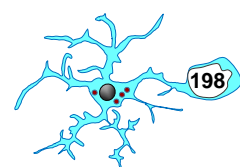
model was lower than in KA [Abiega et al., 2016]. Microglial multinucleation can be induced in vitro by inflammatory cytokines, resulting from incomplete cytokinesis [Hornik et al., 2014]. In agreement with this data, we observed that the formation of multinucleated microglia occurred in parallel to the development of an inflammatory response in KA-treated mice [Abiega et al., 2016]. In contrast, we did not observe this phenomenon at 6h and 1d after tMCAo, probably because they were early time points. Nonetheless, it was described the presence of giant multinucleate Iba1$^+$ cells, which presumably were microglia, in autopsy basal ganglia and thalamus samples from hemorrhagic stroke patients [Shtaya et al., 2019]. In HIE, we also observed multinucleated microglia at 3d in both P9 and 3m, although it was an occasional event. This data showed that microglial phagocytosis dysfunction is accompanied by multinucleation, but it is unclear at this point whether the two processes are functionally related.

7.1.7 Mechanisms of microglial phagocytosis impairment

The impairment of microglial phagocytosis associated with these neuropathological conditions is a complex phenomenon triggered by the overlap of different mechanisms, which will be discussed in the next paragraph.

The first mechanism of microglial dysfunction is related to a defect in microglial surveillance. In KA, we found a decreased basal microglial motility in organotypic hippocampal slices as well as in the living-cortex of KA-treated mice compared to saline, which affected both the retraction and protaction of microglial processes [Abiega et al., 2016]. Interestingly, we observed that oxygen and nutrient deprivation (OND), which mimicked the disruption supply of oxygen and nutrients to the brain during MCAo [Holloway and Gavins, 2016], induced a similar effect in microglia. Indeed, our preliminary results show that OND significantly reduce the process velocity of microglial process, leading to a decreased surveillance capacity (Virginia Sierra-Torre´s PhD Thesis project; **Fig. 51**). Therefore, this reduced motility could partially explain the defect in microglial phagocytosis of apoptotic cells observed in OND treatment.

In parallel to a decrease in motility, we found a defect in recognition and phagocytosis initiation, which result in apoptotic cells apposed to microglia but no phagocytosed. Previous results of our group showed that the apoptotic cell recognition receptors Trem2, MerTK, CR3, and GPR34 were significantly decreased during KA-induced seizures, explaining the deficient apoptotic cells targeting in epilepsy [Abiega et al., 2016]. A similar scenario occurs in MCAo, in which several phagocytic receptors, including CX3CR1, MerTK, CD22, TIMD4, CD300LB, CD36, and ITGAM are
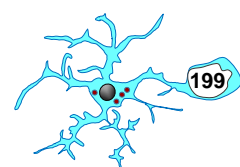
downregulated 3d after brain injury [Rajan et al., 2019]. Together, our findings indicated that the reduced motility and the decreased expression of phagocytosis receptors would explain the defect in microglial phagocytosis of apoptotic cells.

At the molecular level, the impairment of microglial phagocytosis induced by KA is related to ATP. In addition to being released by apoptotic cells [Sierra et al., 2013], ATP is also a neuro- and gliotransmitter that is widely released during epileptic seizures, [Dale and Frenguelli, 2009; Santiago et al., 2011]. We observed that high concentration of ATP disrupted the local "find-me" gradients in hippocampal organotypic slices and in in vivo DG, which lead to a reduction of phagocytosis/apoptosis coupling ratio [Abiega et al., 2016]. Thus, our results showed that the massive release of ATP interferes with the apoptotic cell "find-me" gradients by sending competing ATP signals that microglia cannot discriminate. The excessive extracellular ATP release is a cardinal pathophysiological feature shared by epilepsy, stroke, and HIE [Frenguelli and Wall, 2016; Frenguelli et al., 2007; Jurányi et al., 1999; M. Morais-Lima et al., 2020; Melani et al., 2005, 2012; Pedata et al., 2016; Schock et al., 2007], and therefore, it would also be expected that this nucleotide also plays a critical role in the microglial phagocytosis impairment that we observed in tMCAo and HIE.

Another molecular mechanism related to the phagocytosis impairment is energy depletion, a phenomenon most evident in stroke and HIE but also present in epilepsy. Excessive neuronal firing during status epilepticus provokes an early energetic deficiency at the seizure focus followed by a series of metabolic alterations in the long term [Otáhal et al., 2014] that affect the mitochondrial function [Zsurka and Kunz, 2015], on which phagocytosis heavily relies, at least in macrophages [Park et al., 2011]. In line with this idea, unpublished data from our group indicate that OND reduces microglial degradation of apoptotic cells in vitro (data from Virginia Sierra-Torre´s PhD Thesis project; **Fig. 51**). We speculate that the problems in the degradation step could be due to alterations in the lysosomal compartment, where dead cells are degraded. The lack of oxygen and nutrients might drive an energetic failure within the lysosome, affecting the proton pumps and avoiding the acidification of the lysosome. In fact, the lysosomal pH is shifted to more basic pH values in oxygen and nutrient deprivation conditions (data from Virginia Sierra-Torre´s PhD Thesis project; **Fig. 51**), which might be related to an inefficient lysosomal acidification and function. In addition, our results also show that microglial phagocytosis is rapidly impaired in organotypic hippocampal slices under OND conditions, but this dysfunctional microglial response can be restored after reperfusion (data from Virginia Sierra-Torre´s PhD Thesis project; **Fig. 51**). However, this recovery is not observed in vivo in spite of the transient occlusion of the MCA, because the hypoxia
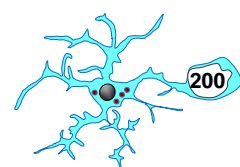
caused in the tissue is extended up to 1d after the injury, as shown by pimonidazole staining. Our findings could be explained by the fact that MCAo induces death and constriction of pericytes apposed to capillaries, leading to a permanent vasoconstriction after reperfusion [Hall et al., 2014]. In summary, our findings indicate that the impairment of microglial phagocytosis depends on multiple mechanisms, including excessive release of ATP and reduced access to nutrients and oxygen, resulting in a reduced motility of microglial process, and dysfunctional recognition of apoptotic cells.
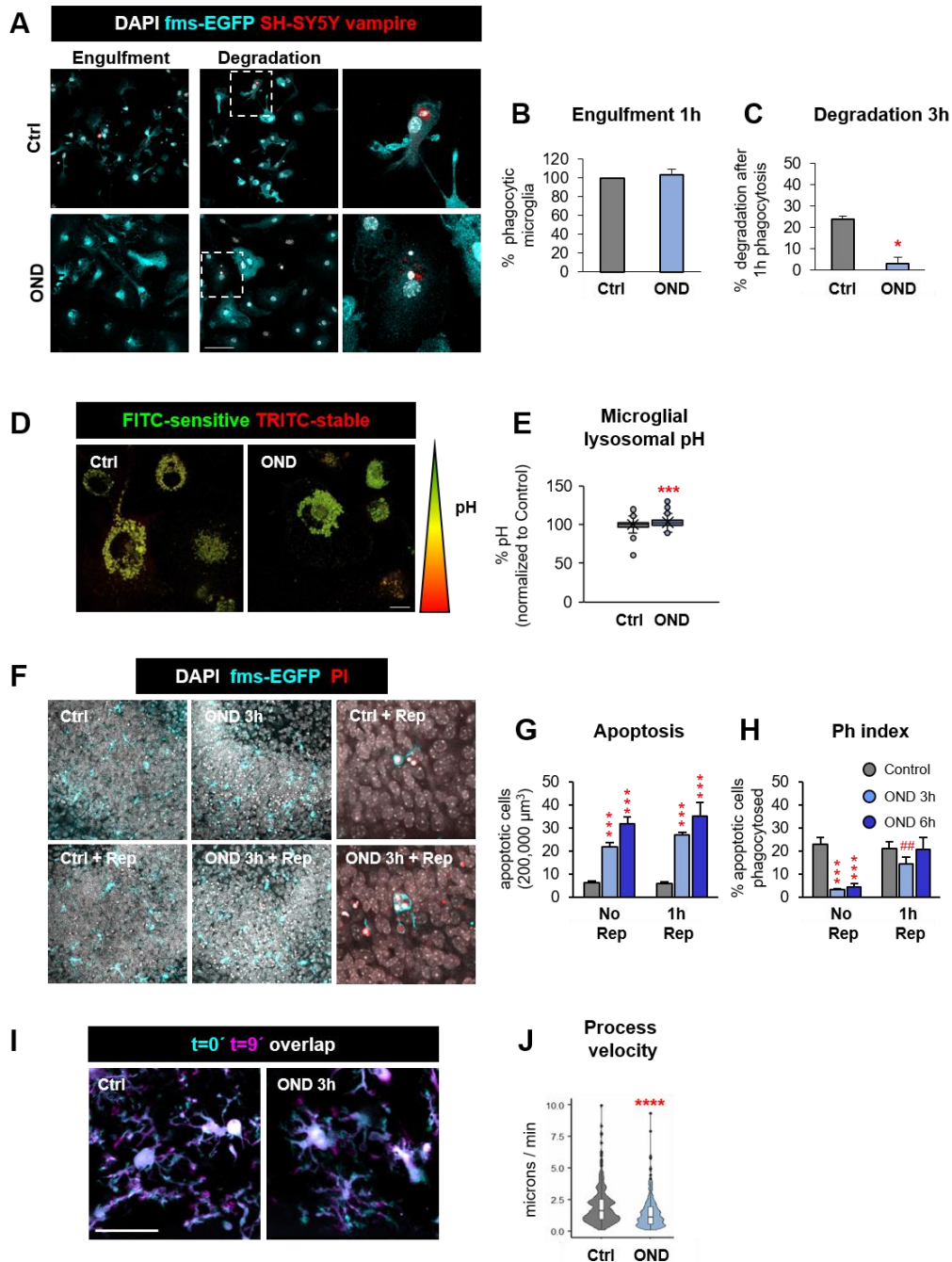
Figure 51. Phagocytosis impairment in OND conditions is related to reduced degradation of apoptotic cells and microglial process motility. [A] *Representative confocal images of primary microglia*

of both engulfment and degradation of apoptotic cells in control and OND conditions. Apoptotic nuclei were detected by pyknosis/karyorrhexis (in white, DAPI), microglia by the transgenic expression of fms-EGFP (in cyan). SH-SY5Y vampire cell line (in red) was used to assess the presence of apoptotic neurons within microglia. [B] Percentage of phagocytic microglia in engulfment step (1h after the addition of apoptotic cells). [C] Percentage of phagocytic microglia in degradation step (3h after the removal of the non-phagocytosed cells). [D] Representative confocal images of microglial lysosomes in control and OND conditions after the incubation with a dextran compound conjugated to two fluorophores: FITC (pH sensitive) and TRITC (pH stable). The ratio between these two fluorophores allows to measure the lysosomal pH. [E] Box plot of the overall lysosomal pH at the microglial population level. [F] Representative confocal images of organotypic hippocampal slices treated with OND at 3h and 6h followed or not by 1h of reperfusion. Apoptotic nuclei were detected by pyknosis/karyorrhexis (in white, DAPI), microglia by the transgenic expression of fms-EGFP (in cyan), membrane permeability (characteristic of necrotic cells) by propidium iodide (PI, in red). [G] Number of apoptotic cells in organotypic hippocampal slices in control and OND conditions at 3h and 6h. [H] Ph index (in % of apoptotic cells) in organotypic hippocampal slices in control and OND at 3h and 6h. [I] Representative 2-photon images of microglia at t=0 (cyan) and at t=9 min (magenta) from control and OND-treated organotypic hippocampal slices. [J] Violin graphs showing the total microglial process velocity independent of the direction of the movement (expressed in microns/min) in control and OND treatment. Bars represent mean ± SEM. The effect of OND on engulfment step [B], degradation step [C], microglial lysosomal pH [E], and process velocity [J] was analyzed using Student´s t test. (*) one symbol indicates p<0.05 and three p<0.005 (vs control). In [B] and [C], n=3 independent experiments; in [E], n= 287 cells (in control) and n=343 cells (in OND); in [G] and [H], n=6-10; in [J], n=12 (control mice): n=98 (cells) and n=335 (processes); n=9 (OND mice): n=57 (cells) and n=222 (processes) from four independent experiments. Scale bar=50µm [A, F], 10µm [D], 20µm [I]; z=10µm [F], 22µm [I]. Data from Virginia Sierra´s PhD Thesis project.

7.1.8 Relevance for human disease

The ultimate goal of animal research is for the information obtained from trials to benefit human clinical research. However, this translation from basic scientific findings in a laboratory to human applications also known as the "bench to beside" process remains a difficult challenge [Perry and Lawrence, 2017; Seyhan, 2019], since the failure rates of human clinical trials are still high [Herson and Traystman, 2014; Wong et al., 2019].

One crucial step in this science translation is the validation of data from animal models in human tissue. Nonetheless, the major limitation to study human brain is the postmortem (PM) delay, which triggers a cascade of events that ultimately, in a relatively short time frame, leading to biological changes in the tissue. Several studies reported that the expression levels of structural proteins and enzymes, integrity of nucleic acid, and changes in the morphology of neurons, receptors for neurotransmitters or their transporters are negatively affected by different PM intervals [Buell, 1982; Hilbig et al.,
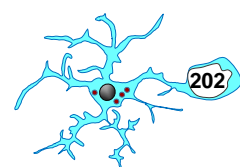
2004; Perry et al., 1981; Spokes, 1979; Williams et al., 1978]. More recently, it was described that different PM delays (average of 29± 2.6h, [Labadorf et al., 2015]) can alter the transcriptional complexity of brain genes in autopsy tissue compared to biopsy samples [Dachet et al., 2021], indicating that PM time represents a crucial limitation to genetic, molecular, biochemical, and anatomical analysis. Importantly, the process of phagocytosis is also affected by PM, as it induces a reduced motility and injury response of microglia [Dibaj et al., 2010]. These findings are replicated by our in vitro model of OND, in which we observed an impairment of phagocytosis associated to a decreased motility of microglial process (data from Virginia Sierra-Torre´s PhD Thesis project; **Fig. 51**). The negative effect of PM on microglia could explain why long PM delays (ranging from 3 to 22h) complicated our interpretation of data obtained from autopsy human tissue of epileptic patients, in which phagocytosis was absent due to a depletion of energy sources in the dead tissue [Dibaj et al., 2010; Dachet et al., 2021]. Therefore, the PM is a crucial factor that should be considered to determine the good quality of tissue in order to study, interpret and conclude the observations.

An alternative to autopsy tissue is biopsy samples, which are close to a living sample of the brain and can be immediately immersed in the fixative, reducing PM-induced changes [Alonso-Nanclares et al., 2008; del Río and DeFelipe, 1994]. This kind of tissue is largely obtained from human brain disorders requiring brain surgery, such as epilepsy and certain brain tumors. In this PhD Thesis, we explored microglial phagocytosis in hippocampal tissue resected from drug resistant MTLE patients (under 40min of postoperative delay before it was fixed), which preserved antigenicity and prevented further neuronal damage and microglial impairment. It should be mentioned that, for obvious reasons, we did not have control samples in this analysis. Our data indicated a similar Ph index, distance to apoptotic cells, microglial density, and microglia tissue volume in hippocampal samples from 4month KA-treated mice and from MTLE patients. In the chronic phase in mouse and human disease, the Ph index indicated that less than half of the apoptotic cells were being degraded by microglia, strongly suggesting that the microglial phagocytic impairment also occur in human MTLE as in our chronic MTLE experimental model. Moreover, we also discovered a novel form of phagocytosis (aster-type) in the human MTLE hippocampus, executed by several ramified microglia with confluent processes towards the apoptotic cell, reminiscent of the microglial response to a laser-induced photo lesion observed by 2-photon imaging in the live mouse cortex [Davalos et al., 2005]. While the functional relevance of the aster-phagocytosis and targeting of live neurons remains to be determined, our findings showed that the cellular
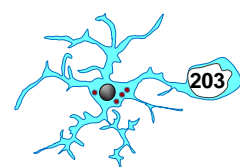
mechanism of cell clearance in the epileptic mouse and human brain were remarkably similar.

In addition, we expanded our microglial phagocytic analysis to non-human primates subjected to tMCAo (*Callithrix jacchus*) in order to get closer to human MCAo and comprehend microglial response under these conditions. After scanning all the brain samples, we only found a few apoptotic cells located in the cortex and hippocampus. This could be explained by the fact that we analyzed the tissue 45d after damage and maybe this period was enough to produce a partial recovery of the parenchyma. It should be mentioned that even though we did not have control samples in this set of experiments, the Ph index was very low compared for instance to mice, which is around 100%. Although these data are preliminary and more analysis is required, it could be indicated that microglial phagocytosis is also impaired in non-human primates after tMCAo. To validate this premise, we are currently analyzing the efficiency of microglia in macaques (*Macaca fascicularis*) subjected to tMCAo as well as human tissue from stroke patients.

7.1.9 Phagocytosis as a therapeutic tool

The impairment of phagocytosis induced a delayed clearance of dead cells, as we observed in our MTLE mouse model [Abiega et al., 2016] and that could also occur in HIE and tMCAo. Therefore, the modulation of microglial phagocytosis could be a critical point in the treatment of brain injury and neurodegenerative diseases. In addition, upcoming studies related to the mechanisms that regulate phagocytosis, such as "find-me" signals release by damaged neurons or apoptotic cells, and/or the phagocytic receptors expressed in microglia, will be crucial for the development of new therapies based on the modulation of microglial phagocytosis. In fact, our group performed a high throughput screening to assess novel pharmacological tools to enhance microglial phagocytosis based on Prestwick Chemical Library, which comprises 600 compounds already approved by European Medicines Agency and Federal Drug Administration with high chemical and pharmacological diversity, and high bioavailability in humans. We identified several candidates to modulate the engulfment and the degradation steps of phagocytosis of apoptotic cells. This pharmacological approach to enhance or restore phagocytic efficiency of microglia could be a therapy to accelerate functional brain recovery from neurodegenerative and neurological diseases. Our results also suggest that simplistic, dichotomic nomenclatures (resting vs activated, M1 vs M2, etc) to describe microglia in neurodegenerative disease do not sufficiently cover the complexity of microglial behavior. Instead, a direct assessment of phagocytosis efficiency and the
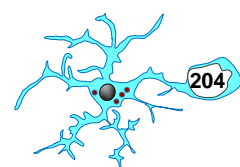
underlying causes of impairment is necessary to set the ground for developing novel therapeutic strategies targeting phagocytosis.

7.2 MICROGLIAL PHAGOCYTOSIS THROUGHOUT ADULTHOOD: A NEUROGENESIS-BASED ANALYSIS

In the last part of this PhD Thesis, we studied another issue related to hippocampal phagocytosis through adulthood: newborn cell survival in the adult hippocampal neurogenic cascade. For this purpose, we performed a systematical analysis using BrdU to trace newborn cells longitudinally (from 2h to 30d of cell life) and transversally (at 1m to 12m).

7.2.1 Critical periods of newborn cell survival are maintained across adulthood

Hippocampal newborn cells decline in two periods: 1, a main early critical period, in which 56% of cells are lost in the first 1-4 days after cell birth, and 2, a secondary late critical period, in which other 25% of newborn cells die from 4-8 days of cell life [Sierra et al., 2010]. In this PhD Thesis, we explored whether these critical periods of survival were maintained throughout adulthood, and therefore whether the adult neurogenic cascade could be used as a model to analyze phagocytosis in older mice. We observed that the main critical period of survival (2d-4d) was maintained across ages (1m, 2m, 6m, and 12m), confirming previous data published by our group [Sierra et al., 2010]. Importantly, the Ph index remains constant during adulthood, indicating that microglial phagocytosis is a critical component of the hippocampal neurogenic niche.

7.2.2 Newborn cell dynamics in the hippocampal niche is similar throughout adulthood and largely depends on the initial number of proliferating neuroprogenitors

The longitudinal dynamics of newborn cells was largely similar in young (1-2m) and mature (6-12m) mice, depending only on the initial number of proliferating neuroprogenitors, labeled with BrdU. The same scenario of longitudinal decay was obtained in juvenile (1m) mice using three different BrdU protocols (1x, 4x, and 8x), disregarding any potential BrdU dilution that could hinder the interpretation of our results. However, one potential limitation of BrdU to label proliferating neuroprogenitors is that the number of labeled cells depends on BBB permeability. Importantly, it was reported
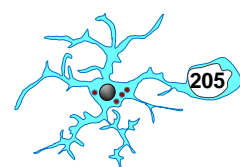
that hippocampal BBB is stable in mice up to 15m of age [del Valle et al., 2009], eliminating the possibility that more BrdU enters the brain with advanced age. Therefore, the initial labeling of neuroprogenitors depended on the relative proportion of different neuroprogenitor subpopulations, their relative mitotic activity, and the relative duration of their cell cycle, particularly of the S phase. The neuroprogenitors labeled with our BrdU protocol were mostly ANPs, as the NSCs are a quiescent population of which only a small fraction is mitotically active [Encinas et al., 2011]. Recently, it was described that NSCs are very heterogeneous population, including radial, horizontal, and omega cells [Lugert et al., 2010; Bonaguidi et al., 2011; Encinas et al., 2011; Martín-Suárez et al., 2019]. Radial NSCs are lost over time [Encinas et al., 2011], potentially diminishing their proliferative capacity along the way [Hattiangady and Shetty, 2008]. Together, these two observations (deforestation vs senescence)[Encinas and Sierra, 2012] was used to explain the depletion of neurogenesis during aging [Kuhn et al., 1996; Knoth et al., 2010; Harris et al., 2021]. In this PhD Thesis, we could not discriminate between these two hypotheses because our BrdU labeling protocol did not allow us to analyze ANPs, radial, and horizontal NSCs separately. Nonetheless, the dynamics of neuroprogenitors (NSCs and ANPs) was homogenously, as they transversally decayed at a constant rate. These data suggested that any changes in one subpopulation may be compensated by opposite changes in another: for instance, an increased cell cycle in NSCs may be compensated by increased number of ANPs with shorter cell cycles, a hypothesis that should be experimentally addressed.

We next studied the transversal decay of proliferating neuroprogenitors and newborn neurons from 1m to 12m, and found that these cells followed an exponential decay with a half-life of 53 and 49d, respectively. This data are in agreement with previous reports that showed a decay of the population of proliferating cells (labeled with Ki67) and the population of neuroblasts (labeled with doublecortin) in mice up to 9m (44 and 53d, respectively)[Ben Abdallah et al., 2010]. It is well-known that hippocampal neurogenesis declines with age [Ben Abdallah et al., 2010; Aizawa et al., 2011; Amrein et al., 2004; Cameron and McKay, 1999; Encinas et al., 2011; Gould et al., 1999; Hattiangady and Shetty, 2008; Kempermann et al., 1998; Kronenberg et al., 2006; Kuhn et al., 1996; Lugert et al., 2010; Manganas et al., 2007; Martín-Suárez et al., 2019; Morgenstern et al., 2008], while it does not occur to the same extent but at a lower rate in the other main neurogenic region, the SVZ [Enwere et al., 2004; Luo et al., 2006; Bouab et al., 2011; Capilla-Gonzalez et al., 2014; Daynac et al., 2016; Obernier et al., 2018]. In many mammalian species, hippocampal neurogenesis exponentially decreases with age, with the sharpest decline associated with sexual maturity,
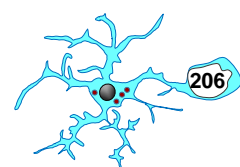
particularly in long-lived animals such as primates [Amrein et al., 2011]. Indeed, we found that in adults the maximum newborn cell decay occurs soon after adolescence both in mice and in humans, with respective half-lives of 1.7m and 25y.

The similarity in the transversal decays of the proliferating neuroprogenitor and newborn neuron population led us to propose that both cell types correlated throughout adulthood. Because until now it has not been possible to trace in real time the offspring of neuroprogenitors, we developed a computational model of the cascade that allowed us to longitudinally trace cohorts of proliferating cells. Using this model, we demonstrated that the well-known decrease of newborn neurons with age [Knoth et al., 2010; Kuhn et al., 1996] was largely due to a decreased number of proliferating neuroprogenitors and not compensated by changes in their survival or differentiation rates. One of the principles of neurogenesis propose that "neurogenesis is not regulated by age" [Kempermann, 2011] because the largest decay of newborn neurons occurs very early (before 2y in the human hippocampus)[Knoth et al., 2010]. However, our data showed another interpretation of this principle, as in fact the rate of production of newborn neurons was independent of age and depended only on the decreased number of proliferating neuroprogenitors.

7.2.3 Neuron and astrocyte productions are inversely regulated across adulthood

We observed that while newborn neurons decreased very fast throughout adulthood (half-life 49d), the newborn astrocyte population decayed at a slower rate (half-life 161d). As a result, the SGZ niche switches from largely neurogenic to similarly neuro-astrogenic. Surprisingly, the production of newborn astrocytes in the hippocampal niche is not well-documented [Gonçalves et al., 2016]. Nonetheless, genetic lineage tracing showed that astrocytes are directly produced from radial NSCs [Bonaguidi et al., 2011; Encinas et al., 2011] in physiological conditions, possibly from an intermediate, bushy radial NSC (beta subtype)[Gebara et al., 2016]. The contribution of horizontal and omega NSCs to astrocyte generation is not well-established [Lugert et al., 2010; Martín-Suárez et al., 2019]. Different proportions of these NSC types or differences in their rate of proliferation and differentiation may account for the increased astrocyte yield we found. In addition, it is possible that the survival of newborn astrocytes increases in mature mice. These different scenarios should be tested experimentally to understand the cellular and molecular mechanisms underlying the neuro-astrogenic switch undergone by the NSCs with increased age.
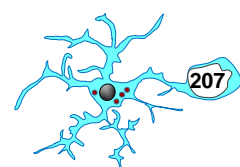
7.2.4 Simulation model to predict the dynamics of hippocampal neurogenesis through adulthood

A few computational models were proposed in the past to study different properties of the hippocampal neuro-astrogenic cascade. For instance, [Aimone et al., 2009] used mathematical modeling to demonstrate the effect of newborn cell addition to the hippocampal network and its impact on memory encoding, particularly pattern separation. Moreover, [Encinas et al., 2011] studied the age-related decay of radial NSCs and ANPs using exponential polynomial functions, leading to the conclusion that radial NSCs decay fast in young animals but their loss slows down as the mice age. In contrast, ANPs decay more slowly at a constant rate, resulting in higher ANPs/radial NSCs in older animals. More recently, two complementary approaches were developed to analyze the cellular dynamics of NSCs. [Ziebell et al., 2014] used ordinary differential equations to model five cellular compartments: NSCs, ANPs, neuroblasts, mature neurons, and astrocytes, each with different rates of self-renewal, proliferation, apoptosis, and differentiation. This computational model concluded that an increased proliferation rate of stem cells depleted the stem cell pool and led to an increased number of astrocytes. These predictions were later demonstrated in a mouse model of epilepsy [Sierra et al., 2015]. The predicted increased numbers of astrocytes matched to some extent with our data in physiological aging, although these studies did not analyze the relative neuronal and astrocytic yields. A more complex computational model by [Li et al., 2017] used multiple Bellman-Harris branching and shifted gamma distributions to analyze the cell cycle duration and transit times between NSCs, ANPs, neuroblasts, mature neurons, and apoptotic cells, concluding that apoptosis is a major factor driving newborn cell dynamics. Contrary to the models, in this PhD Thesis we used a simulation model that did not require analysis of neuroprogenitors behavior (self-renewal, proliferation, apoptosis rates), but rather simplified the analysis by adopting an "end-point" approach in which 1, all neuroprogenitor populations were analyzed together and 2, proliferation, apoptosis and differentiation were combined together in a "black box" of net survival. This approach worked very well for analysis of newborn neurons from 1m to 12m, as indeed their production was largely predicted by the number of proliferating neuroprogenitors, without any significant compensatory effects in proliferation or cell survival. In contrast, our simulation model poorly predicted the generation of astrocytes from proliferating neuroprogenitors from 1m to 12m, suggesting a yet unknown factor driving the production of astrocytes in the mature hippocampus.

Together, our data showed that the hippocampal cascade shifted towards a neuro-astrogenic phenotype with maturity. In physiological conditions, astrocytes have major
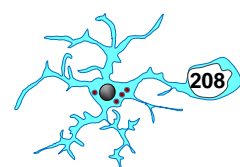
roles in regulating neuronal communication in tripartite synapses [Papouin et al., 2017] and in metabolic buffering [Barros, 2013]. Moreover, preexisting or newborn astrocytes become reactive in a large number of brain diseases, to which they contribute by exacerbating inflammation, compromising BBB function, or releasing neurotoxic compounds [Sofroniew and Vinters, 2010; Sierra et al., 2015]. Therefore, the addition of the slowly decaying newborn astrocytes in the dentate gyrus throughout adulthood may lead to changes of the hippocampal physiology and pathology in the aging hippocampus, to be examined in years to come.

Finally, one relevant question to reveal in this PhD Thesis was whether hippocampal neurogenic cascade can be used to study microglial phagocytosis in older mice. Our findings showed that newborn cells in young (1-2m) and mature (6-12m) mice naturally undergo apoptosis in two critical periods across ages. As the developmental window for cell death in newborn cells is maintained, it is likely that the mechanisms of cell death and recognition by microglia are also maintained. In fact, the basal phagocytic efficiency (Ph index) is maintained at 90-100% up to 12mo [Sierra et al., 2010]. However, the number of apoptotic newborn cells declines with age in parallel with the decreased number of proliferating neuroprogenitors [Sierra et al., 2010]. This issue imposes a limitation on the quantification, as it makes it more difficult to obtain robust estimations of basal phagocytosis efficiency. Nonetheless, the high phagocytic efficiency across adulthood suggests that this baseline could be used to compare with neurodegenerative conditions affecting older mice, such as Alzheimer´s disease.

In summary, in this PhD Thesis we explored apoptosis and microglial phagocytosis from postnatal development to adulthood using as a model the adult hippocampal neurogenic cascade. In the first part of this PhD Thesis, we subjected postnatal microglia (P9-P14) to different apoptotic challenge induced by LPS, EtOH, and HIE, and our data suggested a possible maturation of the microglial phagocytic potential during brain development. In the second part of this PhD thesis, we quantified the phagocytic efficiency in the 2-3m hippocampus under different phagocytic challenges induced by CIR, HIE, tMCAo, and MTLE. While microglia showed their "superphagocytic" facet after CIR, these brain sentinels were remarkably impaired following tMCAo, HIE, and KA treatment. Importantly, this impairment was not compensated by peripheral and resident cell with phagocytic capacity. Moreover, we also found that the dysfunction of phagocytosis was accompanied by phagoptosis. In the last part of this PhD Thesis, we focused on another important point related to microglial phagocytosis in the hippocampal
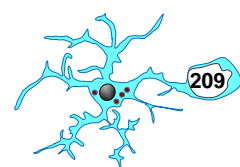
niche: the survival of newborn cells across ages. Our findings showed that the longitudinal dynamics of newborn cell production and survival was largely identical throughout adulthood. In addition, the neurogenic yield of proliferating neuroprogenitors was constant over time: the number of newborn neurons was proportional to the number of proliferating neuroprogenitors from 1m to 12m. Nonetheless, the astrocytic yield of proliferating neuroprogenitor increases in mature mice and was associated with an increased BrdU$^+$ cell net survival, leading to the niche switched from neurogenic to neuro/astrogenic in mature mice. Finally, our findings showed that the hippocampal neurogenic cascade was a useful model to study phagocytosis in older mice. To conclude, microglial phagocytosis is an essential mechanism to maintain brain homeostasis and, more importantly, harnessing their phagocytic potential is a novel therapeutic alternative to accelerate brain recovery in diseases where phagocytosis is impaired, such as ischemia/stroke and epilepsy, but also potentially in others that include AD, PD, MS, or TBI, among others.
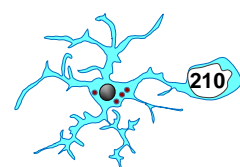
8. CONCLUSIONS

8. CONCLUSIONS

8.1 POSTNATAL MICROGLIAL PHAGOCYTIC POTENTIAL DURING HIPPOCAMPAL DEVELOPMENT

8.1.1 Major findings in LPS challenge

- LPS is not a useful model to induce apoptosis in P9 and P14 mice, and therefore cannot be used to analyze changes in postnatal microglial phagocytic response.

8.1.2 Major findings in EtOH challenge

- EtOH increases the number of apoptotic cells in P9 and P14 mice, however, the phagocytic response to dead cells is completely different in both ages. Although P9 and P14 increase their Ph capacity, only at P14 this tactic allows to maintain phagocytosis and apoptosis tightly coupled, suggesting that microglia experience a development in their phagocytic efficiency between P9 and P14.

8.1.3 Major findings in HIE challenge

- HIE induces apoptotic changes in P9 mice but microglial phagocytosis is uncoupled from apoptosis in spite of the increase in microglial Ph capacity.

- The impairment of microglial phagocytosis coincides with phagoptosis. Nonetheless, this process occurs at a lower level compared to the engulfment of apoptotic cells.

- The impairment of microglial phagocytosis occurs before peripheral monocytes invade the CNS.

- Both RFP$^+$ and RFP$^+$/GFP$^+$ monocytes are poor phagocytes, and do not compensate the microglial phagocytosis disruption.

- P2Y12R is not a useful tool to discriminate resident microglia from monocytes.

8.2 ADULT MICROGLIAL PHAGOCYTIC RESPONSE IN THE HIPPOCAMPUS UNDER NEUROPATHOLOGICAL CONDITIONS

8.2.1 Major findings in CIR challenge
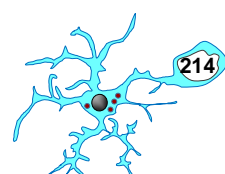
- Microglia become superphagocytic after CIR, as they engulf multiple apoptotic cells at the same time and completely clear the hippocampal parenchyma of apoptotic debris in 24h.

8.2.1 Major findings in HIE, tMCAo, and KA challenge

- Microglial phagocytosis is uncoupled from apoptosis in HIE, tMCAo, and KA because microglia become non-phagocytic.
- Microglia remain the most determinant phagocytes during phagocytosis-apoptosis uncoupling in HIE, tMCAo, and KA.
- Microglial phagocytosis impairment is accompanied by phagoptosis, although this process occurs at a lower level compared to the engulfment of apoptotic cells.

Particular findings in HIE challenge (1d and 3d)

- The impairment of microglial phagocytosis occurs before peripheral monocytes invade the CNS.

- P2Y12R is a useful tool to discriminate resident microglia from monocytes and confirms that double-positive cells (RFP$^+$/GFP$^+$) are also monocytes.

Particular findings in tMCAo challenge (6h and 1d)

- Filament II (F2) is useful to evoke hippocampal injury only in fms-EGFP mice. On the contrary, filament I (F1) is not useful to induce hippocampal damage either in fms-EGFP/CCR2$^{RFP/+}$ and/or fms-EGFP mice.
- tMCAo with F2 leads to sensory and motor coordination dysfunction.
- The presence of peripheral monocytes is low at this early time points after tMCAo, and, therefore, this population does not compensate the microglial phagocytosis impairment.

Particular findings in KA challenge (3d, 7d, and 4m)

- Partial recovery of phagocytosis occurs in subacute stages after KA (3d-7d), although it is not enough to face the increased amount of dead cells.
- Microglia develop a hypertrophic morphology, which accompanies a multinuclearity state at 3-7d after KA.
- Microglia increase their numbers and volume occupied in the brain parenchyma in chronic stages after KA (4m) but these strategies are not enough to compensate the amount of dead cells.
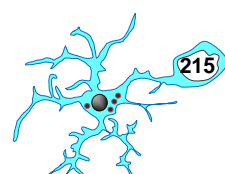
Particular findings in human MTLE patients

- Hippocampal tissue resected from drug-resistant MTLE patients contains many apoptotic cells but microglia only phagocytose a small proportion of them, indicating the impairment of microglia phagocytosis.

- Autopsy hippocampal tissue from epileptic patients (non MTLE) hinders the interpretation of phagocytosis due to long post-mortem (PM) delays. In spite of that, microglia from epileptic patients phagocytose a smaller proportion of apoptotic cells than microglia from controls, showing the impairment of microglia.

8.3 HIPPOCAMPAL NEWBORN CELLS SURVIVAL IN THE NEUROGENIC NICHE ACROSS ADULTHOOD

8.3.1 Major findings at 2h-30d after BrdU administration in 1m-12m mice

- The pattern dynamics of hippocampal newborn cells is maintained across adulthood.

- The majority of hippocampal newborn cells undergo apoptosis in the first 2-4d of their cell life through adulthood, which is efficiently removed from the parenchyma by resident microglia.

- The number of newborn cells differentiates into new neurons is proportional to the number of proliferating neuroprogenitors across ages.

- The number of newborn cells differentiates into new astrocytes increases at 6-12m and is associated with an increased net survival at 30d.

- The young hippocampal cascade shifts from neurogenic to neuro-astrogenic in more mature ages.

- The hippocampal neurogenic cascade is a useful model to study microglial phagocytosis throughout adulthood.
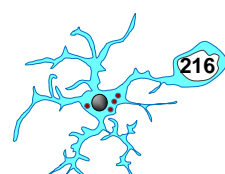
9. BIBLIOGRAPHY

9. BIBLIOGRAPHY

~A~

Abbott, N.J., Patabendige, A.A.K., Dolman, D.E.M., Yusof, S.R., and Begley, D.J. (2010). Structure and function of the blood-brain barrier. Neurobiol. Dis. *37*, 13–25.

Abd-El-Basset, E., and Fedoroff, S. (1995). Effect of bacterial wall lipopolysaccharide (LPS) on morphology, motility, and cytoskeletal organization of microglia in cultures. J. Neurosci. Res. *41*, 222–237.

Ben Abdallah, N.M.B., Slomianka, L., Vyssotski, A.L., and Lipp, H.P. (2010). Early age-related changes in adult hippocampal neurogenesis in C57 mice. Neurobiol. Aging *31*, 151–161.

Abiega, O., Beccari, S., Diaz-Aparicio, I., Nadjar, A., Layé, S., Leyrolle, Q., Gómez-Nicola, D., Domercq, M., Pérez-Samartín, A., Sánchez-Zafra, V., et al. (2016). Neuronal Hyperactivity Disturbs ATP Microgradients, Impairs Microglial Motility, and Reduces Phagocytic Receptor Expression Triggering Apoptosis/Microglial Phagocytosis Uncoupling. PLOS Biol. *14 e100246*.

Acharya, M.M., Green, K.N., Allen, B.D., Najafi, A.R., Syage, A., Minasyan, H., Le, M.T., Kawashita, T., Giedzinski, E., Parihar, V.K., et al. (2016). Elimination of microglia improves cognitive function following cranial irradiation. Sci. Rep. *6*, 31545.

Aguilera, K., and Brekken, R. (2014). Hypoxia Studies with Pimonidazole in vivo. BIO-PROTOCOL *4*, e1254.

Aguzzi, A., Barres, B.A., and Bennett, M.L. (2013). Microglia: Scapegoat, saboteur, or something else? Science (80-.). *339*, 156–161.

Ahl, M., Avdic, U., Skoug, C., Ali, I., Chugh, D., Johansson, U.E., and Ekdahl, C.T. (2016). Immune response in the eye following epileptic seizures. J. Neuroinflammation *13*, 155.

Aimone, J.B., Wiles, J., and Gage, F.H. (2009). Computational Influence of Adult Neurogenesis on Memory Encoding. Neuron *61*, 187–202.

Aizawa, K., Ageyama, N., Terao, K., and Hisatsune, T. (2011). Primate-specific alterations in neural stem/progenitor cells in the aged hippocampus. Neurobiol. Aging *32*, 140–150.
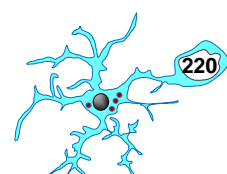
Ajami, B., Bennett, J.L., Krieger, C., Tetzlaff, W., and Rossi, F.M.V. (2007). Local self-renewal can sustain CNS microglia maintenance and function throughout adult life. Nat. Neurosci. *10*, 1538–1543.

Akahoshi, N., Murashima, Y.L., Himi, T., Ishizaki, Y., and Ishii, I. (2007). Increased expression of the lysosomal protease cathepsin S in hippocampal microglia following kainate-induced seizures. Neurosci. Lett. *429*, 136–141.

Akira, S., Takeda, K., and Kaisho, T. (2001). Toll-like receptors: Critical proteins linking innate and acquired immunity. Nat. Immunol. *2*, 675–680.

Al-Macki, N., Miller, S.P., Hall, N., and Shevell, M. (2009). The Spectrum of Abnormal Neurologic Outcomes Subsequent to Term Intrapartum Asphyxia. Pediatr. Neurol. *41*, 399–405.

Albertsson, A.M., Bi, D., Duan, L., Zhang, X., Leavenworth, J.W., Qiao, L., Zhu, C., Cardell, S., Cantor, H., Hagberg, H., et al. (2014). The immune response after hypoxia-ischemia in a mouse model of preterm brain injury. J. Neuroinflammation *11*, 153.

Alexander, C., and Rietschel, E.T. (2001). Bacterial lipopolysaccharides and innate immunity. J. Endotoxin Res. *7*, 167–202.

Alexander, M., Garbus, H., Smith, A.L., Rosenkrantz, T.S., and Fitch, R.H. (2014). Behavioral and histological outcomes following neonatal HI injury in a preterm (P3) and term (P7) rodent model. Behav. Brain Res. *259*, 8–96.

Alfonso-Loeches, S., Pascual-Lucas, M., Blanco, A.M., Sanchez-Vera, I., and Guerri, C. (2010). Pivotal role of TLR4 receptors in alcohol-induced neuroinflammation and brain damage. J. Neurosci. *30*, 8285–8295.

Ali, I., Chugh, D., and Ekdahl, C.T. (2015). Role of fractalkine-CX3CR1 pathway in seizure-induced microglial activation, neurodegeneration, and neuroblast production in the adult rat brain. Neurobiol. Dis. *74*, 194–203.

Alkayed, N.J., Harukuni, I., Kimes, A.S., London, E.D., Traystman, R.J., and Hurn, P.D. (1998). Gender-linked brain injury in experimental stroke. Stroke *29*, 159–165.

Allen, S.J., Watson, J.J., Shoemark, D.K., Barua, N.U., and Patel, N.K. (2013). GDNF, NGF and BDNF as therapeutic options for neurodegeneration. Pharmacol. Ther. *138*, 155–175.

Alonso-Nanclares, L., Gonzalez-Soriano, J., Rodriguez, J.R., and DeFelipe, J. (2008). Gender differences in human cortical synaptic density. Proc. Natl. Acad. Sci. U. S. A.
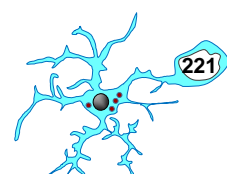
105, 14615–14619.

El Amki, M., Clavier, T., Perzo, N., Bernard, R., Guichet, P.O., and Castel, H. (2015). Hypothalamic, thalamic and hippocampal lesions in the mouse MCAO model: Potential involvement of deep cerebral arteries? J. Neurosci. Methods *254*, 80–85.

Amrein, I., Slomianka, L., Poletaeva, I.I., Bologova, N. V., and Lipp, H.P. (2004). Marked species and age-dependent differences in cell proliferation and neurogenesis in the hippocampus of wild-living rodents. Hippocampus *14*, 1000–1010.

Amrein, I., Isler, K., and Lipp, H.P. (2011). Comparing adult hippocampal neurogenesis in mammalian species and orders: Influence of chronological age and life history stage. Eur. J. Neurosci. *34*, 978–987.

Ansar, S., Chatzikonstantinou, E., Wistuba-Schier, A., Mirau-Weber, S., Fatar, M., Hennerici, M.G., and Meairs, S. (2014). Characterization of a New Model of Thromboembolic Stroke in C57 black/6J mice. Transl. Stroke Res. *5*, 526–533.

Ansari, S., Azari, H., McConnell, D.J., Afzal, A., and Mocco, J. (2011). Intraluminal middle cerebral artery occlusion (MCAO) model for ischemic stroke with laser doppler flowmetry guidance in mice. J. Vis. Exp. *51*, 2879.

Anttila, J.E., Whitaker, K.W., Wires, E.S., Harvey, B.K., and Airavaara, M. (2017). Role of microglia in ischemic focal stroke and recovery: focus on Toll-like receptors. Prog. Neuro-Psychopharmacology Biol. Psychiatry *79*, 3–14.

Arai, K., Lok, J., Guo, S., Hayakawa, K., Xing, C., and Lo, E.H. (2011). Cellular mechanisms of neurovascular damage and repair after stroke. J. Child Neurol. *26*, 1193–1198.

Arandjelovic, S., and Ravichandran, K.S. (2015). Phagocytosis of apoptotic cells in homeostasis. Nat. Immunol. *16*, 907–917.

Arcuri, C., Mecca, C., Bianchi, R., Giambanco, I., and Donato, R. (2017). The pathophysiological role of microglia in dynamic surveillance, phagocytosis and structural remodeling of the developing CNS. Front. Mol. Neurosci. *10*, 191.

Arida, R.M., Scorza, F.A., De Araujo Peres, C., and Cavalheiro, E.A. (1999). The course of untreated seizures in the pilocarpine model of epilepsy. Epilepsy Res. *34*, 99–107.

Arnold, S.A., Rivera, L.B., Miller, A.F., Carbon, J.G., Dineen, S.P., Xie, Y., Castrillon, D.H., Sage, E.H., Puolakkainen, P., Bradshaw, A.D., et al. (2010). Lack of host SPARC enhances vascular function and tumor spread in an orthotopic murine model of
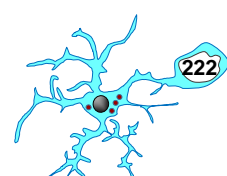
pancreatic carcinoma. DMM Dis. Model. Mech. *3*, 57–72.

Asatryan, L., Ostrovskaya, O., Lieu, D., and Davies, D.L. (2018). Ethanol differentially modulates P2X4 and P2X7 receptor activity and function in BV2 microglial cells. Neuropharmacology *128*, 11–21.

Avignone, E., Ulmann, L., Levavasseur, F., Rassendren, F., and Audinat, E. (2008). Status epilepticus induces a particular microglial activation state characterized by enhanced purinergic signaling. J. Neurosci. *28*, 9133–9144.

Ayata, P., Badimon, A., Strasburger, H.J., Duff, M.K., Montgomery, S.E., Loh, Y.H.E., Ebert, A., Pimenova, A.A., Ramirez, B.R., Chan, A.T., et al. (2018). Epigenetic regulation of brain region-specific microglia clearance activity. Nat. Neurosci. *21*, 1049–1060.

~B~

Babb, T.L., Pereira-Leite, J., Mathern, G.W., and Pretorius, J.K. (1995). Kainic acid induced hippocampal seizures in rats: comparisons of acute and chronic seizures using intrahippocampal versus systemic injections. Ital. J. Neurol. Sci. *16*, 39–44.

Bae, E.K., Jung, K.H., Chu, K., Lee, S.T., Kim, J.H., Park, K. II, Kim, M., Chung, C.K., Lee, S.K., and Roh, J.K. (2010). Neuropathologic and clinical features of human medial temporal lobe epilepsy. J. Clin. Neurol. *6*, 73–80.

Balduini, W., De Angelis, V., Mazzoni, E., and Cimino, M. (2000). Long-lasting behavioral alterations following a hypoxic/ischemic brain injury in neonatal rats. Brain Res. *859*, 318–325.

Baldwin, A.C., and Kielian, T. (2004). Persistent immune activation associated with a mouse model of Staphylococcus aureus-induced experimental brain abscess. J. Neuroimmunol. *151*, 24–32.

Balkaya, M., Kröber, J., Gertz, K., Peruzzaro, S., and Endres, M. (2013a). Characterization of long-term functional outcome in a murine model of mild brain ischemia. J. Neurosci. Methods *213*, 179–187.

Balkaya, M., Kröber, J.M., Rex, A., and Endres, M. (2013b). Assessing post-stroke behavior in mouse models of focal ischemia. J. Cereb. Blood Flow Metab. *33*, 330–338.

Ballerini, P., Di Iorio, P., Ciccarelli, R., Nargi, E., D'Alimonte, I., Traversa, U., Rathbone, M.P., and Caciagli, F. (2002). Glial cells express multiple ATP binding cassette proteins which are involved in ATP release. Neuroreport *13*, 1789–1792.
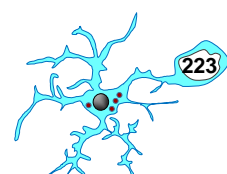
Banati, R.B., Gehrmann, J., Schubert, P., and Kreutzberg, G.W. (1993). Cytotoxicity of microglia. Glia *7*, 111–118.

Banerjee, M., Sasse, V.A., Wang, Y., Maulik, M., and Kar, S. (2015). Increased levels and activity of cathepsins B and D in kainate-induced toxicity. Neuroscience *284*, 360–373.

Bannerman, D.M., Deacon, R.M.J., Offen, S., Friswell, J., Grubb, M., and Rawlins, J.N.P. (2002). Double dissociation of function within the hippocampus: Spatial memory and hyponeophagia. Behav. Neurosci. *116*, 884–901.

Barak, B., Feldman, N., and Okun, E. (2014). Toll-like receptors as developmental tools that regulate neurogenesis during development: an update. Front. Neurosci. *8*, 272.

Barber, G.N. (2001). Host defense, viruses and apoptosis. Cell Death Differ. *8*, 113–126.

Bardutzky, J., Shen, Q., Henninger, N., Bouley, J., Duong, T.Q., and Fisher, M. (2005). Differences in ischemic lesion evolution in different rat strains using diffusion and perfusion imaging. Stroke *36*, 2000–2005.

Barker-Haliski, M., and Steve White, H. (2015). Glutamatergic mechanisms associated with seizures and epilepsy. Cold Spring Harb. Perspect. Med. *5*, a022863.

Barres, B.A., Hart, I.K., Coles, H.S.R., Burne, J.F., Voyvodic, J.T., Richardson, W.D., and Raff, M.C. (1992). Cell death and control of cell survival in the oligodendrocyte lineage. Cell *70*, 31–46.

Barros, L.F. (2013). Metabolic signaling by lactate in the brain. Trends Neurosci. *36*, 396–404.

Barton, E.A., Baker, C., and Leigh Leasure, J. (2017). Investigation of sex differences in the microglial response to binge ethanol and exercise. Brain Sci. *7*, 139.

Beamer, E., Fischer, W., and Engel, T. (2017). The ATP-gated P2X7 receptor as a target for the treatment of drug-resistant epilepsy. Front. Neurosci. *11*, 21.

Beccari, S., Diaz-Aparicio, I., and Sierra, A. (2018). Quantifying Microglial Phagocytosis of Apoptotic Cells in the Brain in Health and Disease. Curr. Protoc. Immunol. *122*, e49.

Beckers, L., Ory, D., Geric, I., Declercq, L., Koole, M., Kassiou, M., Bormans, G., and Baes, M. (2018). Increased Expression of Translocator Protein (TSPO) Marks Pro-inflammatory Microglia but Does Not Predict Neurodegeneration. Mol. Imaging Biol. *20*, 94–102.
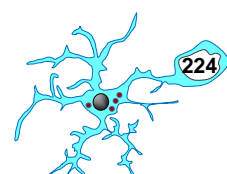
Bédard, A., Tremblay, P., Chernomoretz, A., and Vallières, L. (2007). Identification of genes preferentially expressed by microglia and upregulated during cuprizone-induced inflammation. Glia *55*, 777–789.

Beech, J.S., Williams, S.C.R., Campbell, C.A., Bath, P.M.W., Parsons, A.A., Hunter, A.J., and Menon, D.K. (2001). Further characterisation of a thromboembolic model of stroke in the rat. Brain Res. *895*, 18–24.

Behrens, E.M., Gadue, P., Gong, S.Y., Garrett, S., Stein, P.L., and Cohen, P.L. (2003). The mer receptor tyrosine kinase: Expression and function suggest a role in innate immunity. Eur. J. Immunol. *33*, 2160–2167.

Belov Kirdajova, D., Kriska, J., Tureckova, J., and Anderova, M. (2020). Ischemia-Triggered Glutamate Excitotoxicity From the Perspective of Glial Cells. Front. Cell. Neurosci. *14*, 51.

Ben-Ari, Y., and Cossart, R. (2000). Kainate, a double agent that generates seizures: Two decades of progress. Trends Neurosci. *23*, 580–587.

Ben-Ari, Y., and Lagowska, J. (1978). [Epileptogenic action of intra-amygdaloid injection of kainic acid]. C. R. Acad. Sci. Hebd. Seances Acad. Sci. D. *287*, 813–816.

Benmamar-Badel, A., Owens, T., and Wlodarczyk, A. (2020). Protective Microglial Subset in Development, Aging, and Disease: Lessons From Transcriptomic Studies. Front. Immunol. *11*, 430.

Bennett, M.L., and Barres, B.A. (2017). A genetically distinct microglial subset promotes myelination. EMBO J. *36*, 3269–3271.

Bennett, M.L., Bennett, F.C., Liddelow, S.A., Ajami, B., Zamanian, J.L., Fernhoff, N.B., Mulinyawe, S.B., Bohlen, C.J., Adil, A., Tucker, A., et al. (2016). New tools for studying microglia in the mouse and human CNS. Proc. Natl. Acad. Sci. U. S. A. *113*, E1738–E1746.

Beridze, M., Sanikidze, T., Shakarishvili, R., Intskirveli, N., and Bornstein, N.M. (2011). Selected acute phase CSF factors in ischemic stroke: Findings and prognostic value. BMC Neurol. *11*, 41.

Berti, R., Williams, A.J., Moffett, J.R., Hale, S.L., Velarde, L.C., Elliott, P.J., Yao, C., Dave, J.R., and Tortella, F.C. (2002). Quantitative real-time RT-PCR analysis of inflammatory gene expression associated with ischemia-reperfusion brain injury. J. Cereb. Blood Flow Metab. *22*, 1068–1079.
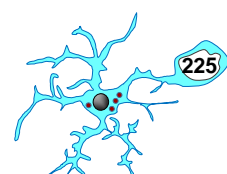
Betjemann, J.P., and Lowenstein, D.H. (2015). Status epilepticus in adults. Lancet Neurol. *14*, 615–624.

Beynon, S.B., and Walker, F.R. (2012). Microglial activation in the injured and healthy brain: What are we really talking about? Practical and theoretical issues associated with the measurement of changes in microglial morphology. Neuroscience *225*, 162–171.

Del Bigio, M.R., and Becker, L.E. (1994). Microglial aggregation in the dentate gyrus: A marker of mild hypoxic-ischaemic brain insult in human infants. Neuropathol. Appl. Neurobiol. *20*, 144–151.

Bihel, E., Pro-Sistiaga, P., Letourneur, A., Toutain, J., Saulnier, R., Insausti, R., Bernaudin, M., Roussel, S., and Touzani, O. (2010). Permanent or transient chronic ischemic stroke in the non-human primate: Behavioral, neuroimaging, histological, and immunohistochemical investigations. J. Cereb. Blood Flow Metab. *30*, 273–285.

Bihel, E., Roussel, S., Toutain, J., Bernaudin, M., and Touzani, O. (2011). Diffusion tensor MRI reveals chronic alterations in white matter despite the absence of a visible ischemic lesion on conventional MRI: A nonhuman primate study. Stroke *42*, 1412–1419.

Black, R.E., Cousens, S., Johnson, H.L., Lawn, J.E., Rudan, I., Bassani, D.G., Jha, P., Campbell, H., Walker, C.F., Cibulskis, R., et al. (2010). Global, regional, and national causes of child mortality in 2008: a systematic analysis. Lancet *375*, 1969–1987.

Blasi, E., Barluzzi, R., Mazzolla, R., Tancini, B., Saleppico, S., Puliti, M., Pitzurra, L., and Bistoni, F. (1995). Role of nitric oxide and melanogenesis in the accomplishment of anticryptococcal activity by the BV-2 microglial cell line. J. Neuroimmunol. *58*, 111–116.

Bogousslavsky, J., Melle, G. Van, and Regli, F. (1988). The lausanne stroke registry: Analysis of 1,000 consecutive patients with first stroke. Stroke *19*, 1083–1092.

Boison, D. (2013). Adenosine and seizure termination: Endogenous mechanisms. Epilepsy Curr. *13*, 35–37.

Boison, D. (2016). Adenosinergic signaling in epilepsy. Neuropharmacology *104*, 131–139.

Bolmont, T., Haiss, F., Eicke, D., Radde, R., Mathis, C.A., Klunk, W.E., Kohsaka, S., Jucker, M., and Calhoun, M.E. (2008). Dynamics of the microglial/amyloid interaction indicate a role in plaque maintenance. J. Neurosci. *28*, 4283–4292.

Bolognini, N., Russo, C., and Edwards, D.J. (2016). The sensory side of post-stroke motor rehabilitation. Restor. Neurol. Neurosci. *34*, 571–586.
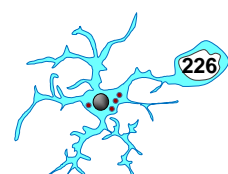
Bona, E., Andersson, A.L., Blomgren, K., Gilland, E., Puka-Sundvall, M., Gustafson, K., and Hagberg, H. (1999). Chemokine and inflammatory cell response to hypoxia-ischemia in immature rats. Pediatr. Res. *45*, 500–509.

Bonaguidi, M.A., Wheeler, M.A., Shapiro, J.S., Stadel, R.P., Sun, G.J., Ming, G.L., and Song, H. (2011). In vivo clonal analysis reveals self-renewing and multipotent adult neural stem cell characteristics. Cell *145*, 1142–1155.

Bonan, C.D., Walz, R., Pereira, G.S., Worm, P. V., Battastini, A.M.O., Cavalheiro, E.A., Izquierdo, I., and Sarkis, J.J.F. (2000). Changes in synaptosomal ectonucleotidase activities in two rat models of temporal lobe epilepsy. Epilepsy Res. *39*, 229–238.

Bonestroo, H.J.C., Nijboer, C.H.A., Van Velthoven, C.T.J., Kavelaars, A., Hack, C.E., Van Bel, F., and Heijnen, C.J. (2013). Cerebral and hepatic inflammatory response after neonatal hypoxia-ischemia in newborn rats. Dev. Neurosci. *35*, 197–211.

Bonfoco, E., Krainc, D., Ankarcrona, M., Nicotera, P., and Lipton, S.A. (1995). Apoptosis and necrosis: Two distinct events induced, respectively, by mild and intense insults with N-methyl-D-aspartate or nitric oxide/superoxide in cortical cell cultures. Proc. Natl. Acad. Sci. U. S. A. *92*, 7162–7166.

Bonifati, D.M., and Kishore, U. (2007). Role of complement in neurodegeneration and neuroinflammation. Mol. Immunol. *44*, 999–1010.

Borges, K., Gearing, M., McDermott, D.L., Smith, A.B., Almonte, A.G., Wainer, B.H., and Dingledine, R. (2003). Neuronal and glial pathological changes during epileptogenesis in the mouse pilocarpine model. Exp. Neurol. *182*, 21–34.

Boström, M., Kalm, M., Karlsson, N., Hellström Erkenstam, N., and Blomgren, K. (2013). Irradiation to the young mouse brain caused long-term, progressive depletion of neurogenesis but did not disrupt the neurovascular niche. J. Cereb. Blood Flow Metab.

Bouab, M., Paliouras, G.N., Aumont, A., Forest-Bérard, K., and Fernandes, K.J.L. (2011). Aging of the subventricular zone neural stem cell niche: Evidence for quiescence-associated changes between early and mid-adulthood. Neuroscience *173*, 135–149.

Bouet, V., Boulouard, M., Toutain, J., Divoux, D., Bernaudin, M., Schumann-Bard, P., and Freret, T. (2009). The adhesive removal test: A sensitive method to assess sensorimotor deficits in mice. Nat. Protoc. *4*, 1560–1564.

Bouët, V., Freret, T., Toutain, J., Divoux, D., Boulouard, M., and Schumann-Bard, P. (2007). Sensorimotor and cognitive deficits after transient middle cerebral artery occlusion in the mouse. Exp. Neurol. *203*, 555–567.
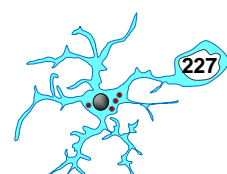
Bouilleret, V., Ridoux, V., Depaulis, A., Marescaux, C., Nehlig, A., and Le Gal La Salle, G. (1999). Recurrent seizures and hippocampal sclerosis following intrahippocampal kainate injection in adult mice: Electroencephalography, histopathology and synaptic reorganization similar to mesial temporal lobe epilepsy. Neuroscience *89*, 717–729.

Boyadjieva, N.I., and Sarkar, D.K. (2010). Role of microglia in ethanol's apoptotic action on hypothalamic neuronal cells in primary cultures. Alcohol. Clin. Exp. Res. *34*, 1835–1842.

Boyer, P.D. (1999). What makes ATP synthase spin? Nature *402*, 247–249.

Boylan, L.S., Flint, L.A., Labovitz, D.L., Jackson, S.C., Starner, K., and Devinsky, O. (2004). Depression but not seizure frequency predicts quality of life in treatment-resistant epilepsy. Neurology *62*, 258–261.

Braeuninger, S., and Kleinschnitz, C. (2009). Rodent models of focal cerebral ischemia: procedural pitfalls and translational problems. Exp. Transl. Stroke Med. *1*, 8.

Brown, G.C., and Neher, J.J. (2012). Eaten alive! Cell death by primary phagocytosis: "Phagoptosis." Trends Biochem. Sci. *37*, 325–332.

Brown, G.C., and Neher, J.J. (2014). Microglial phagocytosis of live neurons. Nat. Rev. Neurosci. *15*, 209–216.

Brumback, T., Cao, D., and King, A. (2007). Effects of alcohol on psychomotor performance and perceived impairment in heavy binge social drinkers. Drug Alcohol Depend. *91*, 10–17.

Buchan, A.M., Xue, D., and Slivka, A. (1992). A new model of temporary focal neocortical ischemia in the rat. Stroke *23*, 273–279.

Buell, S.J. (1982). Golgi-cox and rapid golgi methods as applied to autopsied human brain tissue: Widely disparate results. J. Neuropathol. Exp. Neurol. *41*, 500–507.

Burns, K., Duggan, B., Atkinson, E.A., Famulski, K.S., Nemer, M., Bleackley, R.C., and Michalak, M. (1994). Modulation of gene expression by calreticulin binding to the glucocorticoid receptor. Nature *367*, 476–480.

Burnstock, G. (2016). An introduction to the roles of purinergic signalling in neurodegeneration, neuroprotection and neuroregeneration. Neuropharmacology *104*, 4–17.

Butler, C.A., Alma, P., Kitchener, E., Allendorf, D.H., Puigdellívol, M., and Brown, G.C. (2021). Microglial phagocytosis of neurons in neurodegeneration, and its regulation. J.
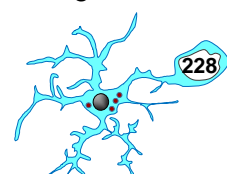
Neurochem.

Butovsky, O., Jedrychowski, M.P., Moore, C.S., Cialic, R., Lanser, A.J., Gabriely, G., Koeglsperger, T., Dake, B., Wu, P.M., Doykan, C.E., et al. (2014). Identification of a unique TGF-β-dependent molecular and functional signature in microglia. Nat. Neurosci. *17*, 131–143.

Buttgereit, A., Lelios, I., Yu, X., Vrohlings, M., Krakoski, N.R., Gautier, E.L., Nishinakamura, R., Becher, B., and Greter, M. (2016). Sall1 is a transcriptional regulator defining microglia identity and function. Nat. Immunol. *17*, 1397–1406.

Buttini, M., Appel, K., Sauter, A., Gebicke-Haerter, P.J., and Boddeke, H.W.G.M. (1996). Expression of tumor necrosis factor alpha after focal cerebral ischaemia in the rat. Neuroscience *71*, 1–16.

Byrne, A., and Reen, D.J. (2002). Lipopolysaccharide Induces Rapid Production of IL-10 by Monocytes in the Presence of Apoptotic Neutrophils. J. Immunol.

~C~

Caberoy, N.B., Alvarado, G., Bigcas, J.L., and Li, W. (2012). Galectin-3 is a new MerTK-specific eat-me signal. J. Cell. Physiol. *227*, 401–407.

Cámara-Lemarroy, C.R., Guzmán-De La Garza, F.J., and Fernández-Garza, N.E. (2010). Molecular inflammatory mediators in peripheral nerve degeneration and regeneration. Neuroimmunomodulation *17*, 314–324.

Cameron, H.A., and McKay, R.D.G. (1999). Restoring production of hippocampal neurons in old age. Nat. Neurosci. *2*, 894–897.

Campbell, B.C.V., De Silva, D.A., Macleod, M.R., Coutts, S.B., Schwamm, L.H., Davis, S.M., and Donnan, G.A. (2019). Ischaemic stroke. Nat. Rev. Dis. Prim. *5*, 70.

Cangalaya, C., Stoyanov, S., Fischer, K.D., and Dityatev, A. (2020). Light-induced engagement of microglia to focally remodel synapses in the adult brain. Elife *9*, e58435.

Cánovas-Ahedo, M., and Alonso-Alconada, D. (2019). Combined therapy in neonatal hypoxic-ischaemic encephalopathy. An. Pediatr.

Capilla-Gonzalez, V., Cebrian-Silla, A., Guerrero-Cazares, H., Garcia-Verdugo, J.M., and Quiñones-Hinojosa, A. (2014). Age-related changes in astrocytic and ependymal cells of the subventricular zone. Glia *62*, 790–803.

Carmichael, S.T. (2005). Rodent models of focal stroke: Size, mechanism, and purpose.
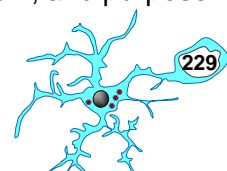
NeuroRx *2*, 396–409.

Castellanos, M., Castillo, J., García, M.M., Leira, R., Serena, J., Chamorro, A., and Dávalos, A. (2002). Inflammation-mediated damage in progressing lacunar infarctions a potential therapeutic target. Stroke *33*, 982–987.

Cavalheiro, E.A., Santos, N.F., and Priel, M.R. (1996). The pilocarpine model of epilepsy in mice. Epilepsia *37*, 1015–1019.

Cenik, B.K., Ostapoff, K.T., Gerber, D.E., and Brekken, R.A. (2013). BIBF 1120 (nintedanib), a triple angiokinase inhibitor, induces hypoxia but not EMT and blocks progression of preclinical models of lung and pancreatic cancer. Mol. Cancer Ther. *12*, 992–1001.

Chakrabarty, P., Jansen-West, K., Beccard, A., Ceballos-Diaz, C., Levites, Y., Verbeeck, C., Zubair, A.C., Dickson, D., Golde, T.E., and Das, P. (2010). Massive gliosis induced by interleukin-6 suppresses Aβ deposition in vivo: evidence against inflammation as a driving force for amyloid deposition. FASEB J. *24*, 548–559.

Chalak, L.F., Sánchez, P.J., Adams-Huet, B., Laptook, A.R., Heyne, R.J., and Rosenfeld, C.R. (2014). Biomarkers for severity of neonatal hypoxic-ischemic encephalopathy and outcomes in newborns receiving hypothermia therapy. J. Pediatr. *164*, 468-74.e1.

Chao, M. V. (2003). Neurotrophins and their receptors: A convergence point for many signalling pathways. Nat. Rev. Neurosci. *4*, 299–309.

Chaparro-Huerta, V., Flores-Soto, M.E., Merin Sigala, M.E., Barrera de León, J.C., Lemus-Varela, M. de L., Torres-Mendoza, B.M. de G., and Beas-Zárate, C. (2017). Proinflammatory Cytokines, Enolase and S-100 as Early Biochemical Indicators of Hypoxic-Ischemic Encephalopathy Following Perinatal Asphyxia in Newborns. Pediatr. Neonatol. *58*, 70–76.

Chapman, A.G. (2000). Glutamate and epilepsy. J. Nutr. *130*, 1043S-5S.

Chappell-Maor, L., Kolesnikov, M., Kim, J.S., Shemer, A., Haimon, Z., Grozovski, J., Boura-Halfon, S., Masuda, T., Prinz, M., and Jung, S. (2020). Comparative analysis of CreER transgenic mice for the study of brain macrophages: A case study. Eur. J. Immunol. *50*, 353–362.

Chekeni, F.B., Elliott, M.R., Sandilos, J.K., Walk, S.F., Kinchen, J.M., Lazarowski, E.R., Armstrong, A.J., Penuela, S., Laird, D.W., Salvesen, G.S., et al. (2010). Pannexin 1 channels mediate "find-me" signal release and membrane permeability during apoptosis.
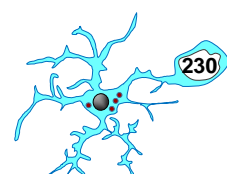
Nature *467*, 863–867.

Chen, C., Leys, D., and Esquenazi, A. (2013). The interaction between neuropsychological and motor deficits in patients after stroke. Neurology *80*, S27-34.

Chen, H.-R., Sun, Y.-Y., Chen, C.-W., Kuo, Y.-M., Kuan, I.S., Tiger Li, Z.-R., Short-Miller, J.C., Smucker, M.R., and Kuan, C.-Y. (2020). Fate mapping via CCR2-CreER mice reveals monocyte-to-microglia transition in development and neonatal stroke. Sci. Adv. *6*, eabb2119.

Chen, L., Deng, H., Cui, H., Fang, J., Zuo, Z., Deng, J., Li, Y., Wang, X., and Zhao, L. (2018). Inflammatory responses and inflammation-associated diseases in organs. Oncotarget *9*, 7204–7218.

Cheng, M.H., Lin, L.L., Liu, J.Y., and Liu, A.J. (2012). The outcomes of stroke induced by middle cerebral artery occlusion in different strains of mice. CNS Neurosci. Ther. *18*, 794–795.

Cheng, X.T., Xie, Y.X., Zhou, B., Huang, N., Farfel-Becker, T., and Sheng, Z.H. (2018). Characterization of LAMP1-labeled nondegradative lysosomal and endocytic compartments in neurons. J. Cell Biol. *217*, 3127–3139.

Cherry, J.D., Olschowka, J.A., and O'Banion, M.K. (2014). Neuroinflammation and M2 microglia: The good, the bad, and the inflamed. J. Neuroinflammation *11*, 98.

Chiu, I.M., Morimoto, E.T.A., Goodarzi, H., Liao, J.T., O'Keeffe, S., Phatnani, H.P., Muratet, M., Carroll, M.C., Levy, S., Tavazoie, S., et al. (2013). A neurodegeneration-specific gene-expression signature of acutely isolated microglia from an amyotrophic lateral sclerosis mouse model. Cell Rep. *4*, 385–401.

Choudhary, G.S., Al-harbi, S., and Almasan, A. (2015). Caspase-3 Activation Is a Critical Determinant of Genotoxic Stress-Induced Apoptosis. Methods Mol. Biol. *414*, 13–21.

Chu, J., and Praticò, D. (2011). 5-lipoxygenase as an endogenous modulator of amyloid beta formation in vivo. Ann. Neurol. *69*, 34–46.

Chung, H., Brazil, M.I., Soe, T.T., and Maxfield, F.R. (1999). Uptake, degradation, and release of fibrillar and soluble forms of Alzheimer's amyloid β-peptide by microglial cells. J. Biol. Chem. *274*, 32301–32308.

Cisneros-Mejorado, A., Pérez-Samartín, A., Gottlieb, M., and Matute, C. (2014). ATP Signaling in Brain: Release, Excitotoxicity and Potential Therapeutic Targets. Cell. Mol. Neurobiol. *35*, 1–6.
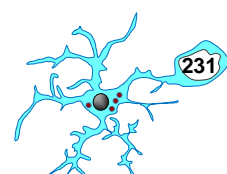
Clausen, B.H., Lambertsen, K.L., Babcock, A.A., Holm, T.H., Dagnaes-Hansen, F., and Finsen, B. (2008). Interleukin-1 beta and tumor necrosis factor-alpha are expressed by different subsets of microglia and macrophages after ischemic stroke in mice. J. Neuroinflammation *5*, 46.

Colton, C.A., Snell-Callanan, J., and Chernyshev, O.N. (1998). Ethanol induced changes in superoxide anion and nitric oxide in cultured microglia. Alcohol. Clin. Exp. Res. *22*, 710–716.

Costardi, J.V.V., Nampo, R.A.T., Silva, G.L., FerreiraRibeiro, M.A., Stella, H.J., BredaStella, M., and Malheiros, S.V.P. (2015). A review on alcohol: From the central action mechanism to chemical dependency. Rev. Assoc. Med. Bras. *61*, 381–387.

Cotrina, M.L., Kang, J., Lin, J.H.C., Bueno, E., Hansen, T.W., He, L., Liu, Y., and Nedergaard, M. (1998). Astrocytic gap junctions remain open during ischemic conditions. J. Neurosci. *18*, 2520–2537.

Coull, J.A.M., Beggs, S., Boudreau, D., Boivin, D., Tsuda, M., Inoue, K., Gravel, C., Salter, M.W., and De Koninck, Y. (2005). BDNF from microglia causes the shift in neuronal anion gradient underlying neuropathic pain. Nature *438*, 1017–1021.

Cowell, R.M., Xu, H., Galasso, J.M., and Silverstein, F.S. (2002). Hypoxic-ischemic injury induces macrophage inflammatory protein-1α expression in immature rat brain. Stroke *33*, 795–801.

Crews, F.T., and Nixon, K. (2009). Mechanisms of neurodegeneration and regeneration in alcoholism. Alcohol Alcohol. *44*, 115–127.

Crews, F.T., Zou, J., and Coleman Jr, L.G. (2021). Extracellular microvesicles promote microglia-- mediated pro-inflammatory responses to ethanol. J Neurosci Res.

Crompton, M. (1999). The mitochondrial permeability transition pore and its role in cell death. Biochem. J. *341*, 233–249.

Crowley, L.C., Marfell, B.J., and Waterhouse, N.J. (2016). Detection of DNA fragmentation in apoptotic cells by TUNEL. Cold Spring Harb. Protoc. *10*.

Cumming, T.B., Marshall, R.S., and Lazar, R.M. (2013). Stroke, cognitive deficits, and rehabilitation: Still an incomplete picture. Int. J. Stroke *8*, 38–45.

Cunha, C., Gomes, C., Vaz, A.R., and Brites, D. (2016). Exploring New Inflammatory Biomarkers and Pathways during LPS-Induced M1 Polarization. Mediators Inflamm.

Cunningham, C.L., Martínez-Cerdeño, V., and Noctor, S.C. (2013a). Microglia regulate
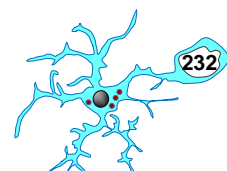
the number of neural precursor cells in the developing cerebral cortex. J. Neurosci.

Cunningham, C.L., Martínez-Cerdeño, V., and Noctor, S.C. (2013b). Microglia regulate the number of neural precursor cells in the developing cerebral cortex. J. Neurosci. *33*, 4216–4233.

Czapski, G.A., Gajkowska, B., and Strosznajder, J.B. (2010). Systemic administration of lipopolysaccharide induces molecular and morphological alterations in the hippocampus. Brain Res. *1356*, 85–94.

~D~

D'Arcy, M.S. (2019). Cell death: a review of the major forms of apoptosis, necrosis and autophagy. Cell Biol. Int. *43*, 582–592.

Dachet, F., Brown, J.B., Valyi-Nagy, T., Narayan, K.D., Serafini, A., Boley, N., Gingeras, T.R., Celniker, S.E., Mohapatra, G., and Loeb, J.A. (2021). Selective time-dependent changes in activity and cell-specific gene expression in human postmortem brain. Sci. Rep. *11*.

Dale, N., and Frenguelli, B. (2009). Release of Adenosine and ATP During Ischemia and Epilepsy. Curr. Neuropharmacol. *7*, 160–179.

Dalmau, I., Vela, J.M., González, B., Finsen, B., and Castellano, B. (2003). Dynamics of microglia in the developing rat brain. J. Comp. Neurol. *458*, 144–157.

Dando, S.J., Mackay-Sim, A., Norton, R., Currie, B.J., St. John, J.A., Ekberg, J.A.K., Batzloff, M., Ulett, G.C., and Beacham, I.R. (2014). Pathogens penetrating the central nervous system: Infection pathways and the cellular and molecular mechanisms of invasion. Clin. Microbiol. Rev. *27*, 691–726.

Davalos, D., Grutzendler, J., Yang, G., Kim, J. V., Zuo, Y., Jung, S., Littman, D.R., Dustin, M.L., and Gan, W.B. (2005). ATP mediates rapid microglial response to local brain injury in vivo. Nat. Neurosci.

Dayer, A.G., Ford, A.A., Cleaver, K.M., Yassaee, M., and Cameron, H.A. (2003). Short-term and long-term survival of new neurons in the rat dentate gyrus. J. Comp. Neurol. *460*, 563–572.

Daynac, M., Morizur, L., Chicheportiche, A., Mouthon, M.A., and Boussin, F.D. (2016). Age-related neurogenesis decline in the subventricular zone is associated with specific cell cycle regulation changes in activated neural stem cells. Sci. Rep. *6*.
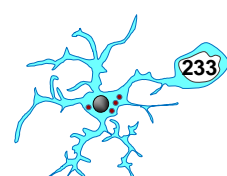
Denes, A., Vidyasagar, R., Feng, J., Narvainen, J., McColl, B.W., Kauppinen, R.A., and Allan, S.M. (2007). Proliferating resident microglia after focal cerebral ischaemia in mice. J. Cereb. Blood Flow Metab. *27*, 1941–1953.

Devi, L.A. (2000). G-protein-coupled receptor dimers in the lime light. Trends Pharmacol. Sci. *21*, 324–326.

Diaz-Aparicio, I., Beccari, S., Abiega, O., and Sierra, A. (2016). Clearing the corpses: Regulatory mechanisms, novel tools, and therapeutic potential of harnessing microglial phagocytosis in the diseased brain. Neural Regen. Res. *11*, 1533–1539.

Diaz-Aparicio, I., Paris, I., Sierra-Torre, V., Plaza-Zabala, A., Rodríguez-Iglesias, N., Márquez-Ropero, M., Beccari, S., Huguet, P., Abiega, O., Alberdi, E., et al. (2020). Microglia actively remodel adult hippocampal neurogenesis through the phagocytosis secretome. J. Neurosci. *40*, 1453–1482.

Dibaj, P., Steffens, H., Nadrigny, F., Neusch, C., Kirchhoff, F., and Schomburg, E.D. (2010). Long-lasting post-mortem activity of spinal microglia in situ in mice. J. Neurosci. Res.

Dickson, D.W., Farlo, J., Davies, P., Crystal, H., Fuld, P., and Yen, S.H.C. (1988). Alzheimer's disease. A double-labeling immunohistochemical study of senile plaques. Am. J. Pathol. *132*, 86–101.

Diesselberg, C., Ribes, S., Seele, J., Kaufmann, A., Redlich, S., Bunkowski, S., Hanisch, U.K., Michel, U., Nau, R., and Schütze, S. (2018). Activin A increases phagocytosis of Escherichia coli K1 by primary murine microglial cells activated by toll-like receptor agonists. J. Neuroinflammation *15*.

Dinarello, C.A. (2000). Proinflammatory cytokines. Chest *118*, 503–508.

Dirnagl, U. (2010). Rodent Models of Stroke.

Dirnagl, U., Iadecola, C., and Moskowitz, M.A. (1999). Pathobiology of ischaemic stroke: An integrated view. Trends Neurosci. *22*, 391–397.

Domercq, M., Vazquez-Villoldo, N., and Matute, C. (2013). Neurotransmitter signaling in the pathophysiology of microglia. Front. Cell. Neurosci. *7*.

Domingues, H.S., Portugal, C.C., Socodato, R., and Relvas, J.B. (2016). Oligodendrocyte, astrocyte, and microglia crosstalk in myelin development, damage, and repair. Front. Cell Dev. Biol. *4*.

Doná, F., Conceição, I.M., Ulrich, H., Ribeiro, E.B., Freitas, T.A., Nencioni, A.L.A., and
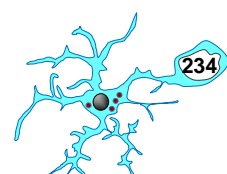
da Silva Fernandes, M.J. (2016). Variations of ATP and its metabolites in the hippocampus of rats subjected to pilocarpine-induced temporal lobe epilepsy. Purinergic Signal. *12*, 295–302.

Dong, X., Luo, M., Huang, G., Zhang, J., Tong, F., Cheng, Y., Cai, Q., Dong, J., Wu, G., and Cheng, J. (2015). Relationship between irradiation-induced neuro-inflammatory environments and impaired cognitive function in the developing brain of mice. Int. J. Radiat. Biol. *91*, 224–239.

Donnan, G.A., Fisher, M., Macleod, M., and Davis, S.M. (2008). Stroke. Lancet *371*, 612–623.

Doyle, A., McGarry, M.P., Lee, N.A., and Lee, J.J. (2012). The construction of transgenic and gene knockout/knockin mouse models of human disease. Transgenic Res. *21*, 327–349.

Drew, P.D., Johnson, J.W., Douglas, J.C., Phelan, K.D., and Kane, C.J.M. (2015). Pioglitazone blocks ethanol induction of microglial activation and immune responses in the hippocampus, cerebellum, and cerebral cortex in a mouse model of fetal alcohol spectrum disorders. Alcohol. Clin. Exp. Res. *39*, 445–454.

Driscoll, D.J.O., Felice, V.D., Kenny, L.C., Boylan, G.B., and O'Keeffe, G.W. (2018). Mild prenatal hypoxia-ischemia leads to social deficits and central and peripheral inflammation in exposed offspring. Brain. Behav. Immun. *69*, 418–427.

Duveau, V., Pouyatos, B., Bressand, K., Bouyssières, C., Chabrol, T., Roche, Y., Depaulis, A., and Roucard, C. (2016). Differential Effects of Antiepileptic Drugs on Focal Seizures in the Intrahippocampal Kainate Mouse Model of Mesial Temporal Lobe Epilepsy. CNS Neurosci. Ther. *22*, 497–506.

Dziewulska, D., and Mossakowski, M.J. (2003). Cellular expression of tumor necrosis factor α and its receptors in human ischemic stroke. Clin. Neuropathol. *22*, 35–40.

~E~

Ehlers, M.R.W. (2000). CR3: A general purpose adhesion-recognition receptor essential for innate immunity. Microbes Infect. *2*, 289–294.

Eid, T., Williamson, A., Lee, T.S.W., Petroff, O.A., and De Lanerolle, N.C. (2008). Glutamate and astrocytes - Key players in human mesial temporal lobe epilepsy? Epilepsia *49 Suppl 2*, 42–52.
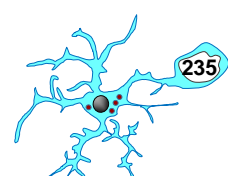
Ekdahl, C.T., Claasen, J.H., Bonde, S., Kokaia, Z., and Lindvall, O. (2003). Inflammation is detrimental for neurogenesis in adult brain. Proc. Natl. Acad. Sci. U. S. A. *100*, 13632–13637.

Elkabes, S., DiCicco-Bloom, E.M., and Black, I.B. (1996). Brain microglia/macrophages express neurotrophins that selectively regulate microglial proliferation and function. J. Neurosci. *16*, 2508–2521.

Elliott, M.R., Chekeni, F.B., Trampont, P.C., Lazarowski, E.R., Kadl, A., Walk, S.F., Park, D., Woodson, R.I., Ostankovich, M., Sharma, P., et al. (2009). Nucleotides released by apoptotic cells act as a find-me signal to promote phagocytic clearance. Nature *461*, 282–286.

Elmore, S. (2007). Apoptosis: A Review of Programmed Cell Death. Toxicol. Pathol. *35*.

Elmquist, J.K., Scammell, T.E., and Saper, C.B. (1997). Mechanisms of CNS response to systemic immune challenge: The febrile response. Trends Neurosci. *20,* 565–570.

Encinas, J.M., and Enikolopov, G. (2008). Identifying and Quantitating Neural Stem and Progenitor Cells in the Adult Brain. In Methods in Cell Biology, pp. 243–272.

Encinas, J.M., and Sierra, A. (2012). Neural stem cell deforestation as the main force driving the age-related decline in adult hippocampal neurogenesis. Behav. Brain Res. *227*, 433–439.

Encinas, J.M., Vaahtokari, A., and Enikolopov, G. (2006). Fluoxetine targets early progenitor cells in the adult brain. Proc. Natl. Acad. Sci. U. S. A. *103*, 8233–8238.

Encinas, J.M., Michurina, T. V., Peunova, N., Park, J.H., Tordo, J., Peterson, D.A., Fishell, G., Koulakov, A., and Enikolopov, G. (2011). Division-coupled astrocytic differentiation and age-related depletion of neural stem cells in the adult hippocampus. Cell Stem Cell.

Engel, T., Gomez-Villafuertes, R., Tanaka, K., Mesuret, G., Sanz-Rodriguez, A., Garcia-Huerta, P., Miras-Portugal, M.T., Henshall, D.C., and Diaz-Hernandez, M. (2012). Seizure suppression and neuroprotection by targeting the purinergic P2X7 receptor during status epilepticus in mice. FASEB J. *26*, 1616–1628.

Engel, T., Alves, M., Sheedy, C., and Henshall, D.C. (2016). ATPergic signalling during seizures and epilepsy. Neuropharmacology *104*, 140–153.

Enwere, E., Shingo, T., Gregg, C., Fujikawa, H., Ohta, S., and Weiss, S. (2004). Aging results in reduced epidermal growth factor receptor signaling, diminished olfactory
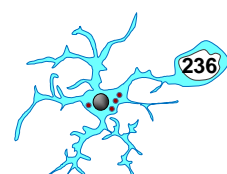
neurogenesis, and deficits in fine olfactory discrimination. J. Neurosci. *24*, 8354–8365.

Erickson, E.K., Blednov, Y.A., Harris, R.A., and Mayfield, R.D. (2019). Glial gene networks associated with alcohol dependence. Sci. Rep. *9*.

Eriksson, C., Zou, L.P., Ahlenius, S., Winblad, B., and Schultzberg, M. (2000). Inhibition of kainic acid induced expression of interleukin-1β and interleukin-1 receptor antagonist mRNA in the rat brain by NMDA receptor antagonists. Mol. Brain Res. *85*, 103–113.

Eyo, U.B., Peng, J., Swiatkowski, P., Mukherjee, A., Bispo, A., and Wu, L.J. (2014). Neuronal hyperactivity recruits microglial processes via neuronal NMDA receptors and microglial P2Y12 receptors after status epilepticus. J. Neurosci. *34*, 10528–10540.

Eyo, U.B., Peng, J., Murugan, M., Mo, M., Lalani, A., Xie, P., Xu, P., Margolis, D.J., and Wu, L.J. (2016). Regulation of physical microglia–neuron interactions by fractalkine signaling after status epilepticus. ENeuro *3*, ENEURO.0209-16.2016.

~F~

Fabene, P.F., Bramanti, P., and Constantin, G. (2010). The emerging role for chemokines in epilepsy. J. Neuroimmunol. *224*, 22–27.

Fadok, V.A., Voelker, D.R., Campbell, P.A., Cohen, J.J., Bratton, D.L., and Henson, P.M. (1992). Exposure of phosphatidylserine on the surface of apoptotic lymphocytes triggers specific recognition and removal by macrophages. J. Immunol. *48*, 2207–2216.

Fadok, V.A., Bratton, D.L., Konowal, A., Freed, P.W., Westcott, J.Y., and Henson, P.M. (1998). Macrophages that have ingested apoptotic cells in vitro inhibit proinflammatory cytokine production through autocrine/paracrine mechanisms involving TGF-β, PGE2, and PAF. J. Clin. Invest. *101*, 890–898.

Famitafreshi, H., and Karimian, M. (2020). Prostaglandins as the Agents That Modulate the Course of Brain Disorders. Degener. Neurol. Neuromuscul. Dis. *2020:10*, 1–13.

Fang, S.H., Wei, E.Q., Zhou, Y., Wang, M.L., Zhang, W.P., Yu, G.L., Chu, L.S., and Chen, Z. (2006). Increased expression of cysteinyl leukotriene receptor-1 in the brain mediates neuronal damage and astrogliosis after focal cerebral ischemia in rats. Neuroscience *140*, 969–979.

Fang, S.H., Zhou, Y., Chu, L.S., Zhang, W.P., Wang, M.L., Yu, G.L., Peng, F., and Wei, E.Q. (2007). Spatio-temporal expression of cysteinyl leukotriene receptor-2 mRNA in rat brain after focal cerebral ischemia. Neurosci. Lett. *412*, 78–83.
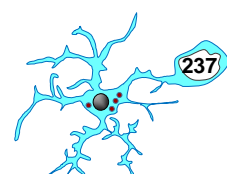
Fang, W., Zhai, X., Han, D., Xiong, X., Wang, T., Zeng, X., He, S., Liu, R., Miyata, M., Xu, B., et al. (2018). CCR2-dependent monocytes/macrophages exacerbate acute brain injury but promote functional recovery after ischemic stroke in mice. Theranostics *8*, 3530–3543.

Fatemi, A., Wilson, M.A., and Johnston, M. V. (2009). Hypoxic-Ischemic Encephalopathy in the Term Infant. Clin. Perinatol. *36*, 835–vii.

Faustino-Mendes, T., Machado-Pereira, M., Castelo-Branco, M., and Ferreira, R. (2018). The ischemic immature brain: Views on current experimental models. Front. Cell. Neurosci. *12:277*.

Feng, L., Murugan, M., Bosco, D.B., Liu, Y., Peng, J., Worrell, G.A., Wang, H.L., Ta, L.E., Richardson, J.R., Shen, Y., et al. (2019). Microglial proliferation and monocyte infiltration contribute to microgliosis following status epilepticus. Glia *67*, 1434–1448.

Fernandez-Lizarbe, S., Pascual, M., and Guerri, C. (2009). Critical Role of TLR4 Response in the Activation of Microglia Induced by Ethanol. J. Immunol. *183*, 4733–4744.

Fernández-López, D., Natarajan, N., Ashwal, S., and Vexler, Z.S. (2014). Mechanisms of perinatal arterial ischemic stroke. J. Cereb. Blood Flow Metab. *34*, 921–932.

Ferrer, I., Bernet, E., Soriano, E., Del Rio, T., and Fonseca, M. (1990). Naturally occurring cell death in the cerebral cortex of the rat and removal of dead cells by transitory phagocytes. Neuroscience *39*, 451–458.

Fisch, U., Brégère, C., Geier, F., Chicha, L., and Guzman, R. (2020). Neonatal hypoxia-ischemia in rat elicits a region-specific neurotrophic response in SVZ microglia. J. Neuroinflammation *17*.

Fisher, R.S., Acevedo, C., Arzimanoglou, A., Bogacz, A., Cross, J.H., Elger, C.E., Engel, J., Forsgren, L., French, J.A., Glynn, M., et al. (2014). ILAE Official Report: A practical clinical definition of epilepsy. Epilepsia *55*, 475–482.

Fisher, R.S., Cross, J.H., French, J.A., Higurashi, N., Hirsch, E., Jansen, F.E., Lagae, L., Moshé, S.L., Peltola, J., Roulet Perez, E., et al. (2017). Operational classification of seizure types by the International League Against Epilepsy: Position Paper of the ILAE Commission for Classification and Terminology. Epilepsia *58*, 522–530.

Fluri, F., Schuhmann, M.K., and Kleinschnitz, C. (2015). Animal models of ischemic stroke and their application in clinical research. Drug Des. Devel. Ther. *9*, 3445–3454.
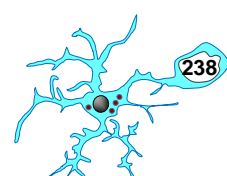
Ford, A.L., Goodsall, A.L., Hickey, W.F., and Sedgwick, J.D. (1995). Normal adult ramified microglia separated from other central nervous system macrophages by flow cytometric sorting. Phenotypic differences defined and direct ex vivo antigen presentation to myelin basic protein-reactive CD4C T cells compared. J. Immunol *154*, 4309–4321.

Forsgren, L., Hauser, W.A., Olafsson, E., Sander, J.W.A.S., Sillanpää, M., and Tomson, T. (2005). Mortality of epilepsy in developed countries: A review. Epilepsia *46*, 18–27.

Foster, J.R. (2001). The functions of cytokines and their uses in toxicology. Int. J. Exp. Pathol. *82*, 171–192.

Fourgeaud, L., Traves, P.G., Tufail, Y., Leal-Bailey, H., Lew, E.D., Burrola, P.G., Callaway, P., Zagorska, A., Rothlin, C. V., Nimmerjahn, A., et al. (2016). TAM receptors regulate multiple features of microglial physiology. Nature *532*, 240–244.

Fowler, J.F. (1989). The linear-quadratic formula and progress in fractionated radiotherapy. Br. J. Radiol. *62*, 679–694.

Franke, H., Günther, A., Grosche, J., Schmidt, R., Rossner, S., Reinhardt, R., Faber-Zuschratter, H., Schneider, D., and Illes, P. (2004). P2X7 receptor expression after ischemia in the cerebral cortex of rats. J. Neuropathol. Exp. Neurol. *63*, 686–699.

Fraser, D.A., Pisalyaput, K., and Tenner, A.J. (2010). C1q enhances microglial clearance of apoptotic neurons and neuronal blebs, and modulates subsequent inflammatory cytokine production. J. Neurochem. *112*, 733–743.

Frautschy, S.A., Yang, F., Irrizarry, M., Hyman, B., Saido, T.C., Hsiao, K., and Cole, G.M. (1998). Microglial response to amyloid plaques in APPsw transgenic mice. Am. J. Pathol. *152*, 307–317.

French, J.A., Koepp, M., Naegelin, Y., Vigevano, F., Auvin, S., Rho, J.M., Rosenberg, E., Devinsky, O., Olofsson, P.S., and Dichter, M.A. (2017). Clinical studies and anti-inflammatory mechanisms of treatments. Epilepsia *58*, 69–82.

Frenguelli, B.G., and Wall, M.J. (2016). Combined electrophysiological and biosensor approaches to study purinergic regulation of epileptiform activity in cortical tissue. J. Neurosci. Methods *260*, 202–214.

Frenguelli, B.G., Wigmore, G., Llaudet, E., and Dale, N. (2007). Temporal and mechanistic dissociation of ATP and adenosine release during ischaemia in the mammalian hippocampus. J. Neurochem. *101*, 1400–1413.
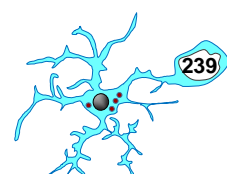
Freret, T., Bouet, V., Toutain, J., Saulnier, R., Pro-Sistiaga, P., Bihel, E., MacKenzie, E.T., Roussel, S., Schumann-Bard, P., and Touzani, O. (2008). Intraluminal thread model of focal stroke in the non-human primate. J. Cereb. Blood Flow Metab. *28*, 786–796.

Fricker, M., Oliva-Martín, M.J., and Brown, G.C. (2012a). Primary phagocytosis of viable neurons by microglia activated with LPS or Aβ is dependent on calreticulin/LRP phagocytic signalling. J. Neuroinflammation *9:196*.

Fricker, M., Neher, J.J., Zhao, J.W., Théry, C., Tolkovsky, A.M., and Brown, G.C. (2012b). MFG-E8 mediates primary phagocytosis of viable neurons during neuroinflammation. J. Neurosci. *2*, 2657–2666.

Friedman, B.A., Srinivasan, K., Ayalon, G., Meilandt, W.J., Lin, H., Huntley, M.A., Cao, Y., Lee, S.H., Haddick, P.C.G., Ngu, H., et al. (2018). Diverse Brain Myeloid Expression Profiles Reveal Distinct Microglial Activation States and Aspects of Alzheimer's Disease Not Evident in Mouse Models. Cell Rep. *22*, 832–847.

Fritsch, B., Reis, J., Gasior, M., Kaminski, R.M., and Rogawski, M.A. (2014). Role of GluK1 kainate receptors in seizures, epileptic discharges, and epileptogenesis. J. Neurosci. *34*, 5765–5775.

Fumagalli, S., Perego, C., Ortolano, F., and De Simoni, M.G. (2013). CX3CR1 deficiency induces an early protective inflammatory environment in ischemic mice. Glia *61*, 827–842.

Funk, C.D. (2001). Prostaglandins and leukotrienes: Advances in eicosanoid biology. Science (80-.). *294*, 1871–1875.

Fuxe, K., Bjelke, B., Andbjer, B., Grahn, H., Rimondini, R., and Agnati, L.F. (1997). Endothelin-1 induced lesions of the frontoparietal cortex of the rat. A possible model of focal cortical ischemia. Neuroreport *8*, 2623–2629.

~G~

Gaber, M.W., Sabek, O.M., Fukatsu, K., Wilcox, H.G., Kiani, M.F., and Merchant, T.E. (2003). Differences in ICAM-1 and TNF-α expression between large single fraction and fractionated irradiation in mouse brain. Int. J. Radiat. Biol. *79*, 359–366.

Gaikwad, S., and Agrawal-Rajput, R. (2015). Lipopolysaccharide from Rhodobacter sphaeroides Attenuates Microglia-Mediated Inflammation and Phagocytosis and Directs Regulatory T Cell Response. Int. J. Inflam. *2015:36132*.
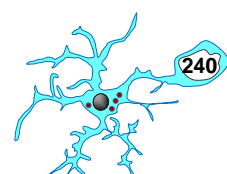
Gaitatzis, A., and Sander, J.W. (2004). The mortality of epilepsy revisited. Epileptic Disord. *6*, 3–13.

Garcia-Bonilla, L., Faraco, G., Moore, J., Murphy, M., Racchumi, G., Srinivasan, J., Brea, D., Iadecola, C., and Anrather, J. (2016). Spatio-temporal profile, phenotypic diversity, and fate of recruited monocytes into the post-ischemic brain. J. Neuroinflammation *13(1):285*.

Gardai, S.J., McPhillips, K.A., Frasch, S.C., Janssen, W.J., Starefeldt, A., Murphy-Ullrich, J.E., Bratton, D.L., Oldenborg, P.A., Michalak, M., and Henson, P.M. (2005). Cell-surface calreticulin initiates clearance of viable or apoptotic cells through trans-activation of LRP on the phagocyte. Cell *123*, 321–334.

Gardai, S.J., Bratton, D.L., Ogden, C.A., and Henson, P.M. (2006). Recognition ligands on apoptotic cells: a perspective. J. Leukoc. Biol. *79*, 896–903.

Garré, J.M., and Yang, G. (2018). Contributions of monocytes to nervous system disorders. J. Mol. Med. *96*, 873–883.

Gautiar, E.L., Shay, T., Miller, J., Greter, M., Jakubzick, C., Ivanov, S., Helft, J., Chow, A., Elpek, K.G., Gordonov, S., et al. (2012). Gene-expression profiles and transcriptional regulatory pathways that underlie the identity and diversity of mouse tissue macrophages. Nat. Immunol. *13*, 1118–1128.

Gebara, E., Bonaguidi, M.A., Beckervordersandforth, R., Sultan, S., Udry, F., Gijs, P.J., Lie, D.C., Ming, G.L., Song, H., and Toni, N. (2016). Heterogeneity of Radial Glia-Like Cells in the Adult Hippocampus. Stem Cells *34*, 997–1010.

Geissmann, F., Manz, M.G., Jung, S., Sieweke, M.H., Merad, M., and Ley, K. (2010). Development of monocytes, macrophages, and dendritic cells. Science (80-.). *327*, 656–661.

Gelosa, P., Lecca, D., Fumagalli, M., Wypych, D., Pignieri, A., Cimino, M., Verderio, C., Enerbäck, M., Nikookhesal, E., Tremoli, E., et al. (2014). Microglia is a key player in the reduction of stroke damage promoted by the new antithrombotic agent ticagrelor. J. Cereb. Blood Flow Metab. *34*, 979–988.

Gerriets, T., Li, F., Silva, M.D., Meng, X., Brevard, M., Sotak, C.H., and Fisher, M. (2003). The macrosphere model: Evaluation of a new stroke model for permanent middle cerebral artery occlusion in rats. J. Neurosci. Methods *122*, 201–211.

Gibson, C.L., Coughlan, T.C., and Murphy, S.P. (2005). Glial nitric oxide and ischemia. Glia *50*, 417–426.
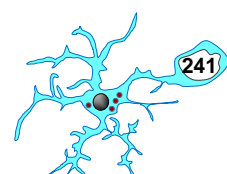
Gilpin, N.W., and Koob, G.F. (2008). Neurobiology of alcohol dependence: Focus on motivational mechanisms. Alcohol Res. Heal. *31*, 185–195.

Ginhoux, F., and Guilliams, M. (2016). Tissue-Resident Macrophage Ontogeny and Homeostasis. Immunity *44*, 439–449.

Ginhoux, F., and Prinz, M. (2015). Origin of microglia: Current concepts and past controversies. Cold Spring Harb. Perspect. Biol. *7(8):a0205*.

Ginhoux, F., Greter, M., Leboeuf, M., Nandi, S., See, P., Gokhan, S., Mehler, M.F., Conway, S.J., Ng, L.G., Stanley, E.R., et al. (2010). Fate mapping analysis reveals that adult microglia derive from primitive macrophages. Science (80-.). *330*, 841–845.

Ginhoux, F., Lim, S., Hoeffel, G., Low, D., and Huber, T. (2013). Origin and differentiation of microglia. Front. Cell. Neurosci. *7:45*.

Girardi, F., Allemani, C., and Coleman, M.P. (2019). Worldwide trends in survival from common childhood brain tumors: A systematic review. J. Glob. Oncol. *5*, 1–25.

Göb, E., Reymann, S., Langhauser, F., Schuhmann, M.K., Kraft, P., Thielmann, I., Göbel, K., Brede, M., Homola, G., Solymosi, L., et al. (2015). Blocking of plasma kallikrein ameliorates stroke by reducing thromboinflammation. Ann. Neurol. *77*, 784–803.

Goffin, K., Nissinen, J., Van Laere, K., and Pitkänen, A. (2007). Cyclicity of spontaneous recurrent seizures in pilocarpine model of temporal lobe epilepsy in rat. Exp. Neurol. *205*, 501–505.

Gofman, L., Cenna, J.M., and Potula, R. (2014). P2X4 Receptor Regulates Alcohol-Induced Responses in Microglia. J. Neuroimmune Pharmacol. *9*, 668–678.

Goldmann, T., Wieghofer, P., Jordão, M.J.C., Prutek, F., Hagemeyer, N., Frenzel, K., Amann, L., Staszewski, O., Kierdorf, K., Krueger, M., et al. (2016). Origin, fate and dynamics of macrophages at central nervous system interfaces. Nat. Immunol. *17*, 797–805.

Gómez-Nicola, D., Schetters, S.T.T., and Hugh Perry, V. (2014). Differential role of CCR2 in the dynamics of microglia and perivascular macrophages during prion disease. Glia *62*, 1041–1052.

Gomez Perdiguero, E., Klapproth, K., Schulz, C., Busch, K., Azzoni, E., Crozet, L., Garner, H., Trouillet, C., De Bruijn, M.F., Geissmann, F., et al. (2015). Tissue-resident macrophages originate from yolk-sac-derived erythro-myeloid progenitors. Nature.
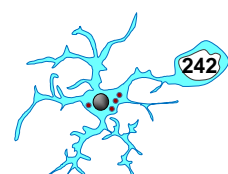
Gonçalves, J.T., Schafer, S.T., and Gage, F.H. (2016). Adult Neurogenesis in the Hippocampus: From Stem Cells to Behavior. Cell *167*, 897–914.

Gonzales-Portillo, G.S., Reyes, S., Aguirre, D., Pabon, M.M., and Borlongan, C. V. (2014). Stem cell therapy for neonatal hypoxic-ischemic encephalopathy. Front. Neurol. *5:147*.

Gould, E., Reeves, A.J., Fallah, M., Tanapat, P., Gross, C.G., and Fuchs, E. (1999). Hippocampal neurogenesis in adult Old World primates. Proc. Natl. Acad. Sci. U. S. A. *96*, 5263–5267.

Gouveia, K., and Hurst, J.L. (2017). Optimising reliability of mouse performance in behavioural testing: The major role of non-aversive handling. Sci. Rep. *7*.

Grabert, K., Michoel, T., Karavolos, M.H., Clohisey, S., Kenneth Baillie, J., Stevens, M.P., Freeman, T.C., Summers, K.M., and McColl, B.W. (2016). Microglial brain regionâ 'dependent diversity and selective regional sensitivities to aging. Nat. Neurosci. *19*, 504–516.

Granberg, P.O. (1991). Alcohol and cold. Arct. Med Res *50*, 43–47.

Grathwohl, S.A., Kälin, R.E., Bolmont, T., Prokop, S., Winkelmann, G., Kaeser, S.A., Odenthal, J., Radde, R., Eldh, T., Gandy, S., et al. (2009). Formation and maintenance of Alzheimer's disease β-amyloid plaques in the absence of microglia. Nat. Neurosci. *2*, 1361–1363.

Green, A.R. (2008). Pharmacological approaches to acute ischaemic stroke: Reperfusion certainly, neuroprotection possibly. Br. J. Pharmacol. *153*, S325-38.

Greene-Schloesser, D., Robbins, M.E., Peiffer, A.M., Shaw, E.G., Wheeler, K.T., and Chan, M.D. (2012). Radiation-induced brain injury: A review. Front. Oncol. *2:73*.

Grifasi, I.R., Evans, W.A., Rexha, A.D., Sako, L.W., and Marshall, S.A. (2019). A comparison of hippocampal microglial responses in aged and young rodents following dependent and non-dependent binge drinking. Int. Rev. Neurobiol. *148,* 305–343.

Griffith, J.W., Sokol, C.L., and Luster, A.D. (2014). Chemokines and chemokine receptors: Positioning cells for host defense and immunity. Annu. Rev. Immunol. *32*, 659–702.

Gude, D.R., Alvarez, S.E., Paugh, S.W., Mitra, P., Yu, J., Griffiths, R., Barbour, S.E., Milstien, S., and Spiegel, S. (2008). Apoptosis induces expression of sphingosine kinase 1 to release sphingosine-1-phosphate as a "come-and-get-me" signal. FASEB J. *22*,
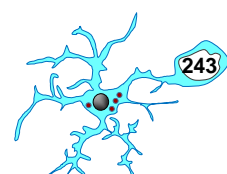
2629–2638.

Guergues, J., Wohlfahrt, J., Zhang, P., Liu, B., and Stevens, S.M. (2020). Deep proteome profiling reveals novel pathways associated with pro-inflammatory and alcohol-induced microglial activation phenotypes. J. Proteomics *220*.

Gulyás, B., Tóth, M., Schain, M., Airaksinen, A., Vas, Á., Kostulas, K., Lindström, P., Hillert, J., and Halldin, C. (2012). Evolution of microglial activation in ischaemic core and peri-infarct regions after stroke: A PET study with the TSPO molecular imaging biomarker [11C]vinpocetine. J. Neurol. Sci. *320*, 110–117.

Gusel'nikova, V. V., and Korzhevskiy, D.E. (2015). NeuN as a neuronal nuclear antigen and neuron differentiation marker. Acta Naturae *7*, 42–47.

Guthrie, P.B., Knappenberger, J., Segal, M., Bennett, M.V.L., Charles, A.C., and Kater, S.B. (1999). ATP released from astrocytes mediates glial calcium waves. J. Neurosci. *19*, 520–528.

Gutiérrez-Fernández, M., Fuentes, B., Rodríguez-Frutos, B., Ramos-Cejudo, J., Vallejo-Cremades, M.T., and Díez-Tejedor, E. (2012). Trophic factors and cell therapy to stimulate brain repair after ischaemic stroke. J. Cell. Mol. Med. *16*, 2280–2290.

Guzzo-Merello, G., Cobo-Marcos, M., and Gallego-Delgado, Maria Garcia-Pavia, P. (2014). Alcoholic cardiomyopathy. World J Cardiol. *6*, 771–781.

~H~

Haage, V., Semtner, M., Vidal, R.O., Hernandez, D.P., Pong, W.W., Chen, Z., Hambardzumyan, D., Magrini, V., Ly, A., Walker, J., et al. (2019). Comprehensive gene expression meta-analysis identifies signature genes that distinguish microglia from peripheral monocytes/macrophages in health and glioma. Acta Neuropathol. Commun. *7(1):20*.

Haga, S., Akai, K., and Ishii, T. (1989). Demonstration of microglial cells in and around senile (neuritic) plaques in the Alzheimer brain - An immunohistochemical study using a novel monoclonal antibody. Acta Neuropathol. *77*, 569–575.

Hagberg, H., Gilland, E., Bona, E., Hanson, L.Å., Hahn-Zoric, M., Blennow, M., Holst, M., McRae, A., and Söder, O. (1996). Enhanced expression of interleukin (IL)-1 and IL-6 messenger RNA and bioactive protein after hypoxia-ischemia in neonatal rats. Pediatr. Res. *40*, 603–609.
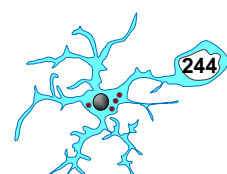
Hagemeyer, N., Hanft, K.M., Akriditou, M.A., Unger, N., Park, E.S., Stanley, E.R., Staszewski, O., Dimou, L., and Prinz, M. (2017). Microglia contribute to normal myelinogenesis and to oligodendrocyte progenitor maintenance during adulthood. Acta Neuropathol. *134*, 441–458.

Haglid, K.G., Wang, S., Qiner, Y., and Hamberger, A. (1994). Excitotoxicity - Experimental correlates to human epilepsy. Mol. Neurobiol. *9*, 259–263.

Hall, C.N., Reynell, C., Gesslein, B., Hamilton, N.B., Mishra, A., Sutherland, B.A., Oâ Farrell, F.M., Buchan, A.M., Lauritzen, M., and Attwell, D. (2014). Capillary pericytes regulate cerebral blood flow in health and disease. Nature *508*, 55–60.

Hamdy, N., Eide, S., Sun, H.S., and Feng, Z.P. (2020). Animal models for neonatal brain injury induced by hypoxic ischemic conditions in rodents. Exp. Neurol. *334:113457*.

Hamilton, N.B., and Attwell, D. (2010). Do astrocytes really exocytose neurotransmitters? Nat. Rev. Neurosci. *11*, 227–238.

Hamilton, S.E., Loose, M.D., Qi, M., Levey, A.I., Hille, B., Mcknight, G.S., Idzerda, R.L., and Nathanson, N.M. (1997). Disruption of the m1 receptor gene ablates muscarinic receptor-dependent M current regulation and seizure activity in mice. Proc. Natl. Acad. Sci. U. S. A. *94*, 13311–13316.

Hamley, I.W. (2012). The amyloid beta peptide: A chemist's perspective. role in Alzheimer's and fibrillization. Chem. Rev. *112*, 5147–5192.

Hammond, T.R., Dufort, C., Dissing-Olesen, L., Giera, S., Young, A., Wysoker, A., Walker, A.J., Gergits, F., Segel, M., Nemesh, J., et al. (2019). Single-Cell RNA Sequencing of Microglia throughout the Mouse Lifespan and in the Injured Brain Reveals Complex Cell-State Changes. Immunity *50*, 253-271.e6.

Han, H.S., and Yenari, M.A. (2003). Cellular targets of brain inflammation in stroke. Curr. Opin. Investig. Drugs *4*, 522–529.

Han, J.W., Kwon, S.Y., Won, S.C., Shin, Y.J., Ko, J.H., and Lyu, C.J. (2009). Comprehensive clinical follow-up of late effects in childhood cancer survivors shows the need for early and well-timed intervention. Ann. Oncol. *20*, 1170–1177.

Han, T., Qin, Y., Mou, C., Wang, M., Jiang, M., and Liu, B. (2016a). Seizure induced synaptic plasticity alteration in hippocampus is mediated by IL-1β receptor through PI3K/Akt pathway. Am. J. Transl. Res. *8*, 4499–4509.

Han, W., Umekawa, T., Zhou, K., Zhang, X.M., Ohshima, M., Dominguez, C.A., Harris,
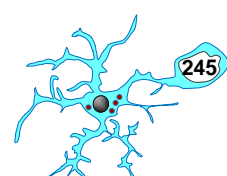
R.A., Zhu, C., and Blomgren, K. (2016b). Cranial irradiation induces transient microglia accumulation, followed by long-lasting inflammation and loss of microglia. Oncotarget *7*, 82305–82323.

Hanayama, R., Tanaka, M., Miwa, K., Shinohara, A., Iwamatsu, A., and Nagata, S. (2002). Identification of a factor that links apoptotic cells to phagocytes. Nature *417*, 182–187.

Harada, H., Wang, Y., Mishima, Y., Uehara, N., Makaya, T., and Kano, T. (2005). A novel method of detecting rCBF with laser-Doppler flowmetry without cranial window through the skull for a MCAO rat model. Brain Res. Protoc. *14*, 165–170.

Harper, C.G., Kril, J.J., and Holloway, R.L. (1985). Brain shrinkage in chronic alcoholics: A pathological study. Br. Med. J. (Clin. Res. Ed). *290*, 501–504.

Harris, L., Rigo, P., Stiehl, T., Gaber, Z.B., Austin, S.H.L., Masdeu, M. del M., Edwards, A., Urbán, N., Marciniak-Czochra, A., and Guillemot, F. (2021). Coordinated changes in cellular behavior ensure the lifelong maintenance of the hippocampal stem cell population. Cell Stem Cell *28*, 863-876.e6.

Hashimoto, D., Chow, A., Noizat, C., Teo, P., Beasley, M.B., Leboeuf, M., Becker, C.D., See, P., Price, J., Lucas, D., et al. (2013). Tissue-resident macrophages self-maintain locally throughout adult life with minimal contribution from circulating monocytes. Immunity *38*, 792–804.

Hata, R., Mies, G., Wiessner, C., Fritze, K., Hesselbarth, D., Brinker, G., and Hossmann, K.-A. (1998). A Reproducible Model of Middle Cerebral Artery Occlusion in Mice: Hemodynamic, Biochemical, and Magnetic Resonance Imaging. J. Cereb. Blood Flow Metab. *18*, 367–375.

Hattiangady, B., and Shetty, A.K. (2008). Aging does not alter the number or phenotype of putative stem/progenitor cells in the neurogenic region of the hippocampus. Neurobiol. Aging *29*, 129–147.

Haynes, S.E., Hollopeter, G., Yang, G., Kurpius, D., Dailey, M.E., Gan, W.B., and Julius, D. (2006). The P2Y12 receptor regulates microglial activation by extracellular nucleotides. Nat. Neurosci. *9*, 1512–1519.

He, J., and Crews, F.T. (2008). Increased MCP-1 and microglia in various regions of the human alcoholic brain. Exp. Neurol. *210*, 349–358.

Hedtjärn, M., Leverin, A.L., Eriksson, K., Blomgren, K., Mallard, C., and Hagberg, H. (2002). Interleukin-18 involvement in hypoxic-ischemic brain injury. J. Neurosci. *22*,
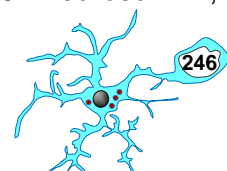
5910–5919.

Hedtjärn, M., Mallard, C., and Hagberg, H. (2004). Inflammatory gene profiling in the developing mouse brain after hypoxia-ischemia. J. Cereb. Blood Flow Metab. *24*, 1333–1351.

Heldmann, U., Mine, Y., Kokaia, Z., Ekdahl, C.T., and Lindvall, O. (2011). Selective depletion of Mac-1-expressing microglia in rat subventricular zone does not alter neurogenic response early after stroke. Exp. Neurol. *229*, 391–398.

Hellwig, S., Masuch, A., Nestel, S., Katzmarski, N., Meyer-Luehmann, M., and Biber, K. (2015). Forebrain microglia from wild-type but not adult 5xFAD mice prevent amyloid-β plaque formation in organotypic hippocampal slice cultures. Sci. Rep. *5:14624*.

Helmut, K., Hanisch, U.K., Noda, M., and Verkhratsky, A. (2011). Physiology of microglia. Physiol. Rev. *91*, 461–553.

Henjum, K., Årskog, V., Jendresen, C.B., Fladby, T., Torp, R., and Nilsson, L.N.G. (2020). Analyzing microglial-associated Aβ in Alzheimer's disease transgenic mice with a novel mid-domain Aβ-antibody. Sci. Rep. *10*.

Henson, P.M., and Hume, D.A. (2006). Apoptotic cell removal in development and tissue homeostasis. Trends Immunol. *27*, 244–250.

Herson, P.S., and Traystman, R.J. (2014). Animal models of stroke: Translational potential at present and in 2050. Future Neurol. *9*, 541–551.

Hicklin, T.R., Wu, P.H., Radcliffe, R.A., Freund, R.K., Goebel-Goody, S.M., Correa, P.R., Proctor, W.R., Lombroso, P.J., and Browning, M.D. (2011). Alcohol inhibition of the NMDA receptor function, long-term potentiation, and fear learning requires striatal-enriched protein tyrosine phosphatase. Proc. Natl. Acad. Sci. U. S. A. *108*, 6650–6655.

Hickman, S.E., Kingery, N.D., Ohsumi, T.K., Borowsky, M.L., Wang, L.C., Means, T.K., and El Khoury, J. (2013). The microglial sensome revealed by direct RNA sequencing. Nat. Neurosci. *16*, 1896–1905.

Hijioka, M., Futokoro, R., Ohto-Nakanishi, T., Nakanishi, H., Katsuki, H., and Kitamura, Y. (2020). Microglia-released leukotriene B4 promotes neutrophil infiltration and microglial activation following intracerebral hemorrhage. Int. Immunopharmacol. *85:106678*.

Hilbig, H., Bidmon, H.J., Oppermann, O.T., and Remmerbach, T. (2004). Influence of post-mortem delay and storage temperature on the immunohistochemical detection of
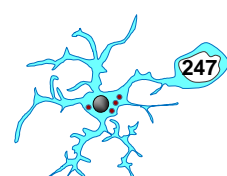
antigens in the CNS of mice. Exp. Toxicol. Pathol. *56*, 159–171.

Hill, J.K., Gunion-Rinker, L., Kulhanek, D., Lessov, N., Kim, S., Clark, W.M., Dixon, M.P., Nishi, R., Stenzel-Poore, M.P., and Eckenstein, F.P. (1999). Temporal modulation of cytokine expression following focal cerebral ischemia in mice. Brain Res. *820*, 45–54.

Hines, D.J., Choi, H.B., Hines, R.M., Phillips, A.G., and MacVicar, B.A. (2013). Prevention of LPS-Induced Microglia Activation, Cytokine Production and Sickness Behavior with TLR4 Receptor Interfering Peptides. PLoS One *8*, e60388.

Hirasawa, T., Ohsawa, K., Imai, Y., Ondo, Y., Akazawa, C., Uchino, S., and Kohsaka, S. (2005). Visualization of microglia in living tissues using Iba1-EGFP transgenic mice. J. Neurosci. Res. *81*, 357–362.

Hoeffel, G., and Ginhoux, F. (2015). Ontogeny of tissue-resident macrophages. Front. Immunol. *6:486*.

Hoeffel, G., and Ginhoux, F. (2018). Fetal monocytes and the origins of tissue-resident macrophages. Cell. Immunol. *330*, 5–15.

Hoeffel, G., Wang, Y., Greter, M., See, P., Teo, P., Malleret, B., Leboeuf, M., Low, D., Oller, G., Almeida, F., et al. (2012). Adult Langerhans cells derive predominantly from embryonic fetal liver monocytes with a minor contribution of yolk sac-derived macrophages. J. Exp. Med. *209*, 1167–1181.

Holloway, P.M., and Gavins, F.N.E. (2016). Modeling Ischemic Stroke in Vitro: Status Quo and Future Perspectives. Stroke *47*, 561–569.

Holmes, G.L. (2015). Cognitive impairment in epilepsy: The role of network abnormalities. Epileptic Disord. *17*, 101–116.

Holness, C.L., and Simmons, D.L. (1993). Molecular cloning of CD68, a human macrophage marker related to lysosomal glycoproteins. Blood *81*, 1607–1613.

Holtman, I.R., Raj, D.D., Miller, J.A., Schaafsma, W., Yin, Z., Brouwer, N., Wes, P.D., Möller, T., Orre, M., Kamphuis, W., et al. (2015). Induction of a common microglia gene expression signature by aging and neurodegenerative conditions: a co-expression meta-analysis. Acta Neuropathol. Commun. *3*.

Honarpisheh, P., Lee, J., Banerjee, A., Blasco-Conesa, M.P., Honarpisheh, P., D'Aigle, J., Mamun, A.A., Ritzel, R.M., Chauhan, A., Ganesh, B.P., et al. (2020). Potential caveats of putative microglia-specific markers for assessment of age-related cerebrovascular neuroinflammation. J. Neuroinflammation *17*.
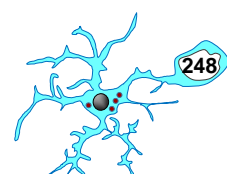
Hong, S., Dissing-Olesen, L., and Stevens, B. (2016). New insights on the role of microglia in synaptic pruning in health and disease. Curr. Opin. Neurobiol. *36*, 128–134.

Hornik, T.C., Neniskyte, U., and Brown, G.C. (2014). Inflammation induces multinucleation of Microglia via PKC inhibition of cytokinesis, generating highly phagocytic multinucleated giant cells. J. Neurochem. *128*, 650–661.

Hoshiko, M., Arnoux, I., Avignone, E., Yamamoto, N., and Audinat, E. (2012). Deficiency of the microglial receptor CX3CR1 impairs postnatal functional development of thalamocortical synapses in the barrel cortex. J. Neurosci. *32*, 15106–15111.

Hosmane, S., Tegenge, M.A., Rajbhandari, L., Uapinyoying, P., Kumar, N.G., Thakor, N., and Venkatesan, A. (2012). Toll/interleukin-1 receptor domain-containing adapter inducing interferon-β mediates microglial phagocytosis of degenerating axons. J. Neurosci. *32*, 7745–7757.

Howells, D.W., Porritt, M.J., Rewell, S.S.J., O'Collins, V., Sena, E.S., Van Der Worp, H.B., Traystman, R.J., and MacLeod, M.R. (2010). Different strokes for different folks: The rich diversity of animal models of focal cerebral ischemia. J. Cereb. Blood Flow Metab. *30*, 1412–1431.

Hu, H., Chen, G., Zhang, J.M., Zhang, W.P., Zhang, L., Ge, Q.F., Yao, H.T., Ding, W., Chen, Z., and Wei, E.Q. (2005). Distribution of cysteinyl leukotriene receptor 2 in human traumatic brain injury and brain tumors. Acta Pharmacol. Sin. *26*, 685–690.

Hu, P., Wang, D., Zhang, Y., Cai, Z., Ye, T., Tong, L., Xu, X., Lu, J., Liu, F., Lu, X., et al. (2020). Apoptosis-triggered decline in hippocampal microglia mediates adolescent intermittent alcohol exposure-induced depression-like behaviors in mice. Neuropharmacology *170:108054*.

Hu, X., Li, P., Guo, Y., Wang, H., Leak, R.K., Chen, S., Gao, Y., and Chen, J. (2012). Microglia/macrophage polarization dynamics reveal novel mechanism of injury expansion after focal cerebral ischemia. Stroke *43*, 3063–3070.

Hughes, C.E., and Nibbs, R.J.B. (2018). A guide to chemokines and their receptors. FEBS J. *285*, 2944–2971.

Hughes, P.M., Botham, M.S., Frentzel, S., Mir, A., and Perry, V.H. (2002). Expression of fractalkine (CX3CL1) and its receptor, CX3CR1, during acute and chronic inflammation in the rodent CNS. Glia *37*, 314–327.

Hughes, P.M., Anthony, D.C., Ruddin, M., Botham, M.S., Rankine, E.L., Sablone, M., Baumann, D., Mir, A.K., and Perry, V.H. (2003). Focal Lesions in the Rat Central Nervous
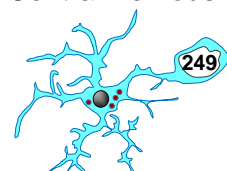
System Induced by Endothelin-1. J. Neuropathol. Exp. Neurol. *62*, 1276–1286.

Hume, D.A., Perry, V.H., and Gordon, S. (1983). Immunohistochemical localization of a macrophage-specific antigen in developing mouse retina: Phagocytosis of dying neurons and differentiation in microglial cells to form a regular array in the plexiform layers. J. Cell Biol. *97*, 253–257.

Huo, K., Sun, Y., Li, H., Du, X., Wang, X., Karlsson, N., Zhu, C., and Blomgren, K. (2012). Lithium reduced neural progenitor apoptosis in the hippocampus and ameliorated functional deficits after irradiation to the immature mouse brain. Mol. Cell. Neurosci. *51*, 32–42.

Hwang, B.Y., Appelboom, G., Ayer, A., Kellner, C.P., Kotchetkov, I.S., Gigante, P.R., Haque, R., Kellner, M., and Connolly, E.S. (2011). Advances in neuroprotective strategies: Potential therapies for intracerebral hemorrhage. Cerebrovasc. Dis. *31*, 211–222.

Hwang, S.Y., Jung, J.S., Kim, T.H., Lim, S.J., Oh, E.S., Kim, J.Y., Ji, K.A., Joe, E.H., Cho, K.H., and Han, I.O. (2006). Ionizing radiation induces astrocyte gliosis through microglia activation. Neurobiol. Dis. *21*, 457–467.

~|~

Iadecola, C., and Anrather, J. (2011). The immunology of stroke: From mechanisms to translation. Nat. Med. *17*, 796–808.

Ieraci, A., and Herrera, D.G. (2006). Nicotinamide protects against ethanol-induced apoptotic neurodegeneration in the developing mouse brain. PLoS Med. *3(4):e101*.

Ifuku, M., Katafuchi, T., Mawatari, S., Noda, M., Miake, K., Sugiyama, M., and Fujino, T. (2012). Anti-inflammatory/anti-amyloidogenic effects of plasmalogens in lipopolysaccharide-induced neuroinflammation in adult mice. J. Neuroinflammation *9:197*.

Ikubo, M., Inoue, A., Nakamura, S., Jung, S., Sayama, M., Otani, Y., Uwamizu, A., Suzuki, K., Kishi, T., Shuto, A., et al. (2015). Structure-activity relationships of lysophosphatidylserine analogs as agonists of G-protein-coupled receptors GPR34, P2Y10, and GPR174. J. Med. Chem. *58*, 4204–4219.

Imamoto, K., and Leblond, C.P. (1978). Radioautographic investigation of gliogenesis in the corpus callosum of young rats II. Origin of microglial cells. J. Comp. Neurol. *180*, 139–163.
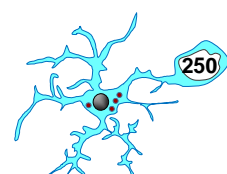
Imura, Y., Morizawa, Y., Komatsu, R., Shibata, K., Shinozaki, Y., Kasai, H., Moriishi, K., Moriyama, Y., and Koizumi, S. (2013). Microglia release ATP by exocytosis. Glia *61*, 1320–1330.

Isailovic, N., Daigo, K., Mantovani, A., and Selmi, C. (2015). Interleukin-17 and innate immunity in infections and chronic inflammation. J. Autoimmun. *60.*

Itagaki, S., McGeer, P.L., Akiyama, H., Zhu, S., and Selkoe, D. (1989). Relationship of microglia and astrocytes to amyloid deposits of Alzheimer disease. J. Neuroimmunol. *24*, 173–182.

Ito, D., Imai, Y., Ohsawa, K., Nakajima, K., Fukuuchi, Y., and Kohsaka, S. (1998). Microglia-specific localisation of a novel calcium binding protein, Iba1. Mol. Brain Res. *57*, 1–9.

Ito, D., Tanaka, K., Suzuki, S., Dembo, T., and Fukuuchi, Y. (2001). Enhanced expression of Iba1, ionized calcium-binding adapter molecule 1, after transient focal cerebral ischemia in rat brain. Stroke *32*, 1208–1215.

Ivacko, J.A., Sun, R., and Silverstein, F.S. (1996). Hypoxic-ischemic brain injury induces an acute microglial reaction in perinatal rats. Pediatr. Res. *39*, 39–47.

~J~

Jana, M., Palencia, C.A., and Pahan, K. (2008). Fibrillar Amyloid-β Peptides Activate Microglia via TLR2: Implications for Alzheimer's Disease. J. Immunol.

Jaworska, J., Ziemka-Nalecz, M., Sypecka, J., and Zalewska, T. (2017). The potential neuroprotective role of a histone deacetylase inhibitor, sodium butyrate, after neonatal hypoxia-ischemia. J. Neuroinflammation *14*, 34.

Jenkins, D.D., Rollins, L.G., Perkel, J.K., Wagner, C.L., Katikaneni, L.P., Bass, W.T., Kaufman, D.A., Horgan, M.J., Languani, S., Givelichian, L., et al. (2012). Serum cytokines in a clinical trial of hypothermia for neonatal hypoxic-ischemic encephalopathy. J. Cereb. Blood Flow Metab. *32*, 1888–1896.

Jenkins, S.J., Ruckerl, D., Thomas, G.D., Hewitson, J.P., Duncan, S., Brombacher, F., Maizels, R.M., Hume, D.A., and Allen, J.E. (2013). IL-4 directly signals tissue-resident macrophages to proliferate beyond homeostatic levels controlled by CSF-1. J. Exp. Med. *210*, 2477–2491.

Jeong, H.-K., Ji, K., Min, K., and Joe, E.-H. (2013). Brain Inflammation and Microglia:
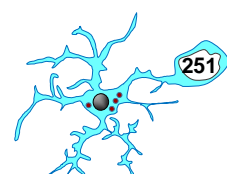
Facts and Misconceptions. Exp. Neurobiol. *22*, 59–67.

Ji, X., Trandafir, C.C., Wang, A., and Kurahashi, K. (2013). Effects of the experimental subarachnoid hemorrhage on the eicosanoid receptors in nicotine-induced contraction of the rat basilar artery. J. Stroke Cerebrovasc. Dis. *22*, 1258–1262.

Jimenez-Pacheco, A., Diaz-Hernandez, M., Arribas-Blázquez, M., Sanz-Rodriguez, A., Olivos-Oré, L.A., Artalejo, A.R., Alves, M., Letavic, M., Teresa Miras-Portugal, M., Conroy, R.M., et al. (2016). Transient P2X7 receptor antagonism produces lasting reductions in spontaneous seizures and gliosis in experimental temporal lobe epilepsy. J. Neurosci. *36*, 5920–5932.

Jin, X., and Yamashita, T. (2016). Microglia in central nervous system repair after injury. J. Biochem. *159*, 491–496.

Jin, M., Jang, E., and Suk, K. (2014). Lipocalin-2 Acts as a Neuroinflammatogen in Lipopolysaccharide-injected Mice. Exp. Neurobiol. *23*, 155–162.

Jinno, S. (2011). Decline in adult neurogenesis during aging follows a topographic pattern in the mouse hippocampus. J. Comp. Neurol. *519*, 451–466.

Joensuu, T., Lehesjoki, A.E., and Kopra, O. (2008). Molecular background of EPM1 - Unverricht-Lundborg disease. Epilepsia *49*, 557–563.

Johnson, C.O., Nguyen, M., Roth, G.A., Nichols, E., Alam, T., Abate, D., Abd-Allah, F., Abdelalim, A., Abraha, H.N., Abu-Rmeileh, N.M., et al. (2019). Global, regional, and national burden of stroke, 1990–2016: a systematic analysis for the Global Burden of Disease Study 2016. Lancet Neurol. *18*, 439–458.

Jones, B.A., Beamer, M., and Ahmed, S. (2010). Fractalkine/CX3CL1: A potential new target for inflammatory diseases. Mol. Interv. *10*, 263–270.

Jordão, M.J.C., Sankowski, R., Brendecke, S.M., Sagar, Locatelli, G., Tai, Y.H., Tay, T.L., Schramm, E., Armbruster, S., Hagemeyer, N., et al. (2019). Neuroimmunology: Single-cell profiling identifies myeloid cell subsets with distinct fates during neuroinflammation. Science (80-.). *363(6425):*, eaat7554.

Jung, K.H., Chu, K., Lee, S.T., Kim, J.H., Kang, K.M., Song, E.C., Kim, S.J., Park, H.K., Kim, M., Lee, S.K., et al. (2009). Region-specific plasticity in the epileptic rat brain: A hippocampal and extrahippocampal analysis. Epilepsia *50*, 537–549.

Jung, S., Aliberti, J., Graemmel, P., Sunshine, M.J., Kreutzberg, G.W., Sher, A., and Littman, D.R. (2000). Analysis of Fractalkine Receptor CX3CR1 Function by Targeted
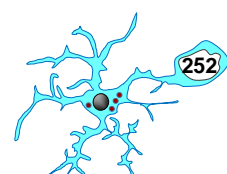
Deletion and Green Fluorescent Protein Reporter Gene Insertion. Mol. Cell. Biol. *20*, 4106–4114.

Jurányi, Z., Sperlágh, B., and Vizi, E.S. (1999). Involvement of P2 purinoceptors and the nitric oxide pathway in [3H]purine outflow evoked by short-term hypoxia and hypoglycemia in rat hippocampal slices. Brain Res. *823*, 183–190.

~K~

Kaiser, T., and Feng, G. (2019). Tmem119-EGFP and Tmem119-creERT2 transgenic mice for labeling and manipulating microglia. ENeuro *6*, ENEURO.0448-18.2019.

Kalinin, S., González-Prieto, M., Scheiblich, H., Lisi, L., Kusumo, H., Heneka, M.T., Madrigal, J.L.M., Pandey, S.C., and Feinstein, D.L. (2018). Transcriptome analysis of alcohol-treated microglia reveals downregulation of beta amyloid phagocytosis. J. Neuroinflammation *15*.

Kalm, M., Lannering, B., Björk-Eriksson, T., and Blomgren, K. (2009). Irradiation-induced loss of microglia in the young brain. J. Neuroimmunol. *206*, 70–75.

Kalozoumi, G., Kel-Margoulis, O., Vafiadaki, E., Greenberg, D., Bernard, H., Soreq, H., Depaulis, A., and Sanoudou, D. (2018). Glial responses during epileptogenesis in Mus musculus point to potential therapeutic targets. PLoS One *13*, e0201742.

Kandratavicius, L., Alves Balista, P., Lopes-Aguiar, C., Ruggiero, R.N., Umeoka, E.H., Garcia-Cairasco, N., Bueno-Junior, L.S., and Leite, J.P. (2014). Animal models of epilepsy: Use and limitations. Neuropsychiatr. Dis. Treat. *10*, 1693–1705.

Kang, T.C., Kim, D.S., Kwak, S.E., Kim, J.E., Won, M.H., Kim, D.W., Choi, S.Y., and Kwon, O.S. (2006). Epileptogenic roles of astroglial death and regeneration in the dentate gyrus of experimental temporal lobe epilepsy. Glia *54*, 258–271.

Kato, H., Kogure, K., Liu, X.H., Araki, T., and Itoyama, Y. (1996). Progressive expression of immunomolecules on activated microglia and invading leukocytes following focal cerebral ischemia in the rat. Brain Res. *734*, 203–212.

Kaur, C., Ling, E.A., and Wong, W.C. (1985). Transformation of Amoeboid Microglial Cells into Microglia in the Corpus Callosum of the Postnatal Rat Brain. An Electron Microscopical Study. Arch. Histol. Jpn. *128*, 847–858.

Kaur, C., Rathnasamy, G., and Ling, E.A. (2013). Roles of activated microglia in hypoxia induced neuroinflammation in the developing brain and the retina. J. Neuroimmune
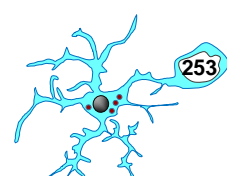
Pharmacol. *8*, 66–78.

Kempermann, G. (2011). Seven principles in the regulation of adult neurogenesis. Eur. J. Neurosci. *33*, 1018–1024.

Kempermann, G., Kuhn, H.G., and Gage, F.H. (1998). Experience-induced neurogenesis in the senescent dentate gyrus. J. Neurosci.

Kempermann, G., Jessberger, S., Steiner, B., and Kronenberg, G. (2004). Milestones of neuronal development in the adult hippocampus. Trends Neurosci.

Keren-Shaul, H., Spinrad, A., Weiner, A., Matcovitch-Natan, O., Dvir-Szternfeld, R., Ulland, T.K., David, E., Baruch, K., Lara-Astaiso, D., Toth, B., et al. (2017). A Unique Microglia Type Associated with Restricting Development of Alzheimer's Disease. Cell *169*, 1276-1290.e17.

Kettenmann, H. (2007). Neuroscience: The brain's garbage men. Nature *446*, 987–989.

Khanna, K.K., and Jackson, S.P. (2001). DNA double-strand breaks: Signaling, repair and the cancer connection. Nat. Genet. *27*, 247–254.

Kierdorf, K., and Prinz, M. (2013). Factors regulating microglia activation. Front. Cell. Neurosci. 7:44.

Kierdorf, K., Erny, D., Goldmann, T., Sander, V., Schulz, C., Perdiguero, E.G., Wieghofer, P., Heinrich, A., Riemke, P., Hölscher, C., et al. (2013a). Microglia emerge from erythromyeloid precursors via Pu.1-and Irf8-dependent pathways. Nat. Neurosci. *16*, 273–280.

Kierdorf, K., Erny, D., Goldmann, T., Sander, V., Schulz, C., Perdiguero, E.G., Wieghofer, P., Heinrich, A., Riemke, P., Hölscher, C., et al. (2013b). Microglia emerge from erythromyeloid precursors via Pu.1-and Irf8-dependent pathways. Nat. Neurosci.

Kim, C.C., Nakamura, M.C., and Hsieh, C.L. (2016). Brain trauma elicits non-canonical macrophage activation states. J. Neuroinflammation *13*, 117.

Kinchen, J.M., and Ravichandran, K.S. (2008). Phagosome maturation: Going through the acid test. Nat. Rev. Mol. Cell Biol. *9*, 781–795.

Kitagawa, K., Matsumoto, M., Yang, G., Mabuchi, T., Yagita, Y., Hori, M., and Yanagihara, T. (1998). Cerebral ischemia after bilateral carotid artery occlusion and intraluminal suture occlusion in mice: Evaluation of the patency of the posterior communicating artery. J. Cereb. Blood Flow Metab. *18*, 570–579.
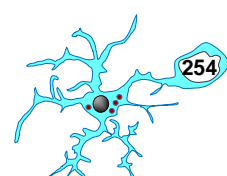
Kivimäki, M., Singh-Manoux, A., Batty, G.D., Sabia, S., Sommerlad, A., Floud, S., Jokela, M., Vahtera, J., Beydoun, M.A., Suominen, S.B., et al. (2020). Association of Alcohol-Induced Loss of Consciousness and Overall Alcohol Consumption With Risk for Dementia. JAMA Netw. Open *3(9):e2016*.

Kleinschnitz, C., Braeuninger, S., Pham, M., Austinat, M., Nölte, I., Renné, T., Nieswandt, B., Bendszus, M., and Stoll, G. (2008). Blocking of platelets or intrinsic coagulation pathway-driven thrombosis does not prevent cerebral infarctions induced by photothrombosis. Stroke *39*, 1262–1268.

Kloss, C.U.A., Bohatschek, M., Kreutzberg, G.W., and Raivich, G. (2001). Effect of lipopolysaccharide on the morphology and integrin immunoreactivity of ramified microglia in the mouse brain and in cell culture. Exp. Neurol. *168*, 32–46.

Knoth, R., Singec, I., Ditter, M., Pantazis, G., Capetian, P., Meyer, R.P., Horvat, V., Volk, B., and Kempermann, G. (2010). Murine features of neurogenesis in the human hippocampus across the lifespan from 0 to 100 years. PLoS One *5(1):e8809*.

Kochan, T., Singla, A., Tosi, J., and Kumar, A. (2012). Toll-like receptor 2 ligand pretreatment attenuates retinal microglial inflammatory response but enhances phagocytic activity toward Staphylococcus aureus. Infect. Immun. *80*, 2076–2088.

Kocur, M., Schneider, R., Pulm, A.K., Bauer, J., Kropp, S., Gliem, M., Ingwersen, J., Goebels, N., Alferink, J., Prozorovski, T., et al. (2015). IFNβ secreted by microglia mediates clearance of myelin debris in CNS autoimmunity. Acta Neuropathol. Commun. *3:20*.

Koenigsknecht, J., and Landreth, G. (2004). Microglial phagocytosis of fibrillar β-amyloid through a β1 integrin-dependent mechanism. J. Neurosci. *24*, 9838–9846.

Koizumi, J.Y., Nakazawa, T., and Ooneda, G. (1986). Experimental studies of ischemic brain edema. I. A new experimental model of cerebral embolism in rats in which recirculation can be introduced in the ischemic area. Jpn J Stroke 1–8.

Koizumi, S., Ohsawa, K., Inoue, K., and Kohsaka, S. (2013). Purinergic receptors in microglia: Functional modal shifts of microglia mediated by P2 and P1 receptors. Glia *61*, 47–54.

Komiya, H., Takeuchi, H., Ogawa, Y., Hatooka, Y., Takahashi, K., Katsumoto, A., Kubota, S., Nakamura, H., Kunii, M., Tada, M., et al. (2020). CCR2 is localized in microglia and neurons, as well as infiltrating monocytes, in the lumbar spinal cord of ALS mice. Mol. Brain *13*, 64 (20.
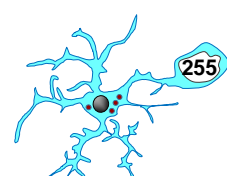
Kondo, S., Kohsaka, S., and Okabe, S. (2011). Long-term changes of spine dynamics and microglia after transient peripheral immune response triggered by LPS in vivo. Mol. Brain *4:27*.

Konishi, H., Kobayashi, M., Kunisawa, T., Imai, K., Sayo, A., Malissen, B., Crocker, P.R., Sato, K., and Kiyama, H. (2017). Siglec-H is a microglia-specific marker that discriminates microglia from CNS-associated macrophages and CNS-infiltrating monocytes. Glia *65*, 1927–1943.

Kotter, M.R., Li, W.W., Zhao, C., and Franklin, R.J.M. (2006). Myelin impairs CNS remyelination by inhibiting oligodendrocyte precursor cell differentiation. J. Neurosci. *26*, 328–332.

Krabbe, G., Halle, A., Matyash, V., Rinnenthal, J.L., Eom, G.D., Bernhardt, U., Miller, K.R., Prokop, S., Kettenmann, H., and Heppner, F.L. (2013). Functional Impairment of Microglia Coincides with Beta-Amyloid Deposition in Mice with Alzheimer-Like Pathology. PLoS One *8(4):e6092*.

Krafft, P.R., Bailey, E.L., Lekic, T., Rolland, W.B., Altay, O., Tang, J., Wardlaw, J.M., Zhang, J.H., and Sudlow, C.L.M. (2012). Etiology of stroke and choice of models. Int. J. Stroke *7*, 398–406.

Kraft, P., Göb, E., Schuhmann, M.K., Göbel, K., Deppermann, C., Thielmann, I., Herrmann, A.M., Lorenz, K., Brede, M., Stoll, G., et al. (2013). FTY720 ameliorates acute ischemic stroke in mice by reducing thrombo-infammation but not by direct neuroprotection. Stroke *44*, 3202–3210.

Kralic, J.E., Ledergerber, D.A., and Fritschy, J.M. (2005). Disruption of the neurogenic potential of the dentate gyrus in a mouse model of temporal lobe epilepsy with focal seizures. Eur. J. Neurosci. *22*, 1916–1927.

Krasemann, S., Madore, C., Cialic, R., Baufeld, C., Calcagno, N., El Fatimy, R., Beckers, L., O'Loughlin, E., Xu, Y., Fanek, Z., et al. (2017). The TREM2-APOE Pathway Drives the Transcriptional Phenotype of Dysfunctional Microglia in Neurodegenerative Diseases. Immunity *47*, 566–581.

Kronenberg, G., Reuter, K., Steiner, B., Brandt, M.D., Jessberger, S., Yamaguchi, M., and Kempermann, G. (2003). Subpopulations of Proliferating Cells of the Adult Hippocampus Respond Differently to Physiologic Neurogenic Stimuli. J. Comp. Neurol. *467*, 455–463.

Kronenberg, G., Bick-Sander, A., Bunk, E., Wolf, C., Ehninger, D., and Kempermann, G.
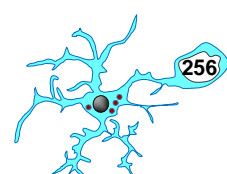
(2006). Physical exercise prevents age-related decline in precursor cell activity in the mouse dentate gyrus. Neurobiol. Aging *27*, 1505–1513.

Krupiński, J., Kałuza, J., Kumar, P., and Kumar, S. (1996). Immunocytochemical studies of cellular reaction in human ischemic brain stroke. MAB anti-CD68 stains macrophages, astrocytes and microglial cells in infarcted area. Folia Neuropathol. *34*, 17–24.

Kuehl, F.A., and Egan, R.W. (1980). Prostagland ins, arachidonic acid, and inflammation. Science (80-.). *210*, 978–984.

Kuhn, H.G., Dickinson-Anson, H., and Gage, F.H. (1996). Neurogenesis in the dentate gyrus of the adult rat: Age-related decrease of neuronal progenitor proliferation. J. Neurosci.

Kumar, A., and Ratan, R.R. (2016). Oxidative Stress and Huntington's Disease: The Good, the Bad, and the Ugly. J. Huntingtons. Dis. *5*, 217–237.

Kurita, H., Kawahara, N., Asai, A., Ueki, K., Shin, M., and Kirino, T. (2001). Radiation-induced apoptosis of oligodendrocytes in the adult rat brain. Neurol. Res. *23*, 869–874.

Kuroiwa, T., Xi, G., Hua, Y., Nagaraja, T.N., Fenstermacher, J.D., and Keep, R.F. (2009). Development of a rat model of photothrombotic ischemia and infarction within the caudoputamen. Stroke *40*, 248–253.

Kzhyshkowska, J., Gratchev, A., and Goerdt, S. (2006). Stabilin-1, a homeostatic scavenger receptor with multiple functions. J. Cell. Mol. Med. *10*, 635–649.

de la Monte, S.M. (1988). Disproportionate atrophy of cerebral white matter in chronic alcoholics. Arch. Neurol. *45*, 990-2.

~L~

Labadorf, A., Hoss, A.G., Lagomarsino, V., Latourelle, J.C., Hadzi, T.C., Bregu, J., MacDonald, M.E., Gusella, J.F., Chen, J.F., Akbarian, S., et al. (2015). RNA sequence analysis of human huntington disease brain reveals an extensive increase in inflammatory and developmental gene expression. PLoS One *10(12)*, e0143563.

Lacroix, S., and Rivest, S. (1998). Effect of acute systemic inflammatory response and cytokines on the transcription of the genes encoding cyclooxygenase enzymes (COX-1 and COX-2) in the rat brain. J. Neurochem. *70*, 452–466.

Lai, A.Y., and Todd, K.G. (2006). Microglia in cerebral ischemia: Molecular actions and interactions. Can. J. Physiol. Pharmacol. *84*, 49–59.
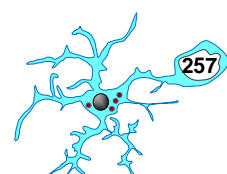
Lai, T.W., Zhang, S., and Wang, Y.T. (2014). Excitotoxicity and stroke: Identifying novel targets for neuroprotection. Prog. Neurobiol. *115*, 157–188.

Lalancette-Hébert, M., Gowing, G., Simard, A., Yuan, C.W., and Kriz, J. (2007). Selective ablation of proliferating microglial cells exacerbates ischemic injury in the brain. J. Neurosci. *27*, 2596–2605.

Lalioti, M.D., Scott, H.S., Buresi, C., Rossier, C., Bottani, A., Morris, M.A., Malafosse, A., and Antonarakis, S.E. (1997). Dodecamer repeat expansion in cystatin B gene in progressive myoclonus epilepsy. Nature *386*, 847–851.

Lambertsen, K.L., Clausen, B.H., Babcock, A.A., Gregersen, R., Fenger, C., Nielsen, H.H., Haugaard, L.S., Wirenfeldt, M., Nielsen, M., Dagnaes-Hansen, F., et al. (2009). Microglia protect neurons against ischemia by synthesis of tumor necrosis factor. J. Neurosci. *29*, 1319–1330.

Lampron, A., Larochelle, A., Laflamme, N., Préfontaine, P., Plante, M.M., Sánchez, M.G., Wee Yong, V., Stys, P.K., Tremblay, M.È., and Rivest, S. (2015). Inefficient clearance of myelin debris by microglia impairs remyelinating processes. J. Exp. Med. *212*, 481–495.

Lan, X., Han, X., Li, Q., Yang, Q.W., and Wang, J. (2017). Modulators of microglial activation and polarization after intracerebral haemorrhage. Nat. Rev. Neurol. *13*, 420–433.

De Lanerolle, N.C., Kim, J.H., Williamson, A., Spencer, S.S., Zaveri, H.P., Eid, T., and Spencer, D.D. (2003). A retrospective analysis of hippocampal pathology in human temporal lobe epilepsy: Evidence for distinctive patient subcategories. Epilepsia *44*, 677–687.

Lau, L.T., and Yu, A.C.H. (2001). Astrocytes produce and release interleukin-1, interleukin-6, tumor necrosis factor alpha and interferon-gamma following traumatic and metabolic injury. J. Neurotrauma *18*, 351–359.

Lauber, K., Bohn, E., Kröber, S.M., Xiao, Y.J., Blumenthal, S.G., Lindemann, R.K., Marini, P., Wiedig, C., Zobywalski, A., Baksh, S., et al. (2003). Apoptotic cells induce migration of phagocytes via caspase-3-mediated release of a lipid attraction signal. Cell *113*, 717–730.

Lauber, K., Blumenthal, S.G., Waibel, M., and Wesselborg, S. (2004). Clearance of apoptotic cells: Getting rid of the corpses. Mol. Cell *14*, 277–287.

Lawson, L.J., Perry, V.H., Dri, P., and Gordon, S. (1990). Heterogeneity in the distribution and morphology of microglia in the normal adult mouse brain. Neuroscience *39*, 151–
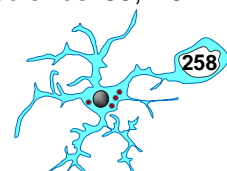
170.

Lazarowski, E.R., Sesma, J.I., Seminario-Vidal, L., and Kreda, S.M. (2011). Molecular Mechanisms of Purine and Pyrimidine Nucleotide Release. Adv. Pharmacol. *61*, 221–261.

Lebedeva, J., Zakharov, A., Ogievetsky, E., Minlebaeva, A., Kurbanov, R., Gerasimova, E., Sitdikova, G., and Khazipov, R. (2017). Inhibition of Cortical Activity and Apoptosis Caused by Ethanol in Neonatal Rats In Vivo. Cereb. Cortex *27*, 1068–1082.

Lee, S.K. (2014). Treatment Strategy for the Patient with Hippocampal Sclerosis Who Failed to the First Antiepileptic Drug. J. Epilepsy Res. *4*, 1–6.

Lee, J.M., Zipfel, G.J., and Choi, D.W. (1999). The changing landscape of ischaemic brain injury mechanisms. Nature *399*, A7-14.

Lee, W.H., Sonntag, W.E., Mitschelen, M., Yan, H., and Lee, Y.W. (2010). Irradiation induces regionally specific alterations in pro-inflammatory environments in rat brain. Int. J. Radiat. Biol. *86*, 132–144.

Legler, D.F., Bruckner, M., Uetz-von Allmen, E., and Krause, P. (2010). Prostaglandin E2 at new glance: Novel insights in functional diversity offer therapeutic chances. Int. J. Biochem. Cell Biol. *42*, 198–201.

Lehnard, S., Lachance, C., Patrizi, S., Lefebvre, S., Follett, P.L., Jensen, F.E., Rosenberg, P.A., Volpe, J.J., and Vartanian, T. (2002). The Toll-Like Receptor TLR4 Is Necessary for Lipopolysaccharide-Induced Oligodendrocyte Injury in the CNS. J. Neurosci. *22*, 2478–2486.

Lehnardt, S. (2010). Innate immunity and neuroinflammation in the CNS: The role of microglia in toll-like receptor-mediated neuronal injury. Glia *58*, 253–263.

Lehrner, J., Kalchmayr, R., Serles, W., Olbrich, A., Pataraia, E., Aull, S., Bacher, J., Leutmezer, F., Gröppel, G., Deecke, L., et al. (1999). Health-related quality of life (HRQOL), activity of daily living (ADL) and depressive mood disorder in temporal lobe epilepsy patients. Seizure *8*, 88–92.

Lemke, G. (2013). Biology of the TAM receptors. Cold Spring Harb. Perspect. Biol. *5*.

Leuner, B., Kozorovitskiy, Y., Gross, C.G., and Gould, E. (2007). Diminished adult neurogenesis in the marmoset brain precedes old age. Proc. Natl. Acad. Sci. U. S. A. *104*, 17169–17173.

Lévesque, M., and Avoli, M. (2013). The kainic acid model of temporal lobe epilepsy.
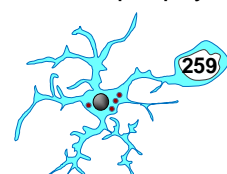
Neurosci. Biobehav. Rev. *37*, 2887–2899.

Lévesque, M., Avoli, M., and Bernard, C. (2016). Animal models of temporal lobe epilepsy following systemic chemoconvulsant administration. J. Neurosci. Methods *260*, 260:45-52.

Levine, S. (1960). Anoxic-ischemic encephalopathy in rats. Am. J. Pathol. *36*, 1–17.

Li, B., Sierra, A., Deudero, J.J., Semerci, F., Laitman, A., Kimmel, M., and Maletic-Savatic, M. (2017). Multitype Bellman-Harris branching model provides biological predictors of early stages of adult hippocampal neurogenesis. BMC Syst. Biol. *11*.

Li, K., Futrell, N., Tovar, J.S., Wang, L.J.C., Wang, D.Z., and Schultz, L.R. (1996). Gender influences the magnitude of the inflammatory response within embolic cerebral infarcts in young rats. Stroke *27*, 498–503.

Li, M.D., Burns, T.C., Kumar, S., Morgan, A.A., Sloan, S.A., and Palmer, T.D. (2015). Aging-like changes in the transcriptome of irradiated microglia. Glia *63*, 754–767.

Li, Q., Liu, D., Pan, F., Ho, C.S.H., and Ho, R.C.M. (2019). Ethanol Exposure Induces Microglia Activation and Neuroinflammation through TLR4 Activation and SENP6 Modulation in the Adolescent Rat Hippocampus. Neural Plast. *1648736*.

Li, T., Pang, S., Yu, Y., Wu, X., Guo, J., and Zhang, S. (2013). Proliferation of parenchymal microglia is the main source of microgliosis after ischaemic stroke. Brain *136*, 3578–3588.

Liddelow, S.A., Guttenplan, K.A., Clarke, L.E., Bennett, F.C., Bohlen, C.J., Schirmer, L., Bennett, M.L., Münch, A.E., Chung, W.S., Peterson, T.C., et al. (2017). Neurotoxic reactive astrocytes are induced by activated microglia. Nature *541*, 481–487.

Lietsche, J., Imran, I., and Klein, J. (2016). Extracellular levels of ATP and acetylcholine during lithium-pilocarpine induced status epilepticus in rats. Neurosci. Lett. *611*, 69–73.

Lin, X., Miao, P., Wang, J., Yuan, F., Guan, Y., Tang, Y., He, X., Wang, Y., and Yang, G.Y. (2013). Surgery-Related Thrombosis Critically Affects the Brain Infarct Volume in Mice Following Transient Middle Cerebral Artery Occlusion. PLoS One *8(9):e7556*.

Linden, J., Fassotte, L., Tirelli, E., Plumier, J.C., and Ferrara, A. (2014). Assessment of behavioral flexibility after middle cerebral artery occlusion in mice. Behav. Brain Res. *258*, 127–137.

Ling, E.A. (1976). Some aspects of amoeboid microglia in the corpus callosum and neighbouring regions of neonatal rats. J. Anat. *121*, 29–45.
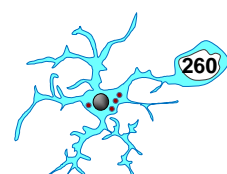
Ling, M., and Murali, M. (2019). Analysis of the Complement System in the Clinical Immunology Laboratory. Clin. Lab. Med. *39*, 579–590.

Linker, R., Gold, R., and Luhder, F. (2009). Function of neurotrophic factors beyond the nervous system: Inflammation and autoimmune demyelination. Crit. Rev. Immunol. *29*, 43–46.

Linnartz, B., Kopatz, J., Tenner, A.J., and Neumann, H. (2012). Sialic acid on the neuronal glycocalyx prevents complement c1 binding and complement receptor-3-mediated removal by microglia. J. Neurosci. *32*, 946–952.

Liu, J., and Feng, Z.C. (2009). Increased umbilical cord plasma interleukin-1β levels was correlated with adverse outcomes of neonatal hypoxic-ischemic encephalopathy. J. Trop. Pediatr. *56*, 178–182.

Liu, B., Wang, K., Gao, H.M., Mandavilli, B., Wang, J.Y., and Hong, J.S. (2001). Molecular consequences of activated microglia in the brain: Overactivation induces apoptosis. J. Neurochem. *77*, 182–189.

Liu, F., Schafer, D.P., and McCullough, L.D. (2009a). TTC, Fluoro-Jade B and NeuN staining confirm evolving phases of infarction induced by middle cerebral artery occlusion. J. Neurosci. Methods *179*, 1–8.

Liu, N.W., Ke, C.C., Zhao, Y., Chen, Y.A., Chan, K.C., Tan, D.T.W., Lee, J.S., Chen, Y.Y., Hsu, T.W., Hsieh, Y.J., et al. (2017). Evolutional Characterization of Photochemically Induced Stroke in Rats: a Multimodality Imaging and Molecular Biological Study. Transl. Stroke Res. *8*, 244–256.

Liu, S., Zhen, G., Meloni, B.P., Campbell, K., and Winn, H.R. (2009b). RODENT STROKE MODEL GUIDELINES FOR PRECLINICAL STROKE TRIALS (1ST EDITION). J. Exp. Stroke Transl. Med. *2*, 2–27.

Liu, T., McDonnell, P.C., Young, P.R., White, R.F., Siren, A.L., Hallenbeck, J.M., Barone, F.C., and Feuerstein, G.Z. (1993). Interleukin-1β mRNA expression in ischemic rat cortex. Stroke *24*, 1746–1750.

Liu, T., Clark, R.K., McDonnell, P.C., Young, P.R., White, R.F., Barone, F.C., and Feuerstein, G.Z. (1994). Tumor necrosis factor-α expression in ischemic neurons. Stroke *25*, 1481–1488.

Loddick, S.A., Turnbull, A. V., and Rothwell, N.J. (1998). Cerebral interleukin-6 is neuroprotective during permanent focal cerebral ischemia in the rat. J. Cereb. Blood Flow Metab. *18*, 176–179.
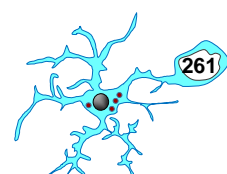
Loftis, J.M., Huckans, M., and Morasco, B.J. (2010). Neuroimmune mechanisms of cytokine-induced depression: Current theories and novel treatment strategies. Neurobiol. Dis. *37*, 519–533.

Longa, E.Z., Weinstein, P.R., Carlson, S., and Cummins, R. (1989). Reversible middle cerebral artery occlusion without craniectomy in rats. Stroke *20*, 84–91.

Lopez-Atalaya, J.P., Askew, K.E., Sierra, A., and Gomez-Nicola, D. (2018). Development and maintenance of the brain's immune toolkit: Microglia and non-parenchymal brain macrophages. Dev. Neurobiol. *78*, 561–579.

Lu, Z., Elliott, M.R., Chen, Y., Walsh, J.T., Klibanov, A.L., Ravichandran, K.S., and Kipnis, J. (2011). Phagocytic activity of neuronal progenitors regulates adult neurogenesis. Nat. Cell Biol. *13*, 1076–1083.

Lucas, S.M., Rothwell, N.J., and Gibson, R.M. (2006). The role of inflammation in CNS injury and disease. Br. J. Pharmacol. *147*, S232-40.

Lugert, S., Basak, O., Knuckles, P., Haussler, U., Fabel, K., Götz, M., Haas, C.A., Kempermann, G., Taylor, V., and Giachino, C. (2010). Quiescent and active hippocampal neural stem cells with distinct morphologies respond selectively to physiological and pathological stimuli and aging. Cell Stem Cell *6*, 445–456.

Lund, S., Christensen, K.V., Hedtjärn, M., Mortensen, A.L., Hagberg, H., Falsig, J., Hasseldam, H., Schrattenholz, A., Pörzgen, P., and Leist, M. (2006). The dynamics of the LPS triggered inflammatory response of murine microglia under different culture and in vivo conditions. J. Neuroimmunol. *180*, 71–87.

Luo, J., Daniels, S.B., Lennington, J.B., Notti, R.Q., and Conover, J.C. (2006). The aging neurogenic subventricular zone. Aging Cell *5*, 139–152.

~M~

M. Morais-Lima, T., C. Vicentini, J., V.P. Alberto, A., H.M. de Freitas, P., M. Perret, C., C. da Silva Ferreira, N., Sarmah, D., Sinha, B., Das, G., Bhattacharya, P., et al. (2020). The Role of Purinergic Signaling in the Pathophysiology of Perinatal Hypoxic-Ischemic Encephalopathy. In Receptors P1 and P2 as Targets for Drug Therapy in Humans, p.

Madden, S.D., and Cotter, T.G. (2008). Cell death in brain development and degeneration: Control of caspase expression may be key! Mol. Neurobiol. *37*, 1–6.

Madsen, T.M., Kristjansen, P.E.G., Bolwig, T.G., and Wörtwein, G. (2003). Arrested
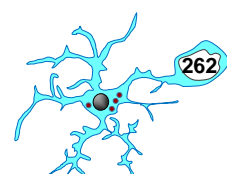
neuronal proliferation and impaired hippocampal function following fractionated brain irradiation in the adult rat. Neuroscience *119*, 635–642.

Maeda, K., Hata, R., and Hossmann, K.A. (1999). Regional metabolic disturbances and cerebrovascular anatomy after permanent middle cerebral artery occlusion in C57Black/6 and SV129 mice. Neurobiol. Dis. *6*, 101–108.

Maggi, L., Scianni, M., Branchi, I., D'Andrea, I., Lauro, C., and Limatola, C. (2011). CX 3CR1 deficiency alters hippocampal-dependent plasticity phenomena blunting the effects of enriched environment. Front. Cell. Neurosci. *5*.

Magnus, T., Chan, A., Grauer, O., Toyka, K. V., and Gold, R. (2001). Microglial Phagocytosis of Apoptotic Inflammatory T Cells Leads to Down-Regulation of Microglial Immune Activation. J. Immunol. *167*, 5004–5010.

Magnus, T., Chan, A., Linker, R.A., Toyka, K. V., and Gold, R. (2002). Astrocytes are less efficient in the removal of apoptotic lymphocytes than microglia cells: Implications for the role of glial cells in the inflamed central nervous system. J. Neuropathol. Exp. Neurol. *61*, 760–766.

Mah, L.J., El-Osta, A., and Karagiannis, T.C. (2010). γh2AX: A sensitive molecular marker of DNA damage and repair. Leukemia *24*, 679–686.

Majumdar, A., Chung, H., Dolios, G., Wang, R., Asamoah, N., Lobel, P., and Maxfield, F.R. (2008). Degradation of fibrillar forms of Alzheimer's amyloid β-peptide by macrophages. Neurobiol. Aging *29*, 707–715.

Makale, M.T., McDonald, C.R., Hattangadi-Gluth, J.A., and Kesari, S. (2016). Mechanisms of radiotherapy-associated cognitive disability in patients with brain tumours. Nat. Rev. Neurol. *13*, 52–64.

Mandrekar, S., Jiang, Q., Lee, C.Y.D., Koenigsknecht-Talboo, J., Holtzman, D.M., and Landreth, G.E. (2009). Microglia mediate the clearance of soluble aβ through fluid phase macropinocytosis. J. Neurosci. *29*, 4252–4262.

Mandyam, C.D., Harburg, G.C., and Eisch, A.J. (2007). Determination of key aspects of precursor cell proliferation, cell cycle length and kinetics in the adult mouse subgranular zone. Neuroscience *146*, 108–122.

Maneu, V., Yáñez, A., Murciano, C., Molina, A., Gil, M.L., and Gozalbo, D. (2011). Dectin-1 mediates in vitro phagocytosis of Candida albicans yeast cells by retinal microglia. FEMS Immunol. Med. Microbiol. *63*, 148–150.
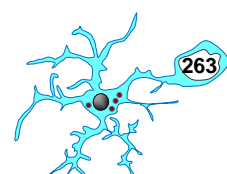
Manganas, L.N., Zhang, X., Li, Y., Hazel, R.D., Smith, S.D., Wagshul, M.E., Henn, F., Benveniste, H., Djurić, P.M., Enikolopov, G., et al. (2007). Magnetic resonance spectroscopy identifies neural progenitor cells in the live human brain. Science (80-.). *318*, 980–985.

Manoharan, S., Guillemin, G.J., Abiramasundari, R.S., Essa, M.M., Akbar, M., and Akbar, M.D. (2016). The Role of Reactive Oxygen Species in the Pathogenesis of Alzheimer's Disease, Parkinson's Disease, and Huntington's Disease: A Mini Review. Oxid. Med. Cell. Longev. *2016:85905*.

Marazziti, D., Baroni, S., Catena-Dell'Osso, M., Schiavi, E., Ceresoli, D., Conversano, C., Dell'Osso, L., and Picano, E. (2012). Cognitive, Psychological and Psychiatric Effects of Ionizing Radiation Exposure. Curr. Med. Chem. *19*, 1864–1869.

Marchi, N., Granata, T., Freri, E., Ciusani, E., Ragona, F., Puvenna, V., Teng, Q., Alexopolous, A., and Janigro, D. (2011). Efficacy of anti-inflammatory therapy in a model of acute seizures and in a population of pediatric drug resistant epileptics. PLoS One *6(3):e1820*.

Marsaglia, G., and Bray, T.A. (1964). A Convenient Method for Generating Normal Variables. SIAM Rev. *6*, 260–264.

Marshall, S.A., McClain, J.A., Kelso, M.L., Hopkins, D.M., Pauly, J.R., and Nixon, K. (2013). Microglial activation is not equivalent to neuroinflammation in alcohol-induced neurodegeneration: The importance of microglia phenotype. Neurobiol. Dis. *54*, 239–251.

Marshall, S.A., McClain, J.A., Wooden, J.I., and Nixon, K. (2020). Microglia Dystrophy Following Binge-Like Alcohol Exposure in Adolescent and Adult Male Rats. Front. Neuroanat. *14: 52*.

Martín-Suárez, S., Valero, J., Muro-García, T., and Encinas, J.M. (2019). Phenotypical and functional heterogeneity of neural stem cells in the aged hippocampus. Aging Cell *18*, e12958.

Martinc, B., Grabnar, I., and Vovk, T. (2012). The Role of Reactive Species in Epileptogenesis and Influence of Antiepileptic Drug Therapy on Oxidative Stress. Curr. Neuropharmacol. *10*, 328–343.

Masino, S.A., Kawamura, M., and Ruskin, D.N. (2014). Adenosine receptors and epilepsy. Current evidence and future potential. Int. Rev. Neurobiol. *119*, 233–255.

Masuda, T., Sankowski, R., Staszewski, O., Böttcher, C., Amann, L., Sagar, Scheiwe,
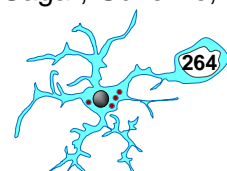
C., Nessler, S., Kunz, P., van Loo, G., et al. (2019). Spatial and temporal heterogeneity of mouse and human microglia at single-cell resolution. Nature *566*, 388–392.

Masuda, T., Amann, L., Sankowski, R., Staszewski, O., Lenz, M., D´Errico, P., Snaidero, N., Costa Jordão, M.J., Böttcher, C., Kierdorf, K., et al. (2020). Novel Hexb-based tools for studying microglia in the CNS. Nat. Immunol. *21*, 802–815.

Matcovitch-Natan, O., Winter, D.R., Giladi, A., Aguilar, S.V., Spinrad, A., Sarrazin, S., Ben-Yehuda, H., David, E., González, F.Z., Perrin, P., et al. (2016). Microglia development follows a stepwise program to regulate brain homeostasis. Science (80-.). *353(6301)*.

Mathon, B., Bédos Ulvin, L., Adam, C., Baulac, M., Dupont, S., Navarro, V., Cornu, P., and Clemenceau, S. (2015). Surgical treatment for mesial temporal lobe epilepsy associated with hippocampal sclerosis. Rev. Neurol. (Paris). *171*, 315–325.

Mathys, H., Adaikkan, C., Gao, F., Young, J.Z., Manet, E., Hemberg, M., De Jager, P.L., Ransohoff, R.M., Regev, A., and Tsai, L.H. (2017). Temporal Tracking of Microglia Activation in Neurodegeneration at Single-Cell Resolution. Cell Rep. *21*, 366–380.

Mawuenyega, K.G., Sigurdson, W., Ovod, V., Munsell, L., Kasten, T., Morris, J.C., Yarasheski, K.E., and Bateman, R.J. (2010). Decreased clearance of CNS β-amyloid in Alzheimer's disease. Science (80-.). *330(6012):*

McAuley, M.A. (1995). Rodent models of focal ischemia. Cerebrovasc. Brain Metab. Rev. *7*, 153–180.

McClain, J.A., Morris, S.A., Deeny, M.A., Marshall, S.A., Hayes, D.M., Kiser, Z.M., and Nixon, K. (2011). Adolescent binge alcohol exposure induces long-lasting partial activation of microglia. Brain. Behav. Immun. *25*, S120-8.

McColl, B.W., Carswell, H. V., McCulloch, J., and Horsburgh, K. (2004). Extension of cerebral hypoperfusion and ischaemic pathology beyond MCA territory after intraluminal filament occlusion in C57Bl/6J mice. Brain Res. *997*, 15–23.

McGonigal, R., Cunningham, M.E., Yao, D., Barrie, J.A., Sankaranarayanan, S., Fewou, S.N., Furukawa, K., Yednock, T.A., and Willison, H.J. (2016). C1q-targeted inhibition of the classical complement pathway prevents injury in a novel mouse model of acute motor axonal neuropathy. Acta Neuropathol. Commun. *4:23*.

McKinsey, G.L., Lizama, C.O., Keown-Lang, A.E., Niu, A., Santander, N., Larpthaveesarp, A., Chee, E., Gonzalez, F.F., and Arnold, T.D. (2020). A new genetic strategy for targeting microglia in development and disease. Elife *9:e54590*.
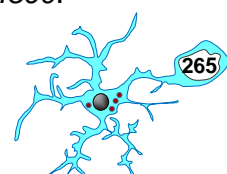
McRae, A., Gilland, E., Bona, E., and Hagberg, H. (1995). Microglia activation after neonatal hypoxic-ischemia. Dev. Brain Res. *84*, 245–252.

Melani, A., Turchi, D., Vannucchi, M.G., Cipriani, S., Gianfriddo, M., and Pedata, F. (2005). ATP extracellular concentrations are increased in the rat striatum during in vivo ischemia. Neurochem. Int. *47*, 442–448.

Melani, A., Amadio, S., Gianfriddo, M., Vannucchi, M.G., Volontè, C., Bernardi, G., Pedata, F., and Sancesario, G. (2006). P2X7 receptor modulation on microglial cells and reduction of brain infarct caused by middle cerebral artery occlusion in rat. J. Cereb. Blood Flow Metab. *26*, 974–982.

Melani, A., Corti, F., Stephan, H., Müller, C.E., Donati, C., Bruni, P., Vannucchi, M.G., and Pedata, F. (2012). Ecto-ATPase inhibition: ATP and adenosine release under physiological and ischemic in vivo conditions in the rat striatum. Exp. Neurol. *233*, 193–204.

Memezawa, H., Smith, M.L., and Siesjo, B.K. (1992). Penumbral tissues salvaged by reperfusion following middle cerebral artery occlusion in rats. Stroke *23*, 552–559.

Mennicken, F., Maki, R., De Souza, E.B., and Quirion, R. (1999). Chemokines and chemokine receptors in the CNS: A possible role in neuroinflammation and patterning. Trends Pharmacol. Sci. *20*, 73–78.

Menzel, F., Kaiser, N., Haehnel, S., Rapp, F., Patties, I., Schöneberg, N., Haimon, Z., Immig, K., and Bechmann, I. (2018). Impact of X-irradiation on microglia. Glia *66*, 15–33.

Meyer-Luehmann, M., Spires-Jones, T.L., Prada, C., Garcia-Alloza, M., De Calignon, A., Rozkalne, A., Koenigsknecht-Talboo, J., Holtzman, D.M., Bacskai, B.J., and Hyman, B.T. (2008). Rapid appearance and local toxicity of amyloid-β plaques in a mouse model of Alzheimer's disease. Nature *451*, 720–724.

Michael, J., Unger, M.S., Poupardin, R., Schernthaner, P., Mrowetz, H., Attems, J., and Aigner, L. (2020). Microglia depletion diminishes key elements of the leukotriene pathway in the brain of Alzheimer's Disease mice. Acta Neuropathol. Commun. *8(1):129*.

Michaelidesová, A., Konířová, J., Bartůněk, P., and Zíková, M. (2019). Effects of radiation therapy on neural stem cells. Genes (Basel). *10(9):640*.

Michelozzi, C., and Cognard, C. (2019). The role of interventional neuroradiology in treatment of hemorrhagic stroke. Press. Medicale *48*, 684–695.
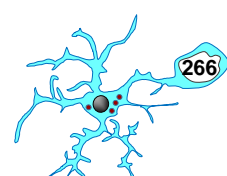
Michenfelder, J.D., Milde, J.H., and Sundt, T.M. (1976). Cerebral Protection by Barbiturate Anesthesia: Use After Middle Cerebral Artery Occlusion in Java Monkeys. Arch. Neurol. *33*, 345–350.

Middeldorp, J., and Hol, E.M. (2011). GFAP in health and disease. Prog. Neurobiol. *93*, 421–443.

Miguel, P.M., Schuch, C.P., Rojas, J.J., Carletti, J.V., Deckmann, I., Martinato, L.H.M., Pires, A.V., Bizarro, L., and Pereira, L.O. (2015). Neonatal Hypoxia-Ischemia Induces Attention-Deficit Hyperactivity Disorder-Like Behavior in Rats. Behav. Neurosci. *129*, 309–320.

Mildner, A., Huang, H., Radke, J., Stenzel, W., and Priller, J. (2017). P2Y12 receptor is expressed on human microglia under physiological conditions throughout development and is sensitive to neuroinflammatory diseases. Glia *65*, 375–387.

Milkovic, L., Cipak Gasparovic, A., Cindric, M., Mouthuy, P.A., and Zarkovic, N. (2019). Short Overview of ROS as Cell Function Regulators and Their Implications in Therapy Concepts. Cells *8(8):793*.

Millar, L.J., Shi, L., Hoerder-Suabedissen, A., and Molnár, Z. (2017). Neonatal hypoxia ischaemia: Mechanisms, models, and therapeutic challenges. Front. Cell. Neurosci. *11:78*.

Min, Y., Yan, L., Wang, Q., Wang, F., Hua, H., Yuan, Y., Jin, H., Zhang, M., Zhao, Y., Yang, J., et al. (2020). Distinct Residential and Infiltrated Macrophage Populations and Their Phagocytic Function in Mild and Severe Neonatal Hypoxic-Ischemic Brain Damage. Front. Cell. Neurosci. *14:244*.

Mirshafiey, A., and Jadidi-Niaragh, F. (2010). Immunopharmacological role of the Leukotriene Receptor Antagonists and inhibitors of leukotrienes generating enzymes in Multiple Sclerosis. Immunopharmacol. Immunotoxicol. *32*, 219–227.

Miyamoto, A., Wake, H., Ishikawa, A.W., Eto, K., Shibata, K., Murakoshi, H., Koizumi, S., Moorhouse, A.J., Yoshimura, Y., and Nabekura, J. (2016). Microglia contact induces synapse formation in developing somatosensory cortex. Nat. Commun. *7*.

Mizobuchi, H., Yamamoto, K., Tsutsui, S., Yamashita, M., Nakata, Y., Inagawa, H., Kohchi, C., and Soma, G.I. (2020). A unique hybrid characteristic having both pro- and anti-inflammatory phenotype transformed by repetitive low-dose lipopolysaccharide in C8-B4 microglia. Sci. Rep. *10*.

Mizumatsu, S., Monje, M.L., Morhardt, D.R., Rola, R., Palmer, T.D., and Fike, J.R.
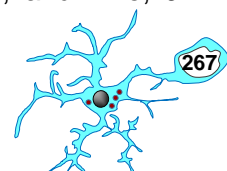
(2003). Extreme sensitivity of adult neurogenesis to low doses of X-irradiation. Cancer Res. *63*, 4021–4027.

Mizutani, M., Pino, P.A., Saederup, N., Charo, I.F., Ransohoff, R.M., and Cardona, A.E. (2012). The Fractalkine Receptor but Not CCR2 Is Present on Microglia from Embryonic Development throughout Adulthood. J. Immunol. *188*, 29–36.

Młodzikowska-Albrecht, J., Steinborn, B., and Zarowski, M. (2007). Cytokines, epilepsy, and antiepileptic drugs - Is there a mutual influence? Pharmacol. Reports *59*, 129–138.

Mohamed, R.M.P., Mokhtar, M.H., Yap, E., Hanim, A., Wahab, N.A., Jaffar, F.H.F., and Kumar, J. (2018). Ethanol-induced changes in PKCe: From cell to behavior. Front. Neurosci. *12: 244*.

Monje, M.L., Mizumatsu, S., Fike, J.R., and Palmer, T.D. (2002). Irradiation induces neural precursor-cell dysfunction. Nat. Med. *8*, 955–962.

Montero, T.D., and Orellana, J.A. (2015). Hemichannels: New pathways for gliotransmitter release. Neuroscience *286*, 45–59.

Montoya, C.P., Campbell-Hope, L.J., Pemberton, K.D., and Dunnett, S.B. (1991). The "staircase test": a measure of independent forelimb reaching and grasping abilities in rats. J. Neurosci. Methods *36*, 219–228.

Moraga, A., Pradillo, J.M., García-Culebras, A., Palma-Tortosa, S., Ballesteros, I., Hernández-Jiménez, M., Moro, M.A., and Lizasoain, I. (2015). Aging increases microglial proliferation, delays cell migration, and decreases cortical neurogenesis after focal cerebral ischemia. J. Neuroinflammation *12:87*.

Morgan, T.E., Nichols, N.R., Pasinetti, G.M., and Finch, C.E. (1993). TGF-β1 mRNA increases in macrophage/microglial cells of the hippocampus in response to deafferentation and kainic acid-induced neurodegeneration. Exp. Neurol. *120*, 291–301.

Morganti, J.M., Jopson, T.D., Liu, S., Gupta, N., and Rosi, S. (2014). Cranial irradiation alters the brain's microenvironment and permits CCR2+ macrophage infiltration. PLoS One *9(4):e9365*.

Morganti, J.M., Riparip, L.K., and Rosi, S. (2016). Call off the dog(ma): M1/M2 polarization is concurrent following traumatic brain injury. PLoS One *11(1):e014*.

Morgenstern, N.A., Lombardi, G., and Schinder, A.F. (2008). Newborn granule cells in the ageing dentate gyrus. J. Physiol. *586*, 3751–3757.

Morin-Brureau, M., Milior, G., Royer, J., Chali, F., LeDuigou, C., Savary, E., Blugeon, C.,
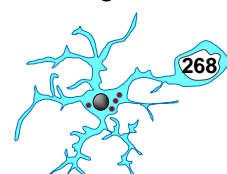
Jourdren, L., Akbar, D., Dupont, S., et al. (2018). Microglial phenotypes in the human epileptic temporal lobe. Brain *141*, 3343–3360.

Morizawa, Y.M., Hirayama, Y., Ohno, N., Shibata, S., Shigetomi, E., Sui, Y., Nabekura, J., Sato, K., Okajima, F., Takebayashi, H., et al. (2017). Reactive astrocytes function as phagocytes after brain ischemia via ABCA1-mediated pathway. Nat. Commun. *8(1):1598*.

Morotti, A., and Goldstein, J.N. (2016). Diagnosis and Management of Acute Intracerebral Hemorrhage. Emerg. Med. Clin. North Am. *34*, 883–899.

Morris, G.P., Wright, A.L., Tan, R.P., Gladbach, A., Ittner, L.M., and Vissel, B. (2016a). A comparative study of variables influencing ischemic injury in the longa and koizumi methods of intraluminal filament middle cerebral artery occlusion in mice. PLoS One *11*, 1–34.

Morris, G.P., Wright, A.L., Tan, R.P., Gladbach, A., Ittner, L.M., and Vissel, B. (2016b). A comparative study of variables influencing ischemic injury in the longa and koizumi methods of intraluminal filament middle cerebral artery occlusion in mice. PLoS One *11*, 1–34.

Morris, S.A., Eaves, D.W., Smith, A.R., and Nixon, K. (2010). Alcohol inhibition of neurogenesis: A mechanism of hippocampal neurodegeneration in an adolescent alcohol abuse model. Hippocampus *34*, 883–899.

Morrison, H.W., and Filosa, J.A. (2013). A quantitative spatiotemporal analysis of microglia morphology during ischemic stroke and reperfusion. J. Neuroinflammation *10:4*.

Moskowitz, M.A., Lo, E.H., and Iadecola, C. (2010). The science of stroke: Mechanisms in search of treatments. Neuron *67*, 181–198.

Möykkynen, T., and Korpi, E.R. (2012). Acute Effects of Ethanol on Glutamate Receptors. Basic Clin. Pharmacol. Toxicol. *111*, 4–13.

Mozaffarian, D., Benjamin, E.J., Go, A.S., Arnett, D.K., Blaha, M.J., Cushman, M., Das, S.R., Ferranti, S. De, Després, J.P., Fullerton, H.J., et al. (2016). Heart disease and stroke statistics-2016 update a report from the American Heart Association. Circulation *133(4):e38*.

Mukherjee, S., Ghosh, R.N., and Maxfield, F.R. (1997). ENDOCYTOSIS [Review]. Physiol. Rev. *77*, 759–803.
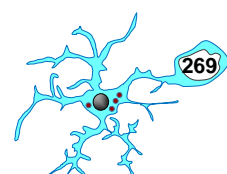
Murabe, Y., and Sano, Y. (1982). Morphological studies on neuroglia - VI. Postnatal development of microglial cells. Cell Tissue Res. *225*, 469–485.

Murabe, Y., and Sano, Y. (1983). Morphological studies on neuroglia - VII. Distribution of "brain macrophages" in brains of neonatal and adult rats, as determined by means of immunohistochemistry. Cell Tissue Res. *229*, 85–95.

Muro-García, T., Martín-Suárez, S., Espinosa, N., Valcárcel-Martín, R., Marinas, A., Zaldumbide, L., Galbarriatu, L., Sierra, A., Fuentealba, P., and Encinas, J.M. (2019). Reactive Disruption of the Hippocampal Neurogenic Niche After Induction of Seizures by Injection of Kainic Acid in the Amygdala. Front. Cell Dev. Biol. *7:158*.

~N~

Nagata, K., Ohashi, K., Nakano, T., Arita, H., Zong, C., Hanafusa, H., and Mizuno, K. (1996). Identification of the product of growth arrest-specific gene 6 as a common ligand for Axl, Sky, and Mer receptor tyrosine kinases. J. Biol. Chem. *271*, 30022–30027.

Nagata, S., Hanayama, R., and Kawane, K. (2010). Autoimmunity and the Clearance of Dead Cells. Cell *140*, 619–630.

Nair, S., Sobotka, K.S., Joshi, P., Gressens, P., Fleiss, B., Thornton, C., Mallard, C., and Hagberg, H. (2019). Lipopolysaccharide-induced alteration of mitochondrial morphology induces a metabolic shift in microglia modulating the inflammatory response in vitro and in vivo. Glia *67*, 1047–1061.

Nakamura, Y., Si, Q.S., and Kataoka, K. (1999). Lipopolysaccharide-induced microglial activation in culture: Temporal profiles of morphological change and release of cytokines and nitric oxide. Neurosci. Res. *35*, 95–100.

Nakashima, M.N., Yamashita, K., Kataoka, Y., Yamashita, Y.S., and Niwa, M. (1995). Time course of nitric oxide synthase activity in neuronal, glial, and endothelial cells of rat striatum following focal cerebral ischemia. Cell. Mol. Neurobiol. *15*, 341–349.

Nalivaeva, N.N., and Rybnikova, E.A. (2019). Editorial: Brain hypoxia and ischemia: New insights into neurodegeneration and neuroprotection. Front. Neurosci. *13*, 770.

Naumann, N., Siratska, O., Gahr, M., and Rösen-Wolff, A. (2005). P-glycoprotein expression increases ATP release in respiratory cystic fibrosis cells. J. Cyst. Fibros. *4*, 157–168.

Navarro-Orozco, D., and Sánchez-Manso, J.C. (2018). Neuroanatomy, Middle Cerebral
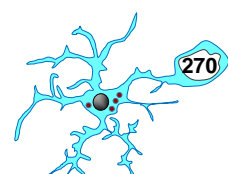
Artery. StatPearls.

Nayak, D., Roth, T.L., and McGavern, D.B. (2014). Microglia development and function. Annu. Rev. Immunol. *32*, 367–402.

Neglia, R., Colombari, B., Peppoloni, S., Orsi, C., Tavanti, A., Senesi, S., and Blasi, E. (2006). Adaptive response of microglial cells to in vitro infection by Candida albicans isolates with different genomic backgrounds. Microb. Pathog. *41*, 251–256.

Neher, J.J., Neniskyte, U., Zhao, J.-W., Bal-Price, A., Tolkovsky, A.M., and Brown, G.C. (2011). Inhibition of Microglial Phagocytosis Is Sufficient To Prevent Inflammatory Neuronal Death. J. Immunol. *186*, 4973–4983.

Neher, J.J., Emmrich, J. V., Fricker, M., Mander, P.K., Théry, C., and Brown, G.C. (2013). Phagocytosis executes delayed neuronal death after focal brain ischemia. Proc. Natl. Acad. Sci. U. S. A. *110*, E4098-107.

Neniskyte, U., and Brown, G.C. (2013). Lactadherin/MFG-E8 is essential for microglia-mediated neuronal loss and phagoptosis induced by amyloid β. J. Neurochem. *126*, 312–317.

Neniskyte, U., Neher, J.J., and Brown, G.C. (2011). Neuronal death induced by nanomolar amyloid β is mediated by primary phagocytosis of neurons by microglia. J. Biol. Chem. *286*, 39904–39913.

Neumann, H., and Takahashi, K. (2007). Essential role of the microglial triggering receptor expressed on myeloid cells-2 (TREM2) for central nervous tissue immune homeostasis. J. Neuroimmunol. *184*, 92–99.

Neumann, J., Henneberg, S., Von Kenne, S., Nolte, N., Müller, A.J., Schraven, B., Görtler, M.W., Reymann, K.G., Gunzer, M., and Riek-Burchardt, M. (2018). Beware the intruder: Real time observation of infiltrated neutrophils and neutrophil-Microglia interaction during stroke in vivo. PLoS One *13(3):e019*.

Nguyen, M.D., Julien, J.P., and Rivest, S. (2002). Innate immunity: The missing link in neuroprotection and neurodegeneration? Nat. Rev. Neurosci. *3*, 216–227.

Niessen, F., Hilger, T., Hoehn, M., and Hossmann, K.A. (2003). Differences in clot preparation determine outcome of recombinant tissue plasminogen activator treatment in experimental thromboembolic stroke. Stroke *34*, 2019–2024.

Nimmerjahn, A., Kirchhoff, F., and Helmchen, F. (2005a). Neuroscience: Resting microglial cells are highly dynamic surveillants of brain parenchyma in vivo. Science (80-
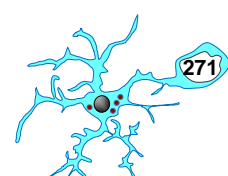
.). *308*, 1314–1318.

Nimmerjahn, A., Kirchhoff, F., and Helmchen, F. (2005b). Resting microglial cells are highly dynamic surveillants of brain parenchyma in vivo. Neuroforum *308*, 1314–1318.

Nitta, N., Heinrich, C., Hirai, H., and Suzuki, F. (2008). Granule cell dispersion develops without neurogenesis and does not fully depend on astroglial cell generation in a mouse model of temporal lobe epilepsy. Epilepsia *49*, 1711–1722.

Nixon, K., and Crews, F.T. (2002). Binge ethanol exposure decreases neurogenesis in adult rat hippocampus. J. Neurochem. *83*, 1087–1093.

Nogles, T.E., and Galuska, M.A. (2020). Middle Cerebral Artery Stroke. StatPearls.

North, R.A. (2002). Molecular physiology of P2X receptors. Physiol. Rev. *82*, 1013–1067.

Nozaki, M., Yoshikawa, M., Ishitani, K., Kobayashi, H., Houkin, K., Imai, K., Ito, Y., and Muraki, T. (2010). Cysteinyl leukotriene receptor antagonists inhibit tumor metastasis by inhibiting capillary permeability. Keio J. Med. *59*, 10–18.

~O~

O'Dell, C.M., Das, A., Wallace, G., Ray, S.K., and Banik, N.L. (2012). Understanding the basic mechanisms underlying seizures in mesial temporal lobe epilepsy and possible therapeutic targets: A review. J. Neurosci. Res. *90*, 913–924.

O'Sullivan, S. (2007). Physical Rehabilitation.

O'Sullivan, S.A., O'Sullivan, C., Healy, L.M., Dev, K.K., and Sheridan, G.K. (2018). Sphingosine 1-phosphate receptors regulate TLR4-induced CXCL5 release from astrocytes and microglia. J. Neurochem. *144*, 736–747.

Obernier, K., and Alvarez-Buylla, A. (2019). Neural stem cells: Origin, heterogeneity and regulation in the adult mammalian brain. Dev. *146(4):dev*.

Obernier, J.A., White, A.M., Swartzwelder, H.S., and Crews, F.T. (2002). Cognitive deficits and CNS damage after a 4-day binge ethanol exposure in rats. Pharmacol. Biochem. Behav. *72*, 521–532.

Obernier, K., Cebrian-Silla, A., Thomson, M., Parraguez, J.I., Anderson, R., Guinto, C., Rodas Rodriguez, J., Garcia-Verdugo, J.M., and Alvarez-Buylla, A. (2018). Adult Neurogenesis Is Sustained by Symmetric Self-Renewal and Differentiation. Cell Stem Cell *22*, 221-234.e8.
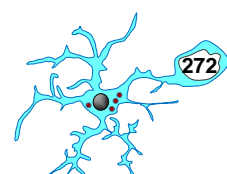
Okuyama, S., Makihata, N., Yoshimura, M., Amakura, Y., Yoshida, T., Nakajima, M., and Furukawa, Y. (2013). Oenothein B suppresses lipopolysaccharide (LPS)-induced inflammation in the mouse brain. Int. J. Mol. Sci. *14*, 9767–9778.

Olney, J.W., Tenkova, T., Dikranian, K., Qin, Y.Q., Labruyere, J., and Ikonomidou, C. (2002). Ethanol-induced apoptotic neurodegeneration in the developing C57BL/6 mouse brain. Dev. Brain Res. *133*, 115–126.

Oorschot, D.E., Sizemore, R.J., and Amer, A.R. (2020). Treatment of neonatal hypoxic-ischemic encephalopathy with erythropoietin alone, and erythropoietin combined with hypothermia: History, current status, and future research. Int. J. Mol. Sci. *21*, 1487.

Opal, S.M., and DePalo, V.A. (2000). Anti-inflammatory cytokines. Chest *117*, 1162–1172.

Orlando, M., Lignani, G., Maragliano, L., Fassio, A., Onofri, F., Baldelli, P., Giovedí, S., and Benfenati, F. (2014). Functional role of ATP binding to synapsin I in synaptic vesicle trafficking and release dynamics. J. Neurosci. *34*, 14752–14768.

Orrenius, S., Zhivotovsky, B., and Nicotera, P. (2003). Regulation of cell death: The calcium-apoptosis link. Nat. Rev. Mol. Cell Biol. *4*, 552–565.

Orset, C., Macrez, R., Young, A.R., Panthou, D., Angles-Cano, E., Maubert, E., Agin, V., and Vivien, D. (2007). Mouse model of in situ thromboembolic stroke and reperfusion. Stroke *38*, 2771–2778.

Orzyłowska, O., Oderfeld-Nowak, B., Zaremba, M., Januszewski, S., and Mossakowski, M. (1999). Prolonged and concomitant induction of astroglial immunoreactivity of interleukin-1beta and interleukin-6 in the rat hippocampus after transient global ischemia. Neurosci. Lett. *263*, 72–76.

Oscar-Berman, M., and Marinković, K. (2007). Alcohol: Effects on neurobehavioral functions and the brain. Neuropsychol. Rev. *17*, 239–257.

Osman, A.M., Sun, Y., Burns, T.C., He, L., Kee, N., Oliva-Vilarnau, N., Alevyzaki, A., Zhou, K., Louhivuori, L., Uhlén, P., et al. (2020). Radiation Triggers a Dynamic Sequence of Transient Microglial Alterations in Juvenile Brain. Cell Rep. *31(9):1076*.

Ostwald, T.J., and MacLennan, D.H. (1974). Isolation of a high affinity calcium binding protein from sarcoplasmic reticulum. J. Biol. Chem. *249*, 974–979.

Otáhal, J., Folbergrová, J., Kovacs, R., Kunz, W.S., and Maggio, N. (2014). Epileptic focus and alteration of metabolism. Int. Rev. Neurobiol. *114:209-43*.
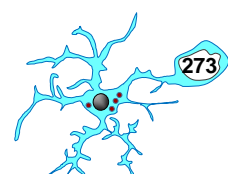
Otxoa-de-Amezaga, A., Miró-Mur, F., Pedragosa, J., Gallizioli, M., Justicia, C., Gaja-Capdevila, N., Ruíz-Jaen, F., Salas-Perdomo, A., Bosch, A., Calvo, M., et al. (2019). Microglial cell loss after ischemic stroke favors brain neutrophil accumulation. Acta Neuropathol. *37*, 321–341.

Overgaard, K., Sereghy, T., Boysen, G., Pedersen, H., Høyer, S., and Diemer, N.H. (1992). A rat model of reproducible cerebral infarction using thrombotic blood clot emboli. J. Cereb. Blood Flow Metab. *12*, 484–490.

~P~

Paloneva, J., Kestilä, M., Wu, J., Salminen, A., Böhling, T., Ruotsalainen, V., Hakola, P., Bakker, A.B.H., Phillips, J.H., Pekkarinen, P., et al. (2000). Loss-of-function mutations in TYROBP (DAP12) result in a presenile dementia with bone cysts. Nat. Genet. *25*, 357–361.

Paloneva, J., Manninen, T., Christman, G., Hovanes, K., Mandelin, J., Adolfsson, R., Bianchin, M., Bird, T., Miranda, R., Salmaggi, A., et al. (2002). Mutations in two genes encoding different subunits of a receptor signaling complex result in an identical disease phenotype. Am. J. Hum. Genet. *71*, 656–662.

Pang, Y., Cai, Z., and Rhodes, P.G. (2000). Effects of lipopolysaccharide on oligodendrocyte progenitor cells are mediated by astrocytes and microglia. J. Neurosci. Res. *62*, 510–520.

Pang, Y., Fan, L.W., Tien, L.T., Dai, X., Zheng, B., Cai, Z., Lin, R.C.S., and Bhatt, A. (2013). Differential roles of astrocyte and microglia in supporting oligodendrocyte development and myelination in vitro. Brain Behav. *3*, 503–514.

Paolicelli, R.C., Bolasco, G., Pagani, F., Maggi, L., Scianni, M., Panzanelli, P., Giustetto, M., Ferreira, T.A., Guiducci, E., Dumas, L., et al. (2011). Synaptic pruning by microglia is necessary for normal brain development. Science (80-.). *333*, 1456–1458.

Papouin, T., Dunphy, J., Tolman, M., Foley, J.C., and Haydon, P.G. (2017). Astrocytic control of synaptic function. Philos. Trans. R. Soc. B Biol. Sci. *372(1715):*

Pardridge, W.M. (2005). The blood-brain barrier: Bottleneck in brain drug development. NeuroRx *2*, 3–14.

Parent, J.M., Yu, T.W., Leibowitz, R.T., Geschwind, D.H., Sloviter, R.S., and Lowenstein, D.H. (1997). Dentate granule cell neurogenesis is increased by seizures and contributes to aberrant network reorganization in the adult rat hippocampus. J. Neurosci. *17*, 3727–
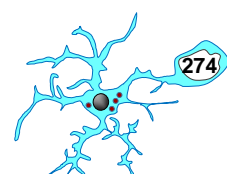
3738.

Parent, J.M., Elliott, R.C., Pleasure, S.J., Barbaro, N.M., and Lowenstein, D.H. (2006). Aberrant seizure-induced neurogenesis in experimental temporal lobe epilepsy. Ann. Neurol. *59*, 81–91.

Parhizkar, S., Arzberger, T., Brendel, M., Kleinberger, G., Deussing, M., Focke, C., Nuscher, B., Xiong, M., Ghasemigharagoz, A., Katzmarski, N., et al. (2019). Loss of TREM2 function increases amyloid seeding but reduces plaque-associated ApoE. Nat. Neurosci. *22*, 191–204.

Park, S.Y., and Kim, I.S. (2017). Engulfment signals and the phagocytic machinery for apoptotic cell clearance. Exp. Mol. Med. *49(5):e331*.

Park, D., Park, D., Han, C.Z., Han, C.Z., Elliott, M.R., Elliott, M.R., Kinchen, J.M., Kinchen, J.M., Trampont, P.C., Trampont, P.C., et al. (2011). Continued clearance of apoptotic cells critically depends on the phagocyte Ucp2 protein. Nature *477*, 220–224.

Park, J.Y., Pillinger, M.H., and Abramson, S.B. (2006). Prostaglandin E2 synthesis and secretion: The role of PGE2 synthases. Clin. Immunol. *119*, 229–240.

Park, S.Y., Jung, M.Y., Lee, S.J., Kang, K.B., Gratchev, A., Riabov, V., Kzhyshkowska, J., and Kim, I.S. (2009). Stabilin-1 mediates phosphatidylserine-dependent clearance of cell cropses in alternatively activated macrophages. J. Cell Sci. *122*, 3365–3373.

Parkhurst, C.N., Yang, G., Ninan, I., Savas, J.N., Yates, J.R., Lafaille, J.J., Hempstead, B.L., Littman, D.R., and Gan, W.B. (2013). Microglia promote learning-dependent synapse formation through brain-derived neurotrophic factor. Cell *155*, 1596–1609.

Parnaik, R., Raff, M.C., and Scholes, J. (2000). Differences between the clearance of apoptotic cells by professional and non-professional phagocytes. Curr. Biol. *10*, 857–860.

Paul, G., and Sullivan, A.M. (2019). Trophic factors for Parkinson's disease: Where are we and where do we go from here? Eur. J. Neurosci. *49*, 440–452.

Pauliah, S.S., Shankaran, S., Wade, A., Cady, E.B., and Thayyil, S. (2013). Therapeutic Hypothermia for Neonatal Encephalopathy in Low- and Middle-Income Countries: A Systematic Review and Meta-Analysis. PLoS One *8(3):e5883*.

Pedata, F., Dettori, I., Coppi, E., Melani, A., Fusco, I., Corradetti, R., and Pugliese, A.M. (2016). Purinergic signalling in brain ischemia. Neuropharmacology *104*, 105–130.

Peißner, W., Kocher, M., Treuer, H., and Gillardon, F. (1999). Ionizing radiation-induced
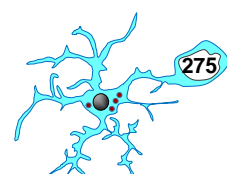
apoptosis of proliferating stem cells in the dentate gyrus of the adult rat hippocampus. Mol. Brain Res. *71*, 61–68.

Pellon, A., Ramirez-Garcia, A., Guruceaga, X., Zabala, A., Buldain, I., Antoran, A., Anguita, J., Rementeria, A., Matute, C., and Hernando, F.L. (2018). Microglial immune response is impaired against the neurotropic fungus Lomentospora prolificans. Cell. Microbiol. *20(8):e128*.

Peña, I. Dela, Borlongan, C., Shen, G., and Davis, W. (2017). Strategies to extend thrombolytic time window for ischemic stroke treatment: An unmet clinical need. J. Stroke *19*, 50–60.

Peng, H., Geil Nickell, C.R., Chen, K.Y., McClain, J.A., and Nixon, K. (2017). Increased expression of M1 and M2 phenotypic markers in isolated microglia after four-day binge alcohol exposure in male rats. Alcohol *62*, 29–40.

Pennacchio, L.A., Lehesjoki, A.E., Stone, N.E., Willour, V.L., Virtaneva, K., Miao, J., D'Amato, E., Ramirez, L., Faham, M., Koskiniemi, M., et al. (1996). Mutations in the gene encoding cystatin B in progressive myoclonus epilepsy (EPM1). Science (80-.). *271*, 1731–1734.

Perez-Pouchoulen, M., VanRyzin, J.W., and McCarthy, M.M. (2015). Morphological and phagocytic profile of microglia in the developing rat cerebellum. ENeuro *2*, ENEURO.0036-15.2015.

Perlman, J.M., Wyllie, J., Kattwinkel, J., Atkins, D.L., Chameides, L., Goldsmith, J.P., Guinsburg, R., Hazinski, M.F., Morley, C., Richmond, S., et al. (2010). Part 11: Neonatal resuscitation: 2010 International Consensus on Cardiopulmonary Resuscitation and Emergency Cardiovascular Care Science with Treatment Recommendations. Circulation *81*, e260-87.

Perrone, S., Weiss, M.D., Proietti, F., Rossignol, C., Cornacchione, S., Bazzini, F., Calderisi, M., Buonocore, G., and Longini, M. (2018). Identification of a panel of cytokines in neonates with hypoxic ischemic encephalopathy treated with hypothermia. Cytokine *111*, 119–124.

Perry, C.J., and Lawrence, A.J. (2017). Hurdles in basic science translation. Front. Pharmacol. *39*, 91–95.

Perry, V.H., and Andersson, P.B. (1992). The inflammatory response in the CNS. Neuropathol. Appl. Neurobiol. *18*, 454–459.

Perry, T.L., Hansen, S., and Gandham, S.S. (1981). Postmortem Changes of Amino
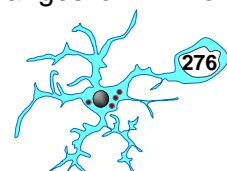
Compounds in Human and Rat Brain. J. Neurochem. *36*, 406–410.

Perry, V.H., Hume, D.A., and Gordon, S. (1985). Immunohistochemical localization of macrophages and microglia in the adult and developing mouse brain. Neuroscience *15*, 313–326.

Perry, V.H., Nicoll, J.A.R., and Holmes, C. (2010). Microglia in neurodegenerative disease. Nat. Rev. Neurol. *6*, 193–201.

Peter, C., Waibel, M., Radu, C.G., Yang, L. V., Witte, O.N., Schulze-Osthoff, K., Wesselborg, S., and Lauber, K. (2008). Migration to apoptotic "find-me" signals is mediated via the phagocyte receptor G2A. J. Biol. Chem. *283*, 5296–5305.

Peter, C., Wesselborg, S., and Lauber, K. (2010). Molecular suicide notes: Last call from apoptosing cells. J. Mol. Cell Biol. *2*, 78–80.

Peters-Golden, M., and Henderson, W.R. (2007). Mechanisms of disease: Leukotrienes. New Engl. J. Med. [NEJM] *3*, 43–51.

Pineda, J.R., Daynac, M., Chicheportiche, A., Cebrian-Silla, A., Sii Felice, K., Garcia-Verdugo, J.M., Boussin, F.D., and Mouthon, M.A. (2013). Vascular-derived TGF-β increases in the stem cell niche and perturbs neurogenesis during aging and following irradiation in the adult mouse brain. EMBO Mol. Med. *5*, 548–562.

Plata-Salamán, C.R., Ilyin, S.E., Turrin, N.P., Gayle, D., Flynn, M.C., Romanovitch, A.E., Kelly, M.E., Bureau, Y., Anisman, H., and McIntyre, D.C. (2000). Kindling modulates the IL-1β system, TNF-α, TGF-β1, and neuropeptide mRNAs in specific brain regions. Mol. Brain Res. *75*, 248–258.

van der Poel, M., Ulas, T., Mizee, M.R., Hsiao, C.C., Miedema, S.S.M., Adelia, Schuurman, K.G., Helder, B., Tas, S.W., Schultze, J.L., et al. (2019). Transcriptional profiling of human microglia reveals grey–white matter heterogeneity and multiple sclerosis-associated changes. Nat. Commun. *10*, 1139.

Pomilio, C., Pavia, P., Gorojod, R.M., Vinuesa, A., Alaimo, A., Galvan, V., Kotler, M.L., Beauquis, J., and Saravia, F. (2016). Glial alterations from early to late stages in a model of Alzheimer's disease: Evidence of autophagy involvement in Aβ internalization. Hippocampus *26*, 194–210.

Poon, I.K.H., Lucas, C.D., Rossi, A.G., and Ravichandran, K.S. (2014). Apoptotic cell clearance: Basic biology and therapeutic potential. Nat. Rev. Immunol. *14*, 166–180.

Popa-Wagner, A., Schröder, E., Schmoll, H., Walker, L.C., and Kessler, C. (1999).
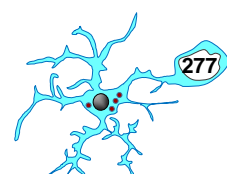
Upregulation of MAP1B and MAP2 in the rat brain after middle cerebral artery occlusion: Effect of age. J. Cereb. Blood Flow Metab. *19*, 425–434.

Preissler, J., Grosche, A., Lede, V., Le Duc, D., Krügel, K., Matyash, V., Szulzewsky, F., Kallendrusch, S., Immig, K., Kettenmann, H., et al. (2015). Altered microglial phagocytosis in GPR34-deficient mice. Glia *63*, 206–215.

Price, C.J.S., Wang, D., Menon, D.K., Guadagno, J. V., Cleij, M., Fryer, T., Aigbirhio, F., Baron, J.C., and Warburton, E.A. (2006). Intrinsic activated microglia map to the peri-infarct zone in the subacute phase of ischemic stroke. Stroke *37*, 749–753.

Prinz, M., Jung, S., and Priller, J. (2019). Microglia Biology: One Century of Evolving Concepts. Cell *179*, 292–311.

PubChem (2021). Compound Summary for CID 702, Ethanol. Natl. Cent. Biotechnol. Inf.

~Q~

Qin, L., Wu, X., Block, M.L., Liu, Y., Breese, G.R., Hong, J.S., Knapp, D.J., and Crews, F.T. (2007). Systemic LPS causes chronic neuroinflammation and progressive neurodegeneration. Glia *55*, 453–462.

Quintas, R., Raggi, A., Giovannetti, A.M., Pagani, M., Sabariego, C., Cieza, A., and Leonardi, M. (2012). Psychosocial difficulties in people with epilepsy: A systematic review of literature from 2005 until 2010. Epilepsy Behav. *55*, 453–462.

~R~

Radic, T., Frieß, L., Vijikumar, A., Jungenitz, T., Deller, T., and Schwarzacher, S.W. (2017). Differential postnatal expression of neuronal maturation markers in the dentate gyrus of mice and rats. Front. Neuroanat. *11:104*.

Radu, B.M., Epureanu, F.B., Radu, M., Fabene, P.F., and Bertini, G. (2017). Nonsteroidal anti-inflammatory drugs in clinical and experimental epilepsy. Epilepsy Res. *131*, 15–27.

Raetz, C.R.H., and Whitfield, C. (2002). Lipopolysaccharide endotoxins. Annu. Rev. Biochem. *71*, 635–700.

Rajan, W.D., Wojtas, B., Gielniewski, B., Gieryng, A., Zawadzka, M., and Kaminska, B. (2019). Dissecting functional phenotypes of microglia and macrophages in the rat brain after transient cerebral ischemia. Glia *67*, 232–245.
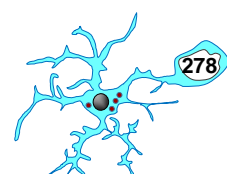
Raleigh, J.A., and Koch, C.J. (1990). Importance of thiols in the reductive binding of 2-nitroimidazoles to macromolecules. Biochem. Pharmacol. *40*, 2457–2464.

Raleigh, J.A., Calkins-Adams, D.P., Rinker, L.H., Ballenger, C.A., Weissler, M.C., Fowler, W.C., Novotny, D.B., and Varia, M.A. (1998). Hypoxia and vascular endothelial growth factor expression in human squamous cell carcinomas using pimonidazole as a hypoxia marker. Cancer Res. *58*, 3765–3768.

Ransohoff, R.M. (2016). A polarizing question: Do M1 and M2 microglia exist. Nat. Neurosci. *19*, 987–991.

Ransohoff, R.M., and Perry, V.H. (2009). Microglial physiology: Unique stimuli, specialized responses. Annu. Rev. Immunol. *27*, 119–145.

Rappold, P.M., Lynd-Balta, E., and Joseph, S.A. (2006). P2X7 receptor immunoreactive profile confined to resting and activated microglia in the epileptic brain. Brain Res. *1089*, 171-8.

Ravichandran, K.S., and Lorenz, U. (2007). Engulfment of apoptotic cells: Signals for a good meal. Nat. Rev. Immunol. *7*, 964–974.

Ravizza, T., Gagliardi, B., Noé, F., Boer, K., Aronica, E., and Vezzani, A. (2008). Innate and adaptive immunity during epileptogenesis and spontaneous seizures: Evidence from experimental models and human temporal lobe epilepsy. Neurobiol. Dis. *29*, 142–160.

Ravizza, T., Balosso, S., Aronica, E., and Vezzani, A. (2010). Brain inflammation and epilepsy. Epilepsy Mech. Model. Transl. Perspect. *58*, 39–47.

Rawji, K.S., and Yong, V.W. (2013). The benefits and detriments of macrophages/microglia in models of multiple sclerosis. Clin. Dev. Immunol. *2013:94897*.

Razavi, S., Nazem, G., Mardani, M., Esfandiari, E., Esfahani, S., and Salehi, H. (2015). Neurotrophic factors and their effects in the treatment of multiple sclerosis. Adv. Biomed. Res. *4:53*.

Ren, M., Lin, Z.J., Qian, H., Choudhury, G.R., Liu, R., Liu, H., and Yang, S.H. (2012). Embolic middle cerebral artery occlusion model using thrombin and fibrinogen composed clots in rat. J. Neurosci. Methods *211*, 296–304.

Rettenbeck, M.L., Rüden, E.L. von, Bienas, S., Carlson, R., Stein, V.M., Tipold, A., and Potschka, H. (2015). Microglial ROS production in an electrical rat post-status epilepticus model of epileptogenesis. Neurosci. Lett. *599*, 146–151.

Reubold, T.F., and Eschenburg, S. (2012). A molecular view on signal transduction by
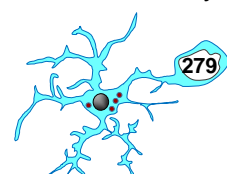
the apoptosome. Cell. Signal. *24*, 1420–1425.

Rezaie, P., Cairns, N.J., and Male, D.K. (1997). Expression of adhesion molecules on human fetal cerebral vessels: Relationship to microglial colonisation during development. Dev. Brain Res. *104*, 175–189.

Rezaie, P., Dean, A., Male, D., and Ulfig, N. (2005). Microglia in the cerebral wall of the human telencephalon at second trimester. Cereb. Cortex *15*, 938–949.

Ribes, S., Ebert, S., Czesnik, D., Regen, T., Zeug, A., Bukowski, S., Mildner, A., Eiffert, H., Hanisch, U.K., Hammerschmidt, S., et al. (2009). Toll-like receptor prestimulation increases phagocytosis of Escherichia coli DH5α and Escherichia coli K1 strains by murine microglial cells. Infect. Immun. *77*, 557–564.

Ricciotti, E., and Fitzgerald, G.A. (2011). Prostaglandins and inflammation. Arterioscler. Thromb. Vasc. Biol. *31*, 986–1000.

Rice, J.E., Vannucci, R.C., and Brierley, J.B. (1981). The influence of immaturity on hypoxic-ischemic brain damage in the rat. Ann. Neurol. *9*, 131–141.

Rice, R.A., Pham, J., Lee, R.J., Najafi, A.R., West, B.L., and Green, K.N. (2017). Microglial repopulation resolves inflammation and promotes brain recovery after injury. Glia *65*, 931–944.

Richardson, H.N., Chan, S.H., Crawford, E.F., Lee, Y.K., Funk, C.K., Koob, G.F., and Mandyam, C.D. (2009). Permanent impairment of birth and survival of cortical and hippocampal proliferating cells following excessive drinking during alcohol dependence. Neurobiol. Dis. *36*, 1–10.

Ricklin, D., Hajishengallis, G., Yang, K., and Lambris, J.D. (2010). Complement: A key system for immune surveillance and homeostasis. Nat. Immunol. *11*, 785–797.

Rietschel, E.T., Kirikae, T., Schade, F.U., Mamat, U., Schmidt, G., Loppnow, H., Ulmer, A.J., Zähringer, U., Seydel, U., Di Padova, F., et al. (1994). Bacterial endotoxin: molecular relationships of structure to activity and function. FASEB J. *8*, 217–225.

Riikonen, J., Jaatinen, P., Rintala, J., Pörsti, I., Karjala, K., and Hervonen, A. (2002). Intermittent ethanol exposure increases the number of cerebellar microglia. Alcohol Alcohol. *37*, 421–426.

del Rio-Hortega, P. (1919). El tercer elemento de los centros nerviosos. Bio Soc Esp Biol *181*.

del Rio-Hortega, P. (1932). Cytology and Cellular Pathology of the Nervous System.
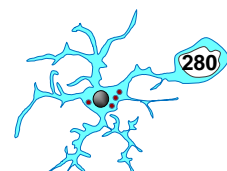
Arch. Intern. Med. *27*, 576.

del Río, M.R., and DeFelipe, J. (1994). A study of SMI 32-stained pyramidal cells, parvalbumin-immunoreactive chandelier cells, and presumptive thalamocortical axons in the human temproal neocortex. J. Comp. Neurol. *342*, 389–408.

Ritzel, R.M., Patel, A.R., Grenier, J.M., Crapser, J., Verma, R., Jellison, E.R., and McCullough, L.D. (2015). Functional differences between microglia and monocytes after ischemic stroke. J. Neuroinflammation *12:106*.

Robbins, M.E.C., and Zhao, W. (2004). Chronic oxidative stress and radiation-induced late normal tissue injury: A review. Int. J. Radiat. Biol. *80*, 251–259.

Robinson, M.J., Macrae, I.M., Todd, M., Reid, J.L., and McCulloch, J. (1990). Reduction of local cerebral blood flow to pathological levels by endothelin-1 applied to the middle cerebral artery in the rat. Neurosci. Lett. *118*, 269–272.

Rocha-Ferreira, E., and Hristova, M. (2015). Antimicrobial peptides and complement in neonatal hypoxia-ischemia induced brain damage. Front. Immunol. *6:56*.

Rocha, N.P., Teixeira, A.L., Coelho, F.M., Caramelli, P., Guimarães, H.C., Barbosa, I.G., da Silva, T.A., Mukhamedyarov, M.A., Zefirov, A.L., Rizvanov, A.A., et al. (2012). Peripheral blood mono-nuclear cells derived from Alzheimer's disease patients show elevated baseline levels of secreted cytokines but resist stimulation with β-amyloid peptide. Mol. Cell. Neurosci. *49*, 77–84.

Rodrigo, R., Fernandez-Gajardo, R., Gutierrez, R., Matamala, J., Carrasco, R., Miranda-Merchak, A., and Feuerhake, W. (2013). Oxidative Stress and Pathophysiology of Ischemic Stroke: Novel Therapeutic Opportunities. CNS Neurol. Disord. - Drug Targets *12*, 698–714.

Roesch, S., Rapp, C., Dettling, S., and Herold-Mende, C. (2018). When immune cells turn bad—tumor-associated microglia/macrophages in glioma. Int. J. Mol. Sci. *19*, 436.

Rogers, J.T., Morganti, J.M., Bachstetter, A.D., Hudson, C.E., Peters, M.M., Grimmig, B.A., Weeber, E.J., Bickford, P.C., and Gemma, C. (2011). CX3CR1 deficiency leads to impairment of hippocampal cognitive function and synaptic plasticity. J. Neurosci. *31*, 16241–16250.

Rola, R., Raber, J., Rizk, A., Otsuka, S., Vandenberg, S.R., Morhardt, D.R., and Fike, J.R. (2004). Radiation-induced impairment of hippocampal neurogenesis is associated with cognitive deficits in young mice. Exp. Neurol. *188*, 316–330.
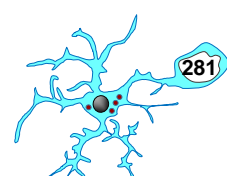
Rosell, D.R., Nacher, J., Akama, K.T., and Mcewen, B.S. (2003). Spatiotemporal distribution of gp130 cytokines and their receptors after status epilepticus: Comparison with neuronal degeneration and microglial activation. Neuroscience *122*, 329–348.

Roseti, C., van Vliet, E.A., Cifelli, P., Ruffolo, G., Baayen, J.C., Di Castro, M.A., Bertollini, C., Limatola, C., Aronica, E., Vezzani, A., et al. (2015). GABAA currents are decreased by IL-1β in epileptogenic tissue of patients with temporal lobe epilepsy: Implications for ictogenesis. Neurobiol. Dis. *82*, 311–320.

Rossouw, G., Irlam, J., and Horn, A.R. (2015). Therapeutic hypothermia for hypoxic ischaemic encephalopathy using low-technology methods: A systematic review and meta-analysis. Acta Paediatr. Int. J. Paediatr. *104*, 1217–1228.

Roth, S., Cao, J., Singh, V., Tiedt, S., Hundeshagen, G., Li, T., Boehme, J.D., Chauhan, D., Zhu, J., Ricci, A., et al. (2021). Post-injury immunosuppression and secondary infections are caused by an AIM2 inflammasome-driven signaling cascade. Immunity *54*, 648-659.e8.

Roughton, K., Kalm, M., and Blomgren, K. (2012). Sex-dependent differences in behavior and hippocampal neurogenesis after irradiation to the young mouse brain. Eur. J. Neurosci.

Roumier, A., Béchade, C., Poncer, J.C., Smalla, K.H., Tomasello, E., Vivier, E., Gundelfinger, E.D., Triller, A., and Bessis, A. (2004). Impaired synaptic function in the microglial KARAP/DAP12-deficient mouse. J. Neurosci. *24*, 11421–11428.

Roumier, A., Pascual, O., Béchade, C., Wakselman, S., Poncer, J.C., Réal, E., Triller, A., and Bessis, A. (2008). Prenatal activation of microglia induces delayed impairment of glutamatergic synaptic function. PLoS One *3(7):e2595*.

Rousselet, E., Kriz, J., and Seidah, N.G. (2012). Mouse model of intraluminal MCAO: cerebral infarct evaluation by cresyl violet staining. J. Vis. Exp. *(69):4038*.

Ruan, C., Sun, L., Kroshilina, A., Beckers, L., De Jager, P., Bradshaw, E.M., Hasson, S.A., Yang, G., and Elyaman, W. (2020). A novel Tmem119-tdTomato reporter mouse model for studying microglia in the central nervous system. Brain. Behav. Immun. *83:180-191*.

Rumajogee, P., Bregman, T., Miller, S.P., Yager, J.Y., and Fehlings, M.G. (2016). Rodent hypoxia-ischemia models for cerebral palsy research: A systematic review. Front. Neurol. *7: 57*.

Rupalla, K., Allegrini, P.R., Sauer, D., and Wiessner, C. (1998). Time course of microglia
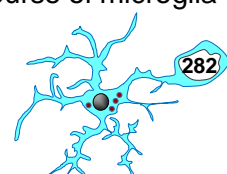
activation and apoptosis in various brain regions after permanent focal cerebral ischemia in mice. Acta Neuropathol. *96*, 172–178.

Ryan, K., Liang, L.P., Rivard, C., and Patel, M. (2014). Temporal and spatial increase of reactive nitrogen species in the kainate model of temporal lobe epilepsy. Neurobiol. Dis. *64*, 8–15.

~S~

Sabir, H., Osredkar, D., Maes, E., Wood, T., and Thoresen, M. (2016). Xenon combined with therapeutic hypothermia is not neuroprotective after severe hypoxia-ischemia in neonatal rats. PLoS One *11(6): e01*.

Saederup, N., Cardona, A.E., Croft, K., Mizutani, M., Cotleur, A.C., Tsou, C.L., Ransohoff, R.M., and Charo, I.F. (2010). Selective chemokine receptor usage by central nervous system myeloid cells in CCR2-red fluorescent protein knock-in mice. PLoS One *5*.

Safaiyan, S., Kannaiyan, N., Snaidero, N., Brioschi, S., Biber, K., Yona, S., Edinger, A.L., Jung, S., Rossner, M.J., and Simons, M. (2016). Age-related myelin degradation burdens the clearance function of microglia during aging. Nat. Neurosci. *19*, 995–998.

Safaiyan, S., Besson-Girard, S., Gberk Kaya, T., Brendel, M., Gokce, O., and Simons Correspondence, M. (2021). White matter aging drives microglial diversity. Neuron *109*, 1100-1117.e10.

Sairanen, T., Carpén, O., Karjalainen-Lindsberg, M.L., Paetau, A., Turpeinen, U., Kaste, M., and Lindsberg, P.J. (2001). Evolution of cerebral tumor necrosis factor-α production during human ischemic stroke. Stroke *32*, 1750–1758.

Salter, M.W., and Stevens, B. (2017). Microglia emerge as central players in brain disease. Nat. Med. *23*, 1018–1027.

Samary, C.S., Ramos, A.B., Maia, L.A., Rocha, N.N., Santos, C.L., Magalhães, R.F., Clevelario, A.L., Pimentel-Coelho, P.M., Mendez-Otero, R., Cruz, F.F., et al. (2018). Focal ischemic stroke leads to lung injury and reduces alveolar macrophage phagocytic capability in rats. Crit. Care *22: 249*.

Sanchez-Alavez, M., Nguyen, W., Mori, S., Wills, D.N., Otero, D., Ehlers, C.L., and Conti, B. (2019). Time course of microglia activation and brain and blood cytokine/chemokine levels following chronic ethanol exposure and protracted withdrawal in rats. Alcohol *76*, 37–45.
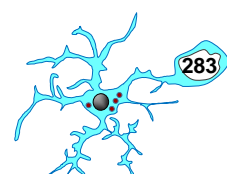
Sankaraneni, R., and Lachhwani, D. (2015). Antiepileptic drugs-a review. Pediatr. Ann. *44(2):e36-*.

Santiago, M.F., Veliskova, J., Patel, N.K., Lutz, S.E., Caille, D., Charollais, A., Meda, P., and Scemes, E. (2011). Targeting pannexin1 improves seizure outcome. PLoS One *6(9):e2517*.

Sasmono, R.T., Oceandy, D., Pollard, J.W., Tong, W., Pavli, P., Wainwright, B.J., Ostrowski, M.C., Himes, S.R., and Hume, D.A. (2003). A macrophage colony-stimulating factor receptor-green fluorescent protein transgene is expressed throughout the mononuclear phagocyte system of the mouse. Blood *101*, 1155–1163.

Savage, N. (2014). Epidemiology: The complexities of epilepsy. Nature *511*, S2-3.

Savage, J.C., St-Pierre, M.K., Hui, C.W., and Tremblay, M.E. (2019). Microglial Ultrastructure in the Hippocampus of a Lipopolysaccharide-Induced Sickness Mouse Model. Front. Neurosci. *13:1340*.

Savarin-Vuaillat, C., and Ransohoff, R.M. (2007). Chemokines and Chemokine Receptors in Neurological Disease: Raise, Retain, or Reduce? Neurotherapeutics *4*, 590–601.

Savill, J., Dransfield, I., Gregory, C., and Haslett, C. (2002). A blast from the past: Clearance of apoptotic cells regulates immune responses. Nat. Rev. Immunol. *2*, 965–975.

Scalzo, F., Nour, M., and Liebeskind, D.S. (2015). Data science of stroke imaging and enlightenment of the penumbra. Front. Neurol. *6:8*.

Schafer, D.P., and Stevens, B. (2015). Microglia function in central nervous system development and plasticity. Cold Spring Harb. Perspect. Biol. *7(10):a020*.

Schafer, D.P., Lehrman, E.K., Kautzman, A.G., Koyama, R., Mardinly, A.R., Yamasaki, R., Ransohoff, R.M., Greenberg, M.E., Barres, B.A., and Stevens, B. (2012). Microglia Sculpt Postnatal Neural Circuits in an Activity and Complement-Dependent Manner. Neuron *74*, 691–705.

Schaffner, S.L., Lussier, A.A., Baker, J.A., Goldowitz, D., Hamre, K.M., and Kobor, M.S. (2020). Neonatal Alcohol Exposure in Mice Induces Select Differentiation- and Apoptosis-Related Chromatin Changes Both Independent of and Dependent on Sex. Front. Genet. *11: 35*.

Schartz, N.D., and Tenner, A.J. (2020). The good, the bad, and the opportunities of the
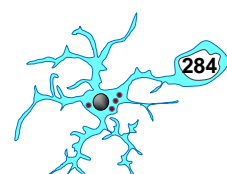
complement system in neurodegenerative disease. J. Neuroinflammation *17*.

Schilling, M., Besselmann, M., Leonhard, C., Mueller, M., Ringelstein, E.B., and Kiefer, R. (2003). Microglial activation precedes and predominates over macrophage infiltration in transient focal cerebral ischemia: A study in green fluorescent protein transgenic bone marrow chimeric mice. Exp. Neurol. *183*, 25–33.

Schletter, J., Heine, H., Ulmer, A.J., and Rietschel, E.T. (1995). Molecular mechanisms of endotoxin activity. Arch. Microbiol. *164*, 383–389.

Schnegg, C.I., Kooshki, M., Hsu, F.C., Sui, G., and Robbins, M.E. (2012). PPARδ prevents radiation-induced proinflammatory responses in microglia via transrepression of NF-κB and inhibition of the PKCα/MEK1/2/ERK1/2/AP-1 pathway. Free Radic. Biol. Med. *52*, 1734–1743.

Schock, S.C., Munyao, N., Yakubchyk, Y., Sabourin, L.A., Hakim, A.M., Ventureyra, E.C.G., and Thompson, C.S. (2007). Cortical spreading depression releases ATP into the extracellular space and purinergic receptor activation contributes to the induction of ischemic tolerance. Brain Res. *1168*, 129–138.

Scholzen, T., and Gerdes, J. (2000). The Ki-67 protein: From the known and the unknown. J. Cell. Physiol. *182*, 311–322.

Schöneberg, T., Meister, J., Knierim, A.B., and Schulz, A. (2018). The G protein-coupled receptor GPR34 – The past 20 years of a grownup. Pharmacol. Ther. *189*, 71–88.

Schulz, C., Perdiguero, E.G., Chorro, L., Szabo-Rogers, H., Cagnard, N., Kierdorf, K., Prinz, M., Wu, B., Jacobsen, S.E.W., Pollard, J.W., et al. (2012). A lineage of myeloid cells independent of myb and hematopoietic stem cells. Science (80-.). *336*, 86–90.

Schwartzkroin, P.A. (1986). Hippocampal slices in experimental and human epilepsy. Adv. Neurol. *44*, 991–1010.

Scorza, C.A., Marques, M.J.G., Gomes da Silva, S., Naffah-Mazzacoratti, M. da G., Scorza, F.A., and Cavalheiro, E.A. (2018). Status epilepticus does not induce acute brain inflammatory response in the Amazon rodent Proechimys, an animal model resistant to epileptogenesis. Neurosci. Lett. *668*, 169–173.

Selip, D.B., Jantzie, L.L., Chang, M., Jackson, M.C., Fitzgerald, E.C., Boll, G., Murphy, A., and Jensen, F.E. (2012). Regional differences in susceptibility to hypoxic-ischemic injury in the preterm brain: Exploring the spectrum from white matter loss to selective grey matter injury in a rat model. Neurol. Res. Int. *2012:72518*.
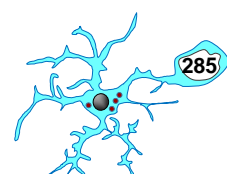
Selkoe, D.J., and Hardy, J. (2016). The amyloid hypothesis of Alzheimer's disease at 25 years. EMBO Mol. Med. *8*, 595–608.

Semmler, A., Okulla, T., Sastre, M., Dumitrescu-Ozimek, L., and Heneka, M.T. (2005). Systemic inflammation induces apoptosis with variable vulnerability of different brain regions. J. Chem. Neuroanat. *30*, 144–157.

Semple, B.D., Blomgren, K., Gimlin, K., Ferriero, D.M., and Noble-Haeusslein, L.J. (2013). Brain development in rodents and humans: Identifying benchmarks of maturation and vulnerability to injury across species. Prog. Neurobiol. *106*, 1–16.

Serbina, N. V., and Pamer, E.G. (2006). Monocyte emigration from bone marrow during bacterial infection requires signals mediated by chemokine receptor CCR2. Nat. Immunol. *7*, 311–317.

Seyhan, A.A. (2019). Lost in translation: the valley of death across preclinical and clinical divide – identification of problems and overcoming obstacles. Transl. Med. Commun. *4*.

Shah, V., and Kochar, P. (2018). Brain Cancer: Implication to Disease, Therapeutic Strategies and Tumor Targeted Drug Delivery Approaches. Recent Pat. Anticancer. Drug Discov. *13*, 70–85.

Shan, Y., Ni, Y., and Gao, Z. (2020). Pannexin-1 Channel Regulates ATP Release in Epilepsy. Neurochem. Res. *45*, 965–971.

Shapiro, L.A., Wang, L., and Ribak, C.E. (2008). Rapid astrocyte and microglial activation following pilocarpine-induced seizures in rats. Epilepsia *49*, 33–41.

Sharma, A.K., Reams, R.Y., Jordan, W.H., Miller, M.A., Thacker, H.L., and Snyder, P.W. (2007). Mesial temporal lobe epilepsy: Pathogenesis, induced rodent models and lesions. Toxicol. Pathol. *35*, 984–999.

Shigeno, T., Teasdale, G.M., McCulloch, J., and Graham, D.I. (2009). Recirculation model following MCA occlusion in rats. J. Neurosurg. *63*, 272–277.

Shimamura, N., Matchett, G., Tsubokawa, T., Ohkuma, H., and Zhang, J. (2006). Comparison of silicon-coated nylon suture to plain nylon suture in the rat middle cerebral artery occlusion model. J. Neurosci. Methods *156*, 161–165.

Shtaya, A., Bridges, L.R., Esiri, M.M., Lam-Wong, J., Nicoll, J.A.R., Boche, D., and Hainsworth, A.H. (2019). Rapid neuroinflammatory changes in human acute intracerebral hemorrhage. Ann. Clin. Transl. Neurol. *6*, 1465–1479.

Siemsen, B.M., Landin, J.D., McFaddin, J.A., Hooker, K.N., Chandler, L.J., and Scofield,
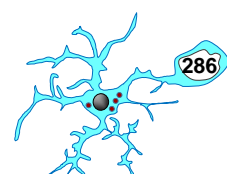
M.D. (2020). Chronic intermittent ethanol and lipopolysaccharide exposure differentially alter Iba1-derived microglia morphology in the prelimbic cortex and nucleus accumbens core of male Long-Evans rats. J. Neurosci. Res. *10.1002/jn.*

Sierra-Torre, V., Plaza-Zabala, A., Bonifazi, P., Abiega, O., Díaz-Aparicio, I., Tegelberg, S., Lehesjoki, A.E., Valero, J., and Sierra, A. (2020). Microglial phagocytosis dysfunction in the dentate gyrus is related to local neuronal activity in a genetic model of epilepsy. Epilepsia *61*, 2593–2608.

Sierra, A., Gottfried-Blackmore, A.C., Mcewen, B.S., and Bulloch, K. (2007). Microglia derived from aging mice exhibit an altered inflammatory profile. Glia *55*, 412–424.

Sierra, A., Encinas, J.M., Deudero, J.J.P., Chancey, J.H., Enikolopov, G., Overstreet-Wadiche, L.S., Tsirka, S.E., and Maletic-Savatic, M. (2010). Microglia shape adult hippocampal neurogenesis through apoptosis-coupled phagocytosis. Cell Stem Cell *7*, 483–495.

Sierra, A., Abiega, O., Shahraz, A., and Neumann, H. (2013). Janus-faced microglia: Beneficial and detrimental consequences of microglial phagocytosis. Front. Cell. Neurosci. *7:6.*

Sierra, A., Tremblay, M.È., and Wake, H. (2014). Never-resting microglia: Physiological roles in the healthy brain and pathological implications. Front. Cell. Neurosci. *8:240.*

Sierra, A., Martín-Suárez, S., Valcárcel-Martín, R., Pascual-Brazo, J., Aelvoet, S.A., Abiega, O., Deudero, J.J., Brewster, A.L., Bernales, I., Anderson, A.E., et al. (2015). Neuronal hyperactivity accelerates depletion of neural stem cells and impairs hippocampal neurogenesis. Cell Stem Cell *14 e100246.*

Sierra, A., de Castro, F., del Río-Hortega, J., Rafael Iglesias-Rozas, J., Garrosa, M., and Kettenmann, H. (2016). The "Big-Bang" for modern glial biology: Translation and comments on Pío del Río-Hortega 1919 series of papers on microglia. Glia *64*, 1801–1840.

Sierra, A., Paolicelli, R.C., and Kettenmann, H. (2019). Cien Años de Microglía: Milestones in a Century of Microglial Research. Trends Neurosci. *42*, 778–792.

Sies, H., and Jones, D.P. (2020). Reactive oxygen species (ROS) as pleiotropic physiological signalling agents. Nat. Rev. Mol. Cell Biol. *21*, 363–383.

Da Silva, R.P., and Gordon, S. (1999). Phagocytosis stimulates alternative glycosylation of macrosialin (mouse CD68), a macrophage-specific endosomal protein. Biochem. J. *338*, 687–694.
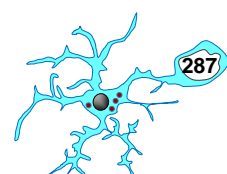
Šimić, G., Kostović, I., Winblad, B., and Bogdanović, N. (1997). Volume and number of neurons of the human hippocampal formation in normal aging and Alzheimer's disease. J. Comp. Neurol. *379*, 482–494.

De Simone, R., Antonietta Ajmone-Cat, M., Tirassa, P., and Minghetti, L. (2003). Apoptotic PC12 cells exposing phosphatidylserine promote the production of anti-inflammatory and neuroprotective molecules by microglial cells. J. Neuropathol. Exp. Neurol. *62*, 208–216.

Siwak-Tapp, C.T., Head, E., Muggenburg, B.A., Milgram, N.W., and Cotman, C.W. (2007). Neurogenesis decreases with age in the canine hippocampus and correlates with cognitive function. Neurobiol. Learn. Mem. *88*, 249–259.

Smith, S.D., and Eskey, C.J. (2011). Hemorrhagic stroke. Radiol. Clin. North Am. *49*, 27–45.

Sofroniew, M. V., and Vinters, H. V. (2010). Astrocytes: Biology and pathology. Acta Neuropathol. *119*, 119(1):7-35.

Sokolowski, J.D., Chabanon-Hicks, C.N., Han, C.Z., Heffron, D.S., and Mandell, J.W. (2014). Fractalkine is a "find-me" signal released by neurons undergoing ethanol-induced apoptosis. Front. Cell. Neurosci. *8:360.*

Song, L., Lee, C., and Schindler, C. (2011). Deletion of the murine scavenger receptor CD68. J. Lipid Res. *52*, 1542–1550.

Spangenberg, E.E., and Green, K.N. (2017). Inflammation in Alzheimer's disease: Lessons learned from microglia-depletion models. Brain. Behav. Immun. *25*, 1352–1354.

Spokes, E.G.S. (1979). An analysis of factors influencing measurements of dopamine, noradrenaline, glutamatedecarboxylase and choline acetylase in human post-mortem brain tissue. Brain *102*, 333–346.

Spratt, N.J., Fernandez, J., Chen, M., Rewell, S., Cox, S., van Raay, L., Hogan, L., and Howells, D.W. (2006). Modification of the method of thread manufacture improves stroke induction rate and reduces mortality after thread-occlusion of the middle cerebral artery in young or aged rats. J. Neurosci. Methods *155*, 285–290.

Squeglia, L.M., Jacobus, J., and Tapert, S.F. (2014). The effect of alcohol use on human adolescent brain structures and systems. Handb. Clin. Neurol. *125*, 501–510.

Stalder, M., Phinney, A., Probst, A., Sommer, B., Staufenbiel, M., and Jucker, M. (1999). Association of microglia with amyloid plaques in brains of APP23 transgenic mice. Am.
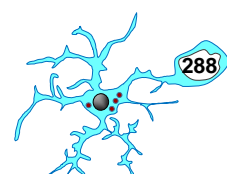
J. Pathol. *154*, 1673–1684.

Stein, M., Keshav, S., Harris, N., and Gordon, S. (1992). Interleukin 4 potently enhances murine macrophage mannose receptor activity: A marker of alternative immunologic macrophage activation. J. Exp. Med. *176*, 287–292.

Stern, M., Savill, J., and Haslett, C. (1996). Human monocyte-derived macrophage phagocytosis of senescent eosinophils undergoing apoptosis: Mediation by α(v)β3/CD36/thrombospondin recognition mechanism and lack of phlogistic response. Am. J. Pathol. *149*, 911–921.

Stowell, R.D., and Majewska, A.K. (2020). Acute ethanol exposure rapidly alters cerebellar and cortical microglial physiology. Eur. J. Neurosci. *10.1111/ej*.

Stowell, R.D., Wong, E.L., Batchelor, H.N., Mendes, M.S., Lamantia, C.E., Whitelaw, B.S., and Majewska, A.K. (2018). Cerebellar microglia are dynamically unique and survey Purkinje neurons in vivo. Dev. Neurobiol. *78*, 627–644.

Strange, B.A., Witter, M.P., Lein, E.S., and Moser, E.I. (2014). Functional organization of the hippocampal longitudinal axis. Nat. Rev. Neurosci. *15, 655–669*.

Streit, W.J., Mrak, R.E., and Griffin, W.S.T. (2004). Microglia and neuroinflammation: A pathological perspective. J. Neuroinflammation *1:14*.

Ström, J.O., Ingberg, E., Theodorsson, A., and Theodorsson, E. (2013). Method parameters' impact on mortality and variability in rat stroke experiments: A meta-analysis. BMC Neurosci. *14*.

Su, F., Bai, F., and Zhang, Z. (2016). Inflammatory Cytokines and Alzheimer's Disease: A Review from the Perspective of Genetic Polymorphisms. Neurosci. Bull. *32*, 469–480.

Subbanna, S., Joshi, V., and Basavarajappa, B.S. (2018). Activity-dependent Signaling and Epigenetic Abnormalities in Mice Exposed to Postnatal Ethanol. Neuroscience *392*, 230–240.

Sugimori, H., Yao, H., Ooboshi, H., Ibayashi, S., and Iida, M. (2004). Krypton laser-induced photothrombotic distal middle cerebral artery occlusion without craniectomy in mice. Brain Res. Protoc. *13*, 189–196.

Sugimoto, K., Nishioka, R., Ikeda, A., Mise, A., Takahashi, H., Yano, H., Kumon, Y., Ohnishi, T., and Tanaka, J. (2014). Activated microglia in a rat stroke model express NG2 proteoglycan in peri-infarct tissue through the involvement of TGF-β1. Glia *62*, 185–198.
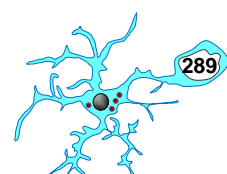
Sun, Y., Calvert, J.W., and Zhang, J.H. (2005). Neonatal hypoxia/ischemia is associated with decreased inflammatory mediators after erythropoietin administration. Stroke *36*, 1672–1678.

Sutherland, G.R., Dix, G.A., and Auer, R.N. (1996). Effect of age in rodent models of focal and forebrain ischemia. Stroke *27*, 1663–1668.

Suzuki, J., Imanishi, E., and Nagata, S. (2016). Xkr8 phospholipid scrambling complex in apoptotic phosphatidylserine exposure. Proc. Natl. Acad. Sci. U. S. A. *113*, 9509–9514.

Suzuki, S., Tanaka, K., Nogawa, S., Nagata, E., Ito, D., Dembo, T., and Fukuuchi, Y. (1999). Temporal profile and cellular localization of interleukin-6 protein after focal cerebral ischemia in rats. J. Cereb. Blood Flow Metab. *19*, 1256–1262.

Szaflarski, J., Burtrum, D., and Silverstein, F.S. (1995). Cerebral hypoxia-ischemia stimulates cytokine gene expression in perinatal rats. Stroke *26*, 1093–1100.

Szemere, E., and Jokeit, H. (2015). Quality of life is social - Towards an improvement of social abilities in patients with epilepsy. Seizure *26*, 12–21.

~T~

Tada, E., Parent, J.M., Lowenstein, D.H., and Fike, J.R. (2000). X-irradiation causes a prolonged reduction in cell proliferation in the dentate gyrus of adult rats. Neuroscience *99*, 33–41.

Taffe, M.A., Kotzebue, R.W., Crean, R.D., Crawford, E.F., Edwards, S., and Mandyam, C.D. (2010). Long-lasting reduction in hippocampal neurogenesis by alcohol consumption in adolescent nonhuman primates. Proc. Natl. Acad. Sci. U. S. A. *107*, 11104–11109.

Tahara, K., Kim, H.D., Jin, J.J., Maxwell, J.A., Li, L., and Fukuchi, K.I. (2006). Role of toll-like receptor signalling in Aβ uptake and clearance. Brain *129*, 3006–3019.

Takagi, S., Furube, E., Nakano, Y., Morita, M., and Miyata, S. (2019). Microglia are continuously activated in the circumventricular organs of mouse brain. J. Neuroimmunol. *331*, 74–86.

Takahashi, Y., Imai, K., Ikeda, H., Kubota, Y., Yamazaki, E., and Susa, F. (2013). Open study of pranlukast add-on therapy in intractable partial epilepsy. Brain Dev. *35*, 236–244.
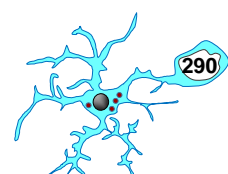
Takasato, M., Osafune, K., Matsumoto, Y., Kataoka, Y., Yoshida, N., Meguro, H., Aburatani, H., Asashima, M., and Nishinakamura, R. (2004). Identification of kidney mesenchymal genes by a combination of microarray analysis and Sall1-GFP knockin mice. Mech. Dev. *121*, 547–557.

Takeuchi, O., and Akira, S. (2010). Pattern Recognition Receptors and Inflammation. Cell *140*, 805–820.

Tamura, A., Graham, D.I., McCulloch, J., and Teasdale, G.M. (1981). Focal cerebral ischaemia in the rat: I. Description of technique and early neuropathological consequences following middle cerebral artery occlusion. J. Cereb. Blood Flow Metab. *1*, 53–60.

Tanaka, T., Ueno, M., and Yamashita, T. (2009). Engulfment of axon debris by microglia requires p38 MAPK activity. J. Biol. Chem. *284*, 21626–21636.

Tang, Y., and Le, W. (2016). Differential Roles of M1 and M2 Microglia in Neurodegenerative Diseases. Mol. Neurobiol. *53*, 1181–1194.

Tarkowski, E., Rosengren, L., Blomstrand, C., Wikkelsö, C., Jensen, C., Ekholm, S., and Tarkowski, A. (1997). Intrathecal release of pro- and anti-inflammatory cytokines during stroke. Clin. Exp. Immunol. *110*, 492–499.

Tarozzo, G., Campanella, M., Ghiani, M., Bulfone, A., and Beltramo, M. (2002). Expression of fractalkine and its receptor, CX3CR1, in response to ischaemia-reperfusion brain injury in the rat. Eur. J. Neurosci. *15*, 1663–1668.

Tatum, W.O. (2012). Mesial temporal lobe epilepsy. J. Clin. Neurophysiol. *29*, 356–365.

Taylor, R.C., Cullen, S.P., and Martin, S.J. (2008). Apoptosis: Controlled demolition at the cellular level. Nat. Rev. Mol. Cell Biol. *9*, 231–241.

Temkin, N.R. (2009). Preventing and treating posttraumatic seizures: The human experience. Epilepsia *50*, 10–13.

Thakur, L., Kojicic, M., Thakur, S.J., Pieper, M.S., Kashyap, R., Trillo-Alvarez, C.A., Javier, F., Cartin-Ceba, R., and Gajic, O. (2009). Alcohol consumption and development of acute respiratory distress syndrome: A population-based study. Int. J. Environ. Res. Public Health *6*, 2426–2435.

Thion, M.S., Ginhoux, F., and Garel, S. (2018). Microglia and early brain development: An intimate journey. Science (80-.). *362*, 185–189.

Thored, P., Heldmann, U., Gomes-Leal, W., Gisler, R., Darsalia, V., Taneera, J., Nygren,
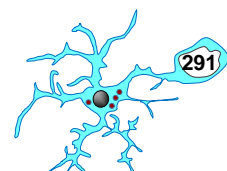
J.M., Jacobsen, S.E., Ekdahl, C.T., Kokaia, Z., et al. (2009). Long-term accumulation of microglia with proneurogenic phenotype concomitant with persistent neurogenesis in adult subventricular zone after stroke. Glia *57*, 835–849.

Thrash, J.C., Torbett, B.E., and Carson, M.J. (2009). Developmental regulation of TREM2 and DAP12 expression in the murine CNS: Implications for nasu-hakola disease. Neurochem. Res. *34*, 38–45.

Thurman, D.J., Beghi, E., Begley, C.E., Berg, A.T., Buchhalter, J.R., Ding, D., Hesdorffer, D.C., Hauser, W.A., Kazis, L., Kobau, R., et al. (2011). Standards for epidemiologic studies and surveillance of epilepsy. Epilepsia *52*, 2–26.

Tian, D.S., Peng, J., Murugan, M., Feng, L.J., Liu, J.L., Eyo, U.B., Zhou, L.J., Mogilevsky, R., Wang, W., and Wu, L.J. (2017). Chemokine CCL2-CCR2 signaling induces neuronal cell death via STAT3 activation and IL-1β production after status epilepticus. J. Neurosci. *37*, 7878–7892.

Tomimatsu, T., Fukuda, H., Endoh, M., Mu, J., Watanabe, N., Kohzuki, M., Fujii, E., Kanzaki, T., Oshima, K., Doi, K., et al. (2002). Effects of neonatal hypoxic-ischemic brain injury on skilled motor tasks and brainstem function in adult rats. Brain Res. *926*, 108–117.

Tomimoto, H., Akiguchi, I., Wakita, H., Kinoshita, A., Ikemoto, A., Nakamura, S., and Kimura, J. (1996). Glial expression of cytokines in the brains of cerebrovascular disease patients. Acta Neuropathol. *92*, 281–287.

Tovar-y-Romo, L.B., Ramírez-Jarquín, U.N., Lazo-Gómez, R., and Tapia, R. (2014). Trophic factors as modulators of motor neuron physiology and survival: Implications for ALS therapy. Front. Cell. Neurosci. *8:61*.

Traystman, R.J. (2003). Animal models of focal and global cerebral ischemia. ILAR J. *44*, 85–95.

Tremblay, M.Ě., Lowery, R.L., and Majewska, A.K. (2010). Microglial interactions with synapses are modulated by visual experience. PLoS Biol. *8(11):e100*.

Trouw, L.A., Blom, A.M., and Gasque, P. (2008). Role of complement and complement regulators in the removal of apoptotic cells. Mol. Immunol. *45*, 1199–1207.

Truman, L.A., Ford, C.A., Pasikowska, M., Pound, J.D., Wilkinson, S.J., Dumitriu, I.E., Melville, L., Melrose, L.A., Ogden, C.A., Nibbs, R., et al. (2008). CX3CL 1/fractalkine is released from apoptotic lymphocytes to stimulate macrophage chemotaxis. Blood *112*, 5026–5036.
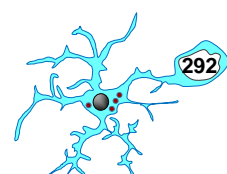
Tsuchiya, D., Hong, S., Kayama, T., Panter, S.S., and Weinstein, P.R. (2003). Effect of suture size and carotid clip application upon blood flow and infarct volume after permanent and temporary middle cerebral artery occlusion in mice. Brain Res. *970*, 131–139.

Türeyen, K., Vemuganti, R., Sailor, K.A., and Dempsey, R.J. (2004). Infarct volume quantification in mouse focal cerebral ischemia: A comparison of triphenyltetrazolium chloride and cresyl violet staining techniques. J. Neurosci. Methods *139*, 203–207.

Turrin, N.P., and Rivest, S. (2004). Innate immune reaction in response to seizures: Implications for the neuropathology associated with epilepsy. Neurobiol. Dis. *16*, 321–334.

Turski, L., Ikonomidou, C., Turski, W.A., Bortolotto, Z.A., and Cavalheiro, E.A. (1989). Review: Cholinergic mechanisms and epileptogenesis. The seizures induced by pilocarpine: A novel experimental model of intractable epilepsy. Synapse *3*, 154–171.

Turski, W.A., Czuczwar, S.J., Kleinrok, Z., and Turski, L. (1983). Cholinomimetics produce seizures and brain damage in rats. Experientia *39*, 1408–1411.

Tuttolomondo, A., Di Raimondo, D., di Sciacca, R., Pinto, A., and Licata, G. (2008). Inflammatory Cytokines in Acute Ischemic Stroke. Curr. Pharm. Des. *14*, 3574–3589.

~U~

Ubogu, E.E., Cossoy, M.B., and Ransohoff, R.M. (2006). The expression and function of chemokines involved in CNS inflammation. Trends Pharmacol. Sci. *27*, 48–55.

Uesugi, M., Kasuya, Y., Hayashi, K., and Goto, K. (1998). SB209670, a potent endothelin receptor antagonist, prevents or delays axonal degeneration after spinal cord injury. Brain Res. *786*, 235–239.

Umekawa, T., Osman, A.M., Han, W., Ikeda, T., and Blomgren, K. (2015). Resident microglia, rather than blood-derived macrophages, contribute to the earlier and more pronounced inflammatory reaction in the immature compared with the adult hippocampus after hypoxia-ischemia. Glia *63*, 2220–2230.

Uribe-Querol, E., and Rosales, C. (2020). Phagocytosis: Our Current Understanding of a Universal Biological Process. Front. Immunol. *11:1066*.

Utsunomiya, H., Takano, K., Okazaki, M., and Mitsudome, A. (1999). Development of the temporal lobe in infants and children: Analysis by MR-based volumetry. Am. J.
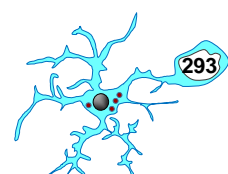
Neuroradiol. *20*, 717–723.

~√~

del Valle, J., Duran-Vilaregut, J., Manich, G., Camins, A., Pallàs, M., Vilaplana, J., and Pelegrí, C. (2009). Time-course of blood-brain barrier disruption in senescence-accelerated mouse prone 8 (SAMP8) mice. Int. J. Dev. Neurosci. *27*, 47–52.

Vallières, L., and Rivest, S. (1997). Regulation of the genes encoding interleukin-6, its receptor, and gp130 in the rat brain in response to the immune activator lipopolysaccharide and the proinflammatory cytokine interleukin-1β. J. Neurochem. *69*, 1668–1683.

Vannucci, R.C., and Vannucci, S.J. (1997). A model of perinatal hypoxic-ischemic brain damage. Ann. N. Y. Acad. Sci. *835*, 234–249.

Vannucci, R.C., Lyons, D.T., and Vasta, F. (1988). Regional cerebral blood flow during hypoxia-ischemia in immature rats. Stroke *19*, 245–250.

VanRyzin, J.W., Marquardt, A.E., Argue, K.J., Vecchiarelli, H.A., Ashton, S.E., Arambula, S.E., Hill, M.N., and McCarthy, M.M. (2019). Microglial Phagocytosis of Newborn Cells Is Induced by Endocannabinoids and Sculpts Sex Differences in Juvenile Rat Social Play. Neuron *102*, 435-449.e6.

Varvel, N.H., Neher, J.J., Bosch, A., Wang, W., Ransohoff, R.M., Miller, R.J., and Dingledine, R. (2016). Infiltrating monocytes promote brain inflammation and exacerbate neuronal damage after status epilepticus. Proc. Natl. Acad. Sci. U. S. A. *13*, E5665-74.

Verdonk, F., Roux, P., Flamant, P., Fiette, L., Bozza, F.A., Simard, S., Lemaire, M., Plaud, B., Shorte, S.L., Sharshar, T., et al. (2016). Phenotypic clustering: A novel method for microglial morphology analysis. J. Neuroinflammation *13*, 153.

Vezzani, A. (2009). PILOCARPINE-INDUCED SEIZURES REVISITED: WHAT DOES THE MODEL MIMIC? Antagonism of Peripheral Inflammation Reduces the Severity of Status Epilepticus. Epilepsy Curr *9*, 146–148.

Vezzani, A., and Granata, T. (2005). Brain inflammation in epilepsy: Experimental and clinical evidence. Epilepsia *46*, 1724–1743.

Vezzani, A., Balosso, S., and Ravizza, T. (2008). The role of cytokines in the pathophysiology of epilepsy. Brain. Behav. Immun. *22*, 797–803.

Vezzani, A., French, J., Bartfai, T., and Baram, T.Z. (2011). The role of inflammation in
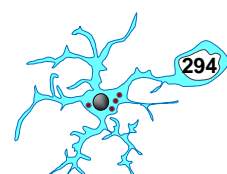
epilepsy. Nat. Rev. Neurol. *7*, 31–40.

Vezzani, A., Friedman, A., and Dingledine, R.J. (2013). The role of inflammation in epileptogenesis. Neuropharmacology *69*, 6–24.

Vila, N., Castillo, J., Dávalos, A., and Chamorro, Á. (2000). Proinflammatory cytokines and early neurological worsening in ischemic stroke. Stroke *31*, 2325–2329.

Vilalta, A., and Brown, G.C. (2018). Neurophagy, the phagocytosis of live neurons and synapses by glia, contributes to brain development and disease. FEBS J. *285(19):35,* 3566–3575.

Viviani, B., Bartesaghi, S., Gardoni, F., Vezzani, A., Behrens, M.M., Bartfai, T., Binaglia, M., Corsini, E., Di Luca, M., Galli, C.L., et al. (2003). Interleukin-1β enhances NMDA receptor-mediated intracellular calcium increase through activation of the Src family of kinases. J. Neurosci. *23*, 8692–8700.

Voll, R.E., Herrmann, M., Roth, E.A., Stach, C., Kalden, J.R., and Girkontaite, I. (1997). Immunosuppressive effects of apoptotic cells [9]. Nature *390*, 350–351.

Vorup-Jensen, T., and Jensen, R.K. (2018). Structural immunology of complement receptors 3 and 4. Front. Immunol. *9:2716*.

~W~

Waje-Andreassen, U., Kråkenes, J., Ulvestad, E., Thomassen, L., Myhr, K.M., Aarseth, J., and Vedeler, C.A. (2005). IL-6: An early marker for outcome in acute ischemic stroke. Acta Neurol. Scand. *111*, 360–365.

Wake, H., Moorhouse, A.J., Jinno, S., Kohsaka, S., and Nabekura, J. (2009). Resting microglia directly monitor the functional state of synapses in vivo and determine the fate of ischemic terminals. J. Neurosci. *29*, 3974–3980.

Walberer, M., Stolz, E., Müller, C., Friedrich, C., Rottger, C., Blaes, F., Kaps, M., Fisher, M., Bachmann, G., and Gerriets, T. (2006). Experimental stroke: Ischaemic lesion volume and oedema formation differ among rat strains (a comparison between Wistar and Sprague-Dawley rats using MRI). Lab. Anim. *40*, 1–8.

Walberer, M., Rueger, M.A., Simard, M.L., Emig, B., Jander, S., Fink, G.R., and Schroeter, M. (2010). Dynamics of neuroinflammation in the macrosphere model of arterio-arterial embolic focal ischemia: An approximation to human stroke patterns. Exp. Transl. Stroke Med. *2(1):22*.
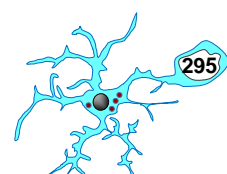
Walker, D.G., and Lue, L.F. (2013). Understanding the neurobiology of CD200 and the CD200 receptor: A therapeutic target for controlling inflammation in human brains? Future Neurol. *8(3):10.22*.

Wang, Y., and Qin, Z.H. (2010). Molecular and cellular mechanisms of excitotoxic neuronal death. Apoptosis *15*, 1382–1402.

Wang, H.J., Zakhari, S., and Jung, M.K. (2010). Alcohol, inflammation, and gut-liver-brain interactions in tissue damage and disease development. World J. Gastroenterol. *16*, 1304–1313.

Wang, X., Yue, T.L., Barone, F.C., White, R.F., Gagnon, R.C., and Feuerstein, G.Z. (1994). Concomitant cortical expression of TNF-α and IL-1β mRNAs follows early response gene expression in transient focal ischemia. Mol. Chem. Neuropathol. *23*, 103–114.

Watson, B.D., Dietrich, W.D., Busto, R., Wachtel, M.S., and Ginsberg, M.D. (1985). Induction of reproducible brain infarction by photochemically initiated thrombosis. Ann. Neurol. *17*, 497–504.

Wattananit, S., Tornero, D., Graubardt, N., Memanishvili, T., Monni, E., Tatarishvili, J., Miskinyte, G., Ge, R., Ahlenius, H., Lindvall, O., et al. (2016). Monocyte-derived macrophages contribute to spontaneous long-term functional recovery after stroke in mice. J. Neurosci. *36*, 4182–4195.

Wegiel, J., and Wisniewski, H.M. (1990). The complex of microglial cells and amyloid star in three-dimensional reconstruction. Acta Neuropathol. *81*, 116–124.

Weinhard, L., Di Bartolomei, G., Bolasco, G., Machado, P., Schieber, N.L., Neniskyte, U., Exiga, M., Vadisiute, A., Raggioli, A., Schertel, A., et al. (2018). Microglia remodel synapses by presynaptic trogocytosis and spine head filopodia induction. Nat. Commun. *9(1):1228*.

Wes, P.D., Holtman, I.R., Boddeke, E.W.G.M., Möller, T., and Eggen, B.J.L. (2016). Next generation transcriptomics and genomics elucidate biological complexity of microglia in health and disease. Glia *64*, 197–213.

Wieghofer, P., and Prinz, M. (2016). Genetic manipulation of microglia during brain development and disease. Biochim. Biophys. Acta - Mol. Basis Dis. *1862*, 299–309.

Wieser, H.G. (2004). Mesial temporal lobe epilepsy with hippocampal sclerosis. Epilepsia *20*, 131–137.
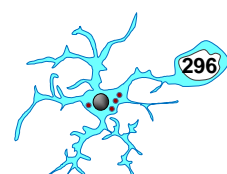
Wijeyesakere, S.J., Bedi, S.K., Huynh, D., and Raghavan, M. (2016). The C-Terminal Acidic Region of Calreticulin Mediates Phosphatidylserine Binding and Apoptotic Cell Phagocytosis. J. Immunol. *196*, 3896–3909.

Williams, P.A., Tribble, J.R., Pepper, K.W., Cross, S.D., Morgan, B.P., Morgan, J.E., John, S.W.M., and Howell, G.R. (2016). Inhibition of the classical pathway of the complement cascade prevents early dendritic and synaptic degeneration in glaucoma. Mol. Neurodegener. *11*.

Williams, R.S., Ferrante, R.J., and Caviness, V.S. (1978). The golgi rapid method in clinical neuropathology: The morphologic consequences of suboptimal fixation. J. Neuropathol. Exp. Neurol. *37*, 13–33.

Wolf, S.A., Boddeke, H.W.G.M., and Kettenmann, H. (2017). Microglia in Physiology and Disease. Annu. Rev. Physiol. *79*, 619–643.

Wolf, Y., Yona, S., Kim, K.W., and Jung, S. (2013). Microglia, seen from the CX3CR1 angle. Front. Cell. Neurosci. *7:26*.

Wong, C.H., Siah, K.W., and Lo, A.W. (2019). Estimation of clinical trial success rates and related parameters. Biostatistics *20*, 273–286.

Woodruff, T.M., Thundyil, J., Tang, S.C., Sobey, C.G., Taylor, S.M., and Arumugam, T. V. (2011). Pathophysiology, treatment, and animal and cellular models of human ischemic stroke. Mol. Neurodegener. *6*.

World Stroke Organization (2019). World Stroke Organization. WSO global stroke fact sheet. WSO. WSO.

Wu, P.H., and Phillis, J.W. (1978). Distribution and release of adenosine triphosphate in rat brain. Neurochem. Res. *3(5):563-7*, 563–571.

Wu, A., Wei, J., Kong, L.Y., Wang, Y., Priebe, W., Qiao, W., Sawaya, R., and Heimberger, A.B. (2010). Glioma cancer stem cells induce immunosuppressive macrophages/microglia. Neuro. Oncol. *12*, 1113–1125.

Wu, L.J., Wu, G., Sharif, M.R.A., Baker, A., Jia, Y., Fahey, F.H., Luo, H.R., Feener, E.P., and Clapham, D.E. (2012). The voltage-gated proton channel Hv1 enhances brain damage from ischemic stroke. Nat. Neurosci. *15*, 565–573.

Wu, Q., Combs, C., Cannady, S.B., Geldmacher, D.S., and Herrup, K. (2000). Beta-amyloid activated microglia induce cell cycling and cell death in cultured cortical neurons. Neurobiol. Aging *21*, 797–806.
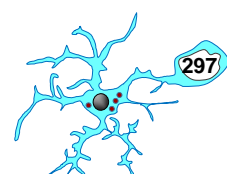
Wu, Y., Singh, S., Georgescu, M.M., and Birge, R.B. (2005). A role for Mer tyrosine kinase in αvβ5 integrin-mediated phagocytosis of apoptotic cells. J. Cell Sci. *118*, 539–553.

~X~

Xiao, A.J., Chen, W., Xu, B., Liu, R., Turlova, E., Barszczyk, A., Sun, C.L., Liu, L., Deurloo, M., Wang, G.L., et al. (2015). Marine compound Xyloketal B reduces neonatal Hypoxic-ischemic brain injury. Mar. Drugs *13*, 29–47.

Xu, J., Wang, T., Wu, Y., Jin, W., and Wen, Z. (2016a). Microglia Colonization of Developing Zebrafish Midbrain Is Promoted by Apoptotic Neuron and Lysophosphatidylcholine. Dev. Cell *38*, 214–222.

Xu, J., Yu, T., Pietronigro, E.C., Yuan, J., Arioli, J., Pei, Y., Luo, X., Ye, J., Constantin, G., Mao, C., et al. (2020). Peli1 impairs microglial Aβ phagocytosis through promoting C/EBPβ degradation. PLoS Biol. *18*.

Xu, P., Xu, Y., Hu, B., Wang, J., Pan, R., Murugan, M., Wu, L.J., and Tang, Y. (2015). Extracellular ATP enhances radiation-induced brain injury through microglial activation and paracrine signaling via P2X7 receptor. Brain. Behav. Immun. *50*, 87–100.

Xu, X., Lai, Y., and Hua, Z.C. (2019). Apoptosis and apoptotic body: Disease message and therapeutic target potentials. Biosci. Rep. *39(1):BSR2*.

Xu, Y., Hu, W., Liu, Y., Xu, P., Li, Z., Wu, R., Shi, X., and Tang, Y. (2016b). P2Y6 Receptor-Mediated Microglial Phagocytosis in Radiation-Induced Brain Injury. Mol. Neurobiol. *53*, 3552–3564.

Xue, J., Schmidt, S. V., Sander, J., Draffehn, A., Krebs, W., Quester, I., DeNardo, D., Gohel, T.D., Emde, M., Schmidleithner, L., et al. (2014a). Transcriptome-Based Network Analysis Reveals a Spectrum Model of Human Macrophage Activation. Immunity *40*, 274–288.

Xue, J., Dong, J.H., Huang, G.D., Qu, X.F., Wu, G., and Dong, X.R. (2014b). NF-κB signaling modulates radiation-induced microglial activation. Oncol. Rep. *31*, 2555–2560.

~Y~

Yamasaki, R., Lu, H., Butovsky, O., Ohno, N., Rietsch, A.M., Cialic, R., Wu, P.M., Doykan, C.E., Lin, J., Cotleur, A.C., et al. (2014). Differential roles of microglia and monocytes in the inflamed central nervous system. J. Exp. Med. *31*, 2555–2560.
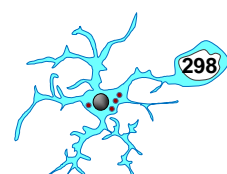
Yan, Z., Khadra, A., Li, S., Tomić, M., Sherman, A., and Stojilkovic, S.S. (2010). Experimental characterization and mathematical modeling of P2X7 receptor channel gating. J. Neurosci. *30*, 14213–14224.

Yanagisawa, M., Kurihara, H., Kimura, S., Goto, K., and Masaki, T. (1988). A novel peptide vasoconstrictor, endothelin, is produced by vascular endothelium and modulates smooth muscle ca2+channels. J. Hypertens. Suppl. *6*, S188-91.

Yang, S.N., and Lai, M.C. (2011). Perinatal hypoxic-ischemic encephalopathy. J. Biomed. Biotechnol. *2011:60981*.

Yang, C.N., Shiao, Y.J., Shie, F.S., Guo, B.S., Chen, P.H., Cho, C.Y., Chen, Y.J., Huang, F.L., and Tsay, H.J. (2011). Mechanism mediating oligomeric Aβ clearance by naïve primary microglia. Neurobiol. Dis. *42*, 221–230.

Yang, G., Kitagawa, K., Matsushita, K., Mabuchi, T., Yagita, Y., Yanagihara, T., and Matsumoto, M. (1997). C57BL/6 strain is most susceptible to cerebral ischemia following bilateral common carotid occlusion among seven mouse strains: Selective neuronal death in the murine transient forebrain ischemia. Brain Res. *752*, 209–218.

Yang, L., Yang, J., Li, G., Li, Y., Wu, R., Cheng, J., and Tang, Y. (2017). Pathophysiological Responses in Rat and Mouse Models of Radiation-Induced Brain Injury. Mol. Neurobiol. *54*, 1022–1032.

Yanuck, S.F. (2019). Microglial Phagocytosis of Neurons: Diminishing Neuronal Loss in Traumatic, Infectious, Inflammatory, and Autoimmune CNS Disorders. Front. Psychiatry *10:712*.

Yao, R., Pan, R., Shang, C., Li, X., Cheng, J., Xu, J., and Li, Y. (2020). Translocator Protein 18 kDa (TSPO) Deficiency Inhibits Microglial Activation and Impairs Mitochondrial Function. Front. Pharmacol. *11:986*.

Yeo, H.G., Hong, J.J., Lee, Y., Yi, K.S., Jeon, C.Y., Park, J., Won, J., Seo, J., Ahn, Y.J., Kim, K., et al. (2019). Increased CD68/TGFβ co-expressing microglia/macrophages after transient middle cerebral artery occlusion in rhesus monkeys. Exp. Neurobiol. *28*, 458–473.

Yeo, S.I., Kim, J.E., Ryu, H.J., Seo, C.H., Lee, B.C., Choi, I.G., Kim, D.S., and Kang, T.C. (2011). The roles of fractalkine/CX3CR1 system in neuronal death following pilocarpine-induced status epilepticus. J. Neuroimmunol. *234,* 93–102.

Yona, S., Kim, K.W., Wolf, Y., Mildner, A., Varol, D., Breker, M., Strauss-Ayali, D., Viukov, S., Guilliams, M., Misharin, A., et al. (2013). Fate Mapping Reveals Origins and
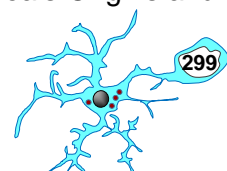
Dynamics of Monocytes and Tissue Macrophages under Homeostasis. Immunity *38*, 79–91.

Yoshikawa, K., Kita, Y., Kishimoto, K., and Shimizu, T. (2006). Profiling of eicosanoid production in the rat hippocampus during kainic acid-induced seizure: Dual phase regulation and differential involvement of COX-1 AND COX-2. J. Biol. Chem. *281*, 14663–14669.

You, L.H., Yan, C.Z., Zheng, B.J., Ci, Y.Z., Chang, S.Y., Yu, P., Gao, G.F., Li, H.Y., Dong, T.Y., and Chang, Y.Z. (2017). Astrocyte hepcidin is a key factor in LPS-induced neuronal apoptosis. Cell Death Dis. *8(3):e2676*.

~Z~

Zaremba, J., and Losy, J. (2001). Early TNF-α levels correlate with ischaemic stroke severity. Acta Neurol. Scand. *104*, 288–295.

Zhan, Y., Paolicelli, R.C., Sforazzini, F., Weinhard, L., Bolasco, G., Pagani, F., Vyssotski, A.L., Bifone, A., Gozzi, A., Ragozzino, D., et al. (2014). Deficient neuron-microglia signaling results in impaired functional brain connectivity and social behavior. Nat. Neurosci. *17*, 400–406.

Zhang, G.X., Li, J., Ventura, E., and Rostami, A. (2002). Parenchymal microglia of naïve adult C57BL/6J mice express high levels of B7.1, B7.2, and MHC class II. Exp. Mol. Pathol. *73*, 35–45.

Zhang, J., Xiao, X., Liu, W., Demirci, G., and Li, X.C. (2009). Inhibitory receptors of the immune system: Functions and therapeutic implications. Cell. Mol. Immunol. *6*, 407–414.

Zhang, W.P., Hu, H., Zhang, L., Ding, W., Yao, H.T., Chen, K. Da, Sheng, W.W., Chen, Z., and Wei, E.Q. (2004). Expression of cysteinyl leukotriene receptor 1 in human traumatic brain injury and brain tumors. Neurosci. Lett. *363*, 247–251.

Zhang, Z., Zhang, Z., Lu, H., Yang, Q., Wu, H., and Wang, J. (2017). Microglial Polarization and Inflammatory Mediators After Intracerebral Hemorrhage. Mol. Neurobiol. *54*, 1874–1886.

Zhao, C.Z., Zhao, B., Zhang, X.Y., Huang, X.Q., Shi, W.Z., Liu, H.L., Fang, S.H., Lu, Y.B., Zhang, W.P., Tang, F.D., et al. (2011). Cysteinyl leukotriene receptor 2 is spatiotemporally involved in neuron injury, astrocytosis and microgliosis after focal cerebral ischemia in rats. Neuroscience *189:1-11*.
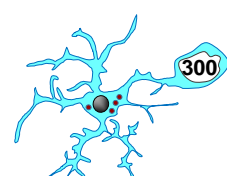
Zhao, S.C., Ma, L.S., Chu, Z.H., Xu, H., Wu, W.Q., and Liu, F. (2017). Regulation of microglial activation in stroke. Acta Pharmacol. Sin. *38*, 445–458.

Zhao, X., Eyo, U.B., Murugan, M., and Wu, L.J. (2018a). Microglial interactions with the neurovascular system in physiology and pathology. Dev. Neurobiol. *78*, 604–617.

Zhao, Y., Wu, X., Li, X., Jiang, L.L., Gui, X., Liu, Y., Sun, Y., Zhu, B., Piña-Crespo, J.C., Zhang, M., et al. (2018b). TREM2 Is a Receptor for β-Amyloid that Mediates Microglial Function. Neuron *97*, 1023–1031.

Zhao, Y.N., Wang, F., Fan, Y.X., Ping, G.F., Yang, J.Y., and Wu, C.F. (2013). Activated microglia are implicated in cognitive deficits, neuronal death, and successful recovery following intermittent ethanol exposure. Behav. Brain Res. *236*, 270–282.

Zheng, C., Zhou, X.W., and Wang, J.Z. (2016). The dual roles of cytokines in Alzheimer's disease: Update on interleukins, TNF-α, TGF-β and IFN-γ. Transl. Neurodegener. *5:7*.

Zhu, C., Wang, X., Xu, F., Bahr, B.A., Shibata, M., Uchiyama, Y., Hagberg, H., and Blomgren, K. (2005). The influence of age on apoptotic and other mechanisms of cell death after cerebral hypoxia-ischemia. Cell Death Differ. *12*, 162–176.

Zhu, P., Hata, R., Cao, F., Gu, F., Hanakawa, Y., Hashimoto, K., and Sakanaka, M. (2008). Ramified microglial cells promote astrogliogenesis and maintenance of neural stem cells through activation of Stat3 function. FASEB J. *22*, 3866-77.

Ziebell, F., Martin-Villalba, A., and Marciniak-Czochra, A. (2014). Mathematical modelling of adult hippocampal neurogenesis: Effects of altered stem cell dynamics on cell counts and bromodeoxyuridine-labelled cells. J. R. Soc. Interface *11(94):201*.

Zimmermann, H. (1996). Biochemistry, localization and functional roles of ecto-nucleotidases in the nervous system. Prog. Neurobiol. *49*, 589–618.

Zizzo, G., Hilliard, B.A., Monestier, M., and Cohen, P.L. (2012). Efficient Clearance of Early Apoptotic Cells by Human Macrophages Requires M2c Polarization and MerTK Induction. J. Immunol. *189*, 3508–3520.

del Zoppo, G.J., Poeck, K., Pessin, M.S., Wolpert, S.M., Furlan, A.J., Ferbert, A., Alberts, M.J., Zivin, J.A., Wechsler, L., Busse, O., et al. (1992). Recombinant tissue plasminogen activator in acute thrombotic and embolic stroke. Ann. Neurol. *32*, 78–86.

Zsurka, G., and Kunz, W.S. (2015). Mitochondrial dysfunction and seizures: The neuronal energy crisis. Lancet Neurol. *14*, 956–966.

Zuroff, L., Daley, D., Black, K.L., and Koronyo-Hamaoui, M. (2017). Clearance of
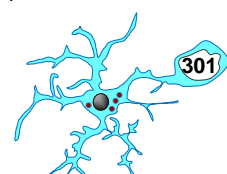
cerebral Aβ in Alzheimer's disease: reassessing the role of microglia and monocytes. Cell. Mol. Life Sci. *74*, 2167–2201.